

BUILDING AND TESTING COSMOLOGICAL MODELS:  
From Friedmann to Weyl-Cartan

---

Inaugural-Dissertation

zur

Erlangung des Doktorgrades

der Mathematischen-Naturwissenschaftlichen Fakultät

der Universität zu Köln

vorgelegt von

**Dirk Pützfeld**

aus Köln

2003

**Berichterstatter**

Prof. Dr. F.W. Hehl

Prof. Dr. C. Kiefer

Tag der mündlichen Prüfung: 2003-06-04

# Contents

<b>Zusammenfassung</b>	<b>1</b>
<b>Overview</b>	<b>5</b>
<b>1 Cosmology in General Relativity</b>	<b>9</b>
1.1 Introduction . . . . .	9
1.2 Field equations . . . . .	10
1.3 Properties . . . . .	13
1.4 Distance-redshift relations . . . . .	18
1.4.1 Luminosity distance . . . . .	18
1.4.2 Magnitude-redshift relation . . . . .	23
1.5 Thermodynamics . . . . .	24
1.6 Nucleosynthesis . . . . .	29
1.7 History of the universe . . . . .	47
1.8 Dimensions . . . . .	50
<b>2 Metric-affine gauge theory</b>	<b>51</b>
2.1 Introduction . . . . .	51
2.2 MAG in general . . . . .	51
2.3 The triplet ansatz . . . . .	53
2.4 Weyl-Cartan spacetime . . . . .	57
2.5 Dimensions . . . . .	59
<b>3 Cosmology in alternative gravity theories</b>	<b>61</b>
3.1 Introduction . . . . .	61
3.2 A cosmological model in Weyl-Cartan spacetime . . . . .	62
3.3 Field equations and Noether identities . . . . .	65
3.4 Special case $\xi(t, r) \rightarrow \zeta(t)$ . . . . .	68
3.5 Solutions . . . . .	71
3.5.1 $\Lambda \neq 0$ solutions . . . . .	71
3.5.2 $\Lambda = 0$ solutions . . . . .	73
3.5.3 Summary . . . . .	74
3.6 Magnitude-redshift relation . . . . .	76
3.7 Numerical results . . . . .	79

3.7.1	Data sets	79
3.7.2	Fitting method	80
3.7.3	Best-fit parameters	80
3.8	Summary	83
3.9	Alternative approach	89
3.10	Other models	92
3.10.1	Triplet model of Obukhov et al.	92
3.10.2	Weyl-Cartan model of Babourova et al.	93
3.10.3	Numerical results	94
3.11	Nucleosynthesis	95
3.11.1	Temperature of neutrinos and photons	96
3.11.2	Distribution functions	98
3.11.3	$^4\text{He}$ abundance	98
3.11.4	Comparison with the precision estimate	102
3.12	Summary	103
3.12.1	Combined constraints	103
3.12.2	The future	104
3.13	Dimensions	106
<b>A</b>	<b>Conventions and identities</b>	<b>107</b>
A.1	Exterior calculus and the hodge dual	107
A.2	Identities	109
<b>B</b>	<b>Units and numbers</b>	<b>111</b>
B.1	Units	111
B.2	Constants	112
B.3	Elementary particles and electromagnetic spectrum	115
<b>C</b>	<b>Decompositions</b>	<b>117</b>
C.1	Decomposing the curvature 2-form	117
C.2	Decomposing the torsion 2-form	119
C.3	Decomposing the nonmetricity 1-form	119
C.4	Decomposition of the linear connection	120
<b>D</b>	<b>Computer stuff</b>	<b>121</b>
D.1	General routines	122
D.1.1	Decomposition routines	122
D.1.2	Noether identities	128
D.1.3	Triplet ansatz in vacuum	129
D.1.4	Extended Weyl-Cartan Lagrangian	130
D.2	Cosmology	131
D.2.1	Standard model	131
D.2.2	Extended Weyl-Cartan model	133

<b>E Miscellany</b>	<b>143</b>
E.1 Field equations and Noether identities for $\xi = \xi(t, r)$ . . . . .	143
E.2 Field equations and Noether identities for $\zeta = \zeta(t)$ . . . . .	144
E.3 Robertson-Walker metric . . . . .	144
E.3.1 Riemannian connection . . . . .	144
E.3.2 Weyl-Cartan connection . . . . .	145
E.4 SN Ia data set . . . . .	145
E.5 Symmetric tracefree part of the second field equation . . . . .	148
<b>Bibliography</b>	<b>151</b>
<b>Index</b>	<b>169</b>
<b>Acknowledgements</b>	<b>173</b>
<b>Erklärung</b>	<b>173</b>
<b>Teilveröffentlichungen</b>	<b>173</b>
<b>Lebenslauf</b>	<b>175</b>



# List of Figures

1.1	Hubble flow . . . . .	11
1.2	Scale factors and equivalence redshift . . . . .	14
1.3	Age function . . . . .	18
1.4	Hubble law . . . . .	22
1.5	CMB spectrum (COBE/FIRAS) . . . . .	28
1.6	Neutron-to-baryon ratio in the FLRW model . . . . .	38
1.7	Neutron-to-baryon ratio in the FLRW model with chemical potential . . . . .	40
1.8	Equilibrium abundance fractions and time-temperature relation . . . . .	42
1.9	Parameter dependence of the ${}^4\text{He}$ abundance . . . . .	44
1.10	History of the universe in the standard picture . . . . .	48
2.1	Spacetime overview . . . . .	59
3.1	Scale factors for solutions with $\Lambda = 0$ . . . . .	76
3.2	Weyl 1-form $Q$ for solutions with $\Lambda = 0$ . . . . .	77
3.3	$\chi^2$ -distribution and best-fits for the FLRW model . . . . .	81
3.4	$\chi^2$ -distribution and best-fits for the Weyl-Cartan model . . . . .	83
3.5	Contours of the deceleration parameter . . . . .	86
3.6	Sign of the deceleration factor for both models . . . . .	87
3.7	Magnitude-redshift relation at high redshifts . . . . .	88
3.8	Magnitude-redshift relation for the alternative approach ( $\lambda = 0$ ) . . . . .	91
3.9	Magnitude-redshift relation for the alternative approach ( $\lambda \neq 0$ ) . . . . .	94
3.10	$\chi^2$ -distribution for the alternative approach . . . . .	95
3.11	Comparison of the conditions for the capture temperature . . . . .	100
3.12	${}^4\text{He}$ abundance and observational limits . . . . .	100
3.13	Comparison with the precision estimate . . . . .	102
3.14	Last-scattering surface . . . . .	104
3.15	Angle subtended by the horizon . . . . .	105
D.1	Computer algebra systems . . . . .	121
D.2	Test of the downhill simplex method . . . . .	122





# List of Tables

1.1	Assumptions made up to this point . . . . .	24
1.2	Discovery of the CMB . . . . .	26
1.3	Assumptions made up to this point . . . . .	27
1.4	Nuclear binding energies . . . . .	30
1.5	Assumptions made in order to derive $Y_n$ . . . . .	37
1.6	Nuclear reactions used in BBN calculations . . . . .	43
1.7	Light element abundance measurements . . . . .	46
1.8	Light element abundances from reviews . . . . .	47
1.9	Dimensions . . . . .	50
2.1	Summary of definitions . . . . .	54
2.2	Dimensions . . . . .	59
3.1	Model assumptions . . . . .	71
3.2	Ansatz $\Lambda \neq 0, w = \text{const}$ . . . . .	73
3.3	Ansatz $\Lambda \neq 0, w = w(t)$ . . . . .	73
3.4	Ansatz $\Lambda = 0, w = w(t)$ . . . . .	74
3.5	SN Ia data sets . . . . .	79
3.6	Grids used for minimization . . . . .	80
3.7	Best-fit parameters (FLRW model) . . . . .	82
3.8	Best-fit parameters (Weyl-Cartan model) . . . . .	83
3.9	Best-fit parameters other groups (FLRW model) . . . . .	84
3.10	Best-fit parameters other groups (non-standard models) . . . . .	85
3.11	Best-fit parameters for the alternative approach . . . . .	92
3.12	Best-fit parameters for the alternative approach ( $\lambda \neq 0$ ) . . . . .	95
3.13	${}^4\text{He}$ abundance limits on $\Omega_\psi$ . . . . .	101
3.14	Dimensions . . . . .	106
B.1	Natural units . . . . .	111
B.2	Operators and natural units . . . . .	111
B.3	SI system of units . . . . .	112
B.4	Fundamental constants in SI units . . . . .	113
B.5	Fundamental constants in cgs units . . . . .	113
B.6	Planck quantities . . . . .	113
B.7	Reduced Planck quantities . . . . .	114

B.8	Conversion factors, constants, and mnemonics . . . . .	114
B.9	Elementary particles (leptons & quarks) . . . . .	115
B.10	Electromagnetic spectrum . . . . .	115
B.11	Bosons and Hadrons . . . . .	116
E.1	SN Ia data set for fitting . . . . .	145
E.2	Acronyms . . . . .	172

# Zusammenfassung

Die Kosmologie repräsentiert heutzutage eines der sich am schnellsten entwickelnden Teilgebiete der Physik. Hervorgerufen durch eine große Zahl an neuen Beobachtungsdaten wurden große Fortschritte in Richtung eines *kosmologischen Standardmodells* gemacht [86]–[103]. Experimente von kosmologischem Interesse umfassen sowohl die Vermessung des kosmischen Mikrowellenhintergrunds (COBE, BOOMERANG, MAXIMA, WMAP), die Beobachtung von Supernovae des Typs Ia (SCP, HIGH-z Search Team), die Bestimmung der primordialen Elementhäufigkeiten als auch die Vermessung der großräumigen Verteilung leuchtender Materie im Universum (SDSS, 2dFGRS, XMM-LSS). Diese Experimente erlauben es uns verschiedene kosmologische Modelle zu testen und deren Parameterraum einzuschränken. In den späten neunziger Jahren führte insbesondere die Messung der scheinbaren Helligkeiten von stark rotverschobenen Supernovae des Typs Ia durch Perlmutter et al., Riess et al. und Schmidt et al. [121]–[126] zu einer wahren Flut an neuen Arbeiten. Die mit diesen Arbeiten verknüpfte Euphorie hatte mehrere Gründe. Einerseits führen die Messungen, falls man sie innerhalb des Standardmodells der Kosmologie interpretiert, zu dem Schluss, dass sich das Universum momentan in einer beschleunigten Phase der Expansion befindet. Andererseits scheint innerhalb dieses Modells die Wiedereinführung der kosmologischen Konstante unvermeidlich. Diese Konstante muss zudem mehr als 70% der kritischen Energiedichte zur Gesamtenergiedichte des Universums beitragen, um die Supernova-Daten zu beschreiben. Die Kosmologen wurden also von der Tatsache überrascht, dass unser Universum von einer bisher nicht direkt nachgewiesenen Energieform dominiert zu sein scheint. Heutzutage spricht man in diesem Kontext von der sogenannten *dunklen Energie*, in Analogie zur dunklen Materie.

Aus theoretischer Sicht führten die beschriebenen Entdeckungen zu einem regelrechten Erklärungsnotstand. Fragen in diesem Zusammenhang sind: Was ist die dunkle Energie? Ist ein hoher Dunkleenergieanteil kompatibel mit den anderen kosmologischen Tests? Gibt es kosmologische Modelle, die nicht auf einen hohen Dunkleenergieanteil angewiesen sind? Fragen dieser Art bringen uns zum Hauptanliegen dieser Arbeit, nämlich den Aufbau und Test alternativer kosmologischer Szenarien. Im Gegensatz zum kosmologischen Standardmodell, welches auf der Allgemeinen Relativitätstheorie (ART) basiert [22, 23, 26], werden die hier vorgestellten kosmologischen Modelle im Rahmen der sogenannten metrisch-affinen Gravitation (MAG) angesiedelt sein [44]. Bei der MAG handelt es sich um die eichtheoretische Formulierung einer alternativen Gravitations-

theorie, die im Gegensatz zur ART nicht auf eine pseudo-Riemann'sche Raumzeitstruktur beschränkt ist. Innerhalb dieser Theorie treten neue geometrische Größen auf, die *Torsion* und *Nichtmetrizität*, welche als zusätzliche Feldstärken analog zur Krümmung im allgemein-relativistischen Fall fungieren. Im Gegensatz zur ART gibt es bisher nur wenige Arbeiten zur Beobachtungslage von MAG-basierten kosmologischen Modellen. Eines unserer Hauptziele ist daher die quantitative Bestimmung der Parameter solcher Modelle mithilfe von aktuellen Beobachtungsdaten.

Im ersten Kapitel dieser Arbeit geben wir einen Überblick über das Standardmodell der Kosmologie. Wir beginnen mit der Herleitung der Feldgleichungen und lösen diese in einigen Spezialfällen. Dabei werden die wichtigsten kosmologischen Parameter eingeführt. Im Folgenden diskutieren wir zwei verschiedene kosmologische Tests, die Relation zwischen Größenklasse und Rotverschiebung sowie die primordiale Synthese von Helium. Insbesondere der Zusammenhang zwischen Helligkeit und Abstand eines astrophysikalischen Objekts weist eine starke Abhängigkeit von den Parametern des zugrundeliegenden kosmologischen Modells auf. In Kombination mit den Supernova-Daten ergibt sich daraus ein wichtiger Test der späten Phase des Universums. Im Gegensatz dazu findet die primordiale Nukleosynthese der leichten Elemente in den ersten Minuten der kosmischen Evolution statt und dient damit als Test für kosmologische Modelle in der Frühphase des Universums. Im Verlauf der Diskussion werden wir insbesondere die Beziehung zwischen Test und zugrundeliegendem kosmologischen Modell herausarbeiten sowie auf die momentane Beobachtungslage eingehen. Abschließend geben wir einen allgemeinen Überblick über die wichtigsten Ereignisse innerhalb des kosmologischen Standardmodells.

Im zweiten Kapitel führen wir die Feldgleichungen der MAG sowie die darin enthaltenen geometrischen Objekte ein. Im Anschluss konzentrieren wir uns auf die Diskussion von zwei interessanten Spezialfällen der MAG. Zum einen handelt es sich dabei um den von Obukhov et al. [74] entdeckten Triplett-Ansatz, in welchem die MAG-Feldgleichungen äquivalent zu denen der Einstein-Proca-Theorie sind. Zum anderen repräsentiert die sogenannte Weyl-Cartan-Raumzeit einen weiteren Spezialfall der metrisch-affinen Geometrie. In dieser verschwindet der gesamte spurfreie Anteil der Nichtmetrizität, und der symmetrische Anteil der Krümmung reduziert sich auf den Spurantil. Hierbei vereinfacht sich insbesondere die zweite MAG-Feldgleichung.

Nach diesen Vorbereitungen suchen wir im dritten Kapitel nach *überlebensfähigen* alternativen kosmologischen Modellen im Kontext der MAG. Nach einer kurzen Übersicht über das momentane Angebot an nicht-Standardszenarien präsentieren wir ein neues Modell auf Basis der Weyl-Cartan-Raumzeit. Innerhalb des ersten Teils von Kapitel drei leiten wir die Feldgleichungen dieses Modells her und suchen nach exakten Lösungen. Anschließend arbeiten wir den Zusammenhang zwischen Größenklasse und Rotverschiebung aus und suchen auf numerischem Weg nach den Modellparametern, die sich aus der Anpassung dieser Relation an die Supernova-Daten ergeben. Diese Analysen führen

wir sowohl für das kosmologische Standardmodell als auch für das Weyl-Cartan-Szenario durch. Im Anschluss widmen wir uns einem interessanten Spezialfall unseres neuen Modells und vergleichen diesen mit den Untersuchungen von zwei anderen Arbeitsgruppen. Die Untersuchung der Supernova-Daten liefert dabei eine obere Schranke für den Beitrag der nicht-Riemann'schen Größen zur Gesamtenergiedichte des Universums. Im weiteren Verlauf bestimmen wir den Anteil des primordial produzierten Heliums und können damit den Parameterraum dieses Modellzweiges weiter einschränken.

Die komplizierte Struktur der Feldgleichungen macht Berechnungen sowohl innerhalb der MAG als auch im Rahmen der ART zu einem zeitaufwändigen Unterfangen. Man ist daher auf die Verwendung von Computeralgebra-Systemen wie `Reduce` und `Maple` angewiesen. Einen Teil der in dieser Arbeit verwendeten Routinen für `Reduce` haben wir daher im Anhang D zusammengetragen. Insbesondere die dort aufgeführten Implementationen zur Zerlegung der Krümmung, Torsion und Nichtmetrizität sowie des Triplett-Lagrangians sind für die Wiederverwendung in zukünftigen Programmen geeignet.

Die Anhänge A und B enthalten eine Zusammenfassung unserer Konventionen sowie eine kurze Einführung in das äußere Kalkül [39]. Außerdem geben wir dort die Werte mehrerer Konstanten an die wir in unseren numerischen Berechnungen verwendet haben. Anhang C enthält die irreduziblen Zerlegungen der Krümmung, Torsion und Nichtmetrizität gemäß der in [44, 48] verwendeten Konventionen.



# Overview

Today cosmology appears to be one of the fastest growing fields of physics. Triggered by a wealth of new observational data, there has been a great leap forward to what is nowadays summarized under the name *cosmological standard model* [86]–[103]. Experiments of cosmological interest range from measurements of the cosmic microwave background (COBE, BOOMERANG, MAXIMA, WMAP), the observation of type Ia supernovae (SCP, HIGH-z Search Team), the determination the light elements abundances, to surveys mapping the large-scale distribution of luminous matter in the universe (SDSS, 2dFGRS, XMM-LSS). These experiments allow us to test different cosmological models and to put constraints on the parameters within these models. Especially the measurements of the apparent magnitudes of several high redshift type Ia supernovae, published by Perlmutter et al., Riess et al., and Schmidt et al. in the late nineties [121]–[126], led to a flood of new works. The reason for this excitement was twofold. Firstly, these measurements, if interpreted within the standard model, suggest that the universe is currently undergoing an accelerated phase of expansion. Secondly, the data strongly suggest the reintroduction of a cosmological constant that contributes more than 70% of the critical density to the total energy density of the universe. To state it the other way round, cosmologists were surprised by the fact that our universe seems to be dominated by some unknown and up to this date undetected form of energy, which is nowadays commonly called *dark energy*.

From a theoretical point of view these measurements raise several interesting questions: What is the nature of dark energy? Is a high amount of dark energy compatible with the other cosmological tests? Are there cosmological models that do not require dark energy? This brings us to the aim of this work, i.e., to build and test alternative cosmological scenarios. In contrast to the cosmological standard model, which is based on General Relativity (GR) [22, 23, 26], we try to construct viable models within the realm of the so-called metric-affine theory of gravity (MAG) [44] that is no longer tied to a pseudo-Riemannian spacetime structure. Within this theory there are new geometrical quantities, namely torsion and nonmetricity that act as additional field strengths similarly to the curvature in the general relativistic case. From an observational point of view the status of MAG based cosmological models is rather vague. Hence one of the main aims of this work is to obtain quantitative estimates for the parameters in such models.

In the first chapter we provide an overview of the standard model of cosmology. We derive the field equations and solve them for some special cases. Thereby we introduce all of the important cosmological parameters. Especially, we thoroughly discuss two different cosmological tests, the so-called magnitude-redshift relation and the primordial synthesis of helium. The connection between the luminosity and the distance of astrophysical objects is closely related to several cosmological parameters and therefore provides, in combination with the SN Ia data, a crucial cosmological test at late stages of the universe. In contrast, the primordial synthesis of light elements is thought to take place during the first minutes of the cosmic evolution and, accordingly, provides a test bed for new scenarios in the early universe. We put special emphasis on the discussion of the parameter dependency of these tests and sketch the current observational situation. The chapter is rounded by a broad brushed overview of the main events which occurred during the evolution of the universe within the standard picture.

The second chapter contains an overview of the field equations of MAG and the geometric quantities therein. Within this rather general introduction, we provide more details on two interesting special cases of MAG. The first one is the so-called triplet ansatz by which, as was shown by Obukhov et al. in [74], the theory becomes effectively equivalent to the Einstein-Proca theory. The second one is represented by the Weyl-Cartan spacetime for which the traceless part of the nonmetricity vanishes and the symmetric part of the curvature is reduced to its trace part. In particular, this constraint simplifies the structure of the second MAG field equation.

After these preparations, chapter three is devoted to the search for viable alternative cosmological models within the framework of MAG. After a brief report on currently available non-standard scenarios, we present a new cosmological model in Weyl-Cartan spacetime. Within the first part of the chapter we derive the field equations of this model and search for exact solutions. We then work out the magnitude-redshift relation within this new setup. Subsequently, we perform a numerical analysis of the SN Ia data within the cosmological standard model and the alternative scenario. Thereby, we constrain the parameters within both models. Additionally, we investigate an interesting special case of our model and compare it to the results of two other groups. We also perform an analysis of the SN Ia data within this branch of the model and obtain a numerical bound on the non-Riemannian contribution to the total density of the universe. The comparison of this result to the primordial helium abundance, which we infer from a semi-analytical nucleosynthesis calculation, enables us to put a very strong quantitative limit on the model parameters.

Due to the complicated structure of the field equations, the search for solutions in MAG as well as in GR is very time consuming. Hence we made extensive use of the computer algebra systems `Reduce` and `Maple`. Some of the routines for `Reduce` are displayed in appendix D. Especially the decomposition routines for the curvature, torsion, and nonmetricity as well as the implementation of the triplet Lagrangian are reusable in future calculations.



In appendices A and B we summarize our conventions (including those of the calculus of exterior differential forms) and the numerical values of several constants as used in the numerical calculations of this work. Appendix C contains the irreducible decomposition of the curvature, the torsion, and the nonmetricity (cf. [44, 48]).



# Chapter 1

## Cosmology in General Relativity

### 1.1 Introduction

In the following sections we give a short survey of some topics which are nowadays summarized under the term *standard cosmological model*. In section 1.2 we derive the field equations of the FLRW model (Friedmann, Lemaître, Robertson, and Walker) and discuss some of its basic properties in 1.3. In sections 1.4–1.6 we review two cosmological tests, the magnitude-redshift relation and the primordial synthesis of helium which will be used to test the non-standard models in chapter 3. Although we tried to keep this work as self contained as possible, the reader might want to turn to one of the standard textbooks on cosmology [1]–[5]. For a collection of influential works in cosmology the reader should consult [6]. Let us note that [19] contains a very individual assessment of the cosmological standard model.

Without going into observational detail we mention here only two assumptions which lead us to consider models of the FLRW type: (i) a global expansion and (ii) the homogeneity and isotropy of space. The first assumption goes back to an observation of Hubble [120], who found, by means of measuring the redshift and the luminosity of extragalactic nebulae, a linear relationship between the radial velocity  $v$  and the distance  $r$  ascribed to the nebulae with respect to an earthbound observer. This relationship is expressed in the famous Hubble law

$$v = H_0 d, \tag{1.1}$$

where  $H_0$  denotes the so-called Hubble constant. Let us stress that this law does *not* single out a preferred observer in the universe as one might intuitively guess, cf. figure 1.1. The velocity  $v$  in the above formula arises from the original interpretation of the observed redshift as Doppler shift. In the context of General Relativity (GR) this observation can also be interpreted as a global expansion of the spacetime. We derive this result in section 1.3. The notion *redshift*, associated with the global expansion, and the notion *Doppler shift*, associated with the peculiar motion of stars, are often used synonymously in astrophysical context. However they are completely different physical effects, see [9]

for a review which stresses this difference and the discussion in [7]. In order to take care of the first assumption (i), a cosmological model should incorporate something like a global scale factor  $S(t)$ , which describes the size of the universe. The second assumption (ii) relies on the fact that matter seems to be distributed very homogeneously in the universe at least in a statistical manner. These two assumptions motivate our ansatz for the metric and the energy-momentum in the next section.

## 1.2 Field equations

In this section we derive the field equations of the FLRW model. The assumption of homogeneity and isotropy leads to the so-called Robertson-Walker metric. Using spherical coordinates  $(t, r, \theta, \phi)$  and the coframe

$$\vartheta^{\hat{0}} = dt, \quad \vartheta^{\hat{1}} = \frac{S(t)}{\sqrt{1 - kr^2}} dr, \quad \vartheta^{\hat{2}} = S(t) r d\theta, \quad \vartheta^{\hat{3}} = S(t) r \sin \theta d\phi, \quad (1.2)$$

the line element is given by

$$ds^2 = -\vartheta^{\hat{0}} \otimes \vartheta^{\hat{0}} + \vartheta^{\hat{1}} \otimes \vartheta^{\hat{1}} + \vartheta^{\hat{2}} \otimes \vartheta^{\hat{2}} + \vartheta^{\hat{3}} \otimes \vartheta^{\hat{3}}. \quad (1.3)$$

The function  $S(t)$  represents the cosmic scale factor, and  $k$  can be chosen, after an appropriate rescaling of the coordinates, to be  $+1$ ,  $-1$ , or  $0$  for spaces with constant positive, negative, or zero spatial curvature, respectively. A straightforward calculation yields the components of the Einstein 3-form  $G_\alpha := \frac{1}{2} \eta_{\alpha\beta\gamma} \wedge \tilde{R}^{\beta\gamma}$ , see also appendices A and C (here and in the following we introduce the abbreviation  $\dot{\phantom{x}} = \frac{\partial}{\partial t}$ ):

$$G_{\hat{0}} = -\frac{3}{S^2} \left( \dot{S}^2 + k \right) \vartheta^{\hat{1}} \wedge \vartheta^{\hat{2}} \wedge \vartheta^{\hat{3}}, \quad (1.4)$$

$$G_{\hat{1}} = \frac{1}{S^2} \left( 2\ddot{S}S + \dot{S}^2 + k \right) \vartheta^{\hat{0}} \wedge \vartheta^{\hat{2}} \wedge \vartheta^{\hat{3}}, \quad (1.5)$$

$$G_{\hat{2}} = \frac{1}{S^2} \left( -2\ddot{S}S - \dot{S}^2 - k \right) \vartheta^{\hat{0}} \wedge \vartheta^{\hat{1}} \wedge \vartheta^{\hat{3}}, \quad (1.6)$$

$$G_{\hat{3}} = \frac{1}{S^2} \left( 2\ddot{S}S + \dot{S}^2 + k \right) \vartheta^{\hat{0}} \wedge \vartheta^{\hat{1}} \wedge \vartheta^{\hat{2}}. \quad (1.7)$$

The only thing missing in order to set up the field equations is an appropriate matter model. As motivated in the introduction we assume that energy and matter are smeared out smoothly over the spacetime. Thus, we choose the energy-momentum 3-form of an ideal fluid with pressure  $p$ , energy-density  $\mu$ , and four-velocity  $u^\alpha$ <sup>1</sup>, i.e.

$$\Sigma_\alpha^{\text{fluid}} = \Sigma_{\alpha\beta} \eta^\beta, \quad (1.8)$$

where

$$\Sigma^{\alpha\beta} = (\mu + p) u^\alpha u^\beta + p g^{\alpha\beta}. \quad (1.9)$$

---

<sup>1</sup>In the comoving frame we have  $u^\alpha = \delta_0^\alpha$ .

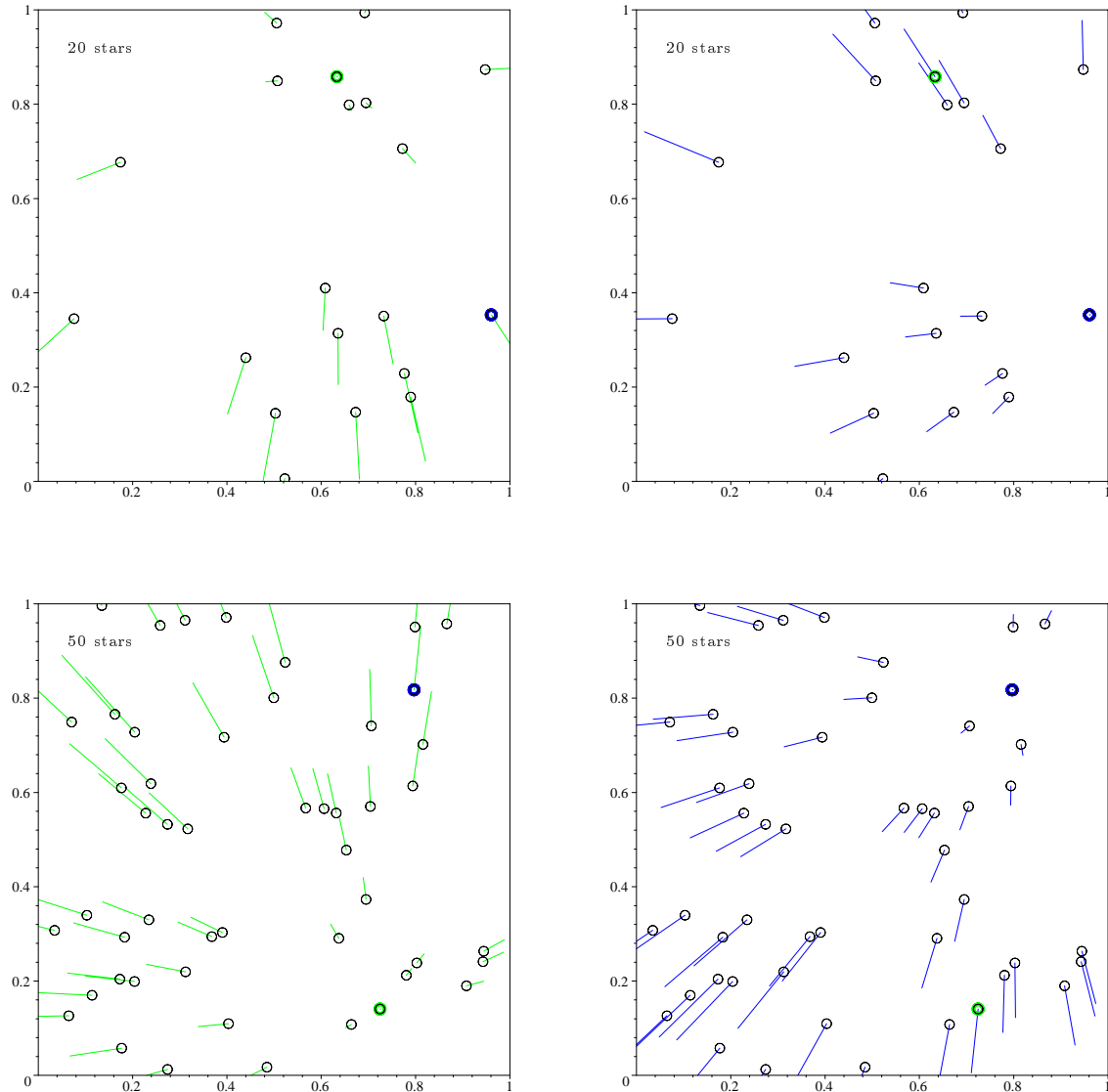


Figure 1.1: The figures above show a random distribution of 20 and 50 stars. The green/blue lines denote the radial velocities with respect to the green/blue reference star. In the initial configurations (in green) on the lhs we have chosen a radial velocity distribution similar to the Hubble law, cf. eq. (1.1). On the rhs we calculated the radial velocities from the lhs with respect to a new, arbitrarily chosen, reference star (marked with the blue circle). As becomes clear by comparing the lhs with the rhs the Hubble law does not single out a preferred observer in the universe. In contrast to what one might intuitively guess.

Now the Einstein field equation with cosmological constant,

$$\eta_{\alpha\beta\gamma} \wedge \tilde{R}^{\beta\gamma} + 2\lambda\eta_\alpha = 2\kappa\Sigma_\alpha^{\text{fluid}}, \quad (1.10)$$

yield the following set of field equations:

$$\frac{2}{S^2} \left( -3\dot{S}^2 + \kappa\mu S^2 - 3k + \lambda S^2 \right) = 0, \quad (1.11)$$

$$\frac{2}{S^2} \left( 2\ddot{S}S + \dot{S}^2 + \kappa p S^2 + k - \lambda S^2 \right) = 0. \quad (1.12)$$

We rewrite (1.11) and (1.12),

$$\left( \frac{\dot{S}}{S} \right)^2 + \frac{k}{S^2} - \frac{\lambda}{3} = \frac{\kappa}{3}\mu, \quad (1.13)$$

$$2\frac{\ddot{S}}{S} + \left( \frac{\dot{S}}{S} \right)^2 + \frac{k}{S^2} - \lambda = -\kappa p, \quad (1.14)$$

and recover the well known form of the so-called Friedmann equations, cf. [1]–[5]. Hence the field equations (1.10) turn into a set of ordinary differential equations for the scale factor  $S(t)$ . The functions  $\mu$ ,  $p$  and the parameters  $k$ ,  $\lambda$  depend on the model we decide to consider. Note that  $\mu$  and  $p$  are related by an equation of state  $p = p(\mu)$ ,  $p = \frac{1}{3}\mu$  in case of a radiation-dominated universe, e.g.

## Epochs

During its evolution the universe goes through different epochs, that are characterized by the respective equation of state. The inspection of (1.13)–(1.14) reveals that the solution for the scale factor  $S(t)$  depends on the choice of this equation of state. In addition to the field equations we have one Noether identity. In a Riemannian spacetime, cf. eq. (2.9), this identity reads

$$\tilde{D}\Sigma_\alpha = 0. \quad (1.15)$$

Let us assume that the equation of state takes the form  $p(t) = w\mu(t)$ , with  $w = \text{const.}$  Using (1.2)–(1.3), and (1.8), equation (1.15) turns into

$$\dot{\mu}S = -3\dot{S}(\mu + p) \stackrel{p=w\mu}{\Rightarrow} \mu = \varkappa_w S^{-3(1+w)} \sim S^{-3(1+w)}, \quad (1.16)$$

where  $\varkappa_w$  is an integration constant. Thus, we found a relation between the energy density and the scale factor, which depends on the constant  $w$  from the equation of state. Substituting back (1.16) into (1.13) yields

$$\left( \frac{\dot{S}}{S} \right)^2 + \frac{k}{S^2} - \frac{\lambda}{3} = \frac{\kappa}{3}\varkappa_w S^{-3(1+w)}. \quad (1.17)$$

**Special cases** A frequently discussed case is the spatially flat one with vanishing cosmological constant. Ignoring all emerging constants in the solution for  $S(t)$ , equation (1.17) yields

$$\left(\frac{\dot{S}}{S}\right)^2 = \frac{\kappa}{3}\varkappa_w S^{-3(1+w)} \quad \lambda=k=0, \varkappa_w=1, p=w\mu, w\neq-1 \quad S \sim t^{\frac{2}{3(1+w)}}. \quad (1.18)$$

Substituting this scaling behavior into (1.16) we have  $\mu \sim t^{-2}$  for all  $w \neq -1$ .

In case of a flat vacuum dominated model with non-vanishing cosmological constant, we can infer from (1.13)

$$\left(\frac{\dot{S}}{S}\right)^2 - \frac{\lambda}{3} = 0 \quad k=\mu=0 \quad S \sim e^{\sqrt{\lambda/3}t}. \quad (1.19)$$

Hence, for the special cases mentioned above we have the following scaling laws for the cosmic scale factor:  $S \sim t^{2/3}$  matter dominated,  $S \sim \sqrt{t}$  radiation dominated, and  $S \sim e^{\sqrt{\lambda/3}t}$  vacuum dominated.

## 1.3 Properties

In this section we collect some of the characteristic properties and definitions related to the FLRW model. We put special emphasis on their dependence on the underlying gravity theory.

### Critical density

In case of a flat universe  $k = 0$  the Hubble rate  $H := \dot{S}/S$  and the density  $\mu$  are related via a unique function  $\mu_c = \mu(H)$ , which is often called the *critical density*. The critical density is obtained via the first Friedmann equation (1.13); in case of a vanishing cosmological constant we have<sup>2</sup>

$$H^2 + \frac{k}{S^2} = \frac{\kappa}{3}\mu = \frac{8\pi G}{3}\mu \quad k=0 \quad \mu_c := \frac{3H^2}{8\pi G}. \quad (1.20)$$

This quantity is called *critical density* because it distinguishes between open, flat, or closed universes

$$\mu = \left(H^2 + \frac{k}{S^2}\right) \frac{3}{8\pi G} \quad \Rightarrow \quad \mu_{k=-1} < \mu_c < \mu_{k=1}. \quad (1.21)$$

---

<sup>2</sup>We make use of natural units (cf. app. B), i.e.  $\hbar = c = 1$ . Thus, the gravitational coupling constant becomes  $\kappa = \frac{8\pi G}{c^2} = 8\pi G$ .

Thus, the critical density can be determined by measuring the current value of the Hubble function. We introduce the dimensionless *density parameter*  $\Omega_w$  as ratio of the actual and the critical density

$$\Omega_w = \frac{\mu}{\mu_c} = \frac{8\pi G}{3H^2}\mu = \frac{\kappa}{3H^2}\mu. \quad (1.22)$$

We use  $w$  as an index since we did not specify the equation of state. In general dust, radiation, etc. contribute to the energy density in (1.22). In case of a non-vanishing cosmological constant  $\lambda$  the first Friedmann equation can be written in terms of the total density parameter  $\Omega_{\text{total}} = \Omega_w + \Omega_\lambda := \frac{\kappa}{3H^2}\mu + \frac{\lambda}{3H^2}$ , yielding

$$H^2 + \frac{k}{S^2} - \frac{\lambda}{3} = \frac{\kappa}{3}\mu \quad \Leftrightarrow \quad \Omega_{\text{total}} - 1 = \frac{k}{S^2 H^2}. \quad (1.23)$$

The value of the total density parameter distinguishes between the three possible geometries of the 3-dimensional subspace, i.e.

$$\Omega_{\text{total}} \begin{cases} < 1 \\ = 1 \\ > 1 \end{cases} \Rightarrow k \begin{cases} < 0 & \text{open} \\ = 0 & \text{flat} \\ > 0 & \text{closed} \end{cases}. \quad (1.24)$$

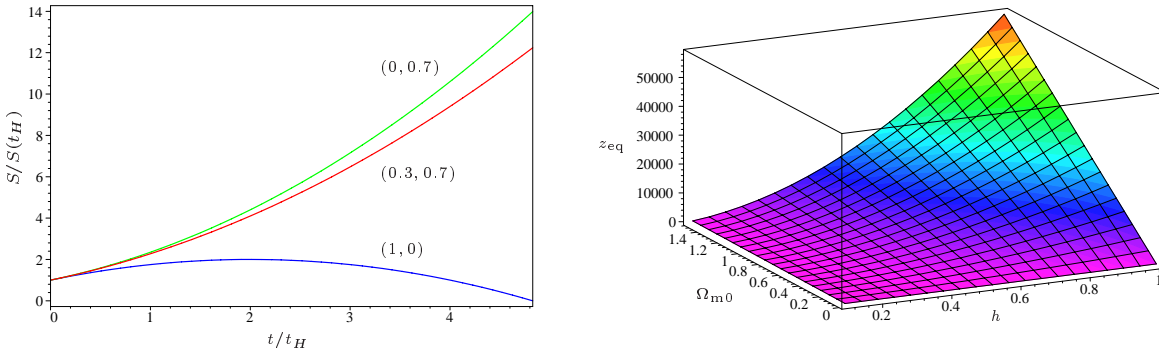


Figure 1.2: On the lhs we plotted the evolution of the scale factor for three different models, the notation is  $(\Omega_{m0}, \Omega_{\lambda0})$ . The plot has been arbitrarily normalised to unity at  $t_H = H_0^{-1}$ . Note that the three solutions correspond to the three different cases  $k = -1, 0, 1$ . On the rhs the matter-radiation equivalence redshift  $z_{\text{eq}}$  is displayed. The parameter  $h$  enters due to the uncertainty in  $H_0 = 100 h \frac{\text{km}}{\text{s Mpc}}$ .

## Horizons

A fundamental question in cosmology concerns the size of causally related regions. Hence one has to determine the maximal distance which light can travel during a given time. In case this distance is finite, there exists a so-called *particle horizon*.



**Particle horizon** The distance travelled by an unimpeded photon, which was emitted at  $r = 0$  and reaches an observer at  $r$ , is given by

$$d_{\text{H}}(t) := \int_0^r d\tilde{r} \sqrt{g_{rr}} = S(t) \int_0^r \frac{d\tilde{r}}{\sqrt{1 - k\tilde{r}^2}}. \quad (1.25)$$

Due to the spherical symmetry of the Robertson-Walker metric, we only need to take into account the radial slice ( $d\theta = d\phi = 0$ ), hence we arrive at

$$\begin{aligned} ds^2 &= -dt^2 + \frac{S(t)^2}{1 - kr^2} dr^2 = 0 \\ \Rightarrow \int_0^t \frac{d\tilde{t}}{S(\tilde{t})} &= \int_0^r \frac{d\tilde{r}}{\sqrt{1 - k\tilde{r}^2}} \Rightarrow d_{\text{H}}(t) = S(t) \int_0^t \frac{d\tilde{t}}{S(\tilde{t})}. \end{aligned} \quad (1.26)$$

Therefore this distance depends on the scale factor  $S$ . For the simple solution in (1.18) we find, for  $w \neq -1$ ,  $d_{\text{H}}(t) \sim \frac{3t(1+w)}{1+3w} = \frac{2}{(1+3w)H}$ . In the case that the explicit solution for  $S$  is not known, it is more comfortable to rewrite (1.26) in the following way

$$d_{\text{H}}(t) = S(t) \int_0^{S(t)} \frac{dS(\tilde{t})}{\dot{S}(\tilde{t}) S(\tilde{t})} = S(t) \int_0^{S(t)} \frac{dS(\tilde{t})}{H(\tilde{t})}. \quad (1.27)$$

**Event horizon** If  $d_{\text{H}}(t \rightarrow \infty)$  remains finite a given photon cannot travel into regions beyond this distance; an event horizon emerges. The existence of such a horizon, as one can imagine intuitively, depends on whether the universe is de- or accelerating. In fact the night sky would look quite uninteresting in an ever accelerating universe, since it will appear perfectly dark after a certain time.

## Singularity

In order to investigate the question of whether the FLRW model exhibits any essential singularities we inspect the curvature invariant

$$\star \left( \tilde{R}_{\alpha\beta} \wedge \star \tilde{R}^{\alpha\beta} \right) = -\frac{6}{S^4} \left( \left( \dot{S}^2 + k \right)^2 + \left( \ddot{S} S \right)^2 \right). \quad (1.28)$$

Thus, the existence of a singularity depends on the solution for the cosmic scale factor up to its second derivative. For the simple solution in (1.18) the invariant in equation (1.28) diverges for arbitrary values of  $w$  and  $k$  if  $t$  tends to zero. Then we have a universe which originates from an initial singularity. Since no one really expects that the simple FLRW description is still valid at Planck scales such a statement seems to be of very limited interest. Nevertheless there have been many attempts to construct models which avoid the initial singularity. In [66], e.g., an additional scalar field is introduced leading to a bouncing universe.

## Redshift

As announced in the introduction the cosmological standard model should lead to a redshift of distant sources due to the global expansion. In order to establish a connection between the cosmic scale factor and the spectral shift in the emission lines of a distant source, a galaxy, e.g., we assume that the propagation of light can be treated as a classical wave phenomenon. The Robertson-Walker line element yields

$$ds^2 = 0 \stackrel{\theta=\phi=\text{const}}{\Rightarrow} \int_{t_1}^{t_0} \frac{dt}{S(t)} = \int_{r_0}^{r_1} \frac{dr}{\sqrt{1 - kr^2}}. \quad (1.29)$$

where the light is emitted by a source at  $(t_1, r_1)$  and detected by an observer at  $(t_0, r_0)$ . Thus, we gained a relation between the coordinate distance and the time of travel. By putting  $r_0 = 0$  we obtain

$$\int_0^{r_1} \frac{dr}{\sqrt{1 - kr^2}} = f(r_1) = \int_{t_1}^{t_0} \frac{dt}{S(t)}. \quad (1.30)$$

Shifting the time of the emission  $t_1 \rightarrow t_1 + \delta t_1$  will result in a shift of the detection time, i.e.  $t_0 \rightarrow t_0 + \delta t_0$ . Since the lhs of (1.30) does not depend on the time of emission or detection we can infer

$$\int_{t_1}^{t_0} \frac{dt}{S(t)} = \int_{t_1 + \delta t_1}^{t_0 + \delta t_0} \frac{dt}{S(t)} \Leftrightarrow \int_{t_0}^{t_0 + \delta t_0} \frac{dt}{S(t)} = \int_{t_1}^{t_1 + \delta t_1} \frac{dt}{S(t)} \quad (1.31)$$

$$\delta t_{0,1} \ll t_{0,1} \rightarrow S(t) = \text{const} \Rightarrow \frac{\delta t_0}{S(t_0)} = \frac{\delta t_1}{S(t_1)}. \quad (1.32)$$

Interpreting  $\delta t_{0,1}$  as the times between two wavecrests at emission and at detection respectively, and relating them to the wavelength  $\delta t_{0,1} \sim \lambda_{0,1}$ , one obtains

$$\frac{\lambda_1}{\lambda_0} = \frac{S(t_1)}{S(t_0)}. \quad (1.33)$$

Using the common astronomical definition for the redshift

$$z := \frac{\lambda_0}{\lambda_1} - 1 \rightarrow \begin{cases} < 0 & \text{blueshifted} \\ > 0 & \text{redshifted} \end{cases}, \quad (1.34)$$

we find the following relation between the scale factor and the redshift in a Robertson-Walker spacetime:

$$1 + z = \frac{S(t_0)}{S(t_1)}. \quad (1.35)$$

Hence, if the universe is expanding, distant sources exhibit a redshift. The derivation presented above makes use of three crucial assumptions: (i) the propagation of light is completely determined by the metric, (ii) the dispersion relation  $\lambda\nu = c$  is valid at all times, and (iii) the observed wavelengths are small compared to the size of the universe.

Let us now derive an alternative form of the Friedmann equation. For that purpose we make use of the expression for the redshift (1.35) and the relation between the scale factor and the density (1.16). With  $\Omega_k := -\frac{k}{S^2 H^2}$  equation (1.23) turns into

$$\Omega_w + \Omega_\lambda + \Omega_k = 1. \quad (1.36)$$

For ordinary matter ( $w = 0$ ), the Friedmann equation can now be rewritten as follows:

$$\begin{aligned} H^2 &= \frac{\kappa}{3} \mu_m - \frac{k}{S^2} + \frac{\lambda}{3} \stackrel{(1.16)}{\Rightarrow} H^2 = \frac{\kappa \mathcal{Z}_0}{3S^3} - \frac{k}{S^2} + \frac{\lambda}{3} \\ \Leftrightarrow H^2 &= \frac{\kappa}{3} \mu_{m0} \left(\frac{S_0}{S}\right)^3 - \frac{k}{S_0^2} \left(\frac{S_0}{S}\right)^2 + \frac{\lambda}{3} \\ \stackrel{(1.35)}{\Rightarrow} H^2 &= H_0^2 \left( \frac{\kappa}{3H_0^2} \mu_{m0} (1+z)^3 - \frac{k}{S_0^2 H_0^2} (1+z)^2 + \frac{\lambda}{3H_0^2} \right) \\ \Leftrightarrow H^2 &= H_0^2 (\Omega_{m0} (1+z)^3 + \Omega_{k0} (1+z)^2 + \Omega_{\lambda0}) \\ \stackrel{(1.36)}{\Rightarrow} H^2 &= H_0^2 [(1+z)^2 (1+z \Omega_{m0}) - z (2+z) \Omega_{\lambda0}]. \end{aligned} \quad (1.37)$$

Relation (1.37) will play a crucial role in section 1.4.1, where we derive an expression for the luminosity distance in the FLRW model.

### Age

We rewrite the Hubble parameter in terms of the redshift as follows:

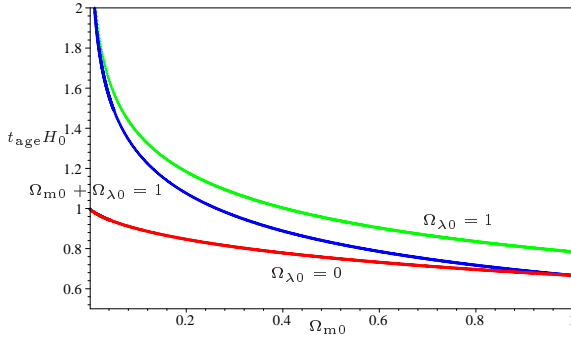
$$H = \frac{d}{dt} \log \left( \frac{S}{S_0} \right) = \frac{d}{dt} \log \left( \frac{1}{1+z} \right) = -\frac{1}{1+z} \frac{dz}{dt} \quad (1.38)$$

$$\stackrel{(1.37)}{\Rightarrow} \frac{dt}{dz} = -H_0^{-1} (1+z)^{-1} [(1+z)^2 (1+z \Omega_{m0}) - z (2+z) \Omega_{\lambda0}]^{-\frac{1}{2}} \quad (1.39)$$

$$\Rightarrow t_0 - t_1 = H_0^{-1} \int_{z_0}^{z_1} (1+z)^{-1} [(1+z)^2 (1+z \Omega_{m0}) - z (2+z) \Omega_{\lambda0}]^{-\frac{1}{2}} dz. \quad (1.40)$$

Thus, for a signal emitted at the big bang ( $t_1 = 0$ ) and detected at  $t_0$ , we find the age of the universe in terms of the redshift, the Hubble parameter, and the density parameters as:

$$t_{\text{age}}(z, H_0, \Omega_{m0}, \Omega_{\lambda0}) = H_0^{-1} \int_z^\infty (1+\tilde{z})^{-1} [(1+\tilde{z})^2 (1+\tilde{z} \Omega_{m0}) - \tilde{z} (2+\tilde{z}) \Omega_{\lambda0}]^{-\frac{1}{2}} d\tilde{z}. \quad (1.41)$$



$\Omega_{m0}$	$\Omega_{\lambda0}$	$H_0 \left[ \frac{\text{km}}{\text{s Mpc}} \right]$	Age [Gyr]
0.3	1	55	19.1
0.3	0.7	55	17.1
0.5	0.5	55	14.7
1	0	55	11.8
1.5	-0.5	55	10.3
0.3	0.7	65	14.5

Figure 1.3: Age function of the FLRW model in Hubble units for different parameter sets cf. eq. (1.41). The so-called Hubble time  $H_0^{-1}$  can be viewed as the basic timescale of the universe. In the table on the rhs we calculated the age of the universe for some specific parameter choices; see [8] for details on the observational procedures involved in estimating  $H_0$ .

## 1.4 Distance-redshift relations

In the next sections we basically focus on two different tests, i.e. the magnitude-redshift relation, and the synthesis of light elements, especially helium 4, in the early universe. The reason to consider these two tests in detail is threefold. Firstly, they can be viewed as tests of different epochs of our universe. Secondly, their observational underpinning is quite robust. Thirdly, they show strong dependence on the cosmological model. Admittedly most of these statements are also correct for other tests, like the ones involving the cosmic microwave background and the formation of structure. But, as we will show in the next sections, the two tests considered by us do not require much additional phenomenology. The reader might object that the prerequisite of the validity of the standard model of particle physics is far from being minimal. However particle physics is very well tested in the laboratory at energies relevant for nucleosynthesis.

### 1.4.1 Luminosity distance

In order to assign a distance to objects one introduces the so-called luminosity distance. This distance notion is based on the assumption that distant luminous objects appear fainter to us than nearby ones. The astronomical definition reads

$$\begin{aligned}
 d_{\text{luminosity}} &:= \left( \frac{\text{energy per time produced by source}}{\text{energy per time per area detected by observer}} \right)^{\frac{1}{2}} \\
 &= \left( \frac{\text{luminosity}}{4\pi \times \text{flux}} \right)^{\frac{1}{2}} = \left( \frac{\check{L}}{4\pi \check{F}} \right)^{\frac{1}{2}}.
 \end{aligned} \tag{1.42}$$

Hence, by measuring  $\check{F}$  and with knowledge of  $\check{L}$  (via a standard candle, a supernova, e.g.) we are able to determine the distance  $d_{\text{luminosity}}$ . Of course this distance definition requires the knowledge of how much light is emitted by the source at least during a specific time interval. Therefore, we either need an observer who measures the flux at the point of emission in the rest frame of the standard candle or an appropriate model of the source. Since we are talking about very distant objects, we have to rely on the latter method which belongs to the realm of astrophysics. We will not discuss different star models in this work, for a discussion concerning type Ia supernovae the reader is referred to [18, 143].

The question we have to ask ourselves is: How is the luminosity distance related to the parameters of the FLRW model? Since energy is conserved the following equation is supposed to hold

$$\check{L} \delta t_1 \delta \lambda_1 = \check{F} \delta t_0 \delta \lambda_0 A_0. \quad (1.43)$$

Here  $A_0$  denotes the area of the 2-sphere at the time of detection  $t = t_0$ . The factors  $\delta t_{0,1}$ , and  $\delta \lambda_{0,1}$  take into account the different length and time scales at emission and detection due to global expansion. The distance  $d_{\text{FLRW}}$  between an object at  $r = r_1$ , which emits light at  $t = t_1$ , and an observer at  $r = r_0 = 0$ , who detects the light at  $t = t_0$ , is given by

$$d_{\text{FLRW}} = S(t_0) r_1 \quad \Rightarrow \quad A_0 = 4\pi d_{\text{FLRW}}^2 = 4\pi S^2(t_0) r_1^2. \quad (1.44)$$

Thus, with the help of equations (1.33)–(1.35) the observed flux is given by

$$\check{F} = \frac{\check{L}}{4\pi S^2(t_0) r_1^2} \frac{\delta t_1 \delta \lambda_1}{\delta t_0 \delta \lambda_0} \stackrel{(1.33) \pm (1.35)}{=} \frac{\check{L}}{4\pi S^2(t_0) r_1^2} (1+z)^{-2}. \quad (1.45)$$

Comparison with (1.42) yields

$$d_{\text{luminosity}} = S(t_0) r_1 (1+z). \quad (1.46)$$

Additionally one wants to replace  $r_1$  by the scale factor  $S$ . We make use of equation (1.30) and obtain

$$\begin{aligned} f(r_1) &= \int_0^{r_1} \frac{dr}{\sqrt{1-kr^2}} = \int_{t_1}^{t_0} \frac{dt}{S(t)} = \begin{cases} \arcsin(r_1) & k = +1 \\ r_1 & \text{for } k = 0 \\ \operatorname{arcsinh}(r_1) & k = -1 \end{cases} \\ \Rightarrow r_1 &= \begin{cases} \sin\left(\int_{t_1}^{t_0} \frac{dt}{S(t)}\right) & k = +1 \\ \int_{t_1}^{t_0} \frac{dt}{S(t)} & \text{for } k = 0 \\ \sinh\left(\int_{t_1}^{t_0} \frac{dt}{S(t)}\right) & k = -1 \end{cases} \\ \Rightarrow d_{\text{luminosity}} &= S(t_0) (1+z) \times \begin{cases} \sin\left(\int_{t_1}^{t_0} \frac{dt}{S(t)}\right) & k = +1 \\ \int_{t_1}^{t_0} \frac{dt}{S(t)} & \text{for } k = 0 \\ \sinh\left(\int_{t_1}^{t_0} \frac{dt}{S(t)}\right) & k = -1 \end{cases}. \end{aligned} \quad (1.47)$$

Thus, we are able to express  $r_1$  via the scale factor. In order to derive  $r_1$  explicitly we need a solution of the Friedmann equations (1.13)–(1.14). Note that we did *not* make use of the field equations of the underlying gravity theory up to this point. This fact will be crucial when we derive an expression for the luminosity distance within an cosmological model which is not based on general relativity in section 3.6. As we will show in the following subsection there is an elegant way to rewrite the luminosity distance in terms of the density parameters, which makes use of the expression for the Hubble parameter as derived in equation (1.37). At this point the field equations come into play.

**Special case** In case of a Friedmann model which contains only ordinary matter and a contribution from the cosmological constant one can derive the following expression for the luminosity distance. This expression will play a crucial role when we perform fits to the observational data of distant supernovae in section 3.7. Again we make use of the Robertson-Walker line element, yielding

$$\begin{aligned}
\frac{dr}{\sqrt{1-kr^2}} &= \frac{dt}{S} \stackrel{(1.35)}{\Leftrightarrow} \frac{S_0}{\sqrt{1-kr^2}} dr = (1+z) dt \\
\stackrel{(1.39)}{\Rightarrow} S_0 \int_0^{r_1} \frac{dr}{\sqrt{1-kr^2}} &= H_0^{-1} \int_0^{z_1} \frac{dz}{\sqrt{(1+z)^2 (1+z\Omega_{m0}) - z(2+z)\Omega_{\lambda0}}} \\
\Rightarrow \Theta^{-1}[r_1] &= (H_0 S_0)^{-1} \int_0^{z_1} \frac{dz}{\sqrt{(1+z)^2 (1+z\Omega_{m0}) - z(2+z)\Omega_{\lambda0}}} \\
\Rightarrow d_{\text{luminosity}} &= S_0 (1+z) \Theta \left[ (H_0 S_0)^{-1} \int_0^z F[\tilde{z}] d\tilde{z} \right]. \tag{1.48}
\end{aligned}$$

Where we made use of the following definitions

$$\Theta[x] := \begin{cases} \sin(x) & k = +1 \\ x & \text{for } k = 0 \\ \sinh(x) & k = -1 \end{cases} \tag{1.49}$$

and

$$F[\tilde{z}] := [(1+\tilde{z})^2 (1+\tilde{z}\Omega_{m0}) - \tilde{z}(2+\tilde{z})\Omega_{\lambda0}]^{-\frac{1}{2}}. \tag{1.50}$$

By means of the definition of  $\Omega_k$  we can rewrite equation (1.48) as follows:

$$\begin{aligned}
d_{\text{luminosity}} &= \frac{(1+z)}{H_0 \sqrt{|\Omega_{k0}|}} \Theta \left[ \sqrt{|\Omega_{k0}|} \int_0^z F[\tilde{z}] d\tilde{z} \right] \\
&\stackrel{(1.36)}{=} \frac{(1+z)}{H_0 \sqrt{|1-\Omega_{m0}-\Omega_{\lambda0}|}} \Theta \left[ \sqrt{|1-\Omega_{m0}-\Omega_{\lambda0}|} \int_0^z F[\tilde{z}] d\tilde{z} \right]. \tag{1.51}
\end{aligned}$$

Thus, within a Friedmann model with ordinary matter and a cosmological constant the luminosity distance turns out to be a function of the corresponding density parameters, the Hubble constant, and the redshift, i.e.  $d_{\text{luminosity}} = d_{\text{luminosity}}(z, H_0, \Omega_{m0}, \Omega_{\lambda0})$ . This is a remarkable result since  $d_{\text{luminosity}}$  depends only on the present day values of the model parameters and the redshift.

**Hubble's law** Another way to rewrite (1.46) is to expand the scale factor around  $t = t_0$ ,

$$S(t) = S(t_0) + \dot{S}(t_0)(t - t_0) + \frac{1}{2}\ddot{S}(t_0)(t - t_0)^2 + \mathcal{O}((t - t_0)^3). \quad (1.52)$$

With<sup>3</sup>

$$H_0 := \frac{\dot{S}(t_0)}{S(t_0)}, \quad q_0 := -\frac{\ddot{S}(t_0)S(t_0)}{\dot{S}^2(t_0)} = -\frac{\ddot{S}(t_0)}{H_0^2 S(t_0)}, \quad (1.53)$$

equation (1.52) turns into

$$\frac{S(t)}{S(t_0)} = 1 + H_0(t - t_0) - \frac{1}{2}q_0 H_0^2 (t - t_0)^2 + \mathcal{O}((t - t_0)^3) \quad (1.54)$$

$$\stackrel{(1.35)}{\Rightarrow} z = H_0(t_0 - t) + \left(\frac{q_0}{2} + 1\right) H_0^2 (t_0 - t)^2 + \mathcal{O}((t - t_0)^3), \quad (1.55)$$

where we made use of another Taylor expansion in the last line<sup>4</sup>. Additionally, we can expand the functions in equation (1.47) around small values of  $r_1$

$$\int_{t_1}^{t_0} \frac{dt}{S(t)} = \begin{cases} r_1 + \mathcal{O}(r_1^3) & k = +1 \\ r_1 & \text{for } k = 0 \\ r_1 + \mathcal{O}(r_1^3) & k = -1 \end{cases}$$

$$\stackrel{(1.54)}{\Rightarrow} r_1 = S(t_0)^{-1} \int_{t_1}^{t_0} dt \left[ 1 - H_0(t - t_0) + \left(\frac{q_0}{2} + 1\right) H_0^2 (t - t_0)^2 + \mathcal{O}((t - t_0)^3) \right]$$

$$\Rightarrow r_1 = S(t_0)^{-1} \left[ (t_0 - t_1) + \frac{1}{2} H_0 (t_0 - t_1)^2 + \mathcal{O}(H_0^2) \right]. \quad (1.56)$$

Solving (1.55) for  $(t_0 - t)$  finally yields

$$(t_0 - t) = H_0^{-1} \left[ z - \left(1 + \frac{q_0}{2}\right) z^2 + \mathcal{O}(H_0^2) \right]$$

$$\Rightarrow r_1 = (S(t_0)H_0)^{-1} \left[ z - \frac{1}{2}(1 + q_0) z^2 + \mathcal{O}(H_0^2) \right]$$

$$\stackrel{(1.46)}{\Rightarrow} d_{\text{luminosity}} = H_0^{-1} (1 + z) \left[ z - \frac{1}{2}(1 + q_0) z^2 + \mathcal{O}(H_0^2) \right]$$

$$\Rightarrow H_0 d_{\text{luminosity}} = z + \frac{1}{2}(1 - q_0) z^2 + \mathcal{O}(z^3). \quad (1.57)$$

Thus, in first order, we recover the linear Hubble law (1.1). The model parameter  $q_0$  leads, if  $q_0 \neq 1$ , to a significant deviation from the linear Hubble law at moderate redshifts, cf. figure 1.4. Thus, we have found a method to determine one parameter of the cosmological model by measuring the luminosity-redshift relation. One can introduce

<sup>3</sup> $q_0$  is called *deceleration parameter*, since it indicates whether the universe is accelerating ( $q_0 \neq 0$ ) or not ( $q_0 = 0$ ).

<sup>4</sup> $\frac{1}{1+x-cx^2} = 1 - x + (c+1)x^2 + \mathcal{O}(x^3)$

additional parameters  $q_i$  up to the desired level of accuracy, which enter the expansion for  $S(t)$  in equation (1.52). Of course these parameters are in principle also determined by measuring the luminosity-redshift relation.

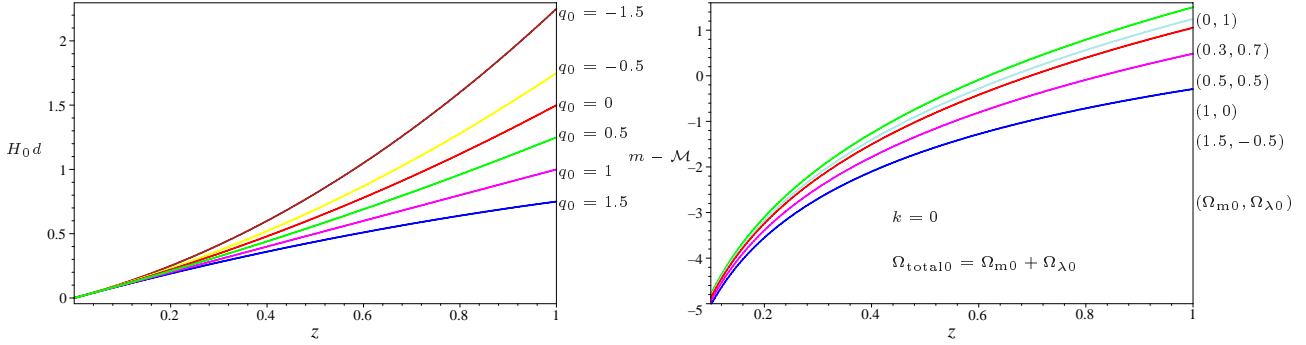


Figure 1.4: On the lhs row we plotted the deviation from the linear Hubble law resulting from the Taylor series expansion of the scale factor  $S$ , cf. eq. (1.57). The only model dependent parameter within this approximation is given by the deceleration factor  $q_0$ . This approximated law is only valid up to small redshifts  $z$ . On the rhs we plotted the magnitude-redshift relation, cf. eq. (1.63), in case of a model with ordinary matter ( $w = 0$ ) and a cosmological constant for a flat ( $\Omega_{\text{total}0} = 1$ ) scenario.

**Deceleration parameter** There are several other ways to express the luminosity distance via the field equations and the parameters of the FLRW model. From equation (1.57) one can read off that  $d_{\text{luminosity}} = d_{\text{luminosity}}(H_0, z, q_0)$ . In the following we rewrite  $q_0$  in terms of the density parameter. Substitution of (1.13) into (1.14) yields

$$\begin{aligned} \left( \frac{\ddot{S}}{S} \right) &= -\frac{\kappa}{6} (3p + \mu) + \frac{\lambda}{3} \\ \stackrel{p=w\mu}{\Rightarrow} q &:= -\frac{\ddot{S}}{SH^2} = \frac{1}{2} \frac{\kappa\mu}{3H^2} (1 + 3w) - \frac{\lambda}{3H^2} \\ \stackrel{(1.23), t=t_0}{\Rightarrow} q_0 &= \frac{(1 + 3w)}{2} \Omega_{w0} - \Omega_{\lambda0}. \end{aligned} \quad (1.58)$$

Thus, we obtain the luminosity distance (up to the second order) in terms of the density parameters, the Hubble constant, the redshift, and the constant which enters the equation of state, i.e.  $d_{\text{luminosity}} = d_{\text{luminosity}}(H_0, z, \Omega_{w0}, \Omega_{\lambda0}, w)$ . Another way to derive the relation between the deceleration parameter and the density parameters in the Friedmann equation is the following. Starting from the definition in (1.53) we obtain

$$q = -\frac{\ddot{S}}{\dot{S}^2} = \frac{d}{dt} H^{-1} - 1 \stackrel{(1.38)}{=} - (1 + z) H \frac{d}{dz} H^{-1} - 1. \quad (1.59)$$



Substitution of the Hubble parameter from equation (1.37) yields

$$q = \frac{1}{2} \frac{(3z(1+z) + 1 + z^2) \Omega_{\text{m}0} - 2\Omega_{\lambda 0}}{z(z+1)^2 \Omega_{\text{m}0} - z(2+z) \Omega_{\lambda 0} + (1+z)^2}. \quad (1.60)$$

Setting  $z = 0$  leads to same result for  $q_0$  as in equation (1.58).

**Other notions of distance** There exist several other distance notions besides the luminosity distance. One of the most prominent examples is the Dyer-Roeder distance cf. [154, 155, 156], where one introduces an additional parameter for the lumpiness of the matter. Without going into detail we want to remind the reader that the correct choice of the notion of distance in cosmology is still subject to discussions.

### 1.4.2 Magnitude-redshift relation

Due to historical reasons astrophysicists often use the so-called magnitude as unit for the luminosity of a stellar object. The relation between the distance-redshift relation and the so-called magnitude redshift relation, cf. [121, 123], is given by<sup>5</sup>

$$\begin{aligned} m(z, H_0, \Omega_{\text{w}0}, \Omega_{\lambda 0}, w, M) &:= M + 5 \log \left( \frac{d_{\text{luminosity}}}{\text{length}} \right) + 25 \\ &= M + 5 \log(H_0 d_{\text{luminosity}}) - 5 \log \left( \frac{H_0}{\text{length}} \right) + 25, \end{aligned} \quad (1.61)$$

where  $M$  represents the absolute bolometric magnitude of the observed star. By introducing a new constant  $\mathcal{M} := M - 5 \log H_0 + 25$  we are able to express the distance-redshift relation in equation (1.61) in a compact way as magnitude-redshift relation

$$\begin{aligned} &m(z, H_0, \Omega_{\text{m}0}, \Omega_{\lambda 0}, M) \\ &= \mathcal{M} + 5 \log \left( \frac{(1+z)}{\sqrt{|1 - \Omega_{\text{m}0} - \Omega_{\lambda 0}|}} \Theta \left[ \sqrt{|1 - \Omega_{\text{m}0} - \Omega_{\lambda 0}|} \int_0^z F[\tilde{z}] d\tilde{z} \right] \right). \end{aligned} \quad (1.62)$$

This relation is commonly used to extract cosmological parameters, as the density parameters associated with ordinary matter and the cosmological constant, by performing fits to data sets which were produced by the observation of standard candles, i.e. objects of known absolute magnitude. Equation (1.62) will be of use in later sections where we perform fits to a real data set, cf. section 3.7. Table 1.1 contains a collection of all assumptions made during the derivation of the magnitude-redshift relation within the cosmological standard model. Note that from a historical point of view the work of Mattig [132] played an influential role. Therein the magnitude-redshift relation for vanishing cosmological constant is derived.

---

<sup>5</sup>Note that  $\log$  denotes the logarithm to base 10, i.e.  $\log(e) \approx 0.4342$ .

Table 1.1: Assumptions made up to this point.

<b>Ansatz/Assumption</b>	<b>Equation</b>
General Relativity as underlying gravity theory	(1.10)
Metric is of Robertson-Walker type (i.e. homogeneity and isotropy)	(1.2)–(1.3)
Photons follow null curves (i.e. are determined by the metric)	(1.29)
Observed wavelengths small compared to size of the universe	(1.32)
Dispersion relation valid at all times, and peculiar movement of the source neglectable	(1.33)
Sources of known constant absolute magnitude	(1.61)
Photons travel unimpeded between source and observer, i.e. no gravitational potentials or dust between source and observer	(1.2)–(1.9)

In order to be complete we mention here the approximated version of the magnitude-redshift relation in terms of the deceleration parameter as derived in equation (1.58)

$$m - \mathcal{M} = 5 \log \left( z + \frac{1}{2} \left( \underbrace{1 - \frac{(1+3w)}{2} \Omega_{w0} + \Omega_{\lambda 0}}_{-q_0} \right) z^2 + \mathcal{O}(z^3) \right). \quad (1.63)$$

This result explains what is commonly known as the degeneracy of the magnitude-redshift relation. Since only the linear combination of the density parameters enters in (1.63).

**Gravitational lensing** Finally, let us remark that there might also be a systematic change in the luminosity of SN Ia due to weak gravitational lensing. A discussion of different lensing models and their impact on the SN Ia luminosity can be found in [149, 150, 151], e.g. We will not take care of systematic effects from lensing in this work.

## 1.5 Thermodynamics

Within the following section we will briefly derive some very useful relations between thermodynamical and cosmological quantities. From a historical point of view, cf. table 1.2, the theoretical developments concerning the thermodynamic history of the universe laid the foundation of the hot big bang model. In 1963 Penzias and Wilson accidentally discovered the cosmic microwave background. The CMB became one of the most important pillars in support of the big bang model, in which the universe cools down from an early hot phase to the present temperature of about 2.7 K. In figure 1.5 we depicted

the spectrum observed by the FIRAS<sup>6</sup> instrument aboard the COBE<sup>7</sup> satellite which was launched in 1989.

### Temperature

In a homogeneous universe the distribution function of a specific particle species  $i$  does not depend on the spatial coordinates, i.e.  $f_i(x, q, t) = f_i(q, t)$ . Here  $q$  denotes the momentum. The number density, energy density, and pressure of a particle species of type  $i$  are defined by

$$n_i : = \frac{g_i}{(2\pi)^3} \int f_i(q_i, t) d^3 q_i, \quad (1.64)$$

$$\mu_i : = \frac{g_i}{(2\pi)^3} \int E_i f_i(q_i, t) d^3 q_i, \quad (1.65)$$

$$p_i : = \frac{g_i}{(2\pi)^3} \int \frac{|q_i|^2}{3E_i} f_i(q_i, t) d^3 q_i, \quad (1.66)$$

where  $g_i$  is the spin degeneracy factor of the species and  $E_i = \sqrt{m_i^2 + q_i^2}$ . Since we consider spatial homogeneous distribution functions  $d^3 q_i \rightarrow q_i^2 dq_i d\Omega = 4\pi q_i^2 dq_i$ . Hence for an ideal Fermi or Bose gas the equilibrium energy density takes the form

$$\mu_i = \int_0^\infty \frac{g_i}{2\pi^2} \left[ e^{\frac{E_i - \varrho_i}{T_i}} \pm 1 \right]^{-1} E_i q_i^2 dq_i. \quad (1.67)$$

Here  $\varrho_i$  denotes the chemical potential, and the sign selects between Fermi or Bose statistics. This relation for the energy density is only valid if the particles are in thermal equilibrium. In the limit  $m_i, \varrho_i \ll T_i$  the energy density is given by

$$\begin{aligned} \mu_i &= \int_0^\infty \frac{g_i}{2\pi^2} \left[ e^{\frac{q_i}{T_i}} \pm 1 \right]^{-1} q_i^3 dq_i \\ &= \begin{cases} \frac{7}{8} \frac{\pi^2}{30} g_{Fi} T_i^4 & \text{for fermions} \\ \frac{\pi^2}{30} g_{Bi} T_i^4 & \text{for bosons} \end{cases}. \end{aligned} \quad (1.68)$$

Hence the total energy density of all species is given by

$$\mu_{\text{total}} = \sum_i \mu_i = \left( \frac{7}{8} \sum_{i=\text{fermions}} g_{Fi} T_i^4 + \sum_{i=\text{bosons}} g_{Bi} T_i^4 \right) \frac{\pi^2}{30}. \quad (1.69)$$

In case all particle species have the same temperature we can infer

$$\mu_{\text{total}} = \sum_i \mu_i = \left( \frac{7}{8} \sum_{i=\text{fermions}} g_{Fi} + \sum_{i=\text{bosons}} g_{Bi} \right) \frac{\pi^2}{30} T^4. \quad (1.70)$$

<sup>6</sup>Far InfraRed Absolute Spectrophotometer.

<sup>7</sup>COsmic Background Explorer.

Table 1.2: Discovery of the CMB.

1931	Lemaître	Formulated idea of a hot beginning
1934	Tolman	Thermodynamic history of an expanding universe
1941	Adams	Interstellar emission lines, later identified with molecules at $T \sim 2.3$ K
1942	Chandrasekhar & Henrich	Theory of therm. equilibrium & frozen abundances at high energies lead to observed cosmic abundances of elements
1942, 46	Gamow	Pointed out necessity of a dynamic model
1948	Alpher, Bethe, Gamow	Elements built up by rapid neutron capture
1948	Gamow	Estimated baryon number density $n$ at $T \sim 10^9$ K ( $T \sim n^{\frac{1}{3}} \rightarrow T_0 \sim 4$ K)
1948	Alpher & Herman	Corrected some numerical errors $T_0 \sim 5$ K
1950	Bell Labs	Start work on satellite communication
1959	NASA	Launched ECHO (passive reflector, 100 ft diameter balloon made of aluminized polyester, orbit 800-900 nmi, 960 MHz, 2390 MHz)
1961	Bell Labs	Construction of a horn antenna at Holmdel (NJ), 50 km from Princeton
1963	Penzias & Wilson	Antenna unused, conversion into a radio telescope, too high backgrounds
1964	Smimov	Rediscussed work of Gamow, arrived at $T_0 \sim 1 - 10$ K
1964	Doroshkevich & Novikov	Pointed out useful bound on radiation temperature from Bell reports
1965	Penzias & Wilson	Meeting with Princeton group, two papers on the observed background and the theoretical model in the same journal issue
1978	Penzias & Wilson	Nobel price

Refs. [206]–[213]

Table 1.3: Necessary assumptions for (1.72).

Ansatz/Assumption	Equation
Species are in thermal equilibrium	(1.67)
Temperature is high with respect to $m_i$ and $q_i$	(1.68)
Species interact with each other, i.e. have the same temperature	(1.70)

Of course we can only assume that all species have the same temperature if their interaction rate  $\Gamma_i$  is sufficiently high. The term in parenthesis, i.e. the effective number of degrees of freedom, depends on the underlying model of particle physics. Let us assume that this number depends only on the global temperature. Thus, with the definition

$$g_{\text{total}}(T) := \left( \frac{7}{8} \sum_{i=\text{fermions}} g_{\text{Fi}} + \sum_{i=\text{bosons}} g_{\text{Bi}} \right), \quad (1.71)$$

the total energy density turns out to be

$$\mu_{\text{total}} = \frac{\pi^2}{30} g_{\text{total}}(T) T^4. \quad (1.72)$$

If the temperature is high enough, which is the case in the early radiation dominated phase of the universe, the assumptions summarized in table 1.3 are fulfilled. Hence (1.72) with an appropriate  $g_{\text{total}}$  is applicable. By means of equation (1.16) we can derive a relation between the scale factor and the temperature, thereby establishing a link between thermodynamics and cosmology:

$$\mu_{\text{total}} \stackrel{(1.16)}{=} \sum_w \varkappa_w S^{-3(1+w)} \stackrel{(1.71)}{=} \frac{\pi^2}{30} g_{\text{total}}(T) T^4. \quad (1.73)$$

Hence we obtain the scaling behavior  $T \sim S^{-1}$  for a radiation dominated universe. If we make use of the definition for the redshift from (1.35) we arrive at

$$T(z) \sim T_0(1+z). \quad (1.74)$$

The use of the equilibrium formula in (1.67) seems to be justified at least in case of radiation. As depicted in the following figures the deviation from the blackbody law is of the order  $10^{-5}$  K as measured by the FIRAS instrument aboard the COBE satellite.

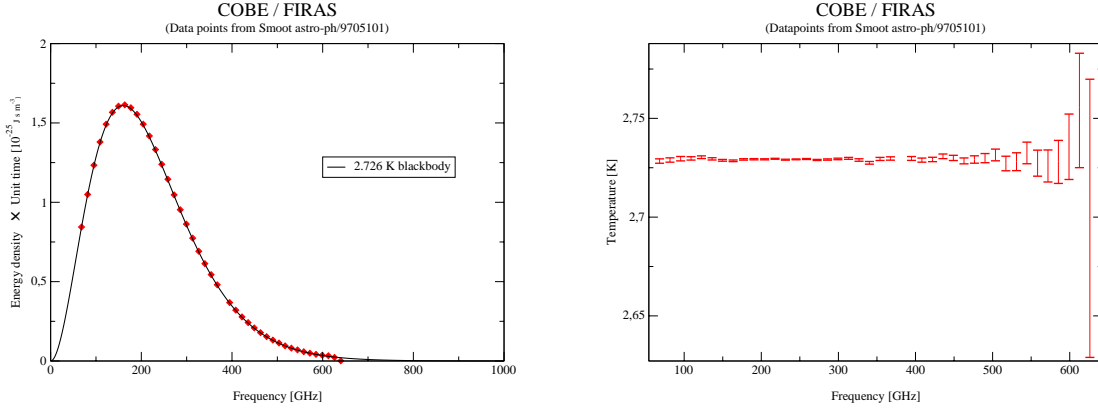


Figure 1.5: Blackbody spectrum at 2.726 K and results from COBE/FIRAS. Note that actual errorbars on the lhs are smaller than the data points, which renders the CMB one of the most perfect blackbodies we know. The datapoints in these plots are taken from [174].

**Expansion rate temperature relation** In case of a vanishing cosmological constant and zero spatial curvature we have the following relation between the Hubble function and the total density (1.72)

$$H^2 = \frac{\kappa}{3} \mu_{\text{total}} \stackrel{(1.73)}{=} \frac{\pi^2}{90} \kappa g_{\text{total}}(T) T^4. \quad (1.75)$$

Hence the expansion rate scales as  $H \sim T^2$ .

### Decoupling

Equation (1.64) allows us to calculate the number density of a given particle species in the limit  $m_i, q_i \ll T_i$ , i.e.

$$\begin{aligned} n_i &= \frac{g_i}{2\pi^2} \int_0^\infty \left[ e^{\frac{q_i}{T_i}} \pm 1 \right]^{-1} q_i^2 dq_i \\ &= \begin{cases} \frac{3}{4} \frac{\zeta(3)}{\pi^2} g_{Fi} T_i^3 & \text{for fermions} \\ \frac{\zeta(3)}{\pi^2} g_{Bi} T_i^3 & \text{for bosons} \end{cases}. \end{aligned} \quad (1.76)$$

Here  $\zeta$  denotes the Riemannian zeta function, with  $\zeta(3) \approx 1.202056903$ . Thus, the number density of a relativistic particle species scales as  $n \sim T^3$ . Let us assume that we have a general process of the form

$$A \overset{\Gamma}{\leftrightarrow} B, \quad (1.77)$$

where  $\Gamma$  denotes the interaction rate. One may write the interaction rate in terms of the number density  $n$ , the cross section  $\sigma$  of the corresponding interaction type, and the

mean velocity of the particles involved, i.e.

$$\Gamma = n\sigma \langle v \rangle. \quad (1.78)$$

By means of (1.76) and (1.78), we can interrelate the temperature and the reaction rate. For relativistic particles we have  $\langle v \rangle = 1$ , and therefore

$$\Gamma \sim T^3 \sigma \sim HT\sigma \rightarrow \frac{\Gamma}{H} \sim T\sigma. \quad (1.79)$$

Here the cross section has to be determined by the underlying particle physics model<sup>8</sup>. The relation in (1.79) establishes a link between different regimes of physics, i.e. elementary particle physics, gravity, and thermodynamics. If the reaction rate drops below the expansion rate, the interaction of the species in (1.77) becomes negligible and we call them *decoupled*. Especially the question of when the neutrinos have decoupled from the electron plasma plays a role for nucleosynthesis, which will be discussed in the next section. Although it will be sufficient for us to know that neutrinos have decoupled from the plasma at temperatures below 2 MeV, one has to keep in mind that decoupling is a non-equilibrium process which has, to certain extent, impact on nucleosynthesis [236]. For a detailed discussion of the decoupling temperature of the neutrinos and their role in cosmology the reader is referred to [105].

In the non-relativistic limit  $T_i \ll m_i$  the number density in (1.64) can be written as

$$\begin{aligned} n_i &:= \frac{g_i}{2\pi^2} \int_0^\infty \left[ e^{\frac{E_i - \epsilon_i}{T_i}} \pm 1 \right]^{-1} q_i^2 dq_i \simeq \frac{g_i}{2\pi^2} \int_0^\infty e^{-\frac{\sqrt{q_i^2 + m_i^2} - \epsilon_i}{T_i}} q_i^2 dq_i \\ &\simeq \frac{g_i}{2\pi^2} e^{-\frac{m_i - \epsilon_i}{T_i}} \int_0^\infty e^{-\frac{q_i^2}{2m_i T_i}} q_i^2 dq_i = g_i \left( \frac{m_i T_i}{2\pi} \right)^{\frac{3}{2}} e^{-\frac{m_i - \epsilon_i}{T_i}}. \end{aligned} \quad (1.80)$$

This relation holds for both, bosons and fermions.

## 1.6 Nucleosynthesis

In this section we review the standard big bang nucleosynthesis (BBN) scenario. Although there have been several suggestions to extend the BBN scenario, we stick to the simplest model, which is still in good agreement with observations.

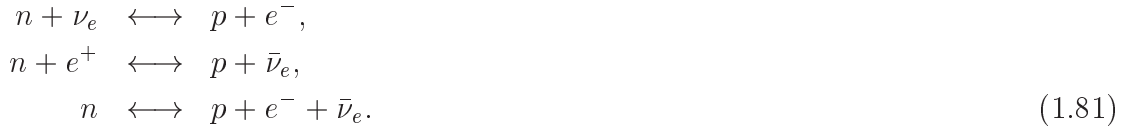
The beginning of nucleosynthesis is characterized by the freeze out of the weak interactions. Hence it is important to know the number density of protons and neutrons at the beginning of nucleosynthesis. The onset of nucleosynthesis is commonly defined by the time at which the temperature of the universe falls below the binding energy of the lightest nuclei, cf. table 1.4. The number density of neutrons and protons is fixed by the following processes

---

<sup>8</sup>Note that the cross section itself might depend on the temperature.

Table 1.4: Nuclear binding energies. Every element heavier than helium is called *metal*. The abundance of such elements is called *metallicity*.

Nuclei	Binding energy [MeV]	Nuclei	Binding energy [MeV]
$^2\text{H}$	2.22	$^8\text{Be}$	56.49
$^3\text{H}$	6.92	$^9\text{Be}$	58.19
$^3\text{He}$	7.72	$^{10}\text{B}$	64.75
$^4\text{He}$	28.29	$^{11}\text{B}$	76.20
$^6\text{Li}$	31.99	$^{12}\text{C}$	92.16
$^7\text{Li}$	39.24		



In the non-relativistic limit (1.80) the ratio of the neutron and proton number density becomes

$$\frac{n_n}{n_p} = \frac{g_n}{g_p} \left( \frac{m_n T_n}{m_p T_p} \right)^{\frac{3}{2}} e^{-\frac{m_n - \varrho_n}{T_n} + \frac{m_p - \varrho_p}{T_p}}. \tag{1.82}$$

From the conservation of the chemical potential in the reactions in (1.81) we find

$$\varrho_n + \varrho_{\nu_e} = \varrho_p + \varrho_{e^-} \xrightarrow{\varrho_{\nu_e}, \varrho_{e^-} \approx 0} \varrho_n = \varrho_p. \tag{1.83}$$

Hence, the equilibrium value of the neutron-to-proton ratio in (1.82) is given by

$$\frac{n_n}{n_p} \approx e^{-\frac{m_n - m_p}{T}} = e^{-\frac{Q}{T}}, \tag{1.84}$$

where  $Q := m_n - m_p \approx 1.29$  MeV denotes the mass difference between neutron and proton. The equilibrium formula in (1.84) remains valid as long as the reaction rate for the first two processes in (1.81) exceeds the expansion rate. It becomes clear from (1.84) that the neutron-to-proton ratio is approximately unity for temperatures well above the mass difference. In case the reaction rate  $\Gamma$  drops below the expansion rate  $H$  the neutron-to-proton ratio will freeze at the value corresponding to the decoupling temperature  $T_D$ , i.e.  $n_n/n_p \approx \exp(-Q/T_D)$ . According to our investigations in section 1.5 this temperature can be determined by calculating the reaction rates for the processes in (1.81). Early quantitative estimates of the reaction rates can be found in [190, 191, 213], for more recent estimates see [1, 237]. In the following sections we present a thorough review of a method which allows us to track the neutron-to-proton ratio in the expanding universe after the weak interaction ceased to keep neutrons and protons in thermodynamical equilibrium. This semi-analytical derivation was developed by Bernstein et al. in [193].



### Neutron-to-baryon ratio

We start with the definition of the ratio of the total number of neutrons to the total number of baryons

$$Y_n := \frac{n_n}{n_n + n_p}. \quad (1.85)$$

Let  $\Gamma_{np}$  and  $\Gamma_{pn}$  be the reaction rates of all weak processes which convert neutrons into protons and vice versa. Of course these functions depend on the temperature, and therefore on time. The rate equation for the time evolution of the neutron-to-baryon ratio is assumed to be given by

$$\frac{dY_n}{dt} = \Gamma_{pn} (1 - Y_n) - \Gamma_{np} Y_n. \quad (1.86)$$

This is a linear first-order differential equation. Rewriting (1.86) and defining two new functions we obtain

$$\dot{Y}_n = \Gamma_{pn} - (\Gamma_{pn} + \Gamma_{np})Y_n \quad \Leftrightarrow \quad \dot{Y}_n + \mathcal{A}Y_n = \mathcal{B}. \quad (1.87)$$

The solution of equation (1.87) is given by [38]

$$Y_n = e^{-\int_{t_0}^t \mathcal{A}(\tilde{t})d\tilde{t}} \left\{ Y_n(t_0) + \int_{t_0}^t \mathcal{B}(\tilde{t}) e^{\int_{t_0}^{\tilde{t}} \mathcal{A}(\hat{t})d\hat{t}} d\tilde{t} \right\}. \quad (1.88)$$

Suppressing the time dependency of the rates, we end up with

$$Y_n = e^{-\int_{t_0}^t (\Gamma_{pn} + \Gamma_{np})d\tilde{t}} \left\{ Y_n(t_0) + \int_{t_0}^t \Gamma_{pn} e^{\int_{t_0}^{\tilde{t}} (\Gamma_{pn} + \Gamma_{np})d\hat{t}} d\tilde{t} \right\}. \quad (1.89)$$

Following the work of Bernstein et al. [193] we assume that this solution is well approximated by

$$Y_n \approx \int_0^t d\tilde{t} \Gamma_{pn} e^{\int_{t_0}^{\tilde{t}} (\Gamma_{pn} + \Gamma_{np})d\hat{t}} := \int_0^t d\tilde{t} \Gamma_{pn} C(t, \tilde{t}). \quad (1.90)$$

Note that  $\frac{d}{dt}C(t, \tilde{t}) = (\Gamma_{pn} + \Gamma_{np}) C(t, \tilde{t})$ . Partial integration yields

$$\begin{aligned} Y_n &= \int_0^t d\tilde{t} \frac{\Gamma_{pn}}{\Gamma_{pn} + \Gamma_{np}} \frac{d}{d\tilde{t}} C(t, \tilde{t}) \\ &= \left. \frac{\Gamma_{pn}}{\Gamma_{pn} + \Gamma_{np}} C(t, \tilde{t}) \right|_0^t - \int_0^t d\tilde{t} C(t, \tilde{t}) \frac{d}{d\tilde{t}} \left( \frac{\Gamma_{pn}}{\Gamma_{pn} + \Gamma_{np}} \right) \end{aligned} \quad (1.91)$$

$$\begin{aligned} &= \left. \frac{\Gamma_{pn}}{\Gamma_{pn} + \Gamma_{np}} C(t, \tilde{t}) \right|_0^t - \int_0^t d\tilde{t} \frac{1}{\Gamma_{pn} + \Gamma_{np}} \frac{dC(t, \tilde{t})}{d\tilde{t}} \frac{d}{d\tilde{t}} \left( \frac{\Gamma_{pn}}{\Gamma_{pn} + \Gamma_{np}} \right) \\ &= \left. \frac{\Gamma_{pn}}{\Gamma_{pn} + \Gamma_{np}} C(t, \tilde{t}) \right|_0^t - \frac{C(t, \tilde{t})}{\Gamma_{pn} + \Gamma_{np}} \frac{d}{d\tilde{t}} \left( \frac{\Gamma_{pn}}{\Gamma_{pn} + \Gamma_{np}} \right) \Big|_0^t \\ &\quad + \int_0^t d\tilde{t} C(t, \tilde{t}) \frac{d}{d\tilde{t}} \left[ \frac{1}{\Gamma_{pn} + \Gamma_{np}} \frac{d}{d\tilde{t}} \left( \frac{\Gamma_{pn}}{\Gamma_{pn} + \Gamma_{np}} \right) \right] \\ &\approx \frac{\Gamma_{pn}}{\Gamma_{pn} + \Gamma_{np}} - \frac{1}{\Gamma_{pn} + \Gamma_{np}} \frac{d}{dt} \left( \frac{\Gamma_{pn}}{\Gamma_{pn} + \Gamma_{np}} \right) + \mathcal{O} \left[ \left( \frac{d\Gamma}{dt} \right)^2, \frac{d^2\Gamma}{dt^2} \right]. \end{aligned} \quad (1.92)$$

In the last step we made use of the fact that the sum of the reaction rates is large compared to the time variation of the rates. Hence we drop all second order terms containing the time derivative of the reaction rates. In the succeeding sections we will use

$$Y_n = \frac{\Gamma_{pn}}{\Gamma_{pn} + \Gamma_{np}} - \int_0^t d\tilde{t} C(t, \tilde{t}) \frac{d}{d\tilde{t}} \left( \frac{\Gamma_{pn}}{\Gamma_{pn} + \Gamma_{np}} \right), \quad (1.93)$$

thereby neglecting the integrating factor in the first term. In order to determine the neutron abundance in (1.93), we need to compute the reaction rates of the involved processes. Following the work of Bernstein et al. we neglect the neutron decay, i.e. the third reaction in eq. (1.81), in a first approximation.

### Reaction rates

After Weinberg [24] the reaction rates for the first two processes in (1.81) are given by

$$\begin{aligned} \Gamma_{n\nu_e \rightarrow pe^-} &= A \int_0^\infty dq_{\nu_e} q_{\nu_e}^2 q_e E_e (1 - f_e) f_{\nu_e}, \\ \Gamma_{ne^+ \rightarrow p\bar{\nu}_e} &= A \int_0^\infty dq_e q_e^2 q_{\nu_e} E_{\nu_e} (1 - f_{\nu_e}) f_e. \end{aligned} \quad (1.94)$$

Here  $f_e$  and  $f_{\nu_e}$  are the distribution functions of the electrons and electron neutrinos, respectively, and  $A$  is an effective coupling constant. If we neglect the chemical potential, the distribution functions entering (1.94) are given by

$$f_{e, \nu_e} = \frac{1}{e^{\frac{E_{e, \nu_e}}{T_{e, \nu_e}}} + 1}. \quad (1.95)$$

**Distribution functions** The distribution functions in (1.95) are also solutions of the collisionless Boltzmann equation in an expanding universe

$$\left( q^\alpha \frac{\partial}{\partial x^\alpha} - \Gamma^\alpha_{\beta\gamma} q^\beta q^\gamma \frac{\partial}{\partial q^\alpha} \right) f(x, q, t) = 0. \quad (1.96)$$

In a homogeneous and isotropic space the distribution function becomes  $f(q, t) \rightarrow f(E, t)$ . Hence, with  $q^\alpha = (E, q^i)$ , eq. (1.96) turns into

$$\left( E \frac{\partial}{\partial t} - \Gamma^0_{\beta\gamma} q^\beta q^\gamma \frac{\partial}{\partial E} \right) f(E, t) = 0. \quad (1.97)$$

For the Robertson-Walker metric in a Riemannian spacetime the connection components are displayed in E.3.1. Substituting these components into equation (1.97) yields

$$\left( E \frac{\partial}{\partial t} - \frac{\dot{S}}{S} g_{ij} q^i q^j \frac{\partial}{\partial E} \right) f(E, t) = 0 \Rightarrow \left( \frac{\partial}{\partial t} - H E \frac{\partial}{\partial E} \right) f(E, t) = 0. \quad (1.98)$$

Note that this is an interesting result with respect to the non-Riemannian models which we investigate in later chapters. Since the connection entering eq. (1.96) might differ from the Levi-Civita connection we can expect a change of eq. (1.98).

We derive a relationship between the reactions listed in (1.94) and the corresponding backreactions, i.e.

$$\begin{aligned} \Gamma_{pe^- \rightarrow n\nu_e} &= A \int_{q_0}^{\infty} dq_e q_e^2 q_{\nu_e} E_{\nu_e} (1 - f_{\nu_e}) f_e, \\ \Gamma_{p\bar{\nu}_e \rightarrow ne^+} &= A \int_{q_0}^{\infty} dq_{\nu_e} q_{\nu_e}^2 q_e E_e (1 - f_e) f_{\nu_e}. \end{aligned} \quad (1.99)$$

From (1.95) we can infer that

$$1 - f_{e,\nu_e} = e^{\frac{E_{e,\nu_e}}{T_{e,\nu_e}}} f_{e,\nu_e}, \quad (1.100)$$

hence

$$\begin{aligned} \Gamma_{pe^- \rightarrow n\nu_e} &= A \int_{p_0}^{\infty} dq_e q_e^2 q_{\nu_e} E_{\nu_e} (1 - f_{\nu_e}) f_e \\ &\stackrel{q_e dq_e = E_e dE_e}{=} A \int_0^{\infty} dE_e q_e q_{\nu_e} E_{\nu_e} E_e (1 - f_{\nu_e}) f_e \\ &\stackrel{dE_e = dq_{\nu_e} = dE_{\nu_e}}{=} A \int_0^{\infty} dq_{\nu_e} q_e q_{\nu_e} E_{\nu_e} E_e (1 - f_{\nu_e}) f_e \\ &\stackrel{E_{\nu_e} = q_{\nu_e}}{=} A \int_0^{\infty} dq_{\nu_e} q_e q_{\nu_e}^2 E_e (1 - f_e) f_{\nu_e} e^{\frac{E_{\nu_e}}{T_{\nu_e}} - \frac{E_e}{T_e}} \\ &\stackrel{T = T_e = T_{\nu_e}}{=} A \int_0^{\infty} dq_{\nu_e} q_e q_{\nu_e}^2 E_e (1 - f_e) f_{\nu_e} e^{-\frac{\Delta m}{T}} \\ &\stackrel{(1.94)}{=} e^{-\frac{\Delta m}{T}} \Gamma_{n\nu_e \rightarrow pe^-}. \end{aligned} \quad (1.101)$$

Here we assumed that the electrons and the neutrinos have the same temperature<sup>9</sup>, i.e.  $T = T_e = T_{\nu_e} = T_\gamma$ , and made use of the definition  $\Delta m := E_e - E_{\nu_e}$ . Accordingly the second reaction in (1.99) can be written as follows:

$$\Gamma_{p\bar{\nu}_e \rightarrow ne^+} = e^{-\frac{\Delta m}{T}} \Gamma_{ne^+ \rightarrow p\bar{\nu}_e}. \quad (1.102)$$

In case the temperature is low compared to the energy of the particles eq. (1.95) turns into

$$f_{e,\nu_e} \approx e^{-\frac{E_{e,\nu_e}}{T}} \quad \rightarrow \quad 1 - f_{e,\nu_e} \approx 1. \quad (1.103)$$

Hence the rate equations listed in (1.94) become

$$\begin{aligned} \Gamma_{n\nu_e \rightarrow pe^-} &\stackrel{(1.103)}{\approx} A \int_0^\infty dq_{\nu_e} q_{\nu_e}^2 q_e E_e e^{-\frac{E_{\nu_e}}{T}}, \\ \Gamma_{ne^+ \rightarrow p\bar{\nu}_e} &\stackrel{(1.103)}{\approx} A \int_0^\infty dq_e q_e^2 q_{\nu_e} E_{\nu_e} e^{-\frac{E_e}{T}}. \end{aligned} \quad (1.104)$$

Energy conservation yields

$$m_n + E_{\nu_e} = m_p + E_e \Leftrightarrow E_e = Q + E_{\nu_e}. \quad (1.105)$$

With the assumption that the electron mass is much smaller than the energies entering eq. (1.104) the rate equations turn into

$$\begin{aligned} \Gamma_{n\nu_e \rightarrow pe^-} &\stackrel{q_{\nu_e} \equiv E_{\nu_e}}{=} A \int_0^\infty dE_{\nu_e} E_{\nu_e}^2 q_e E_e e^{-\frac{E_{\nu_e}}{T}} \\ &\stackrel{q_e \equiv E_e}{=} A \int_0^\infty dE_{\nu_e} E_{\nu_e}^2 (Q + E_{\nu_e})^2 e^{-\frac{E_{\nu_e}}{T}} \\ &\stackrel{CA}{=} 2AT^3 (Q^2 + 6TQ + 12T^2), \end{aligned} \quad (1.106)$$

and

$$\begin{aligned} \Gamma_{ne^+ \rightarrow p\bar{\nu}_e} &\stackrel{q_e \equiv E_e, q_{\nu_e} \equiv E_{\nu_e}}{=} A \int_0^\infty dE_e E_e^2 E_{\nu_e}^2 e^{-\frac{E_e}{T}} \\ &\stackrel{E_{\nu_e} \equiv Q + E_e}{=} A \int_0^\infty dE_e E_e^2 (Q + E_e)^2 e^{-\frac{E_e}{T}} \\ &\stackrel{CA}{=} 2AT^3 (Q^2 + 6TQ + 12T^2) = \Gamma_{n\nu_e \rightarrow pe^-}. \end{aligned} \quad (1.107)$$

Hence the reaction rates turn out to be identical within this first approximation. Let us now investigate the third reaction displayed in (1.81), i.e. the *decay* of the neutron.

---

<sup>9</sup>In general the temperature of the photons and the neutrinos might differ due to annihilation of electrons and positrons. Our first approximation for the rate is justified by the fact that the neutron-to-baryon ratio will reach its asymptotic value before there is a significant deviation between the neutrino and photon temperature.

According to [24], the rate for this process is given by<sup>10</sup>

$$\begin{aligned}
\Gamma_{n \rightarrow p \bar{\nu}_e e^-} &= A \int_0^{q_0} dq_e q_e^2 q_{\nu_e} E_{\nu_e} (1 - f_{\nu_e}) (1 - f_e) \\
&\stackrel{(1.103), E_{\nu_e} = q_{\nu_e}}{\approx} A \int_0^{q_0} dq_e q_e^2 E_{\nu_e}^2 \\
&\stackrel{E_{\nu_e} = Q - E_e}{=} A \int_0^{q_0} dq_e q_e^2 (Q - E_e)^2 = A \int_0^{q_0} dq_e q_e^2 \left( Q - \sqrt{q_e^2 + m_e^2} \right)^2 \\
&\stackrel{CA}{=} A \left\{ \frac{Q^4 q_0}{30} - \frac{3Q^2 m_e^2 q_0}{20} - \frac{2q_0 m_e^4}{15} + \frac{Q}{4} m_e^4 \operatorname{arcsinh} \left( \frac{q_0}{m_e} \right) \right\} \\
&\stackrel{q_0 = \sqrt{Q^2 - m_e^2}}{=} \frac{A \sqrt{Q^2 - m_e^2}}{5} \left( \frac{Q^4}{6} - \frac{3Q^2 m_e^2}{4} - \frac{2m_e^4}{3} \right) + \frac{AQ m_e^4}{4} \operatorname{arccosh} \left( \frac{Q}{m_e} \right).
\end{aligned}$$

The upper integration limit for this process is determined by the positiveness of the neutrino energy, i.e.  $E_{\nu_e} = Q - E_e > 0 \Rightarrow q_e < \sqrt{Q^2 - m_e^2}$ . Of course the integral above determines the decay rate of a free neutron  $\Gamma_{n \rightarrow p \bar{\nu}_e e^-}^{-1}(Q, m_e, A) = \tau$ . This result is consistent with that of Bernstein et al., cf. (2.25a) in [193]. For  $Q = 1.29$  MeV and  $m_e = 0.511$  MeV we have  $\tau^{-1} = 0.01569024 \times A Q^5$ . In order to be compatible with the notation of Bernstein et al. we introduce a new constant  $a := 4/0.01569024 \approx 255$  which absorbs the numerical prefactor in the decay rate. Hence, we end up with

$$\tau^{-1} = \frac{4}{a} A Q^5. \quad (1.108)$$

Additionally, we introduce the dimensionless temperature  $y := Q/T$ . With these definitions we can rewrite the total neutron-to-proton reaction rate as follows

$$\begin{aligned}
\Gamma_{np} &:= \Gamma_{n\nu_e \rightarrow pe^-} + \Gamma_{ne^+ \rightarrow p\bar{\nu}_e} \\
&\stackrel{(1.106), (1.107)}{=} 4AT^5 (y^2 + 6y + 12) \\
&\stackrel{(1.108)}{=} \frac{a}{\tau y^5} (y^2 + 6y + 12).
\end{aligned} \quad (1.109)$$

Hence, we obtained the total reaction rate in terms of the neutron lifetime and the dimensionless temperature. This first approximation does not contain the free neutron decay. In terms of the dimensionless temperature the relation between the forward and backward reaction rates, cf. eq. (1.102), reads<sup>11</sup>

$$\Gamma_{pn} = e^{-y} \Gamma_{np}, \quad (1.110)$$

and the solution for the neutron abundance, i.e. (1.93), can be written as

$$Y_n \stackrel{(1.110)}{=} \frac{1}{1 + e^y} - \int_0^y d\tilde{y} C(y, \tilde{y}) \frac{d}{d\tilde{y}} \left( \frac{1}{1 + e^{\tilde{y}}} \right), \quad (1.111)$$

<sup>10</sup>In the last step we made use of  $\operatorname{arccosh}(\frac{A}{B}) = \operatorname{arcsinh}(\frac{\sqrt{A^2 - B^2}}{B})$ .

<sup>11</sup>Note that eq. (1.105) yields  $Q = \Delta m$ .

with

$$\begin{aligned} C(y, \tilde{y}) &= \exp \left[ \int_y^{\tilde{y}} d\hat{y} \left( \frac{d\hat{t}}{d\hat{y}} \right) (\Gamma_{pn} + \Gamma_{np}) \right] \\ &\stackrel{(1.110)}{=} \exp \left[ \int_y^{\tilde{y}} d\hat{y} \left( \frac{d\hat{t}}{d\hat{y}} \right) (1 + e^{-\hat{y}}) \Gamma_{np} \right]. \end{aligned} \quad (1.112)$$

In order to determine  $d\hat{t}/d\hat{y}$  in (1.112) we make use of eq. (1.16) which can be rewritten in the following form

$$\frac{d}{dt} (\mu S^{3(w+1)}) \stackrel{\text{GR}}{=} 0 \quad \Rightarrow \quad \mu S^{3(w+1)} = \text{const} \quad \stackrel{w=\frac{1}{3}, (1.72)}{\Rightarrow} \quad ST = \text{const}. \quad (1.113)$$

Subsequently

$$\begin{aligned} \left( -\frac{\dot{T}}{T} \right)^2 &= \left( \frac{\dot{S}}{S} \right)^2 = H^2 \stackrel{(1.75)}{=} \frac{\pi^2}{90} \kappa g_{\text{total}} T^4 \\ &\Leftrightarrow \dot{T} = -\sqrt{\frac{\pi^2}{90} \kappa g_{\text{total}} T^3}. \end{aligned} \quad (1.114)$$

Hence, with

$$\frac{dy}{dt} = -Q\dot{T}T^{-2} \stackrel{(1.114)}{=} Q\sqrt{\frac{\pi^2}{90} \kappa g_{\text{total}}} T = Q^2 \sqrt{\frac{\pi^2}{90} \kappa g_{\text{total}}} y^{-1}, \quad (1.115)$$

we can rewrite eq. (1.112)

$$\begin{aligned} C(y, \tilde{y}) &= \exp \left[ \int_y^{\tilde{y}} d\hat{y} \left( Q^2 \sqrt{\frac{\pi^2}{90} \kappa g_{\text{total}}} \right)^{-1} \hat{y} (1 + e^{-\hat{y}}) \Gamma_{np} \right] \\ &\stackrel{(1.109)}{=} \exp \left[ \int_y^{\tilde{y}} d\hat{y} \left( \frac{a}{Q^2 \tau \sqrt{\frac{\pi^2}{90} \kappa g_{\text{total}}}} \right) (1 + e^{-\hat{y}}) \hat{y}^{-4} (\hat{y}^2 + 6\hat{y} + 12) \right] \\ &= \exp \left[ b \int_y^{\tilde{y}} d\hat{y} (1 + e^{-\hat{y}}) \hat{y}^{-4} (\hat{y}^2 + 6\hat{y} + 12) \right]. \end{aligned} \quad (1.116)$$

Where we introduced a new constant<sup>12</sup>  $b := \sqrt{\frac{90 a^2}{Q^4 \tau^2 \pi^2 \kappa g_{\text{total}}}}$  in the last step. Integration yields

$$C(y, \tilde{y}) = \exp \left[ b \left( \frac{4}{\hat{y}^3} + \frac{3}{\hat{y}^2} + \frac{1}{\hat{y}} \right) + b e^{-\hat{y}} \left( \frac{4}{\hat{y}^3} + \frac{1}{\hat{y}^2} \right) \right] \Big|_y^{\tilde{y}}. \quad (1.117)$$

<sup>12</sup>In SI units the numerical value of  $b$  is given by  $\sqrt{\frac{90 a^2}{Q^4 \tau^2 \pi^2 \kappa g_{\text{total}}}} \stackrel{\text{SI}}{=} \frac{0.7323}{\sqrt{g_{\text{total}}}} \stackrel{g_{\text{total}}=\frac{43}{4}}{=} 0.2233$ . Which is consistent with the result of Bernstein et al. Here we used  $\tau = 1013$  s,  $a = 255$  and the conversion factors from appendix B.

Table 1.5: Assumptions made in order to derive  $Y_n$ .

Assumptions	Equation number
Form of the rate equation	(1.86)
Neglect chemical potential	(1.95)
Energy conservation, species have the same temperature	(1.101)
Temperature low compared to energies in distribution functions	(1.103),(1.104)
Electron mass neglected	(1.106),(1.107)
Neutron decay neglected	(1.109)
FLRW field equations valid, radiation dominated epoch	(1.113)

This solution is compatible with eqs. (2.33) and (2.37) of [193]. Finally, the neutron-to-baryon ratio (1.111) becomes

$$\begin{aligned}
Y_n &\stackrel{(1.110)}{=} \frac{1}{1+e^y} + \int_0^y d\tilde{y} C(y, \tilde{y}) \frac{e^{\tilde{y}}}{(1+e^{\tilde{y}})^2} \\
&= \frac{1}{1+e^y} + \int_0^y d\tilde{y} \frac{e^{\tilde{y}}}{(1+e^{\tilde{y}})^2} \exp \left[ b \left( \frac{4}{\hat{y}^3} + \frac{3}{\hat{y}^2} + \frac{1}{\hat{y}} \right) + b e^{-\hat{y}} \left( \frac{4}{\hat{y}^3} + \frac{1}{\hat{y}^2} \right) \right] \Big|_y.
\end{aligned} \tag{1.118}$$

This function describes the evolution of the neutron-to-baryon ratio in terms of the dimensionless temperature, the mass difference between neutron and proton, the mean life time of the neutron, and the total number of degrees of freedom, i.e.  $Y_n = Y_n(y, Q, \tau, g_{\text{total}})$ . We depicted the neutron-to-baryon ratio and its dependence on the parameter  $b$  in figure 1.6. The asymptotic value of  $Y_n$  is given by 0.149 for  $b = 0.251$  and by 0.158 for  $b = 0.223$ , respectively. The assumptions that lead to (1.118) are collected in table 1.5.

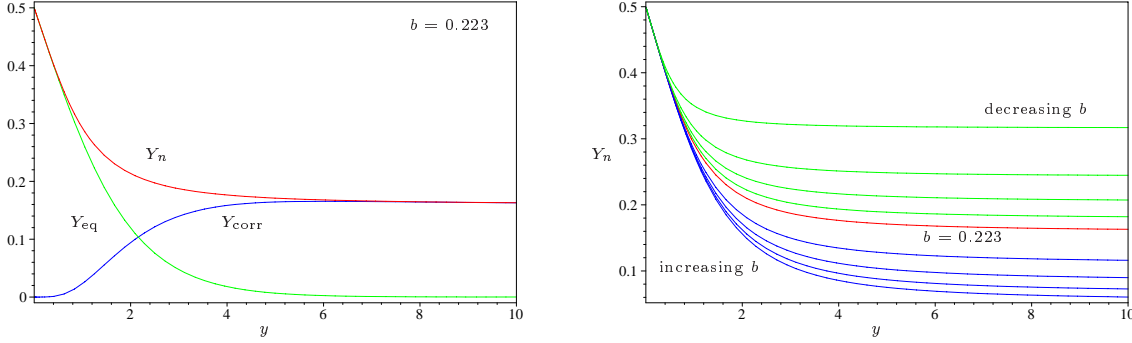


Figure 1.6: On the lhs the solution for the neutron-to-baryon ratio (1.118) is displayed. Here  $Y_{\text{eq}}$  denotes the equilibrium ratio which corresponds to the first term in eq. (1.118). The correction to the equilibrium ratio in an expanding universe is given by the integral in eq. (1.118) and is denoted by  $Y_{\text{corr}}$ . As one can see from the lhs this term becomes important at higher values of  $y$ , i.e. at lower temperatures. On the rhs we sketched the parameter dependence of  $Y_n$ . The red curve corresponds to  $b = 0.223$ , which is also displayed on the lhs. The parameter  $b$  depends on the several other model parameters  $b = b(Q, \tau, g_{\text{total}})$ .

**Chemical potential** In case of a chemical potential for the electron neutrino the distribution function in (1.95) is given by

$$f_{\nu_e, \nu_{\bar{e}}} = \frac{1}{e^{\frac{E_{\nu_e, \nu_{\bar{e}}} \mp \varrho_{\nu_e, \nu_{\bar{e}}}}{T}} + 1} := \frac{1}{e^{\frac{E_{\nu_e, \nu_{\bar{e}}}}{T} \mp \alpha} + 1}. \quad (1.119)$$

The relation between the reaction rates becomes

$$\Gamma_{pn} = e^{-y-\alpha} \Gamma_{np}. \quad (1.120)$$

In contrast to the case without chemical potential, cf. eq. (1.110), the new quantity  $\alpha := \varrho/T$  enters the prefactor. In the following we assume that  $\alpha$  remains constant. The solution for the neutron-to-baryon ratio from (1.93) becomes

$$\begin{aligned} \tilde{Y}_n &\stackrel{(1.120)}{=} \frac{1}{1 + e^{y+\alpha}} - \int_0^y d\tilde{y} C(y, \tilde{y}) \frac{d}{d\tilde{y}} \left( \frac{1}{1 + e^{\tilde{y}+\alpha}} \right) \\ &= \frac{1}{1 + e^{y+\alpha}} + \int_0^y d\tilde{y} C(y, \tilde{y}) \frac{e^{\tilde{y}+\alpha}}{(1 + e^{\tilde{y}+\alpha})^2}. \end{aligned} \quad (1.121)$$

The integrating factor reads

$$\begin{aligned} C(y, \tilde{y}) &= \exp \left[ \int_y^{\tilde{y}} d\hat{y} \left( \frac{d\hat{t}}{d\hat{y}} \right) (\Gamma_{pn} + \Gamma_{np}) \right] \\ &\stackrel{(1.115), (1.120)}{=} \exp \left[ \int_y^{\tilde{y}} d\hat{y} \left( Q^2 \sqrt{\frac{\pi^2}{90} \kappa g_{\text{total}}} \right)^{-1} \hat{y} (1 + e^{-\hat{y}-\alpha}) \Gamma_{np} \right]. \end{aligned} \quad (1.122)$$



In order to derive the reaction rates we assume that the additional factor in the distribution function is small compared to the energies. Hence the electron neutrino distribution function turns into

$$f_{\nu_e} \approx e^{-\frac{E_{\nu_e}}{T} + \alpha} \rightarrow 1 - f_{\nu_e} \approx 1. \quad (1.123)$$

Subsequently the reaction rate in (1.106) becomes

$$\Gamma_{n\nu_e \rightarrow pe^-} = e^\alpha 2AT^3 (Q^2 + 6TQ + 12T^2). \quad (1.124)$$

Therefore the total reaction rate can be written as

$$\begin{aligned} \Gamma_{np} &= (1 + e^\alpha) 2AT^3 (Q^2 + 6TQ + 12T^2) \\ &\stackrel{(1.108)}{=} (1 + e^\alpha) \frac{a}{2\tau Q^5} T^3 (Q^2 + 6TQ + 12T^2) \\ &= (1 + e^\alpha) \frac{a}{2\tau y^5} (y^2 + 6y + 12). \end{aligned} \quad (1.125)$$

The integrating factor (1.122) reads

$$\begin{aligned} C(y, \tilde{y}) &= \exp \left[ \int_y^{\tilde{y}} d\hat{y} \left( \frac{a(1 + e^\alpha)}{2Q^2 \tau \sqrt{\frac{\pi^2}{90} \kappa g_{\text{total}}}} \right) \hat{y}^{-4} (1 + e^{-\hat{y} - \alpha}) (\hat{y}^2 + 6\hat{y} + 12) \right] \\ &= \exp \left[ \frac{b}{2} (1 + e^\alpha) \int_y^{\tilde{y}} d\hat{y} \hat{y}^{-4} (1 + e^{-\hat{y} - \alpha}) (\hat{y}^2 + 6\hat{y} + 12) \right] \\ &= \exp \left[ \frac{b}{2} (1 + e^\alpha) \left( \frac{4}{\hat{y}^3} + \frac{3}{\hat{y}^2} + \frac{1}{\hat{y}} \right) + \frac{b}{2} (1 + e^\alpha) e^{-\hat{y} - \alpha} \left( \frac{4}{\hat{y}^3} + \frac{1}{\hat{y}^2} \right) \right] \Big|_y^{\tilde{y}}. \end{aligned} \quad (1.126)$$

The neutron-to-baryon ratio (1.121) is given by

$$\begin{aligned} \tilde{Y}_n &= \frac{1}{1 + e^{y + \alpha}} + \int_0^y d\tilde{y} \frac{e^{\tilde{y} + \alpha}}{(1 + e^{\tilde{y} + \alpha})^2} \exp \left[ \frac{b}{2} (1 + e^\alpha) \left( \frac{4}{\hat{y}^3} + \frac{3}{\hat{y}^2} + \frac{1}{\hat{y}} \right) \right] \Big|_y^{\tilde{y}} \\ &\quad + \frac{b}{2} (1 + e^\alpha) e^{-\hat{y} - \alpha} \left( \frac{4}{\hat{y}^3} + \frac{1}{\hat{y}^2} \right) \Big|_y^{\tilde{y}}. \end{aligned} \quad (1.127)$$

In figure 1.7 we plotted the neutron-to-baryon ratio  $Y_n = Y_n(y, Q, \tau, g_{\text{total}}, \alpha)$  for different values of the parameter  $\alpha$ .

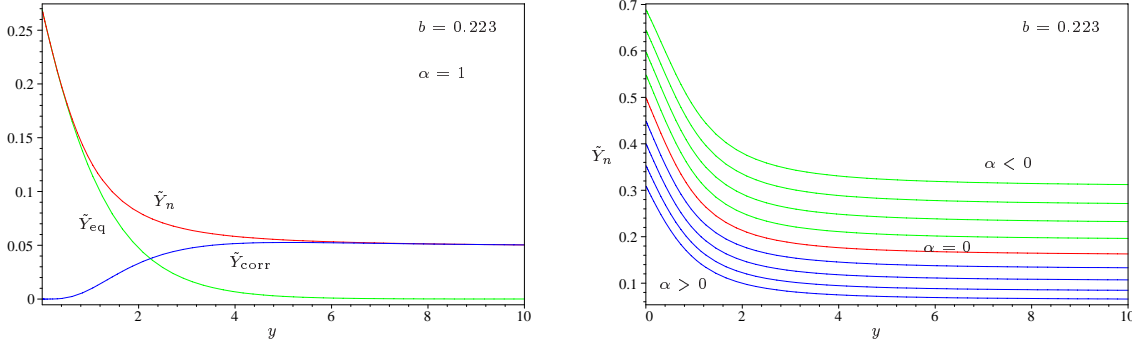


Figure 1.7: On the lhs the neutron-to-baryon ratio from eq. (1.127) is displayed in case of a non-vanishing chemical potential  $\alpha$  of the electron neutrino. Again  $\tilde{Y}_{\text{eq}}$  and  $\tilde{Y}_{\text{corr}}$  denote the equilibrium ratio and the correction due to an expanding universe, corresponding to the first and the second term in eq. (1.127). On the rhs we plotted  $\tilde{Y}_n$  for fixed  $b$  and varying  $\alpha$ . The red curve corresponds to  $\alpha = 0$ . The green curves correspond to negative values of  $\alpha$ , the blue ones to positive  $\alpha$ . Hence the neutron population decreases for positive values of chemical potential.

### Neutron decay

So far we neglected the neutron decay (1.81) in the derivation of (1.118). However since  $Y_n$  does not vary much over the timescale of the neutron decay we assume that the neutron-to-baryon ratio including the decay effect is given by

$$\check{Y}_n = e^{-\frac{t_c}{\tau}} Y_n. \quad (1.128)$$

Where  $t_c$  denotes the time at which the neutrons are captured in nuclei. Since deuterium is the first element to be formed via the reaction N1 from table 1.6 on page 43,  $t_c$  will be determined by the time at which the temperature has dropped below the binding energy of deuterium. In order to establish a relation between the capture time  $t_c$  and the capture temperature  $T_c$  we make use of (1.114):

$$\begin{aligned} \frac{1}{T} \frac{dT}{dt} \Big|_{\text{GR}, k=0} &= -\sqrt{\frac{\pi^2}{90} \kappa g_{\text{total}}} T^2 \\ \Leftrightarrow t - t_1 &= \int_T^\infty dT \sqrt{\frac{90}{\pi^2 \kappa g_{\text{total}}}} T^{-3} = \sqrt{\frac{45}{2\pi^2 \kappa g_{\text{total}}}} T^{-2}. \end{aligned} \quad (1.129)$$

At times at which the neutron decay becomes relevant the neutrino temperature differs from the photon temperature due to  $e^+e^-$  annihilation. Usually the relation between photon and neutrino temperature is assumed to be  $T_\gamma = \left(\frac{11}{4}\right)^{\frac{1}{3}} T_\nu$ . We will derive this result in section 3.11.1. A calculation which takes into account the heating of neutrinos by  $e^+e^-$  annihilations due to their incomplete decoupling from the plasma is given in [236].

If we express the energy density  $\mu_{\text{total}} = \frac{\pi^2}{30} g_\nu T_\nu^4 + \frac{\pi^2}{30} g_\gamma T_\gamma^4 = \frac{\pi^2}{30} \tilde{g}_{\text{total}} T_\nu^4$  in (1.75) via the neutrino temperature (with a  $\tilde{g}_{\text{total}}$  which differs from the standard one), we end up with

$$t = \sqrt{\frac{45}{2\pi^2 \kappa \tilde{g}_{\text{total}}}} T_\nu^{-2} + t_1 = \sqrt{\frac{45}{2\pi^2 \kappa \tilde{g}_{\text{total}}}} \left(\frac{11}{4}\right)^{\frac{2}{3}} T_\gamma^{-2} + t_1. \quad (1.130)$$

Where  $\tilde{g}_{\text{total}} = g_\nu + g_\gamma \left(\frac{11}{4}\right)^{\frac{4}{3}} = \frac{21}{4} + 2 \left(\frac{11}{4}\right)^{\frac{4}{3}} \approx 12.955$ . In the following we assume that the integration constant  $t_1$  is small. Bernstein et al. obtain a value of  $t_1 \approx 2$  s. This result may be different in a non-standard cosmological model. But as a first approximation we will use the value of Bernstein et al. from here on. The relation in (1.130) and its dependence on  $\tilde{g}_{\text{total}}$  is displayed in figure 1.8.

The number density of a particle species in the non-relativistic limit is given by (1.80), hence we have

$$n_i = g_i \left(\frac{m_i T_i}{2\pi}\right)^{\frac{3}{2}} e^{-\frac{m_i - e_i}{T_i}}. \quad (1.131)$$

Assuming that neutrons, protons, and deuterium nuclei have the same temperature  $T_n = T_p = T_D$  we can infer from (1.131) that

$$\begin{aligned} \frac{n_n n_p}{n_D} &= \frac{g_n g_p}{g_D} \left(\frac{m_n m_p T}{2\pi m_D}\right)^{\frac{3}{2}} e^{-\frac{(m_n + m_p - m_D) - (e_n + e_p - e_D)}{T}} \\ &\stackrel{e_D = e_n + e_p}{=} \frac{g_n g_p}{g_D} \left(\frac{m_n m_p T}{2\pi m_D}\right)^{\frac{3}{2}} e^{-\frac{\varepsilon_D}{T}}. \end{aligned} \quad (1.132)$$

In the last step we assumed that the different components are in chemical equilibrium and introduced  $\varepsilon_D := m_n + m_p - m_D$  for the binding energy of deuterium, cf. table 1.4 on page 30. Commonly (1.132) is rewritten in terms of the abundance fractions  $X_i := \frac{n_i}{n_{\text{baryons}}}$  and the baryon-to-photon ratio, which is defined by

$$\eta := \frac{n_{\text{baryons}}}{n_\gamma} \stackrel{(1.76)}{=} \frac{\pi^2}{g_\gamma \zeta(3)} \frac{n_{\text{baryons}}}{T^3}. \quad (1.133)$$

Thus, we end up with<sup>13</sup>

$$\begin{aligned} \frac{X_n X_p}{X_D} &= \frac{n_n n_p}{n_{\text{baryons}} n_D} = \frac{g_n g_p}{g_D} \left(\frac{m_n m_p T}{2\pi m_D}\right)^{\frac{3}{2}} e^{-\frac{\varepsilon_D}{T}} \eta^{-1} \frac{\pi^2}{g_\gamma \zeta(3) T^3} \\ &= \frac{\sqrt{\pi}}{\zeta(3)} \frac{g_n g_p}{g_D g_\gamma} \left(\frac{m_n m_p}{2m_D}\right)^{\frac{3}{2}} \eta^{-1} e^{-\frac{\varepsilon_D}{T}} T^{-\frac{3}{2}} \\ &\stackrel{g_\gamma = g_n = g_p = 2, g_D = 3}{=} \sqrt{\frac{\pi}{18}} \frac{1}{\zeta(3)} \left(\frac{m_n m_p}{m_D}\right)^{\frac{3}{2}} \eta^{-1} e^{-\frac{\varepsilon_D}{T}} T^{-\frac{3}{2}}. \end{aligned} \quad (1.134)$$

<sup>13</sup>Bernstein et al. use the approximation  $m_D \approx 2m_n$  which yields  $\frac{X_n X_p}{X_D} \approx \frac{\sqrt{\pi}}{12\zeta(3)} \left(\frac{m_p}{T}\right)^{\frac{3}{2}} \eta^{-1} e^{-\frac{\varepsilon_D}{T}}$ .

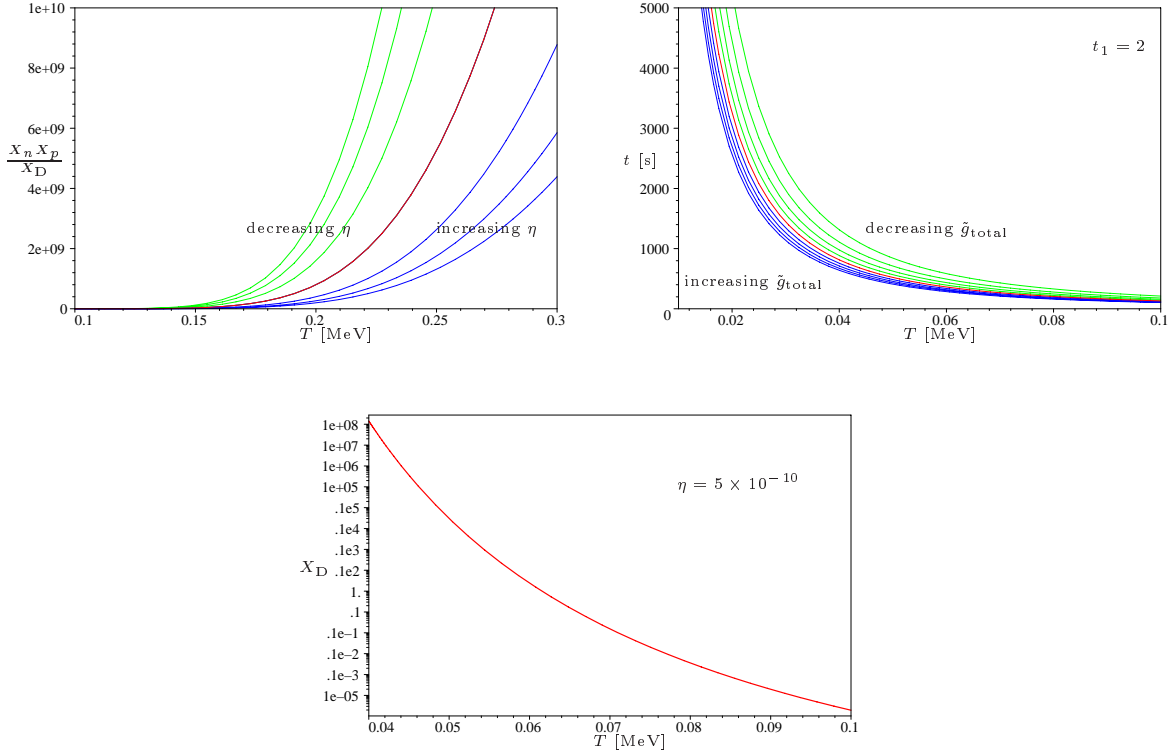


Figure 1.8: On the lhs we plotted the equilibrium fraction from eq. (1.134) for different values of the baryon-to-photon ratio  $\eta$  ( $m_n = 939.5, m_p = 938.2, m_D = 1875.48$  all values in MeV). From the lhs it becomes clear that significant amounts of deuterium are formed if the temperature drops below the binding energy of deuterium. This behavior is usually called the *deuterium bottleneck*, for a more detailed discussion see [192], e.g. On the rhs we plotted the time temperature-relation from eq. (1.130). The red line corresponds to the standard value of 12.995 for  $\tilde{g}_{\text{total}}$ .

The dependence of the baryon-to-photon ratio on the abundance fraction is displayed in figure 1.8. Significant amounts of deuterium are only formed at temperatures well below the binding energy of deuterium. This is mainly due to the small value of  $\eta$ , i.e. the high entropy of the universe. In order to estimate the temperature at which  $X_D \simeq 1$  we rewrite eq. (1.134) by using the formula for the neutron-to-baryon ratio (1.118), i.e.

$$\begin{aligned}
 X_D &= \sqrt{\frac{18}{\pi}} \zeta(3) \left( \frac{m_n m_p}{m_D} \right)^{-\frac{3}{2}} \eta e^{\frac{\epsilon_D}{T}} T^{\frac{3}{2}} Y_n (1 - Y_n) \\
 &\stackrel{Y_n(\infty)}{\approx} \sqrt{\frac{9}{50 \pi}} \zeta(3) \left( \frac{m_n m_p}{m_D} \right)^{-\frac{3}{2}} \eta e^{\frac{\epsilon_D}{T}} T^{\frac{3}{2}}.
 \end{aligned} \tag{1.135}$$

In the last line we substituted the asymptotic numerical value of  $Y_n$ , which approximately yields  $Y_n (1 - Y_n) \approx 0.149 \times (1 - 0.149) \approx 0.1$ . Note that it does not matter if we take  $b = 0.223$  or  $b = 0.251$  in this first approximation since we use the rounded value for

Table 1.6: Nuclear reactions used in BBN calculations.

Symbol	Reaction
N1	$p + n \longleftrightarrow D + \gamma$
N2	$D + D \longleftrightarrow T + p$
N3	$D + n \longleftrightarrow T + \gamma$
N4	$D + D \longleftrightarrow {}^3\text{He} + n$
N5	$D + p \longleftrightarrow {}^3\text{He} + \gamma$
N6	$D + D \longleftrightarrow {}^4\text{He} + \gamma$
N7	$T + p \longleftrightarrow {}^4\text{He} + \gamma$
N8	$T + D \longleftrightarrow {}^4\text{He} + n$
N9	$T + T \longleftrightarrow {}^4\text{He} + 2n$
N10	${}^3\text{He} + n \longleftrightarrow T + p$
N11	${}^3\text{He} + n \longleftrightarrow {}^4\text{He} + \gamma$
N12	${}^3\text{He} + D \longleftrightarrow {}^4\text{He} + p$
N13	${}^3\text{He} + T \longleftrightarrow {}^4\text{He} + p + n$

$Y_n(1 - Y_n)$ . Numerically we obtain  $X_D \simeq 1 \Leftrightarrow T_c \simeq 0.1$  MeV, which corresponds to the time  $t_c \approx 133$  s. For a more detailed estimate of the capture time the reader is referred to reference [193], and section 3.11.3 of this work, which contains a numerical comparison of different capture conditions.

### Synthesis of ${}^4\text{He}$

As we have learned in the last section the nucleosynthesis chain begins with the formation of deuterium, followed by the production of the other light elements via the reactions listed in the table 1.6. More comprehensive reaction networks used in numerical nucleosynthesis calculations can be found in [182, 183, 184, 185, 237]. In the following we assume that almost all neutrons end up in  ${}^4\text{He}$ . Hence, we are able to infer the primordial helium abundance from the neutron-to-baryon ratio, i.e.

$$Y_{4\text{He}} := 4 \frac{n_{4\text{He}}}{n_{\text{baryon}}} = \frac{2n_n}{n_p + n_n} \stackrel{(1.128)}{=} 2\check{Y}_n. \quad (1.136)$$

Bernstein et al. use the reaction rates for the reactions N1, N2, and N8, cf. table 1.6, in order to estimate the capture temperature as  $T_c \simeq 0.086$  MeV, which corresponds to  $t_c \approx 180$  s. Substituting this value for  $t_c$  into eq. (1.128) and using  $\tau = 886.7$  s [84] for the mean life time of the neutron, we end up with

$$Y_{4\text{He}} = 2 e^{-\frac{180}{886.7}} Y_n = 2 \times 0.816 \times 0.149 = 0.243. \quad (1.137)$$

As we will see in the next section the above value lies well within the present observational bounds. The dependence of the helium abundance on various parameters is depicted in figure 1.9.

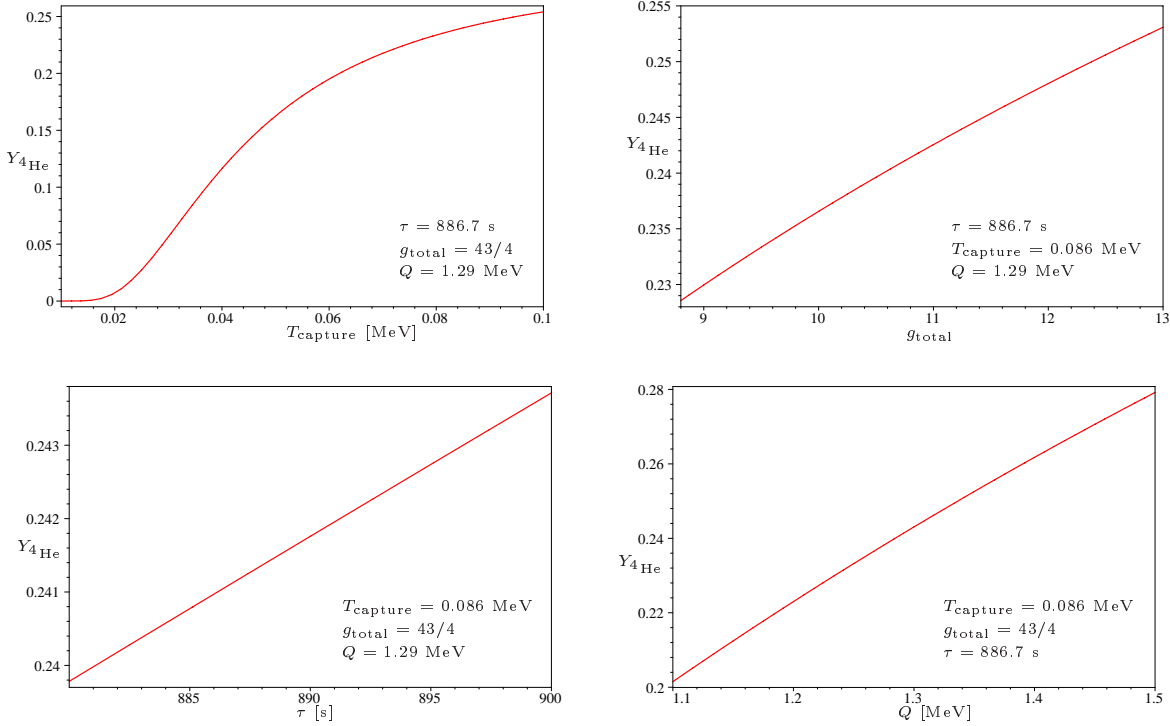


Figure 1.9: On the upper lhs we plotted the dependence of the helium abundance on the capture temperature (note that  $T_{\text{capture}} \approx 0.086$  MeV corresponds to  $t \approx 180$  s). On the upper rhs the helium abundance is plotted for different values of the spin degeneracy factor  $g_{\text{total}}$ . From this plot it becomes clear that additional neutrino species lead to a higher abundance of  ${}^4\text{He}$ . On the lower lhs we plotted the helium abundance for varying neutron mean life time. Note that the experimental bound on  $\tau$  is much tighter than the plotted range, i.e.  $\tau = 886.7 \pm 1.9$  s [84]. On the lower rhs we displayed the dependence on the proton-neutron mass difference.

## Observational situation

In table 1.7 we collected the observational bounds on the light element abundances. This list is by no means exhaustive. One has to keep in mind that these measurements are a delicate subject since they require deep insight into stellar nucleosynthesis and the chemical evolution of galaxies. Hence, we have to rely on the combined observational bounds suggested by the experts in this field collected in table 1.8.

In contrast to deuterium, elements from helium onwards can be produced in stars. Accordingly, there has been a lively discussion in the literature whether the observed helium abundance is really of primordial origin. In presence of heavier elements helium is formed via the so-called CNO cycle, cf. [20], e.g., for a detailed discussion. Back in 1972 the work of Searle and Sargent [234] provisionally settled the ongoing debate when they found a region of very low metallicity, which encompassed nearly the usual abundance

of helium. Nevertheless there are still investigations concerning the primordial origin of helium [233]. Most of these revolving around the amount of helium synthesized in stars, and the applicability of methods, which allow us to extrapolate back to the time of zero metallicity. If totally metal-free stars, so-called population III stars, could be found, one would be able to study the composition of the pristine gas by means of these stars. The recent discovery [232] of a low-mass halo star with a very low iron abundance suggests that such types of stars still exist.

In contrast, no astrophysical site has survived, in which deuterium is produced. Since deuterium is converted into  ${}^3\text{He}$  during pre-main sequence evolution there is only a net destruction of deuterium during star formation. The process which is mainly responsible for a conversion of deuterium into helium is one of the so-called pp chains, i.e.



Since the deuterium abundance strongly depends on the baryon-to-photon ratio  $\eta$  it is often called *baryometer*. From the cosmological point of view the deuterium measurements played a crucial role in the determination of the baryonic mass density of the universe. Only very recent CMB measurements [178, 235] via the WMAP<sup>14</sup> satellite offer a stronger constraint on  $\eta$ . Nevertheless nucleosynthesis represents a very important cosmological test for the very end of the redshift scale.

Let us keep in mind the different methods to measure the abundances listed in table 1.7. Deuterium is mainly observed in cool neutral gas (HI regions),  ${}^3\text{He}$  is studied in hot ionized gas (HII),  ${}^4\text{He}$  is probed via emission of optical recombination lines in HII regions, and  ${}^7\text{Li}$  via the absorption spectra of hot low-mass halo stars [185, 186, 187]. Especially the observation of high-redshift gas clouds of low-metallicity allows us to study deuterium abundance in regions which are nearly primordial, cf. D2, D3, D7, and D8 in table 1.7.

### Computer programs and possible extensions of the standard scenario

In the last sections we reviewed a semi-analytical method for the calculation of the helium abundance. Although we will stick to this method for the rest of this work one should mention some of the computer programs, which were developed in order to track all of the light element abundances during nucleosynthesis. In 1967 Wagoner et al. were the first who implemented a reaction network, which allowed for the numerical computation of the abundances, cf. [188, 189]. Kawano revised this code twice in 1988 [182] and 1992 [183]. The Kawano code and numerous modifications are still in use nowadays. The most recent numerical estimate was provided by Lopez and Turner [237] who build a new code from scratch. This code takes into account several higher order effects and is supposed to estimate the  ${}^4\text{He}$  abundance with a theoretical uncertainty of less than 0.1%.

---

<sup>14</sup>Wilkinson Microwave Anisotropy Probe.

Table 1.7: Light element abundance measurements.

Symbol	Quantity	Year	Observation	Value	Reference
D1	$\frac{n_D}{n_H}$	1972	Solar system observations	$(2.5 \pm 0.5) \times 10^{-5}$	[229]
D2	$\frac{n_D}{n_H}$	1996	Ly- $\alpha$ observations Q1937-1009 ( $z = 3.572$ )	$(2.3 \pm 0.3 \pm 0.3) \times 10^{-5}$	[231]
D3	$\frac{n_D}{n_H}$	1997	Ly- $\alpha$ observations Q1718-4807 ( $z = 0.701$ )	$(20 \pm 5) \times 10^{-5}$	[217]
D4	$\frac{n_D}{n_H}$	1998	Local interstellar medium	$(1.5 \pm 0.1) \times 10^{-5}$	[228]
D5	$\frac{n_D}{n_H}$	1998	Atmosphere of Jupiter	$(2.6 \pm 0.7) \times 10^{-5}$	[227]
D6	$\frac{n_D}{n_H}$	1998	Solar system observations (indirect via $^3\text{He}$ )	$(2.1 \pm 0.5) \times 10^{-5}$	[226]
D7	$\frac{n_D}{n_H}$	1998	Ly- $\alpha$ observations Q1937-1009 (revised estimate)	$(3.24 \pm 0.3) \times 10^{-5}$	[219]
D8	$\frac{n_D}{n_H}$	1998	Ly- $\alpha$ observations Q1009-2956 ( $z = 2.504$ )	$(3.39 \pm 0.25) \times 10^{-5}$	[218]
HE1	$\frac{n_3\text{He}}{n_H}$	1992	Planetary nebulae	$\gtrsim 10^{-3}$	[225]
HE2	$\frac{n_3\text{He}}{n_H}$	1994	Interstellar medium	$[1, 4] \times 10^{-4}$	[223]
HE3	$\frac{n_3\text{He}}{n_H}$	1997	Planetary nebulae	$[0.1, 1] \times 10^{-3}$	[224]
Y1	$Y_{4\text{He}}$	1994	10 low-metallicity, blue compact galaxies	$0.240 \pm 0.005$	[214]
Y2	$Y_{4\text{He}}$	1995	49 low-metallicity, extragalactic HII regions	$0.234 \pm 0.003$	[216]
Y3	$Y_{4\text{He}}$	1998	45 low-metallicity, extragalactic HII regions	$0.244 \pm 0.002$	[215]
L1	$\frac{n_{\text{Li}}}{n_H}$	1997	41 population II halo stars	$(1.729 \pm 0.011) \times 10^{-10}$	[230]



Table 1.8: Light element abundances from reviews.

$\frac{n_D}{n_H}$	$\frac{n_{3\text{He}}}{n_H}$	$Y_{4\text{He}}$	$\frac{n_{7\text{Li}}}{n_H}$	<b>Ref.</b>
$(2.52 \pm 0.49) \times 10^{-5}$	$(1.48 \pm 0.13) \times 10^{-5}$	$0.274 \pm 0.016$		[222]
$[1.9, 3.3] \times 10^{-5}$	$[1.9, 18] \times 10^{-5}$			[221]
	$\leq 3.2 \times 10^{-5}$			[220]
$[2.9, 4] \times 10^{-5}$ ,	$\sim 10^{-3}$	$[0.228, 0.248]$	$[1.2, 1.9] \times 10^{-10}$	[187]
$[1, 3] \times 10^{-4}$				

Since nucleosynthesis depends on very different concepts of particle physics, thermodynamics, and the underlying gravity theory there seems to be no lack of room for extensions. One, rather mild, extension of the standard paradigm is given by a change of the expansion rate. This might be generated by an additional relativistic particle species, corresponding to a change in the model of particle physics. Such a change would enter through the energy density in (1.72). Moreover there might be also a change of the expansion behavior due to a modification of the field equations of the cosmological model [194]–[202]. In case the field equations are similar to the Friedmann equations one can use a changed expression for the energy density in order to describe a set of changed field equations in an effective way. We will learn more about this possibility in section 3.11. A more drastic change, which currently lies beyond the observational scope, involves the time before nucleosynthesis and therefore also its initial conditions. Especially modifications at the time of the QCD phase transition [106] may question one of the basic assumptions of standard BBN, i.e. homogeneity. For an investigation covering nucleosynthesis in a neutron-enriched region the reader is referred to [203].

## 1.7 History of the universe

On the basis of the cosmological standard model, one is able to establish a chronological order of events, which took place during the evolution of the universe. Although we discussed only two of the cosmological tests in detail, the magnitude-redshift relation and the primordial production of  $^4\text{He}$ , we will draw a more complete picture of our current understanding of the universe in this section. In figure 1.10 we sketched some of the events which took place during the evolution of the universe. From an observational point of view there is no direct evidence for processes which occur during the first second.

One prominent example for a mechanism which has to be introduced if one wants to salvage the FLRW description up to the earliest stages is inflation [79, 80]. In order to explain the observed homogeneity of the cosmic microwave background one has to specify a mechanism, which enables different patches of the universe to get in causal contact before the time of decoupling. This is not the case if we assume that the universe expanded with the rate of a radiation dominated FLRW model during its early phase. The emergence of causally disconnected regions is caused by the existence of particle horizons, cf. section 1.3. Inflation, in its simplest version, solves this problem

by introducing an additional scalar field. This field leads to a very rapid expansion at early times such that small uniform regions become large enough to encompass the observed universe, thereby yielding an explanation for the uniformness of the CMB. Since there exists exhaustive literature on the inflationary scenario and its successors we will not discuss it in detail, cf. [11, 14, 15, 81, 82], e.g. Another interesting feature of the inflationary model is given by the fact that it provides an explanation for the small fluctuations in the CMB. These fluctuations are thought to be generated by quantum fluctuations of the inflaton field which are diluted to macroscopic scales during the process of inflation. Thereby they act as seeds for the potential wells in the primordial plasma, which are one of the generators of CMB temperature fluctuations. One might judge the inflationary scenario to be a rather speculative idea which expresses our lack of knowledge about the early evolution of the universe. However it undoubtedly provides a simple solution to several problems within the cosmological standard model. Hence inflation raises the bar for any competitor model, which of course also has to provide an explanation for the density fluctuations. Unless this is the case, no model will be on par with the standard model.

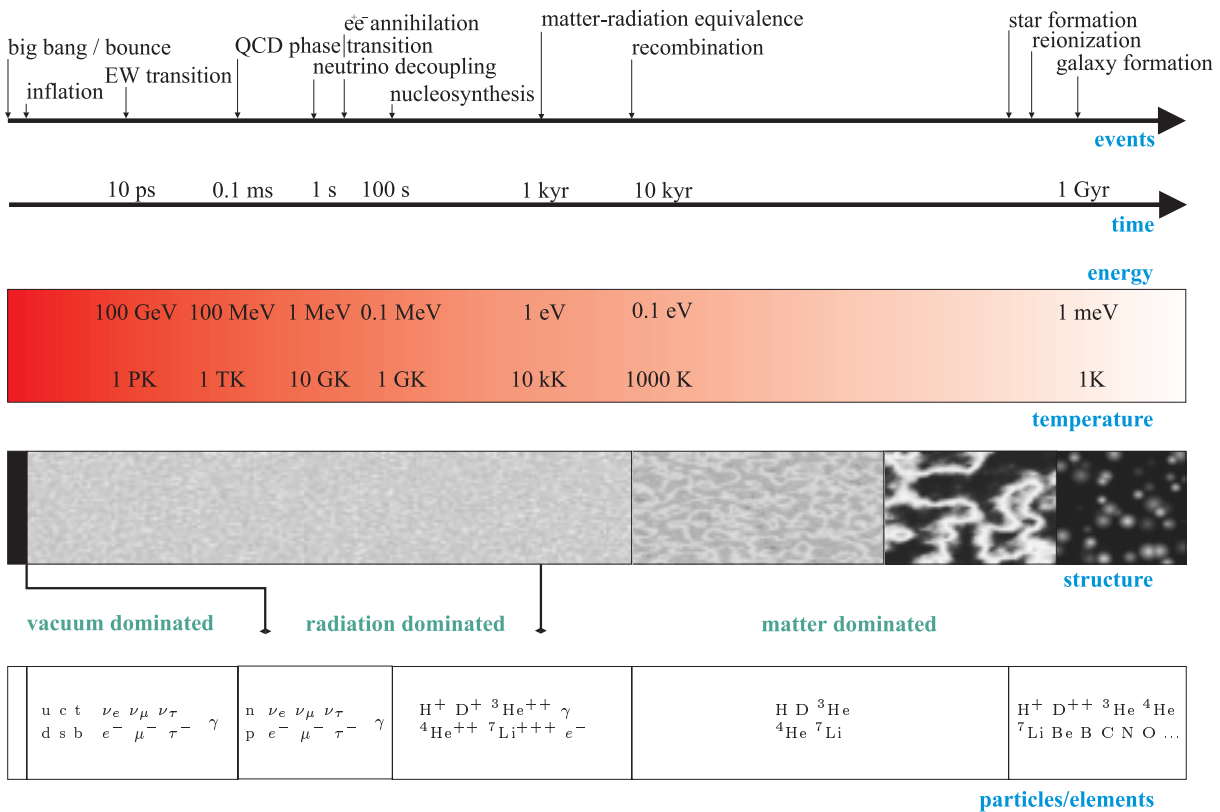


Figure 1.10: History of the universe.

Let us come back to figure 1.10 and the events which have a rather robust observational underpinning. The time after the formation of hadronic matter is believed to be rather well understood. As we have discussed in detail in section 1.6 the synthesis of light elements during the first minutes represents one of the main pillars of the hot big bang model. The next main event takes place at the time at which the temperature of the plasma is low enough to allow for the recombination of the elements. Hence the photons are no longer scattered by free electrons and the universe loses its opaqueness. The density fluctuations of the primordial plasma are imprinted into the photon distribution which is nowadays observed in form of the cosmic microwave background. Since from this moment on the universe is no longer pervaded by a plasma one expects that the energy density in the FLRW equation is dominated by the pressureless component. In other words the universe has entered its matter dominated era. In the upcoming rather long period, long in comparison to the amount of time which has elapsed till the universe became matter dominated, the formation of structure takes place. We will not touch questions of structure formation within this work, the reader is referred to the textbooks [10, 11, 16]. Nevertheless one has to keep in mind that the evolution of density perturbations and their condensation into large-scale structures (LSS) is one of the main topics of modern cosmology which is linked to many observations [75, 76, 77, 78]. Hence any attempt to build a competitive cosmological model will sooner or later lead to investigations concerning the large scale distribution of matter. From a conceptual point of view the cosmological tests linked to the CMB and LSS observations *suffer* a little bit from their complexity, because they need a fair amount of extra phenomenology. This sometimes makes it difficult to clearly segregate the effects caused by a change in the underlying gravity theory.

## 1.8 Dimensions

Table 1.9: Dimensions.

Quantities	<b>1</b>	Length
Geometrical quantities	$[\tilde{R}_{\alpha\beta}], [g_{\alpha\beta}]$	$[\vartheta^\alpha], [G_\alpha]$
Matter quantities		$[\Sigma_\alpha]^{-1}, [\Sigma_{\alpha\beta}]^{-\frac{1}{4}}$
Coordinates	$[\theta], [\phi], [r]$	$[t]$
Constants	$[k], [w]$	$[\kappa]^{\frac{1}{2}}, [\lambda]^{-\frac{1}{2}}, [\mathcal{W}_w]^{-\frac{1}{-4+3(1+w)}}$
Functions	$[\Omega_w], [\Omega_\lambda], [\Omega_{\text{total}}],$ $[\Omega_k], [\Omega_m], [\Theta], [F]$	$[S], [\mu]^{-\frac{1}{4}}, [p]^{-\frac{1}{4}}, [H]^{-1},$ $[\mu_c]^{-\frac{1}{4}}, [d_H], [\mu_{m0}]^{-\frac{1}{4}}$
Miscellany	$[u^\alpha], [z], [q], [m], [M],$ $[\mathcal{M}], [\mu]$	$[d_{\text{luminosity}}], [\check{L}]^{-\frac{1}{2}}, [\check{F}]^{-\frac{1}{4}}$ $[A_0]^{\frac{1}{2}}, [\sigma]^{\frac{1}{2}}$
Thermodynamics	$[f_i], [g_i]$	$[n_i]^{-\frac{1}{3}}, [\mu_i]^{-\frac{1}{4}}, [p_i]^{-\frac{1}{4}},$ $[q_i]^{-1}, [E_i]^{-1}, [\varrho_i]^{-1}, [T_i]^{-1}$
Nucleosynthesis	$[Y_n], [C], [a], [y], [b], [\alpha]$ $[\check{Y}_n], [\check{Y}_n], [X_i], [\eta], [Y_{\text{He}}^4]$	$[Q]^{-1}, [\Gamma_{np}]^{-1}, [\Gamma_{pn}]^{-1}$ $[\mathcal{A}]^{-1}, [\mathcal{B}]^{-1}, [A]^{\frac{1}{4}}, [\tau], [\varepsilon_D]^{-1}$

# Chapter 2

## Metric-affine gauge theory

### 2.1 Introduction

This chapter gives a short overview of metric–affine gauge theory of gravity (MAG) and its subcases. Due to the existence of several introductions dealing with this subject, cf. [44, 46, 47], we will concentrate on summarizing the main results that are necessary to understand the forthcoming chapter. In order to keep our introduction rather concise, most of the mathematical concepts used in this chapter are summarized in the appendices A and C.

### 2.2 MAG in general

In this section we will not be concerned with the question of how to formulate a theory of gravity in a gauge theoretical manner, this was already done in [44, 46] and chapter one of [49], but with the introduction of all necessary notions to set up the field equations.

In MAG we have the metric  $g_{\alpha\beta}$ , the coframe  $\vartheta^\alpha$ , and the connection 1-form  $\Gamma_{\alpha\beta}$  (with values in the Lie algebra of the four-dimensional linear group  $GL(4, R)$ ) as new independent field variables. Here  $\alpha, \beta, \dots = 0, 1, 2, 3$  denote (anholonomic) frame indices. Spacetime is described by a metric-affine geometry with the gravitational field strengths nonmetricity  $Q_{\alpha\beta} := -Dg_{\alpha\beta}$ , torsion  $T^\alpha := D\vartheta^\alpha$ , and curvature  $R_{\alpha}{}^\beta := d\Gamma_{\alpha}{}^\beta - \Gamma_{\alpha}{}^\gamma \wedge \Gamma_{\gamma}{}^\beta$ . A Lagrangian formalism for a matter field  $\Psi$  minimally coupled to the gravitational potentials  $g_{\alpha\beta}$ ,  $\vartheta^\alpha$ ,  $\Gamma_{\alpha}{}^\beta$  has been set up in [44]. Then the dynamics of this theory is specified by a total Lagrangian

$$L = V_{\text{MAG}}(g_{\alpha\beta}, \vartheta^\alpha, Q_{\alpha\beta}, T^\alpha, R_{\alpha}{}^\beta) + L_{\text{mat}}(g_{\alpha\beta}, \vartheta^\alpha, \Psi, D\Psi). \quad (2.1)$$

The variation of the action with respect to the independent gauge potentials leads to

the field equations:

$$\frac{\delta L_{\text{mat}}}{\delta \Psi} = 0, \quad (2.2)$$

$$DM^{\alpha\beta} - m^{\alpha\beta} = \sigma^{\alpha\beta}, \quad (2.3)$$

$$DH_\alpha - E_\alpha = \Sigma_\alpha, \quad (2.4)$$

$$DH^\alpha{}_\beta - E^\alpha{}_\beta = \Delta^\alpha{}_\beta. \quad (2.5)$$

Equations (2.3) and (2.4) are the generalized Einstein equations with the symmetric energy-momentum 4-form  $\sigma^{\alpha\beta}$  and the canonical energy-momentum 3-form  $\Sigma_\alpha$  as sources. Equation (2.5) is an additional field equation which takes into account other aspects of matter, such as spin, shear and dilation currents, represented by the hypermomentum  $\Delta^\alpha{}_\beta$ . We made use of the definitions of the gauge field excitations:

$$H_\alpha := -\frac{\partial V_{\text{MAG}}}{\partial T^\alpha}, \quad H^\alpha{}_\beta := -\frac{\partial V_{\text{MAG}}}{\partial R_{\alpha\beta}}, \quad M^{\alpha\beta} := -2\frac{\partial V_{\text{MAG}}}{\partial Q_{\alpha\beta}}. \quad (2.6)$$

Moreover, we introduce the canonical energy-momentum, the metric stress-energy and the hypermomentum current of the gauge fields,

$$E_\alpha := \frac{\partial V_{\text{MAG}}}{\partial \vartheta^\alpha}, \quad m^{\alpha\beta} := 2\frac{\partial V_{\text{MAG}}}{\partial g_{\alpha\beta}}, \quad E^\alpha{}_\beta := -\vartheta^\alpha \wedge H_\beta - g_{\beta\gamma} M^{\alpha\gamma}, \quad (2.7)$$

and the canonical energy-momentum, the metric stress-energy and the hypermomentum currents of the matter fields,

$$\Sigma_\alpha := \frac{\delta L_{\text{mat}}}{\delta \vartheta^\alpha}, \quad \sigma^{\alpha\beta} := 2\frac{\delta L_{\text{mat}}}{\delta g_{\alpha\beta}}, \quad \Delta^\alpha{}_\beta := \frac{\delta L_{\text{mat}}}{\delta \Gamma_{\alpha\beta}}. \quad (2.8)$$

Provided the matter equations (2.2) are fulfilled, the following Noether identities hold:

$$D\Sigma_\alpha = (e_\alpha \rfloor T^\beta) \wedge \Sigma_\beta - \frac{1}{2} (e_\alpha \rfloor Q_{\beta\gamma}) \sigma^{\beta\gamma} + (e_\alpha \rfloor R_{\beta\gamma}) \wedge \Delta^\beta{}_\gamma, \quad (2.9)$$

$$D\Delta^\alpha{}_\beta = g_{\beta\gamma} \sigma^{\alpha\gamma} - \vartheta^\alpha \wedge \Sigma_\beta. \quad (2.10)$$

By means of (2.9) and (2.10) it can be shown that the field equation (2.3) is redundant, thus we only need to take into account (2.4) and (2.5).

As suggested in [45], the most general parity conserving quadratic Lagrangian expressed in terms of the irreducible pieces of the nonmetricity  $Q_{\alpha\beta}$ , torsion  $T^\alpha$ , and curvature  $R_{\alpha\beta}$  reads:

$$\begin{aligned}
V_{\text{MAG}} = & \frac{1}{2\kappa} \left[ -a_0 R^{\alpha\beta} \wedge \eta_{\alpha\beta} - 2\lambda\eta + T^\alpha \wedge \star \left( \sum_{I=1}^3 a_I {}^{(I)}T_\alpha \right) \right. \\
& + Q_{\alpha\beta} \wedge \star \left( \sum_{I=1}^4 b_I {}^{(I)}Q^{\alpha\beta} \right) \\
& + b_5 ({}^{(3)}Q_{\alpha\gamma} \wedge \vartheta^\alpha) \wedge \star ({}^{(4)}Q^{\beta\gamma} \wedge \vartheta_\beta) \\
& \left. + 2 \left( \sum_{I=2}^4 c_I {}^{(I)}Q_{\alpha\beta} \right) \wedge \vartheta^\alpha \wedge \star T^\beta \right] \\
& - \frac{1}{2\rho} R^{\alpha\beta} \wedge \star \left[ \sum_{I=1}^6 w_I {}^{(I)}W_{\alpha\beta} + \sum_{I=1}^5 z_I {}^{(I)}Z_{\alpha\beta} + w_7 \vartheta_\alpha \wedge (e_\gamma] {}^{(5)}W^\gamma_\beta \right. \\
& \left. + z_6 \vartheta_\gamma \wedge (e_\alpha] {}^{(2)}Z^\gamma_\beta) + \sum_{I=7}^9 z_I \vartheta_\alpha \wedge (e_\gamma] {}^{(I-4)}Z^\gamma_\beta) \right]. \quad (2.11)
\end{aligned}$$

The corresponding lines can be characterized in the following way

$$\begin{aligned}
V_{\text{MAG}} = & \text{weak part} \left[ \begin{aligned} & \text{Einstein-Hilbert + cosmological term + quadratic torsion} \\ & + \text{quadratic nonmetricity} \\ & + \text{quadratic nonmetricity mixed with coframe} \\ & + \text{cross terms with nonmetricity and torsion} \end{aligned} \right] \\
& - \text{strong part} \left[ \text{quadratic curvature + terms mixed with coframe} \right]. \quad (2.12)
\end{aligned}$$

The constants entering (2.11) are the cosmological constant  $\lambda$ , the weak and strong coupling constant  $\kappa$  and  $\rho$ , and the 28 dimensionless parameters

$$a_0, \dots, a_3, b_1, \dots, b_5, c_2, \dots, c_4, w_1, \dots, w_7, z_1, \dots, z_9. \quad (2.13)$$

This Lagrangian and the presently known exact solutions in MAG have been reviewed in [45]. As compared to GR [25, 83], the number of known exact solutions in MAG is relatively small. Important definitions of this section are summarized in table 2.1.

## 2.3 The triplet ansatz

In this section we briefly discuss the results of Obukhov et al. [74]. Note that a similar result for a less general Lagrangian was derived by Dereli et al. in [73]. Starting from the most general gauge Lagrangian  $V_{\text{MAG}}$  as given in the previous section, cf. eq. (2.11), we will now investigate the special case with

$$w_1, \dots, w_7 = 0, \quad z_1, \dots, z_3, z_5, \dots, z_9 = 0, \quad z_4 \neq 0. \quad (2.14)$$

Table 2.1: Summary of definitions made in section 2.2.

Potentials	Field strengths	Excitations	Gauge currents
$g_{\alpha\beta}$	$Q_{\alpha\beta} := -Dg_{\alpha\beta}$	$M^{\alpha\beta} := -2\frac{\partial V}{\partial Q_{\alpha\beta}}$	$m^{\alpha\beta} := 2\frac{\partial V}{\partial g_{\alpha\beta}}$
$\vartheta^\alpha$	$T^\alpha := D\vartheta^\alpha$	$H_\alpha := -\frac{\partial V}{\partial T^\alpha}$	$E_\alpha := \frac{\partial V}{\partial \vartheta^\alpha}$
$\Gamma_\alpha{}^\beta$	$R_\alpha{}^\beta := D\Gamma_\alpha{}^\beta$	$H^\alpha{}_\beta := -\frac{\partial V}{\partial R_\alpha{}^\beta}$	$E^\alpha{}_\beta := \frac{\partial V}{\partial \Gamma_\alpha{}^\beta}$

Thus, we consider a general weak part (i.e. we do not impose that one of the weak coupling constants vanishes initially) but only a very constrained strong part of (2.11). Written explicitly we are left with

$$\begin{aligned}
V_{\text{Triplet}} = & \frac{1}{2\kappa} \left[ -a_0 R^{\alpha\beta} \wedge \eta_{\alpha\beta} - 2\lambda\eta + T^\alpha \wedge \star \left( \sum_{I=1}^3 a_I {}^{(I)}T_\alpha \right) \right. \\
& + Q_{\alpha\beta} \wedge \star \left( \sum_{I=1}^4 b_I {}^{(I)}Q^{\alpha\beta} \right) \\
& + b_5 {}^{(3)}Q_{\alpha\gamma} \wedge \vartheta^\alpha \wedge \star \left( {}^{(4)}Q^{\beta\gamma} \wedge \vartheta_\beta \right) \\
& \left. + 2 \left( \sum_{I=2}^4 c_I {}^{(I)}Q_{\alpha\beta} \right) \wedge \vartheta^\alpha \wedge \star T^\beta \right] \\
& - \frac{z_4}{2\rho} R^{\alpha\beta} \wedge \star {}^{(4)}Z_{\alpha\beta}. \tag{2.15}
\end{aligned}$$

The corresponding lines can be characterized in the following way

$$\begin{aligned}
V_{\text{Triplet}} = & \text{weak part} \left[ \text{Einstein-Hilbert} + \text{cosmological term} + \text{quadratic torsion} \right. \\
& + \text{quadratic nonmetricity} \\
& + \text{quadratic nonmetricity mixed with coframe} \\
& \left. + \text{cross terms with nonmetricity and torsion} \right] \\
& - \text{strong part} \left[ \text{quadratic segmental curvature} \right]. \tag{2.16}
\end{aligned}$$

Thus, the only surviving strong gravity piece in  $V_{\text{Triplet}}$  is given by the square of the dilation part of the segmental curvature  ${}^{(4)}Z_{\alpha\beta} := \frac{1}{4}g_{\alpha\beta}Z$ , cf. appendix C.1. In this case, the result of Obukhov et al. [74] is the following: The curvature  $R_{\alpha\beta}$  may be effectively considered to be Riemannian. Both torsion and nonmetricity may be represented by a



single 1-form  $\omega$ .

$$Q = k_0\omega, \quad \Lambda = k_1\omega, \quad T = k_2\omega, \quad (2.17)$$

$$T^\alpha = {}^{(2)}T^\alpha = \frac{1}{3}\vartheta^\alpha \wedge T, \quad (2.18)$$

$$Q_{\alpha\beta} = {}^{(3)}Q_{\alpha\beta} + {}^{(4)}Q_{\alpha\beta} = \frac{4}{9} \left( \vartheta_{(\alpha} e_{\beta)} \rfloor \Lambda - \frac{1}{4} g_{\alpha\beta} \Lambda \right) + g_{\alpha\beta} Q. \quad (2.19)$$

With the aid of the Riemannian curvature  $\tilde{R}_{\alpha\beta}$  (cf. appendix C.1), the field equation (2.4) looks like the Einstein equation with an energy-momentum source that depends on torsion and nonmetricity. Therefore, the field equation (2.5) turns into a system of differential equations for torsion and nonmetricity alone. In the *vacuum* case, i.e. vanishing energy-momentum  $\Sigma_\alpha$  and hypermomentum  $\Delta_\alpha{}^\beta$  of matter, these differential equations reduce to

$$\frac{a_0}{2} \eta_{\alpha\beta\gamma} \wedge \tilde{R}^{\beta\gamma} + \lambda \eta_\alpha = \kappa \Sigma_\alpha^{(\omega)}, \quad (2.20)$$

$$d^* d\omega + m^2 {}^* \omega = 0. \quad (2.21)$$

The four constants  $m$ ,  $k_0$ ,  $k_1$ , and  $k_2$ , which appear in (2.17) and (2.21), uniquely depend on the parameters of the MAG Lagrangian (2.14)

$$\begin{aligned} k_0 &= 4(a_2 - 2a_0) \left( b_3 + \frac{a_0}{8} \right) - 3(c_3 + a_0)^2, \\ k_1 &= \frac{9}{2}(a_2 - 2a_0)(b_5 - a_0) - 9(c_3 + a_0)(c_4 + a_0), \\ k_2 &= 12 \left( b_3 + \frac{a_0}{8} \right) (c_4 + a_0) - \frac{9}{2}(b_5 - a_0)(c_3 + a_0), \\ m^2 &= \frac{1}{z_4 \kappa} \left( -4b_4 + \frac{3}{2}a_0 + \frac{k_1}{2k_0}(b_5 - a_0) + \frac{k_2}{k_0}(c_4 + a_0) \right). \end{aligned} \quad (2.22)$$

The energy-momentum source of the torsion and nonmetricity  $\Sigma_\alpha^{(\omega)}$  which appears in the effective Einstein equation (2.20) reads

$$\begin{aligned} \Sigma_\alpha^{(\omega)} &= \frac{z_4 k_0^2}{2\rho} \{ (e_\alpha \rfloor d\omega) \wedge {}^* d\omega - (e_\alpha \rfloor {}^* d\omega) \wedge d\omega \\ &\quad + m^2 [(e_\alpha \rfloor \omega) \wedge {}^* \omega + (e_\alpha \rfloor {}^* \omega) \wedge \omega] \}. \end{aligned} \quad (2.23)$$

This energy-momentum is precisely the energy-momentum of a Proca 1-form, thus our constrained Lagrangian (2.15), together with (2.20), and (2.21) is effectively equivalent to an Einstein-Proca Lagrangian  $V_{\text{Einstein-Proca}} = V_{\text{Einstein-Hilbert}} + V_{\text{Proca}}$ , where

$$V_{\text{Proca}} = -\frac{1}{2} d\omega \wedge {}^* d\omega + \frac{1}{2} m^2 \omega \wedge {}^* \omega. \quad (2.24)$$

Consequently, the Einstein-Proca Lagrangian describes a spacetime with a massive 1-form field  $\omega$ . As we can see from (2.24) the parameter  $m$  in (2.21) has the meaning of

the mass parameter of the Proca 1-form  $\omega$ . If  $m$  vanishes the constrained MAG theory is equivalent to the Einstein-Maxwell theory, as can be seen immediately by comparing (2.23) with the energy-momentum of the Maxwell theory

$$\Sigma_\alpha^{\text{Max}} = \frac{1}{2} \{ (e_\alpha \rfloor dA) \wedge \star dA - (e_\alpha \rfloor \star dA) \wedge dA \}, \quad (2.25)$$

where  $A$  denotes the electromagnetic potential 1-form. Inspection of (2.22) reveals that  $m = 0$  leads to an additional constraint among the coupling constants (cf. [49], eq. (3.7)):

$$\begin{aligned} 0 &= -4b_4 + \frac{3}{2}a_0 + \frac{k_1}{2k_0}(b_5 - a_0) + \frac{k_2}{k_0}(c_4 + a_0) \\ &= 32b_4a_2b_3 - 12a_0a_2b_3 - 64b_4a_0b_3 - 24b_3c_4^2 - 48b_3c_4a_0 - 32b_4a_0^2 \\ &\quad - 24b_4c_3^2 + 9a_2b_5a_0 - 6a_2a_0^2 + 9a_0c_3^2 - 48b_4c_3a_0 + 4b_4a_2a_0 - 24a_0^2c_4 \\ &\quad + 9a_0b_5^2 - \frac{9}{2}a_2b_5^2 - 3a_0c_4^2 + 18c_3c_4b_5 - 18c_3c_4a_0 + 18c_3a_0b_5 + 18a_0c_4b_5. \end{aligned} \quad (2.26)$$

For the sake of completeness we display the explicit form of the excitations (cf. [74], p. 7772) derived from the triplet Lagrangian (2.15)

$$\text{Triplet } H_\alpha = -\frac{\partial V_{\text{Triplet}}}{\partial T^\alpha} = -\frac{1}{\kappa} \star \left[ \sum_{I=1}^3 a_I {}^{(I)}T_\alpha + \left( \sum_{I=2}^4 c_I {}^{(I)}Q_{\alpha\beta} \right) \wedge \vartheta^\alpha \right], \quad (2.27)$$

$$\text{Triplet } H^\alpha{}_\beta = -\frac{\partial V_{\text{Triplet}}}{\partial R^\alpha{}_\beta} = \frac{a_0}{2\kappa} \eta^\alpha{}_\beta + \frac{z_4}{\rho} \star ({}^{(4)}Z^\alpha{}_\beta), \quad (2.28)$$

$$\begin{aligned} \text{Triplet } M^{\alpha\beta} &= -2\frac{\partial V_{\text{Triplet}}}{\partial Q_{\alpha\beta}} = -\frac{2}{\kappa} \left[ \star \left( \sum_{I=1}^4 b_I {}^{(I)}Q^{\alpha\beta} \right) + \frac{b_5}{2} (\vartheta^{(\alpha} \wedge \star (Q \wedge \vartheta^{\beta)}) \right. \\ &\quad \left. - \frac{1}{4} g^{\alpha\beta} \star (3Q + \Lambda) \right) + c_2 \vartheta^{(\alpha} \wedge \star {}^{(1)}T^{\beta)} + c_3 \vartheta^{(\alpha} \wedge \star {}^{(2)}T^{\beta)} \\ &\quad \left. + \frac{1}{4} (c_3 - c_4) g^{\alpha\beta} \star T \right], \end{aligned} \quad (2.29)$$

$$\begin{aligned} \text{Triplet } E_\alpha &= e_\alpha \rfloor V_{\text{Triplet}} + (e_\alpha \rfloor T^\beta) \wedge \text{Triplet } H_\beta + (e_\alpha \rfloor R_{\beta\gamma}) \wedge \text{Triplet } H^\beta{}_\gamma \\ &\quad + \frac{1}{2} (e_\alpha \rfloor Q_{\beta\gamma}) \text{Triplet } M^{\beta\gamma}, \end{aligned} \quad (2.30)$$

$$\text{Triplet } E^\alpha{}_\beta = -\vartheta^\alpha \wedge \text{Triplet } H_\beta - \text{Triplet } M^\alpha{}_\beta. \quad (2.31)$$

Here we made use of the definitions  $Q := \frac{1}{4} Q^\alpha{}_{\alpha,\Lambda} := \vartheta^\alpha e^\beta \rfloor (Q_{\alpha\beta} - Q g_{\alpha\beta})$ ,  $T := e_\alpha \rfloor T^\alpha$ .

**Further specialization** In the following we confine ourselves to the case  $m = 0$ . Thus, the field equations of MAG are given by (2.20) and (2.21). The energy-momentum of the triplet is represented by the first part of (2.23). We observe that in case of a closed triplet 1-form  $\omega$ , i.e.  $d\omega = 0$ , the energy-momentum of the triplet field  $\Sigma_\alpha^{(\omega)}$  vanishes. Additionally, the second triplet field equation (2.21) is fulfilled identically. Thus, the

only remaining field equation is (2.20), i.e. the field equation of General Relativity, which in case of vacuum reads as follows (note that we are allowed to choose  $a_0 = 1$ )

$$\frac{1}{2}\eta_{\alpha\beta\gamma} \wedge \tilde{R}^{\beta\gamma} + \lambda\eta_\alpha = 0. \quad (2.32)$$

Consequently, we find a solution of the triplet regime of MAG with *closed*  $\omega$  if we are able to solve (2.32). Of course, this means that every vacuum solution in general relativity (note that we do not have to confine ourselves to the vacuum case) generates a solution of what we will call the *closed* triplet ansatz. But what about the non-Riemannian features like nonmetricity and torsion in our solution? As we mentioned above, the energy-momentum  $\Sigma_\alpha^{(\omega)}$  of the triplet field vanishes if  $\omega$  is closed. Thinking of the classical Maxwell theory, a closed potential 1-form  $A$  immediately leads to vanishing fields strengths, because of  $F = dA$ . Consequently we may express the potential 1-form  $A$  by finding the corresponding 0-form  $\phi$  with  $A = d\phi$ .

As we can see from (2.18) and (2.19), a closed potential  $\omega$  does not necessarily lead to vanishing field strengths in the triplet regime of MAG. Expressing  $\omega$  locally by means of a 0-form  $\psi$ , we arrive at the following notions for torsion  $T^\alpha$  and nonmetricity  $Q_{\alpha\beta}$

$$T^\alpha = \frac{k_2}{3}\vartheta^\alpha \wedge d\psi, \quad (2.33)$$

$$Q_{\alpha\beta} = \frac{4k_1}{9} \left( \vartheta_{(\alpha} e_{\beta)} d\psi - \frac{1}{4}g_{\alpha\beta} d\psi \right) + k_0 g_{\alpha\beta} d\psi. \quad (2.34)$$

With  $\omega = \omega_\mu \vartheta^\mu = d\psi$  the MAG connection, cf. appendix C.4, reduces to

$$\Gamma_{\alpha\beta} = \Gamma_{\alpha\beta}^{\{\}} + \frac{2k_1}{9} \left( \vartheta_{(\alpha} \omega_{\beta)} - \frac{1}{4}g_{\alpha\beta} \omega \right) + \frac{k_0}{2}g_{\alpha\beta} \omega + \left( \frac{k_1}{3} - \frac{2k_2}{3} - k_0 \right) \vartheta_{[\alpha} \omega_{\beta]}. \quad (2.35)$$

## 2.4 Weyl-Cartan spacetime

The Weyl-Cartan spacetime ( $Y_n$ ) is a special case of the metric-affine geometry in which the tracefree part  $\mathcal{Q}_{\alpha\beta}^\times$  of the nonmetricity  $Q_{\alpha\beta}$  vanishes. Thus, the whole nonmetricity is proportional to its trace part, i.e. the Weyl 1-form  $Q := \frac{1}{4}Q^\gamma{}_\gamma$ ,

$$Q_{\alpha\beta} = g_{\alpha\beta} Q = \frac{1}{4}g_{\alpha\beta} Q^\gamma{}_\gamma. \quad (2.36)$$

Therefore the MAG connection, cf. appendix C.4, may be represented as

$$\Gamma_{\alpha\beta} = \Gamma_{\alpha\beta}^{\{\}} - e_{[\alpha} T_{\beta]} + \frac{1}{2}(e_\alpha] e_\beta] T_\gamma) \vartheta^\gamma + \frac{1}{2}g_{\alpha\beta} Q + (e_{[\alpha} Q) \vartheta_{\beta]}. \quad (2.37)$$

**Further specialization** Now let us recall the definition of the material hypermomentum  $\Delta_{\alpha\beta}$  given in (2.8). With  $\Delta_{(\alpha\beta)}^\times := \Delta_{(\alpha\beta)} - \frac{1}{4}g_{\alpha\beta}\Delta^\gamma{}_\gamma = \Delta_{(\alpha\beta)} - \frac{1}{4}g_{\alpha\beta}\Delta$  for the

symmetric tracefree piece, we have:

$$\begin{aligned}
\Delta_{\alpha\beta} &= \text{antisymmetric piece} + \text{symmetric tracefree piece} + \text{trace piece} \\
&= \tau_{\alpha\beta} + \mathbb{A}_{(\alpha\beta)} + \frac{1}{4}g_{\alpha\beta} \Delta \\
&= \text{spin current} + \text{shear current} + \text{dilation current}.
\end{aligned} \tag{2.38}$$

If we assume that the shear current in (2.38) vanishes the second MAG field equation (2.5) decomposes into

$$dH^\alpha{}_\alpha - E^\alpha{}_\alpha = \Delta, \tag{2.39}$$

$$g_{\gamma(\alpha}DH^\gamma{}_{\beta)} - E_{(\alpha\beta)} - \frac{1}{4}g_{\alpha\beta} (dH^\gamma{}_\gamma - E^\gamma{}_\gamma) = 0, \tag{2.40}$$

$$g_{\gamma[\alpha}DH^\gamma{}_{\beta]} - E_{[\alpha\beta]} = \tau_{\alpha\beta}, \tag{2.41}$$

while the first field equation is still given by (2.4). Additionally, we can decompose the second Noether identity (2.10) into

$$\frac{1}{4}g_{\alpha\beta} d\Delta + \vartheta_{(\alpha} \wedge \Sigma_{\beta)} = \sigma_{\alpha\beta}, \tag{2.42}$$

$$D\tau_{\alpha\beta} + Q \wedge \tau_{\alpha\beta} + \vartheta_{[\alpha} \wedge \Sigma_{\beta]} = 0. \tag{2.43}$$

Substituting the Weyl 1-form and the hypermomentum into the first Noether identity (2.9) yields

$$D\Sigma_\alpha = (e_\alpha \rfloor T^\beta) \wedge \Sigma_\beta - \frac{1}{2}(e_\alpha \rfloor Q) \sigma^\beta{}_\beta + (e_\alpha \rfloor R_{[\beta\gamma]}) \wedge \tau^{\beta\gamma} + \frac{1}{4}(e_\alpha \rfloor R) \wedge \Delta. \tag{2.44}$$

Finally, we note that in a  $Y_n$  spacetime the symmetric part of the curvature  $R_{(\alpha\beta)} = Z_{\alpha\beta}$ , i.e. the strain curvature, reduces to its trace part

$$Z_{\alpha\beta} = \frac{1}{4}g_{\alpha\beta}R = \frac{1}{4}g_{\alpha\beta}R^\gamma{}_\gamma = \frac{1}{2}g_{\alpha\beta}dQ. \tag{2.45}$$

In section 3.2 we will consider a cosmological model in the Weyl-Cartan spacetime.

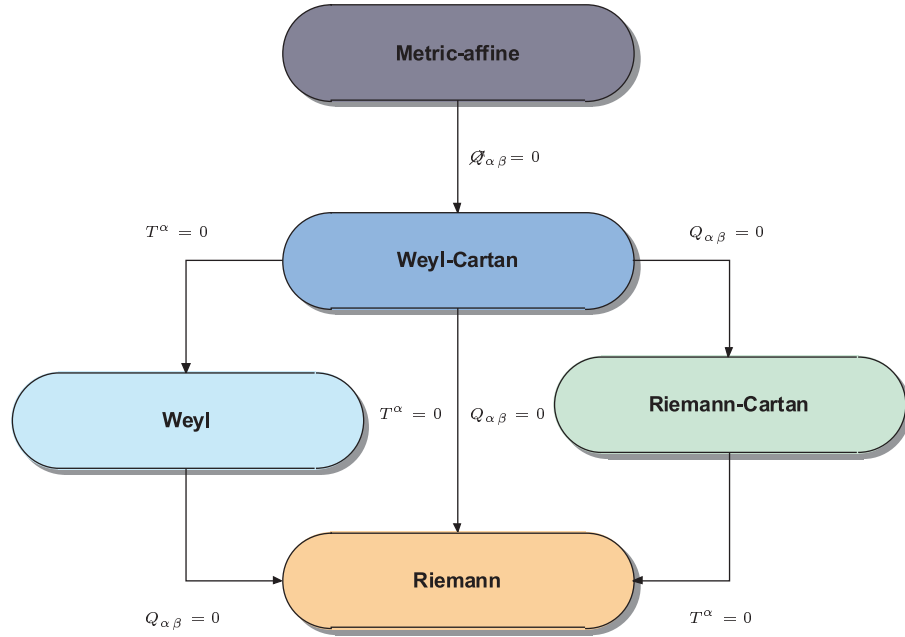


Figure 2.1: Schematic overview of different spacetimes types.

## 2.5 Dimensions

Table 2.2: Dimensions.

Quantities	1	Length
Gauge potentials	$[g_{\alpha\beta}], [\Gamma_{\alpha\beta}]$	$[\vartheta^\alpha]$
Gauge fieldstrengths	$[Q_{\alpha\beta}], [R_{\alpha\beta}], [W_{\alpha\beta}], [Z_{\alpha\beta}], [\tilde{R}_{\alpha\beta}]$	$[T^\alpha]$
Gauge field excitations	$[M^{\alpha\beta}], [H^\alpha_\beta]$	$[H_\alpha]^{-1}$
Gauge field currents	$[E^\alpha_\beta], [m^{\alpha\beta}]$	$[E_\alpha]^{-1}$
Matter currents	$[\Delta_{\alpha\beta}], [\sigma^{\alpha\beta}], [\tau_{\alpha\beta}]$	$[\Sigma_\alpha]^{-1}$
Constants	$[\rho], [a_{0\dots 3}], [b_{1\dots 5}], [c_{2\dots 4}]$ $[w_{1\dots 7}], [z_{1\dots 9}], [k_{0\dots 2}]$	$[\kappa]^{\frac{1}{2}}, [\lambda]^{-\frac{1}{2}}$ $[m]^{-1}$
Triplet potentials	$[\omega], [Q], [\Lambda], [T]$	
Miscellany	$[A], [\psi]$	$[\eta_\alpha]^{\frac{1}{3}}, [\eta_{\alpha\beta}]^{\frac{1}{2}}, [\eta_{\alpha\beta\gamma}], [C_\alpha]$



# Chapter 3

## Cosmology in alternative gravity theories

### 3.1 Introduction

In this chapter we present a new cosmological model in Weyl-Cartan spacetime. For a classification scheme of non-Riemannian spacetimes see figure 2.1 on page 59. In sections 3.2–3.5 we focus on the derivation and solution of the field equations. We work out the magnitude-redshift relation in section 3.6 and perform fits to a SN Ia data set in section 3.7. In section 3.9 we discuss an interesting special case of the model and its observational implications. Subsequently we make contact with the models of two other groups in section 3.10 and constrain their parameters with the help of the magnitude-redshift relation. In section 3.11 we discuss several issues related to nucleosynthesis. Additionally, we constrain the model parameters by means of the observed helium abundance. Finally, we draw our conclusion and give an outlook on future goals in section 3.12.

Before we start with the discussion of a specific model let us briefly comment on some other alternative cosmological scenarios. The current spectrum of alternative models ranges from ad hoc modifications of the Friedmann equation [141], FLRW type models with matter creation [53], over models in higher dimensions [67] to models in non-Riemannian spacetimes [59].

Especially models with extra dimensions received very much attention in the recent literature. The idea that ordinary matter is confined to a submanifold, commonly termed brane, which is embedded in a higher dimensional space, called bulk, has several physical consequences. Some of these models are interesting from a cosmological point of view because they allow to recover the usual Friedmann equation on the brane enriched by high energy corrections, which lead to significant deviations from the cosmological standard scenario in the early universe while preserving the well tested standard scenario at low energies. This brings us to the countless number of models which introduce a modification of the field equations in a phenomenological way, mostly by adding

additional terms in the Friedmann equation or by introducing additional fields on the Lagrangian level. One prominent example of these *add-on's* is inflation, which provided a solution of the horizon problem within the FLRW description in 1981. Most of these add-on's aim for a solution of specific cosmological problems. For example, to lower the amount of the, up to now not directly detected, dark matter and dark energy which is needed within the FLRW description in order to keep track with observations. There have only been few attempts to study the observational impact of cosmological models which require a non-Riemannian spacetime structure.

Some early investigations concerning the search for exact cosmological solutions in an Einstein-Cartan and MAG framework can be found in [59]–[62]. A model involving a Proca like field and its implications for an inflationary era as well as its possible consequences for galactic rotation curves was studied in [63]<sup>1</sup>. An interesting property of this model is given by the avoidance of the initial singularity. Such a behavior was also observed in several Einstein-Cartan scenarios, cf. [54, 59], e.g. Two other examples for models within Riemann-Cartan spacetime are given in [55] and [56], wherein the authors try to assess a limit on the spin-density perturbations from the observed temperature fluctuations of the CMB. Finally, we note that there exist several works in which the relation between Weyl type theories and the inflationary scenario is investigated, cf. [57, 58].

## 3.2 A cosmological model in Weyl-Cartan spacetime

In [68] we considered the following gauge Lagrangian

$$V = \frac{\chi}{2\kappa} R_{\alpha}{}^{\beta} \wedge \eta^{\alpha}{}_{\beta} + \sum_{I=1}^6 a_I R_{\alpha}{}^{\beta} \wedge {}^{*(I)}W^{\alpha}{}_{\beta} + b R_{\alpha}{}^{\beta} \wedge {}^{*(4)}Z^{\alpha}{}_{\beta}. \quad (3.1)$$

Here  $\eta_{\alpha\beta} := {}^*(\vartheta_{\alpha} \wedge \vartheta_{\beta})$ ,  ${}^{(I)}W^{\alpha\beta}$ , and  ${}^{(I)}Z^{\alpha\beta}$  as given in appendix C. Since we are interested in more general gauge Lagrangians (cf. equation (2.11) for a very general one proposed in MAG), we are going to extend (3.1) by means of

$$V_1 = c Q_{\alpha\beta} \wedge {}^{*(4)}Q^{\alpha\beta}. \quad (3.2)$$

Hence, our new Lagrangian reads

$$\begin{aligned} V &= V_{\text{old}} + V_1 \\ &\sim \text{Einstein-Hilbert} + \text{quadratic rotational curvature} \\ &\quad + \text{quadratic strain curvature} + \text{quadratic nonmetricity}. \end{aligned} \quad (3.3)$$

---

<sup>1</sup>Note that also the works [64] and [65] contain a discussion of the equations of motion in a non-Riemannian space, albeit in a non-cosmological context. Another work [52], also in a non-cosmological context, deals with possible observational implications of a MAG based model due to a non-minimal coupling of torsion to the electromagnetic field.



In contrast to our old model [68], we included an explicit nonmetricity term in our Lagrangian. Note that we have the arbitrary constants  $\chi$ ,  $a_{I=1\dots 6}$ ,  $b$ ,  $c$ , and the weak coupling constant  $\kappa$ . The Lagrangian in (3.3) represents a special case of (2.11), what can easily be seen by performing the following substitutions for the constants in (2.11):

$$a_0 \rightarrow -\chi, \quad w_1, \dots, w_6 \rightarrow -2\rho a_1, \dots, -2\rho a_6, \quad b_4 \rightarrow c, \quad z_4 \rightarrow -2\rho b. \quad (3.4)$$

Since a treatment of the full Lagrangian is computationally not feasible at the moment, it is necessary to study successively the impact of additional terms in the Lagrangian. Together with the quadratic rotational curvature and quadratic strain curvature terms, which were already included in our old model [68], we now have an additional post-Riemannian piece in form of a quadratic nonmetricity term. This generalizes the usual Einstein-Hilbert Lagrangian commonly used in general relativistic cosmological models. Note that the Lagrangian in (3.3) does not encompass a term with the cosmological constant. However, as we will show in section 3.4, our ansatz gives rise to an additional constant which, on the level of the field equations, will play the same role as the cosmological constant in the standard model. From (3.3) we can derive the gauge field excitations (cf. section 2.2). They read

$$M^{\alpha\beta} = -4c^{*(4)}Q^{\alpha\beta} = -cg^{\alpha\beta} * Q^\gamma{}_\gamma, \quad (3.5)$$

$$H_\alpha = 0, \quad (3.6)$$

$$\begin{aligned} H^\alpha{}_\beta &= -\frac{\chi}{2\kappa}\eta^\alpha{}_\beta - 2\sum_{I=1}^6 a_I {}^{*(I)}W^\alpha{}_\beta - 2b^{*(4)}Z^\alpha{}_\beta \\ &= -\frac{\chi}{2\kappa}\eta^\alpha{}_\beta - 2\sum_{I=1}^6 a_I {}^{*(I)}W^\alpha{}_\beta - \frac{b}{2}\delta_\beta^\alpha * R^\gamma{}_\gamma. \end{aligned} \quad (3.7)$$

Hence the canonical energy-momentum of the gauge fields is given by

$$\begin{aligned} E_\alpha &= e_\alpha \rfloor V + (e_\alpha \rfloor R_\beta{}^\gamma) \wedge H^\beta{}_\gamma + (e_\alpha \rfloor T^\beta) \wedge H_\beta + \frac{1}{2}(e_\alpha \rfloor Q_{\beta\gamma}) \wedge M^{\beta\gamma} \\ &= e_\alpha \rfloor V + (e_\alpha \rfloor R_\beta{}^\gamma) \wedge H^\beta{}_\gamma + \frac{1}{2}(e_\alpha \rfloor Q_{\beta\gamma}) \wedge M^{\beta\gamma}. \end{aligned} \quad (3.8)$$

In contrast to [68] we now have a non-vanishing gauge hypermomentum

$$\begin{aligned} E^\alpha{}_\beta &= -\vartheta^\alpha \wedge H_\beta - g_{\beta\gamma} M^{\alpha\gamma} \\ &= 4c g_{\beta\gamma} {}^{*(4)}Q^{\alpha\gamma} = c \delta_\beta^\alpha * Q^\nu{}_\nu. \end{aligned} \quad (3.9)$$

The field equations turn into

$$-E_\alpha = \Sigma_\alpha, \quad (3.10)$$

$$dH^\alpha{}_\alpha - E^\alpha{}_\alpha = \Delta, \quad (3.11)$$

$$g_{\gamma(\alpha} D H^\gamma{}_{\beta)} - E_{(\alpha\beta)} - \frac{1}{4} g_{\alpha\beta} (dH^\gamma{}_\gamma - E^\gamma{}_\gamma) = \mathbb{X}_{(\alpha\beta)}, \quad (3.12)$$

$$g_{\gamma[\alpha} D H^\gamma{}_{\beta]} - E_{[\alpha\beta]} = \tau_{\alpha\beta}. \quad (3.13)$$

In eqs. (3.11)–(3.13) we decomposed the second field equation into its trace, tracefree symmetric, and antisymmetric part, cf. section 2.4. Due to the structure of (3.11) we make the following ansatz for the dilation current:

$$\Delta_{\alpha\beta} = \frac{1}{4} g_{\alpha\beta} \Delta = \frac{1}{4} g_{\alpha\beta} (dH^\gamma{}_\gamma - E^\gamma{}_\gamma). \quad (3.14)$$

Hence we confine ourselves to a medium with vanishing spin current and vanishing shear current, i.e.  $\tau_{\alpha\beta} = \mathbb{X}_{(\alpha\beta)} = 0$ . Thus, equations (3.12) and (3.13) turn into

$$\frac{\chi}{2\kappa} Q_{(\alpha}{}^\gamma \wedge \eta_{\gamma|\beta)} - 2 \sum_{I=1}^6 a_I g_{\gamma(\alpha} D^{*(I)} W^{\gamma)}{}_\beta = 0, \quad (3.15)$$

$$g_{\gamma[\alpha} D H^{\gamma]}{}_\beta = 0. \quad (3.16)$$

The derivation of (3.15) is sketched in appendix E.5. From (3.7), and (3.9) we can infer that

$$\Delta_{\alpha\beta} = -\frac{1}{4} g_{\alpha\beta} (2b d^* R^\gamma{}_\gamma + 4c^* Q^\nu{}_\nu). \quad (3.17)$$

In contrast to [68] the derivative of the dilation current does no longer vanish identically due to the new structure of (3.11). Because we have not specified a matter Lagrangian, we have to take into account the Noether identities (cf. section 2.2 and section 2.4), i.e.

$$D\Sigma_\alpha = (e_\alpha] T^\beta) \wedge \Sigma_\beta - \frac{1}{2} (e_\alpha] Q) \sigma^\beta{}_\beta + \frac{1}{4} (e_\alpha] R) \wedge \Delta, \quad (3.18)$$

$$\sigma_{\alpha\beta} = \frac{1}{4} g_{\alpha\beta} d\Delta + \vartheta_{(\alpha} \wedge \Sigma_{\beta)}, \quad (3.19)$$

$$0 = \vartheta_{[\alpha} \wedge \Sigma_{\beta]}. \quad (3.20)$$

We can rewrite eq. (3.19) by using (3.11)

$$\sigma_{\alpha\beta} = -\frac{1}{4} g_{\alpha\beta} dE^\gamma{}_\gamma + \vartheta_{(\alpha} \wedge \Sigma_{\beta)}. \quad (3.21)$$

Equations (3.19)–(3.20) represent the decomposed second Noether identity in case of a vanishing spin and shear current. With (3.21) eq. (3.18) turns into

$$D\Sigma_\alpha = (e_\alpha] T^\beta) \wedge \Sigma_\beta - \frac{1}{2} (e_\alpha] Q) \vartheta^\beta \wedge \Sigma_\beta + \frac{1}{8} (e_\alpha] Q) g^\beta{}_\beta dE^\gamma{}_\gamma + \frac{1}{4} (e_\alpha] R) \wedge \Delta. \quad (3.22)$$

Thus, we have to solve (3.10), (3.11), (3.15), (3.16), (3.18)–(3.20) in order to obtain a solution for our model proposed in (3.3). If we confine ourselves to a Weyl-Cartan spacetime we can make use of (2.45), i.e.  $R^\gamma{}_\gamma \sim dQ$ , hence equation (3.17) turns into

$$\Delta_{\alpha\beta} = -\frac{1}{4} g_{\alpha\beta} (b d^* dQ^\gamma{}_\gamma + c g_{\gamma\mu}{}^* (g^{\mu\gamma} Q^\nu{}_\nu)). \quad (3.23)$$

Thus, for such an ansatz the hypermomentum  $\Delta_{\alpha\beta}$  depends on the nonmetricity and vice versa. Note that the second term in (3.23) depends on the coupling constant of equation

(3.5). Now let us specify the remaining quantities in our model. Equation (3.20) forces the energy-momentum 3-form to be symmetric, thus we choose, with  $\eta^\alpha := \star\vartheta^\alpha$ ,

$$\Sigma_\alpha = \Sigma_{\alpha\beta}\eta^\beta, \quad \text{with} \quad \Sigma_{\alpha\beta} = \text{diag}(\mu(t), p_r(t), p_t(t), p_t(t)). \quad (3.24)$$

Subsequently we can calculate the metric stress-energy  $\sigma_{\alpha\beta}$  from eq. (3.21)

$$\sigma_{\alpha\beta} = -\frac{1}{4}g_{\alpha\beta} d(c g_{\gamma\mu} \star(g^{\mu\gamma}Q^\nu{}_\nu)) + \vartheta_{(\alpha} \wedge (\Sigma_{\beta)\gamma}\eta^\gamma). \quad (3.25)$$

Again we obtained a quantity which depends on the Weyl 1-form, i.e. the trace of the nonmetricity. Since we want to compare our model to the cosmological standard model, we use the Robertson-Walker line element as starting point for our calculations,

$$\vartheta^{\hat{0}} = dt, \quad \vartheta^{\hat{1}} = \frac{S(t)}{\sqrt{1-kr^2}}dr, \quad \vartheta^{\hat{2}} = S(t)r d\theta, \quad \vartheta^{\hat{3}} = S(t)r \sin\theta d\phi, \quad (3.26)$$

with

$$ds^2 = \vartheta^{\hat{0}} \otimes \vartheta^{\hat{0}} - \vartheta^{\hat{1}} \otimes \vartheta^{\hat{1}} - \vartheta^{\hat{2}} \otimes \vartheta^{\hat{2}} - \vartheta^{\hat{3}} \otimes \vartheta^{\hat{3}}. \quad (3.27)$$

As usual,  $S(t)$  denotes the cosmic scale factor and  $k = -1, 0, 1$  determines whether the spatial sections are of constant negative, vanishing or positive Riemannian curvature. Following the model proposed in [68], we choose the torsion to be proportional to the Weyl 1-form

$$T^\alpha = \frac{1}{2}Q \wedge \vartheta^\alpha. \quad (3.28)$$

Hence the torsion consists only of its vector piece  ${}^{(2)}T^\alpha$ . The only thing missing in order to setup the field equations is a proper ansatz for the Weyl 1-form  $Q$ . In [68] we were able to derive  $Q$  from a proper ansatz for the potential of the hypermomentum  $\Delta$ , the so-called polarization 2-form  $P$ . Here we adopt a slightly different point of view. Since we are interested in the impact of different choices of the non-Riemannian quantity  $Q$  we will prescribe directly in the following. Besides of the fact that we gain direct control of the post-Riemannian features of our model, we circumvent the question of which type of matter generates the corresponding hypermomentum. Note that our ansatz in equation (3.24) is in general not compatible with the energy-momentum obtained in equation (3.28) of [50]. Since we do not prescribe a matter Lagrangian and use the Noether identities as constraints on the matter variables, our approach could be termed *phenomenological* as suggested in the first part of [50].

### 3.3 Field equations and Noether identities

In this section we derive the field equations and Noether identities resulting from a specific choice of the 1-form  $Q$ , which controls nearly every feature of our model. We start with a rather general form of  $Q$ , namely

$$Q = \frac{\xi(t, r)}{S(t)} \vartheta^{\hat{0}}, \quad (3.29)$$

where  $\xi(t, r)$  denotes an arbitrary function<sup>2</sup> of the radial coordinate and the time coordinate, and  $S(t)$  is the cosmic scale factor from (3.26). With the help of computer algebra we find that the field equations (3.10), (3.11), and (3.16) yield a set of four equations. In order to compare these new field equations with the ones derived in [68] (cf. eqs. (40)-(43) therein) we rewrite them as follows:

$$\begin{aligned} \chi \left( \left( \frac{\dot{S}}{S} \right)^2 + \frac{k}{S^2} \right) - (a_4 + a_6) \kappa \left( \left( \frac{\ddot{S}}{S} \right)^2 - \left( \left( \frac{\dot{S}}{S} \right)^2 + \frac{k}{S^2} \right)^2 \right) \\ = \frac{\kappa}{3} \left( \mu - 4c \left( \frac{\xi}{S} \right)^2 + b(1 - kr^2) \frac{\xi_{,r}^2}{S^4} \right), \end{aligned} \quad (3.30)$$

$$\begin{aligned} \chi \left( 2 \frac{\ddot{S}}{S} + \left( \frac{\dot{S}}{S} \right)^2 + \frac{k}{S^2} \right) + (a_4 + a_6) \kappa \left( \left( \frac{\ddot{S}}{S} \right)^2 - \left( \left( \frac{\dot{S}}{S} \right)^2 + \frac{k}{S^2} \right)^2 \right) \\ = -\kappa \left( p_r - 4c \left( \frac{\xi}{S} \right)^2 - b(1 - kr^2) \frac{\xi_{,r}^2}{S^4} \right), \end{aligned} \quad (3.31)$$

$$\begin{aligned} \chi \left( 2 \frac{\ddot{S}}{S} + \left( \frac{\dot{S}}{S} \right)^2 + \frac{k}{S^2} \right) + (a_4 + a_6) \kappa \left( \left( \frac{\ddot{S}}{S} \right)^2 - \left( \left( \frac{\dot{S}}{S} \right)^2 + \frac{k}{S^2} \right)^2 \right) \\ = -\kappa \left( p_t - 4c \left( \frac{\xi}{S} \right)^2 + b(1 - kr^2) \frac{\xi_{,r}^2}{S^4} \right), \end{aligned} \quad (3.32)$$

$$\frac{d}{dt} \left( \frac{\ddot{S}}{S} + \left( \frac{\dot{S}}{S} \right)^2 + \frac{k}{S^2} \right) = 0. \quad (3.33)$$

In eq. (3.33) we assumed  $a_4 \neq -a_6$ . We will investigate a relaxation of this condition later. Since we have not specified a matter Lagrangian, we have to be careful with the Noether identities (3.18)-(3.20). For our ansatz (3.29) we obtain two independent equations

$$\dot{S}S^3 (3\mu + p_r + 2p_t) + \dot{\mu}S^4 - 16\dot{S}cS\xi^2 + 2\xi_{,rt}\xi_{,r}b(1 - kr^2) - 8\xi_{,t}cS^2\xi = 0, \quad (3.34)$$

$$\xi_{,rr}\xi_{,r}br(1 - kr^2) + \xi_{,r}^2b(2 - 3kr^2) + 4\xi_{,r}crS^2\xi + S^4(p_t - p_r) = 0. \quad (3.35)$$

As one realizes immediately, the equations (3.30)-(3.33) are very similar to (40)-(43) of [68]. There is only a change on the rhs, i.e. the matter side, of the above equations in form of additional terms contributing to the pressure and energy density. The terms proportional to  $\xi_{,r}$  vanish if we make the same assumptions as in [68], i.e.  $\xi(t, r) \rightarrow \xi(t)$ . Apart from this feature there is another, more subtle, change in (3.30)-(3.33), namely

---

<sup>2</sup>This function is *not* identical with the one used in equation (24) of [68]. It has a slightly different meaning, since we use it here directly in our ansatz for the nonmetricity.

a term of the order  $\xi^2$  controlled by the new coupling constant  $c$  from eq. (3.2)<sup>3</sup>. The Noether identities (3.34) and (3.35) can be transformed into

$$\frac{\partial}{\partial t} (\mu S^4 + \xi_{,r}^2 b (1 - kr^2) - 8c (S\xi)^2) + 4c S^2 \frac{\partial \xi^2}{\partial t} = \frac{1}{4} \frac{dS^4}{dt} (\mu - p_r - 2p_t), \quad (3.36)$$

$$p_r - p_t = \frac{2cr}{S^2} \frac{\partial \xi^2}{\partial r} + \frac{b}{S^4} \left( \frac{r}{2} (1 - kr^2) \frac{\partial \xi_{,r}^2}{\partial r} + (2 - 3kr^2) \xi_{,r}^2 \right). \quad (3.37)$$

Hence we have more sophisticated relation between the radial and tangential stresses than in equation (37) of [68].

Let us now extract some more information from the field equations. Addition of (3.30) and (3.32) yields

$$2\chi \left( \frac{\ddot{S}}{S} + \left( \frac{\dot{S}}{S} \right)^2 + \frac{k}{S^2} \right) = \frac{\kappa}{3} \left( \mu - 3p_t + 8c \left( \frac{\xi}{S} \right)^2 - 2b (1 - kr^2) \frac{\xi_{,r}^2}{S^4} \right). \quad (3.38)$$

Subtracting (3.32) from (3.30) yields

$$\begin{aligned} & 2\chi \frac{\ddot{S}}{S} + 2\kappa (a_4 + a_6) \left( \left( \frac{\ddot{S}}{S} \right)^2 - \left( \left( \frac{\dot{S}}{S} \right)^2 + \frac{k}{S^2} \right)^2 \right) \\ &= -\frac{\kappa}{3} \left( \mu + 3p_t - 16c \left( \frac{\xi}{S} \right)^2 + 4b (1 - kr^2) \frac{\xi_{,r}^2}{S^4} \right). \end{aligned} \quad (3.39)$$

Combination of (3.33) and (3.38) leads to

$$\begin{aligned} 0 & \stackrel{(3.33)}{=} 2\chi \frac{d}{dt} \left( \frac{\ddot{S}}{S} + \left( \frac{\dot{S}}{S} \right)^2 + \frac{k}{S^2} \right) \\ & \stackrel{(3.38)}{=} \frac{\kappa}{3} \frac{d}{dt} \left( \mu - 3p_t + 8c \left( \frac{\xi}{S} \right)^2 - 2b (1 - kr^2) \frac{\xi_{,r}^2}{S^4} \right). \end{aligned} \quad (3.40)$$

The trace of the energy-momentum is

$$\begin{aligned} \Sigma^\gamma_\gamma &= \mu - p_r - 2p_t \\ & \stackrel{(3.37)}{=} \mu - 3p_t - \frac{2cr}{S^2} \frac{\partial \xi^2}{\partial r} + \frac{b}{S^4} \left( \frac{r}{2} (1 - kr^2) \frac{\partial \xi_{,r}^2}{\partial r} + (2 - 3kr^2) \xi_{,r}^2 \right). \end{aligned} \quad (3.41)$$

Since we encountered a system of coupled PDEs we will confine ourselves to a special case in which the field equations turn into a set of coupled ODEs. Note that the above situation is reminiscent of that encountered in anisotropic and inhomogeneous extensions of the FLRW model.

---

<sup>3</sup>Formerly the term of the order  $\xi^2$  was controlled by the coupling constant  $b$  from the Lagrangian in (3.1).

For completeness we list the surviving curvature pieces in case of the ansatz (3.29) below. Note that at this point it is easy to see that the symmetric tracefree part of the second field equation is identically fulfilled in our model. Because the only surviving member of the sum in equation (E.21) is the one for  $I = 4$ . Of course this part vanishes due to the structure of (3.42).

$${}^{(4)}W^{\alpha\beta} = \frac{\ddot{S}S - \dot{S}^2 - k}{2S^2} \vartheta^\alpha \wedge \vartheta^\beta, \quad (3.42)$$

$${}^{(6)}W^{\alpha\beta} = \frac{\ddot{S}S + \dot{S}^2 + k}{2S^2} \vartheta^\alpha \wedge \vartheta^\beta, \quad (3.43)$$

$${}^{(4)}Z_{\hat{0}\hat{0}} = -{}^{(4)}Z_{\hat{1}\hat{1}} = -{}^{(4)}Z_{\hat{2}\hat{2}} = -{}^{(4)}Z_{\hat{3}\hat{3}} = -\frac{\xi_{,r}\sqrt{-kr^2+1}}{2S^2} \vartheta^{\hat{0}} \wedge \vartheta^{\hat{1}}. \quad (3.44)$$

### 3.4 Special case $\xi(t, r) \rightarrow \zeta(t)$

Let us investigate the interesting special case in which  $Q$ , cf. eq. (3.29), is given by a closed 1-form, i.e.

$$Q = \frac{\zeta(t)}{S(t)} \vartheta^{\hat{0}}. \quad (3.45)$$

The field equations are now given by

$$\begin{aligned} \chi \left( \left( \frac{\dot{S}}{S} \right)^2 + \frac{k}{S^2} \right) - (a_4 + a_6) \kappa \left( \left( \frac{\ddot{S}}{S} \right)^2 - \left( \left( \frac{\dot{S}}{S} \right)^2 + \frac{k}{S^2} \right)^2 \right) \\ = \frac{\kappa}{3} \left( \mu - 4c \left( \frac{\zeta}{S} \right)^2 \right), \end{aligned} \quad (3.46)$$

$$\begin{aligned} \chi \left( 2\frac{\ddot{S}}{S} + \left( \frac{\dot{S}}{S} \right)^2 + \frac{k}{S^2} \right) + (a_4 + a_6) \kappa \left( \left( \frac{\ddot{S}}{S} \right)^2 - \left( \left( \frac{\dot{S}}{S} \right)^2 + \frac{k}{S^2} \right)^2 \right) \\ = -\kappa \left( p_r - 4c \left( \frac{\zeta}{S} \right)^2 \right), \end{aligned} \quad (3.47)$$

$$\begin{aligned} \chi \left( 2\frac{\ddot{S}}{S} + \left( \frac{\dot{S}}{S} \right)^2 + \frac{k}{S^2} \right) + (a_4 + a_6) \kappa \left( \left( \frac{\ddot{S}}{S} \right)^2 - \left( \left( \frac{\dot{S}}{S} \right)^2 + \frac{k}{S^2} \right)^2 \right) \\ = -\kappa \left( p_t - 4c \left( \frac{\zeta}{S} \right)^2 \right), \end{aligned} \quad (3.48)$$

$$\frac{d}{dt} \left( \frac{\ddot{S}}{S} + \left( \frac{\dot{S}}{S} \right)^2 + \frac{k}{S^2} \right) = 0. \quad (3.49)$$

Thus, the function  $\zeta$  contributes to the energy density and pressure in a similar way as the function  $\xi$  in [68]. Note that there is no additional contribution from the strain curvature in eqs. (3.46)–(3.49), i.e. no term controlled by the coupling constant  $b$  from our Lagrangian in eq. (3.1). This behavior is explained by the fact that the strain curvature vanishes identically for closed 1-forms in a Weyl-Cartan spacetime. The Noether identities read:

$$\frac{d}{dt} (\mu S^4 - 8c (S\zeta)^2) + 4cS^2 \frac{d\zeta^2}{dt} = \frac{1}{4} \frac{dS^4}{dt} (\mu - p_r - 2p_t), \quad (3.50)$$

$$p_r - p_t = 0. \quad (3.51)$$

In contrast to (3.37), eq. (3.51) forces the radial stress to equal the tangential stress. Addition of (3.46) and (3.48) yields

$$2\chi \left( \frac{\ddot{S}}{S} + \left( \frac{\dot{S}}{S} \right)^2 + \frac{k}{S^2} \right) = \frac{\kappa}{3} \left( \mu - 3p_r + 8c \left( \frac{\zeta}{S} \right)^2 \right). \quad (3.52)$$

Subtracting (3.48) from (3.46), cf. eq. (3.39), yields

$$\begin{aligned} & 2\chi \frac{\ddot{S}}{S} + 2\kappa (a_4 + a_6) \left( \left( \frac{\ddot{S}}{S} \right)^2 - \left( \left( \frac{\dot{S}}{S} \right)^2 + \frac{k}{S^2} \right)^2 \right) \\ &= -\frac{\kappa}{3} \left( \mu + 3p_r - 16c \left( \frac{\zeta}{S} \right)^2 \right). \end{aligned} \quad (3.53)$$

Combination of (3.52) with the field equations leads to

$$\begin{aligned} 0 & \stackrel{(3.49)}{=} \frac{\kappa}{3} \frac{d}{dt} \left( \mu - 3p_r + 8c \left( \frac{\zeta}{S} \right)^2 \right) \\ &= \frac{\kappa}{3} \frac{d}{dt} \left( \Sigma^\gamma_\gamma + 8c \left( \frac{\zeta}{S} \right)^2 \right) \Rightarrow \Sigma^\gamma_\gamma + 8c \left( \frac{\zeta}{S} \right)^2 = \text{const} =: \Xi. \end{aligned} \quad (3.54)$$

Thus, we obtained a *conserved quantity* similar to the one in equation (47) of [68]. The first Noether identity (3.50) takes the form

$$\begin{aligned} \frac{d}{dt} \left[ S^4 \left( \mu - 8c \left( \frac{\zeta}{S} \right)^2 \right) \right] + 4cS^2 \frac{d\zeta^2}{dt} &= \frac{1}{4} \frac{dS^4}{dt} \Sigma^\gamma_\gamma \\ \stackrel{(3.54)}{\Leftrightarrow} \frac{d}{dt} [S^4 (\Xi - \mu)] &= S^4 \frac{d\Sigma^\gamma_\gamma}{dt} + 4cS^2 \frac{d\zeta^2}{dt} + \frac{3}{4} \frac{dS^4}{dt} \Sigma^\gamma_\gamma \\ \Leftrightarrow 4 \frac{\dot{S}}{S} (\Xi - \mu) - \dot{\mu} &= 16c\zeta^2 \frac{\dot{S}}{S^3} - 8c \frac{\dot{\zeta}\zeta}{S^2} + \frac{3\dot{S}}{S} \Sigma^\gamma_\gamma \\ \Leftrightarrow 4 \frac{\dot{S}}{S} \left( \Xi - \mu - \frac{3}{4} \Sigma^\gamma_\gamma \right) - \dot{\mu} &= 8c \left( \frac{\zeta}{S} \right)^2 \left( 2 \frac{\dot{S}}{S} - \frac{\dot{\zeta}}{\zeta} \right). \end{aligned} \quad (3.55)$$

Before we proceed with the search for explicit solutions we collect the remaining field equations:

$$\begin{aligned} \chi \left( \left( \frac{\dot{S}}{S} \right)^2 + \frac{k}{S^2} \right) - (a_4 + a_6) \kappa \left( \left( \frac{\ddot{S}}{S} \right)^2 - \left( \left( \frac{\dot{S}}{S} \right)^2 + \frac{k}{S^2} \right)^2 \right) \\ = \frac{\kappa}{3} \left( \mu - 4c \left( \frac{\zeta}{S} \right)^2 \right), \end{aligned} \quad (3.56)$$

$$\begin{aligned} \chi \left( \Lambda + \frac{\ddot{S}}{S} \right) + (a_4 + a_6) \kappa \left( \left( \frac{\ddot{S}}{S} \right)^2 - \left( \left( \frac{\dot{S}}{S} \right)^2 + \frac{k}{S^2} \right)^2 \right) \\ = -\kappa \left( p_r - 4c \left( \frac{\zeta}{S} \right)^2 \right), \end{aligned} \quad (3.57)$$

$$\frac{\ddot{S}}{S} + \left( \frac{\dot{S}}{S} \right)^2 + \frac{k}{S^2} = \Lambda, \quad (3.58)$$

$$4 \frac{\dot{S}}{S} \left( \Xi - \mu - \frac{3}{4} \Sigma^\gamma_\gamma \right) - \dot{\mu} = 8c \left( \frac{\zeta}{S} \right)^2 \left( 2 \frac{\dot{S}}{S} - \frac{\dot{\zeta}}{\zeta} \right). \quad (3.59)$$

Note that the new constant  $\Lambda$  in (3.57) is defined via (3.58). Comparison of (3.58) with the Friedmann equation (1.14) reveals that  $\Lambda$  plays the same role as the usual cosmological constant. Since we did not include this additional constant in our Lagrangian right from the beginning,  $\Lambda$  might be termed *induced* cosmological constant. Now let us exploit the fact that we are allowed to set the constant  $\Xi = 0$ , which leads to an additional constraint, i.e.

$$\mu = 3p_r - 8c \left( \frac{\zeta}{S} \right)^2. \quad (3.60)$$

Subsequently eq. (3.56) turns into

$$\begin{aligned} \chi \left( \left( \frac{\dot{S}}{S} \right)^2 + \frac{k}{S^2} \right) - (a_4 + a_6) \kappa \left( \left( \frac{\ddot{S}}{S} \right)^2 - \left( \left( \frac{\dot{S}}{S} \right)^2 + \frac{k}{S^2} \right)^2 \right) \\ = \kappa \left( p_r - 4c \left( \frac{\zeta}{S} \right)^2 \right). \end{aligned} \quad (3.61)$$

The second Noether identity (3.59) reads

$$4 \frac{\dot{S}}{S} \mu + \dot{\mu} = 8c \left( \frac{\zeta}{S} \right)^2 \left( \frac{\dot{S}}{S} + \frac{\dot{\zeta}}{\zeta} \right). \quad (3.62)$$

We collect all assumptions made up to this point in table 3.4.



Table 3.1: Model assumptions.

Ansatz/Assump.	Resulting quantity/equation	Equation
$\Sigma_\alpha = \Sigma_{\alpha\beta} \eta^\beta$	Affects the form of the first field eq.	(3.10),(3.24)
$\tau_{\alpha\beta} = \mathbb{X}_{(\alpha\beta)} = 0$	Affects the form of the second field eq.	(3.16)
$T^\alpha = \frac{1}{2}Q \wedge \vartheta^\alpha$	Affects the form of the connection	(2.37),(3.28)
$Q = \frac{\xi(t,r)}{S(t)} \vartheta^{\hat{0}}$	Controls non-Riemannian features/ Affects the form of the field equations	(3.23),(3.29),(2.36), (3.30)-(3.35)
$Q = \frac{\zeta(t)}{S(t)} \vartheta^{\hat{0}}$	Controls non-Riemannian features/ Simplifies field equations	(3.23),(3.45),(2.36), (3.46)-(3.51)
$a_4 \neq -a_6$	Affects the form of the second field eq.	(3.33)
$\Xi = 0$	Relation between $\mu$ and $p_r$	(3.60)
$\Lambda$	Affects the form of the field equations	(3.57)-(3.58)

## 3.5 Solutions

### 3.5.1 $\Lambda \neq 0$ solutions

We solve equation (3.58) for nonvanishing  $\Lambda$ . This equation does not depend on the relation between the energy density and pressure and therefore can be solved independently. This ODE, after a substitution, turns into a Bernoulli ODE, which can be transformed into a linear equation. We obtain two branches for the scale factor. They are given by

$$S = \pm \frac{1}{\sqrt{2\Lambda}} \sqrt{e^{-\sqrt{2\Lambda}t} \left( 2ke^{\sqrt{2\Lambda}t} - \sqrt{2\Lambda}\varkappa_1 e^{2\sqrt{2\Lambda}t} + \sqrt{2\Lambda}\varkappa_2 \right)}, \quad (3.63)$$

where  $\varkappa_1$ , and  $\varkappa_2$  are constants. This solution for the scale factor is valid for all three possible choices of  $k$ . Let us proceed by fixing the equation of state.

We start with the most simple ansatz, i.e. with the introduction of an additional constant  $w$  into the equation of state, which parametrizes the ratio of the energy density and the pressure:

$$w \mu(t) = p_r(t). \quad (3.64)$$

Substituting (3.64) into equation (3.60) yields

$$\mu = -\frac{8c}{1-3w} \left( \frac{\zeta}{S} \right)^2. \quad (3.65)$$

The other field equations are given by

$$\begin{aligned} \chi \left( \left( \frac{\dot{S}}{S} \right)^2 + \frac{k}{S^2} \right) - (a_4 + a_6) \kappa \left( \left( \frac{\ddot{S}}{S} \right)^2 - \left( \left( \frac{\dot{S}}{S} \right)^2 + \frac{k}{S^2} \right)^2 \right) \\ = -\frac{4c\kappa}{3} \left( \frac{\zeta}{S} \right)^2 \left( \frac{1+3w}{1-3w} \right), \end{aligned} \quad (3.66)$$

$$\begin{aligned} \chi \left( \Lambda + \frac{\ddot{S}}{S} \right) + (a_4 + a_6) \kappa \left( \left( \frac{\ddot{S}}{S} \right)^2 - \left( \left( \frac{\dot{S}}{S} \right)^2 + \frac{k}{S^2} \right)^2 \right) \\ = 4c\kappa \left( \frac{\zeta}{S} \right)^2 \left( \frac{1-w}{1-3w} \right), \end{aligned} \quad (3.67)$$

$$\frac{\ddot{S}}{S} + \left( \frac{\dot{S}}{S} \right)^2 + \frac{k}{S^2} = \Lambda, \quad (3.68)$$

$$\frac{24c(1-w)}{3w-1} \left( \frac{\zeta}{S} \right)^2 \left( \frac{\dot{S}}{S} + \frac{\dot{\zeta}}{\zeta} \right) = 0. \quad (3.69)$$

Equation (3.69) has two non-trivial solution, i.e.

$$(i) \zeta = \frac{\iota}{S}, \text{ with } \iota = \text{const}, \quad \text{and} \quad (ii) w = 1. \quad (3.70)$$

Solving the field equations (3.66)-(3.68) by taking into account the first solution in eq. (3.70), we obtain constraints among the coupling constants which are summarized in table 3.2 (note that every set of parameters on the rhs corresponds to a solution of the field equations). These solutions are not very satisfactory since they either lead to vanishing post-Riemannian quantities or, in case of  $\chi = c = 0$ , to a restriction on the Lagrangian level.

Hence we switch to another ansatz for the equation of state, namely

$$w(t)\mu(t) = p_r(t). \quad (3.71)$$

Here we introduced an additional function which controls the relation between the energy density and stresses in a *dynamical* way. Hence, equation (3.69) is now given by

$$-\frac{24c}{(3w-1)^2} \left( \frac{\zeta}{S} \right)^2 \left( \frac{\dot{S}}{S} (1+3w^2-4w) + \frac{\dot{\zeta}}{\zeta} (1+3w^2-4w) + \dot{w} \right) = 0. \quad (3.72)$$

In case of an arbitrary choice of  $\zeta$ , this equation is solved by

$$w = \frac{S^2 \zeta^2 \varkappa_3 - 1}{S^2 \zeta^2 \varkappa_3 - 3}. \quad (3.73)$$

Substituting this solution for  $w$  into the remaining field equations yields additional parameter constraints, summarized in table 3.3. As one realizes immediately none of

Table 3.2: Ansatz  $\Lambda \neq 0, w = \text{const.}$ 

$\zeta$	$S$	Additional constraints
$\zeta = \frac{t}{S}$	$S$ from eq. (3.63)	$\{a_4 = a_6 = c = \chi = 0\},$ $\{a_4 = a_6 = \iota = 0, w = \frac{1}{3}\},$ $\{a_4 = a_6 = \chi = 0, w = 1\},$ $\{a_4 = a_6 = c = 0, w = \frac{1}{3}\},$ $\{a_4 = -a_6, \Lambda = 0, w = \text{const}\}$

Table 3.3: Ansatz  $\Lambda \neq 0, w = w(t).$ 

$\zeta$	$S$	Additional constraints
$\zeta$ arbitrary, $w = \frac{\zeta^2 S^2 \varkappa_3 - 1}{\zeta^2 S^2 \varkappa_3 - 3}$	$S$ from eq. (3.63)	$\{a_4 = -a_6, \Lambda = 0\},$ $\{a_4 = -a_6, \chi = 0, w = 1\},$ $\{a_4 = -a_6, \iota = \chi = 0\}$

the solutions collected in table 3.3 is of use for us. They all lead to unrealistic or forbidden restrictions among the coupling constants in our model. In the following section we therefore switch to the case with vanishing induced cosmological constant  $\Lambda$ .

### 3.5.2 $\Lambda = 0$ solutions

Solving equation (3.68) for vanishing  $\Lambda$ , yields a solution for the scale factor which depends on the constant  $k$

$$k \neq 0 : \quad S = \pm \sqrt{\frac{1}{k} (\varkappa_1 - k^2 (\varkappa_2 + t)^2)}, \quad \text{with } \varkappa_1, \varkappa_2 = \text{const}, \quad (3.74)$$

$$k = 0 : \quad S = \varkappa_1 \text{ or } S = \pm \sqrt{2\varkappa_1 (t + \varkappa_2)}, \quad \text{with } \varkappa_1, \varkappa_2 = \text{const}. \quad (3.75)$$

Motivated by the results for the  $\Lambda \neq 0$  case, we will directly start with the more general equation of state as given in (3.71). The field equations are given by eqs. (3.66)-(3.69) but with  $\Lambda = 0$ . Note that we do not fix the function  $\zeta$ . Using computer algebra we find several solutions which impose additional parameter constraints on our model. These constraints are summarized in the second part of table 3.4.

Additionally, we investigated the case in which we prescribe the solution for the function  $\zeta$  as given in equation (3.70). Then the second Noether identity (3.72) yields:

$$\dot{w} = 0. \quad (3.76)$$

Table 3.4: Ansatz  $\Lambda = 0$ ,  $w = w(t)$ .

$\zeta$	$S$	Add. constraints
$\zeta = \frac{k}{S}$ , $w = \text{const}$	$k \neq 0$ , $S$ from eq. (3.74)	$w = \frac{4cl^2\kappa + \varkappa_1\chi}{4cl^2\kappa + 3\varkappa_1\chi}$
	$k = 0$ , $S = \text{const}$ , cf. eq. (3.75)	$w = 1$
	$k = 0$ , $S$ from eq. (3.75)	$w = \frac{4cl^2\kappa + \varkappa_1^2\chi}{4cl^2\kappa + 3\varkappa_1^2\chi}$
$w = \frac{\zeta^2 S^2 \varkappa_3 - 1}{\zeta^2 S^2 \varkappa_3 - 3}$ , $\zeta$ arbitrary	$k \neq 0$ , $S$ from eq. (3.74)	$\varkappa_3 = -4 \frac{c\kappa}{\varkappa_1\chi}$
	$k = 0$ , $S = \text{const}$ , cf. eq. (3.75)	$c = 0$
	$k = 0$ , $S$ from eq. (3.75)	$\varkappa_3 = -4 \frac{c\kappa}{\varkappa_1^2\chi}$

Thus,  $w$  has to be a constant which can be determined from the remaining field equations after choosing the branch of  $S$  from equations (3.74)-(3.75). The additional parameter constraints for this branch of the model are displayed in the first part of table 3.4. It turns out that the parameter  $w$ , which controls the equation of state, is restricted by the choice of a certain set of constants in our theory, cf. the rhs in the first part of table 3.4.

### 3.5.3 Summary

Let us pause here for a moment in order to recall what we have accomplished so far. Starting from the new Lagrangian in (3.3) we successively derived the general form of the field equations in section 3.2. In section 3.3 we worked out a rather complicated set of field equations for a specific ansatz for the Weyl 1-form (3.29). In section 3.4 we switched to a time dependent ansatz for the Weyl 1-form which yields a set of coupled ordinary differential equations, reminiscent of the Friedmann equations, cf. section 1.2. With these equations at hand we were able to generate a rather broad class of exact solutions, which allow for a flexible equation of state. The resulting constraints on the parameters within our model are collected in tables 3.2–3.4. There seem to be *no* reasonable solutions in case of a non-vanishing induced cosmological constant  $\Lambda$ . Of course this statement is only correct as long as one does not allow for strong restrictions on the Lagrangian level. We focus on the solutions with *vanishing*  $\Lambda$  in the following.

In figure 3.1 we plotted the scale factor for all three possible values of  $k$  and for different values of the parameter  $\varkappa_1$ . As becomes clear from the plot at the lower rhs, we have three qualitatively different solutions depending on the value of  $k$ . As in the Friedmann case the collapsing scenario corresponds to a universe with positive spatial curvature. In figure 3.2 we plotted the function  $Q$  for the solution (3.70). This plot shows that it is possible to construct models in which  $Q$  vanishes at late stages of the universe. Thus, the non-Riemannian quantities *die out* with time in such a scenario. This is a rather desirable feature, one would expect that the spacetime we are living in nowadays is a Riemannian one. From an observational point of view this seems to be true on local scales; at least all experiments carried out so far point to this direction

[27, 28]. One possible exception is given by the recently observed anomalous acceleration of the Pioneer spacecraft [159, 160]. Although we do not investigate this effect here, we remind the reader that our model allows for both, Riemannian and non-Riemannian features. If there is evidence for non-Riemannian structures at the present time, and especially on local scales, we can implement this fact by modifying our ansatz in (3.29) and (3.45), respectively.

In comparison to the usual FLRW model we still have three distinct cases for the evolution of the scale factor, corresponding to the three different choices of  $k$ . Since one of our field equations (3.68) is very similar to the Friedmann equation we obtain the same root type behavior for the scale factor as displayed in figure 3.1. As becomes clear from equation (3.63) an induced cosmological constant would lead to inflationary solutions. In contrast to our old model [68] we were not able to find meaningful parameter constraints for this branch of the model. This drawback might be relaxed if one switches to another ansatz for the Weyl 1-form  $Q$ . Most interestingly the non-Riemannian quantities lead to a contribution to the total energy density of the universe as shown in (3.65). Thus, the scaling behavior of the energy density is no longer determined by the evolution of the scale factor alone. Instead, it additionally depends on our ansatz for the Weyl 1-form. We are going to exploit this fact in the following sections in which we derive the magnitude-redshift relation. One should also keep in mind that an ansatz with a position dependent Weyl 1-form might serve as an interesting source of the observed inhomogeneities in the microwave background.

Recently there has been much interest in exotic equations of state in the literature [108]-[119]. The equations of state considered in most of these works can be summarized under the name unified dark matter models (UDM), since they aim for a description of the dark matter and dark energy by using a single fluid. Such a fluid changes its character during the evolution of the universe, i.e. from a behavior similar to pressureless matter to a cosmological constant like behavior and vice versa. A model which recently has received much attention is the so-called Chaplygin gas, which has the equation of state  $p = -A\mu^\alpha$ , where  $A$  and  $\alpha$  are constants. Such an equation of state was already considered much earlier, cf. [107]. However, the availability of the supernova data and the connection with some higher dimensional cosmological models [113] led to a renewed interest in such an ansatz. Note that our ansatz in (3.71) also allows for Chaplygin like equations of state. Nevertheless our model encompasses sufficiently many parameters. Therefore we focus on the solutions found in sections 3.5.1 and 3.5.2 in the following. Note that there also arose some criticism concerning Chaplygin gas models with respect to the generation of oscillations in the matter power spectrum [119]. The main objection is that the allowed parameter space of Chaplygin gas scenarios, when compared to the results of the 2dF galaxy redshift survey [76], is confined to a region in which the models are virtually equal to the usual FLRW model.

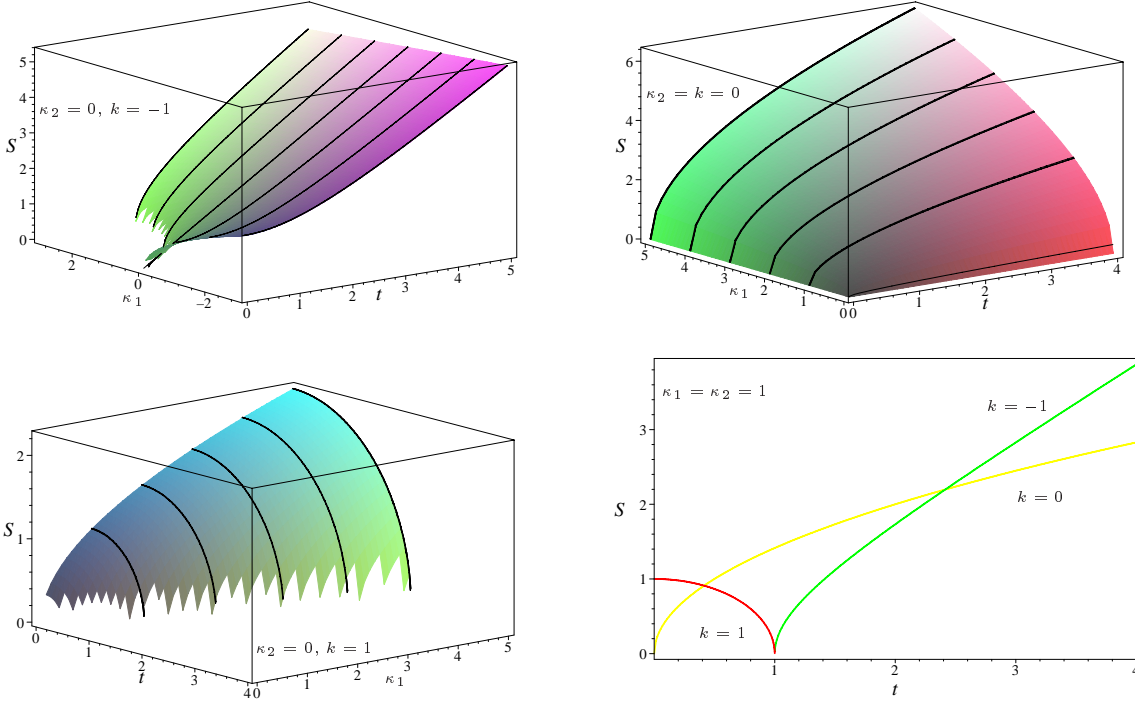


Figure 3.1: Scale factors in case of the  $\Lambda = 0$  branch of the model (we always select the positive sign in front of the scale factor, cf. eqs. (3.74)–(3.75)).

### 3.6 Magnitude-redshift relation

In this section we derive the magnitude-redshift relation. Therefore we make use of the field equations (3.57)–(3.58), (3.61)–(3.62), and the relation between energy-density and pressure (3.60). In sections 1.4.1–1.4.2 we characterized the dependence of the magnitude-redshift relation on the field equations. Since we also made use of the Robertson-Walker metric in our new model we are allowed to use relation (1.38). Hence, our next aim is to express the Hubble rate in terms of the density parameters. From equation (3.58) we infer

$$H^2 = \Lambda - \frac{\ddot{S}}{S} - \frac{k}{S^2}. \quad (3.77)$$

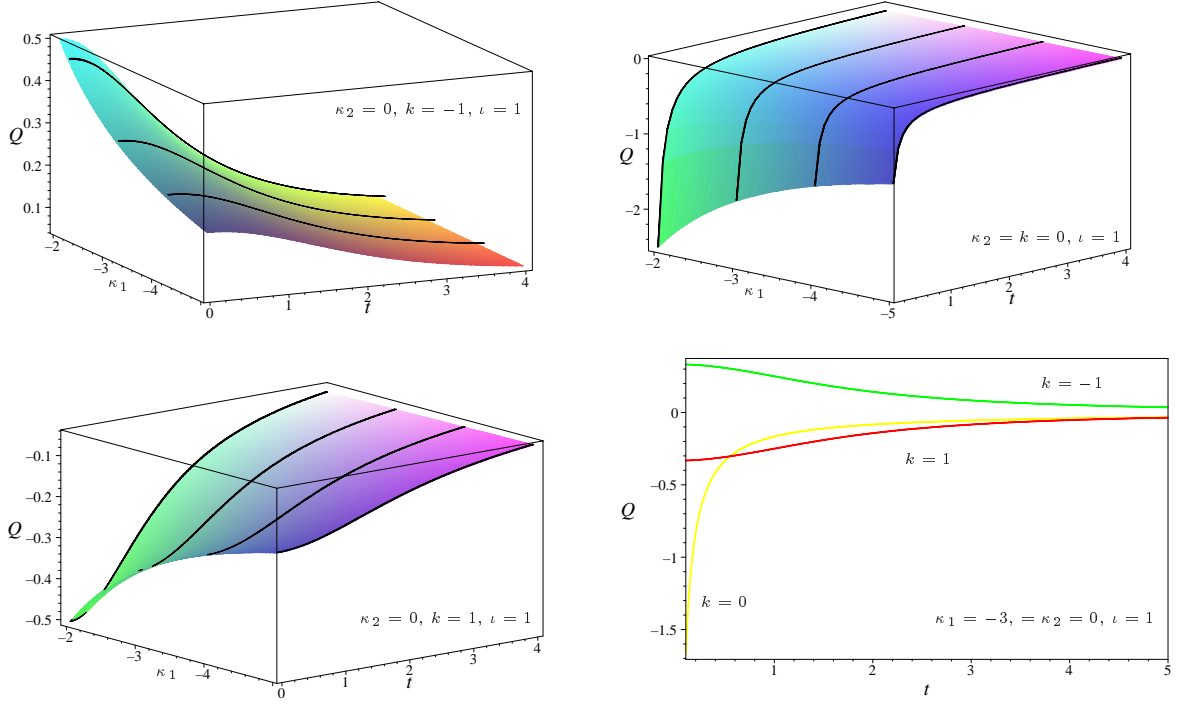


Figure 3.2: Weyl 1-form  $Q$  in case of the  $\Lambda = 0$ ,  $\zeta = \frac{l}{S}$  branch of the model (we always select the positive sign in front of the scale factor, cf. eqs. (3.74)–(3.75)).

In order to eliminate the second order term we make use of equation (3.57). Substituting the solution for  $\ddot{S}/S$  from this equation into (3.77) leads to

$$H^2 = \frac{(\Lambda^2 S^2 - 2\Lambda k) \kappa (a_4 + a_6) - \chi k + \kappa S^2 p_r - 4\kappa c \zeta^2}{(2\kappa\Lambda (a_4 + a_6) + \chi) S^2} \quad (3.78)$$

$$= \frac{H_0^2}{(2\kappa\Lambda (a_4 + a_6) + \chi)} \left\{ \kappa (a_4 + a_6) \left[ \frac{\Lambda^2}{H_0^2} - \frac{2\Lambda k}{H_0^2 S_0^2} \left( \frac{S_0}{S} \right)^2 \right] - \frac{\chi k}{H_0^2 S_0^2} \left( \frac{S_0}{S} \right)^2 + \frac{\kappa p_r}{H_0^2} - \frac{4\kappa c \zeta^2}{H_0^2 S_0^2} \left( \frac{S_0}{S} \right)^2 \right\} \quad (3.79)$$

$$\stackrel{(1.35)}{=} \frac{H_0^2}{(2\kappa\Lambda (a_4 + a_6) + \chi)} \left\{ \kappa (a_4 + a_6) [H_0^2 \Omega_{\Lambda 0}^2 - 2\Lambda \Omega_{k0} (1+z)^2] - \chi \Omega_{k0} (1+z)^2 + \frac{\kappa p_r}{H_0^2} - \frac{4\kappa c \zeta^2}{H_0^2 S_0^2} (1+z)^2 \right\}. \quad (3.80)$$

Here we introduced the density parameters  $\Omega_k := \frac{k}{H^2 S^2}$  and  $\Omega_\Lambda := \frac{\Lambda}{H^2}$ . Subsequently, we have to choose an equation of state and an appropriate ansatz for  $\zeta$ . We choose  $p = w\mu$  with  $w = \text{const}$ , cf. eq. (3.64), and use the solution for  $\mu$  obtained in equation (3.65),

i.e.  $\mu = -\frac{8c}{1-3w} \left(\frac{\zeta}{S}\right)^2$ :

$$H^2 = \frac{H_0^2}{(2\kappa\Lambda(a_4 + a_6) + \chi)} \left\{ \kappa(a_4 + a_6) [H_0^2\Omega_{\Lambda 0}^2 - 2\Lambda\Omega_{k0}(1+z)^2] - \chi\Omega_{k0}(1+z)^2 - \frac{4\kappa c\zeta^2}{H_0^2 S_0^2} \left(\frac{1-w}{1-3w}\right) (1+z)^2 \right\}. \quad (3.81)$$

Using the solution for  $\zeta$  from equation (3.70), i.e.  $\zeta = \iota/S$  with  $\iota = \text{const}$ , we have

$$H^2 = \frac{H_0^2}{(2\kappa H_0^2\Omega_{\Lambda 0}(a_4 + a_6) + \chi)} \left\{ \kappa(a_4 + a_6) [H_0^2\Omega_{\Lambda 0}^2 - 2H_0^2\Omega_{\Lambda 0}\Omega_{k0}(1+z)^2] - \chi\Omega_{k0}(1+z)^2 - 4\Omega_{\zeta 0}(1+z)^4 \left(\frac{1-w}{1+3w}\right) \right\}, \quad (3.82)$$

here we introduced the new density parameter  $\Omega_{\zeta 0} := \frac{\kappa c \iota^2}{H^2 S^4}$  in the last equation. This density parameter clearly dominates at high redshifts due to its  $\sim z^4$  scaling behavior, cf. the last term in (3.82).

**Special case** For a vanishing induced cosmological constant  $\Lambda = 0$ , equation (3.82) turns into

$$H^2 = \frac{H_0^2}{\chi} \left[ 4(1+z)^4\Omega_{\zeta 0} \left(\frac{w-1}{1-3w}\right) - \chi\Omega_{k0}(1+z)^2 \right]. \quad (3.83)$$

If we substitute this expression into equation (1.38) we can derive the luminosity distance analogously to (1.48), i.e.

$$d_{\text{luminosity}}(z, H_0, \Omega_{k0}, \Omega_{\zeta 0}, \chi, w) = \frac{(1+z)}{H_0\sqrt{|\Omega_{k0}|}} \Theta \left[ \sqrt{\frac{|\Omega_{k0}|}{\chi}} \int_0^z G[\tilde{z}] d\tilde{z} \right]. \quad (3.84)$$

Here  $G[\tilde{z}] := \left[ 4(1+\tilde{z})^4\Omega_{\zeta 0} \left(\frac{w-1}{1-3w}\right) - \chi\Omega_{k0}(1+\tilde{z})^2 \right]^{-\frac{1}{2}}$ , and  $\Theta$  is defined as in eq. (1.49). Hence the magnitude-redshift relation, cf. eq. (1.61), is given by

$$\begin{aligned} m(z, H_0, \Omega_{\zeta 0}, \Omega_{k0}, w, M, \chi) &= \mathcal{M} + 5 \log \{ H_0 d_{\text{luminosity}}(z, H_0, \Omega_{\zeta 0}, \Omega_{k0}, \chi, w) \} \\ &= \mathcal{M} + 5 \log \left\{ \frac{(1+z)}{\sqrt{|\Omega_{k0}|}} \Theta \left[ \sqrt{\frac{|\Omega_{k0}|}{\chi}} \int_0^z G[\tilde{z}] d\tilde{z} \right] \right\}. \end{aligned} \quad (3.85)$$

In contrast to the FLRW model, see eq. (1.36), there is no simple relation between the density parameters. Therefore, we cannot eliminate the density parameter  $\Omega_k$  in the equation for the magnitude. In case of a flat model, equation (3.85) reduces to

$$m(z, \Omega_{\zeta 0}, w, M, \chi) = \mathcal{M} + 5 \log \left\{ \frac{(1+z)}{\chi} \left[ \int_0^z \left[ 4(1+\tilde{z})^4\Omega_{\zeta 0} \left(\frac{w-1}{1-3w}\right) \right]^{-\frac{1}{2}} d\tilde{z} \right] \right\}. \quad (3.86)$$



Table 3.5: SN Ia data sets.

Symbol	Number of SN	Reference	Comments
I	18	p. 571, [127, 121]	Calán/Tololo survey
II	42	p. 570, [121]	Supernova Cosmology Project
III	10	p. 1021, [126]	High-z Supernova Search Team
IV	10	p. 1020, [126]	Same as III but MLCS method
V	1	[125]	Farthest SN Ia observed to date
VI	27	p. 1035, [126]	Low-redshift MLCS/template

## 3.7 Numerical results

In this section we present the numerical results obtained by fitting the magnitude-redshift relations (1.51) and (3.85) to a SN Ia data set. We start with a collection of the available data sets. Parts and combinations of these sets were used by different groups to determine the cosmological parameters.

### 3.7.1 Data sets

In table 3.5 we collected the number of supernovae and the references which contain the actual data. These data sets are not directly comparable. Perlmutter et al. [121] provide the effective magnitude  $m_B^{\text{eff}}$  in the B band, while Riess et al. [126] use the so-called distance modulus<sup>4</sup>  $\mu$ . As shown by Wang [137] it is possible to find a relation between these two data sets by comparing a sample of 18 supernovae published by both groups. The definition of the magnitude given in equation (1.61) is compatible with the definition used by Perlmutter et al., and related to the definition of Riess et al. via

$$m = M + \mu = M + 5 \log d_{\text{luminosity}} + 25 = \mathcal{M} + 5 \log H_0 d_{\text{luminosity}}. \quad (3.87)$$

As shown in [137] we have to choose  $M = -19.33 \pm 0.25$  in order to transform the different data sets into each other. This numerical value is obtained from the data points which were measured by the MLCS method of Riess et al., cf. IV in table 3.5. Note that there is an ongoing discussion about the applicability of certain measurement methods and the resulting data sets, cf. [140] e.g. Since these experimental questions lie beyond the scope of this work we have to rely on the data sets provided by the experts in this field. In the following we make use of the data set of Wang which contains 92 data points. This set represents a compilation of the sets I, II, IV, and VI, cf. table 3.5, from which some outliers were removed. The complete data set is displayed in table E.1 on page 145.

<sup>4</sup>Not to be confused with the energy-density in the field equations.

Table 3.6: Grids used for minimization.

Parameters	[Interval, Stepsize]
$\{\Omega_{m0}, \Omega_{\lambda0}\}$	$\{[-2 \dots 4, 0.01], [-2 \dots 4, 0.01]\}$
$\{\Omega_{k0}, \Omega_{\zeta0}, \chi, w\}$	$\{[-2 \dots 4, 0.01], [-1 \dots 1, 0.01], 1, [-1 \dots 0, 0.1]\}$

### 3.7.2 Fitting method

Since we aim for results comparable to the analysis of the combined data set by Wang [137], we are going to minimize [35, 36, 37]<sup>5</sup>

$$\chi^2 := \sum_{i=1}^{92} \frac{[\mu_i^{\text{theory}}(z_i | \text{parameters}) - \mu_i^{\text{measured}}]^2}{\sigma_{\mu i}^2 + \sigma_{mz i}^2}, \quad (3.88)$$

in order to obtain the best-fit parameters within the FLRW and the Weyl-Cartan model. Here  $\mu_i^{\text{theory}}$  denotes the distance modulus at a certain redshift  $z_i$  as defined in (3.87). It can be calculated for a specific choice of the parameters entering the magnitude-redshift relation, cf. eqs. (1.51) and (3.85). The error of the measured distance modulus  $\mu_i^{\text{measured}}$  is given by  $\sigma_{\mu i}$ . The dispersion in the distance modulus  $\sigma_{mz}$  due to the dispersion in the galaxy redshift,  $\sigma_z$ , can be calculated iteratively from

$$\sigma_{mz} := \frac{5}{\ln 10} \left[ \frac{1}{d_{\text{luminosity}}} \frac{\partial d_{\text{luminosity}}}{\partial z} \right] \sigma_z \quad (3.89)$$

according to Wang, cf. equation (13) of [137]. In order to determine the minima of (3.88) we perform a brute force calculation on the grids listed in table 3.6.

Note that there is an ongoing discussion about the appropriate fitting method in the literature, cf. [136] e.g. Although the above fitting method might appear simple in the eyes of most experimentalists, we subscribe to the point of view that any result which cannot be revealed by a simple analysis of the data is inherently suspicious.

### 3.7.3 Best-fit parameters

In table 3.7 and table 3.8 we collected the best-fit parameters obtained by the method described in the previous section. It should be remarked that we did not impose any constraints on our parameters, like spatial flatness, e.g., when performing our search. In figure 3.3 and figure 3.4 we plotted the corresponding distance modulus versus redshift relation together with the data set of Wang from appendix E.4. The  $\chi^2$ -distributions displayed in figure 3.3 and figure 3.4 correspond to the plane encompassing the best-fit parameters found on our grid, i.e. F13 for the FLRW model and C2 for the Weyl-Cartan model. In both figures the 95.4% confidence level corresponds to the outer boundary

<sup>5</sup>Not to be confused with the coupling constant  $\chi$  in the field equations.

of the ellipse. In table 3.9 and table 3.10 we collected the results of several other groups who performed a similar analysis within the FLRW as well as in non-standard scenarios. These collections are by no means exhaustive, therefore we apologize for not having mentioned all the works which are devoted to this subject.

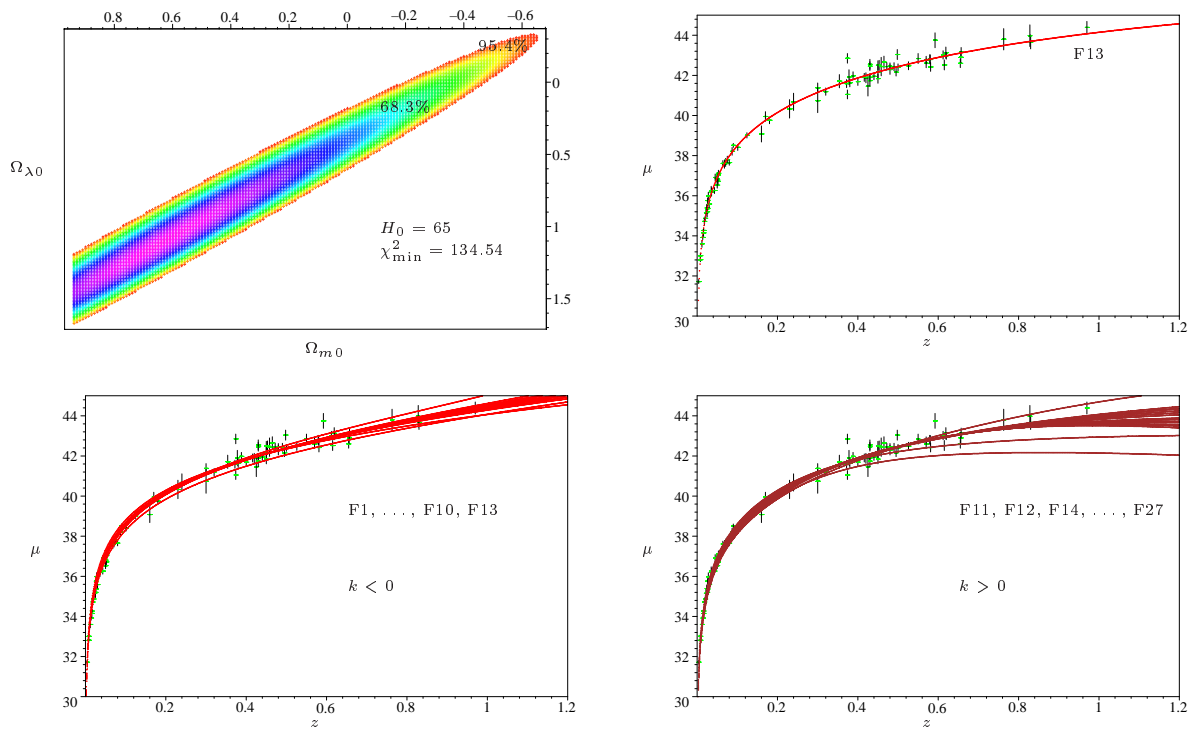


Figure 3.3:  $\chi^2$ -distribution in the  $(\Omega_{m0}, \Omega_{\lambda0})$  plane and magnitude-redshift relation in case of the standard model. On the top lhs the  $\chi^2$ -distribution in the  $H_0 = 65$  plane is shown which also contains the best-fit parameter set F13. On the top rhs we plotted the distance modulus versus the redshift for the best-fit parameter set. The green dots correspond to the experimental data for 92 type Ia SNe as contained in the data set of Wang. In the two other figures we plotted the distance modulus versus the redshift for the other parameter sets in table 3.7.

Table 3.7: Best-fit parameters (FLRW model).  $[H_0] = \text{km s}^{-1}\text{Mpc}^{-1}$ .

<b>Symbol</b>	$H_0$	$\Omega_{m0}$	$\Omega_{\lambda 0}$	$\chi^2$	$\chi^2_{\nu}$	$q_0$
F1	50	0.45	-2.00	401.04	4.50	2.22
F2	54	-0.60	-2.00	256.81	2.88	1.70
F3	55	-0.81	-2.00	230.86	2.59	1.59
F4	56	-1.00	-2.00	208.73	2.34	1.50
F5	57	-1.18	-2.00	190.31	2.13	1.41
F6	58	-1.34	-2.00	175.50	1.97	1.33
F7	59	-2.00	-2.00	188.04	2.11	1.00
F8	60	-1.15	-1.49	155.83	1.75	0.91
F9	61	-0.64	-0.79	148.80	1.67	0.47
F10	62	-1.14	-1.21	145.58	1.63	0.64
F11	63	1.02	1.29	142.53	1.60	-0.78
F12	64	3.10	3.35	233.03	2.61	-1.80
F13	65	0.63	1.10	134.54	1.51	-0.78
F14	66	0.80	1.40	134.91	1.51	-1.00
F15	67	0.92	1.63	137.02	1.53	-1.17
F16	68	0.99	1.80	140.98	1.58	-1.30
F17	69	1.04	1.94	146.84	1.64	-1.42
F18	70	1.07	2.05	154.66	1.73	-1.51
F19	72	1.06	2.17	176.32	1.98	-1.64
F20	73	1.04	2.20	190.23	2.13	-1.68
F21	74	1.02	2.23	206.18	2.31	-1.72
F22	75	0.98	2.23	224.21	2.51	-1.74
F23	76	0.95	2.24	244.30	2.74	-1.76
F24	77	0.91	2.23	266.47	2.99	-1.77
F25	78	0.87	2.22	290.71	3.26	-1.78
F26	79	3.05	3.68	733.20	8.23	-2.15
F27	80	0.13	1.45	374.68	4.20	-1.38

Table 3.8: Best-fit parameters (Weyl-Cartan model).  $[H_0] = \text{km s}^{-1}\text{Mpc}^{-1}$ .

Symbol	$H_0$	$\Omega_{k0}$	$\Omega_{\zeta 0}$	$\chi$	$w$	$\chi^2$	$\chi_\nu^2$	$q_0$
C1	65	-1.07	0.05	1.00	-0.80	138.034	1.56	-0.109
C2	66	-1.03	0.05	1.00	-0.90	138.028	1.56	-0.110
C3	67	-1.01	0.03	1.00	-0.10	138.034	1.56	-0.111
C4	69	-0.95	0.04	1.00	-0.60	138.056	1.56	-0.106
C5	70	-0.92	0.04	1.00	-0.70	138.034	1.56	-0.105
C6	71	-0.90	0.03	1.00	-0.20	138.031	1.56	-0.111
C7	74	-0.83	0.04	1.00	-0.80	138.039	1.56	-0.113
C8	80	-0.71	0.03	1.00	-0.50	138.035	1.56	-0.112

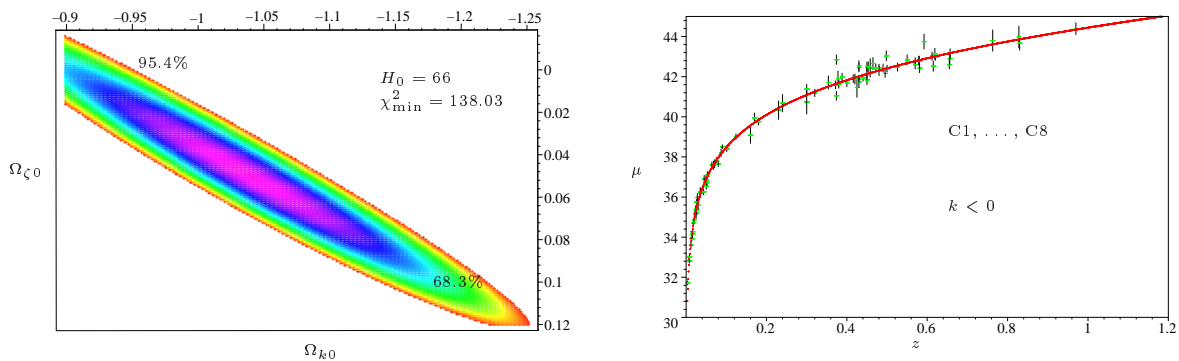


Figure 3.4:  $\chi^2$ -distribution in the  $(\Omega_{k0}, \Omega_{\zeta 0})$  plane and magnitude-redshift relation in case of the Weyl-Cartan model. On the lhs the  $\chi^2$ -distribution in the  $H_0 = 66$  plane is shown, which contains the best-fit parameter set C2. On the rhs we plotted the distance modulus versus the redshift for all parameter sets from table 3.8. Since all of these sets fit the data very well the eight different curves appear as a single line at the selected resolution.

## 3.8 Summary

### Fitting results

As we have shown in the previous section it is possible to describe the observational data within both models. It is noteworthy that, without any additional constraints, a closed FLRW model is favored by the data, as can be read off from the best-fit parameters F13 in table 3.7. In contrast, the best-fit solution within the Weyl-Cartan model, i.e. set C2 in table 3.8, corresponds to an open universe. For the FLRW model our results comply with the ones found by Wang in [137]. If one imposes the condition of spatial flatness, the best-fit parameters are given by (F28, 65, 0.29, 0.71, 135.26, 1.51, -0.56)

Table 3.9: Best-fit parameters other groups (FLRW model).

Symbol	Ref.	Best-fit parameters	Comment
S1	[124]	$\{\Omega_{m0} = -0.2, \Omega_{\lambda0} = 0\}$	
S2	[124]	$\{\Omega_{m0} = 0.4, \Omega_{\lambda0} = 0.6\}$	
P1	[121]	$\{\Omega_{m0} = 0.28, \Omega_{\lambda0} = 0.72\}$	
R1	[126]	$\{\Omega_{m0} = 0.24, \Omega_{\lambda0} = 0.72\}$	MLCS
R2	[126]	$\{\Omega_{m0} = 0.2, \Omega_{\lambda0} = 0.8\}$	Template
G1	[134]	$\{\Omega_{m0} = -0.1, \Omega_{\lambda0} = 0\}$	
G2	[134]	$\{\Omega_{m0} = 0.4, \Omega_{\lambda0} = 0.6\}$	MLCS
G3	[134]	$\{\Omega_{m0} = 0.3, \Omega_{\lambda0} = 0.7\}$	Template
V1	[130]	$\{\Omega_{m0} = 0.28, \Omega_{\lambda0} = 0.72, \mathcal{M} = 23.94\}$	
V2	[130]	$\{\Omega_{m0} = 0.79, \Omega_{\lambda0} = 1.41, \mathcal{M} = 23.91\}$	
V15	[129]	$\{\Omega_{m0} = 0.33, \Omega_{\lambda0} = 0\}$	1997ff included
W1	[137]	$\{H_0 = 65, \Omega_{m0} = 0.7, \Omega_{\lambda0} = 1.2\}$	Combined data set

$[H_0] = \text{km s}^{-1}\text{Mpc}^{-1}$ .

within in the FLRW model, and (C9, 69, 0, -0.28, 1, -0.5, 292.821, 3.32, 1) within the Weyl-Cartan model<sup>6</sup>. Hence, as soon as we assume that the universe is flat we are not able to find parameters which fit the data within our new model, in contrast to the FLRW model where the assumption of spatial flatness worsens the fit only slightly. Therefore we conclude that our model does not support a flat universe, at least not within the parameter intervals we considered here, cf. table 3.6. Note that the fit F28 is compatible with the current cosmological concordance model which encompasses about 30% of matter and a dark energy contribution of about 70%.

### Deceleration factor

The Hubble rate (3.83) enables us to derive the deceleration parameter within the Weyl-Cartan model. With the help of (1.59) we find

$$q = \frac{4\Omega_{\zeta 0} (w - 1) (1 + z)^2}{4\Omega_{\zeta 0} (w - 1) (1 + z)^2 + \chi\Omega_{k0} (3w - 1)}. \quad (3.90)$$

Therefore the best-fit sets F13 and C2, together with (1.58) and (3.90), predict a universe which presently undergoes an accelerating phase of expansion. In case of the Weyl-Cartan model the current value of the deceleration parameter is roughly seven times smaller than in the FLRW case. Figure 3.6 provides an overview of the sign of the deceleration factor in the FLRW and in the Weyl-Cartan model. In case of the latter we

<sup>6</sup>Here we use the same notation as in table 3.7 and table 3.8.

Table 3.10: Best-fit parameters other groups (non-standard models).

Symbol	Ref.	Best-fit parameters	Comment
B1	[135]	$\{\Omega_{m0} = 0.3, \Omega_{\text{Rigid}0} = 0.7\}$	Conformal model
V3	[130]	$\{\Omega_{m0} = 0.49, \Omega_{\lambda0} = 0.51, \mathcal{M} = 23.97\}$	$\lambda \sim S^{-2}$
V4	[130]	$\{\Omega_{m0} = 1.86, \Omega_{\lambda0} = 1.52, \mathcal{M} = 23.95\}$	$\lambda \sim S^{-2}$
V5	[130]	$\{\Omega_{m0} = 0.4, \Omega_{\lambda0} = 0.6, \mathcal{M} = 23.96\}$	$\lambda \sim H^2$
V6	[130]	$\{\Omega_{m0} = 0.98, \Omega_{\lambda0} = 1.53, \mathcal{M} = 23.91\}$	$\lambda \sim H^2$
V7	[130]	$\{\Omega_{m0} = 0.4, \Omega_{\lambda0} = 0.6, \mathcal{M} = 23.96\}$	$\lambda \sim \mu$
V8	[130]	$\{\Omega_{m0} = 1.62, \Omega_{\lambda0} = 1.59, \mathcal{M} = 23.93\}$	$\lambda \sim \mu$
V9	[128]	$\{\Omega_{m0} = 0.54, \Omega_{\lambda0} = 0.46, \mathcal{M} = 24.03\}$	Variable $\lambda$
V10	[128]	$\{\Omega_{m0} = 1.76, \Omega_{\lambda0} = 1.34, \mathcal{M} = 24.03\}$	Variable $\lambda$
V11	[129]	$\{\Omega_{m0} = 0.79, \Omega_{\phi0} = 1.41, w_{\phi} = -1\}$	Quintessence model
V12	[129]	$\{\Omega_{m0} = 0.65, \Omega_{\phi0} = 1.22, w_{\phi} = -1\}$	Quintess. model +1997ff
V13	[129]	$\{\Omega_{m0} = 0.52, \Omega_{\lambda0} = 0.48\}$	$\lambda \sim H^2$ +1997ff
V14	[129]	$\{\Omega_{m0} = 0.6, \Omega_{\lambda0} = 0.4\}$	$\lambda \sim S^{-2}$ +1997ff
V16	[129]	$\{\Omega_{\lambda0} = -0.358, z_{\text{max}} = 5\}$	QSSC model
M1	[116]	$\{\Omega_{M0}^* = 0.26, \alpha = 0.43, H_0 = 72\}$	Chaplygin gas
T1	[139]	$\{z_1 = 0.08, H_0^{II}/H_0^I = 0.87, \Omega_0^I = 0.3, H_0^I = 64, \Omega_0^{II} = 0.6, \lambda_0^{II} = 0.3\}$	Model with local void

$[H_0] = \text{km s}^{-1} \text{Mpc}^{-1}$ .

plotted the distribution in the parameter plane which contains the best-fit C2. Another interesting conclusion can be drawn from the contour lines of the deceleration factor. As displayed in the plot on the top lhs of figure 3.5 the contour lines for a constant deceleration factor within the  $(\Omega_{m0}, \Omega_{\lambda0})$  parameter plane of the FLRW model are nearly perpendicular to the ones for constant  $\Omega_{k0}$ . Hence, if we assume that we can measure  $\Omega_{k0}$  via an independent cosmological test, by studying the fluctuations of the CMB [11, 21, 163, 164], e.g., then we are able to pin down the pair  $(\Omega_{m0}, \Omega_{\lambda0})$  via the intersection of the confidence intervals. The situation within the new model is similar that in the FLRW case, i.e. the curves for constant  $q_0$  and  $\Omega_{k0}$  intersect each other at a non-zero angle. Figure 3.5 contains plots for five different choices of the equation of state parameter  $w$ . As we can see from the plot at the bottom lhs only the choice  $w = 1$  corresponds to a degenerated situation. In this case the deceleration parameter vanishes according to (3.90).

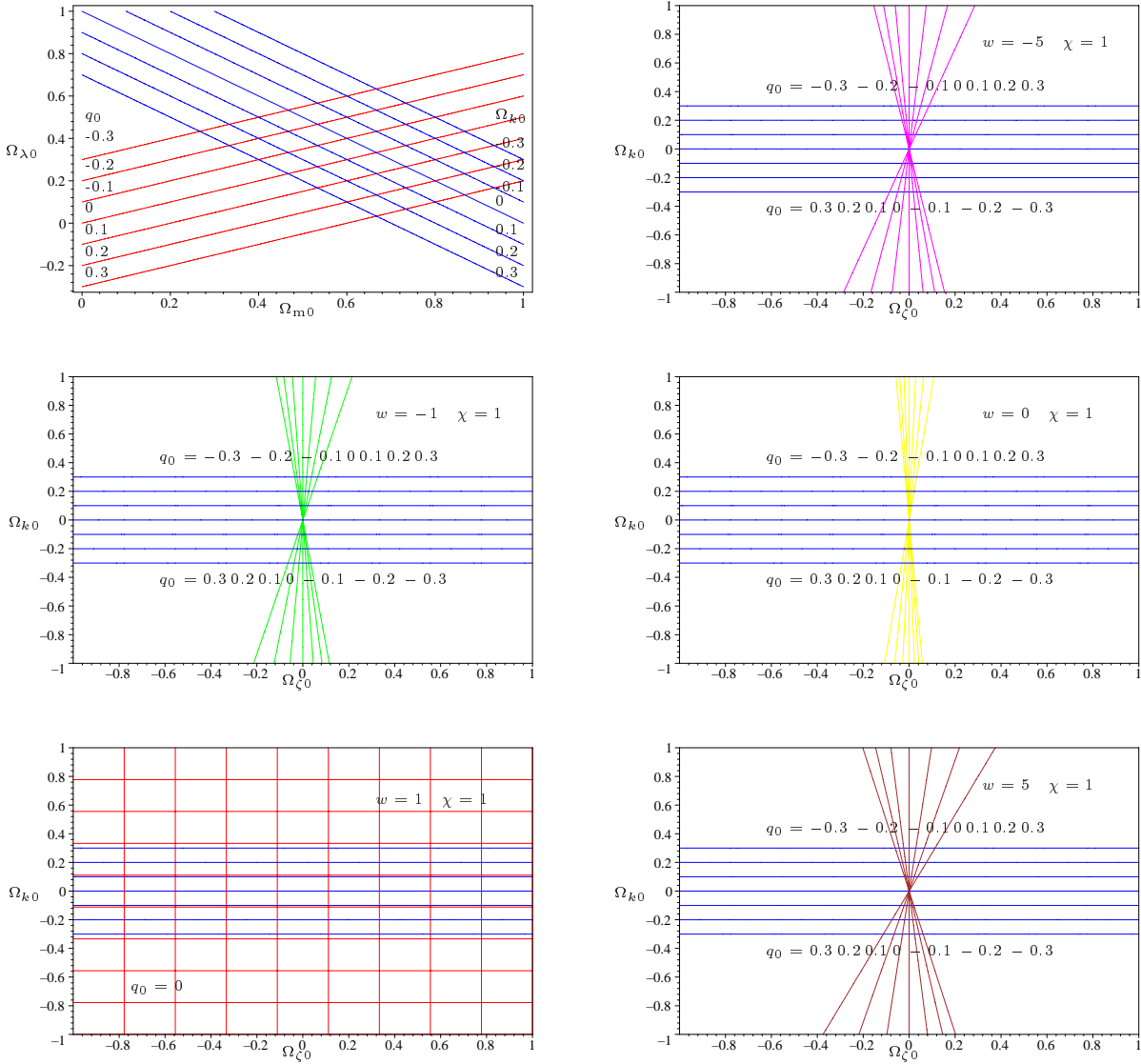


Figure 3.5: Contour lines of the deceleration parameter  $q_0$  and the density parameter  $\Omega_{k0}$  in the  $(\Omega_{m0}, \Omega_{\lambda0})$  and  $(\Omega_{\zeta0}, \Omega_{k0})$  plane, respectively. The figure on the top left corresponds to the standard model which contains only ordinary matter with  $w = 0$  and a contribution from the cosmological constant. The other figures belong to the Weyl-Cartan model in case of different choices of the equation of state parameter  $w$  and a vanishing induced cosmological constant. Note that in case of  $w = 1$  the whole red grid belongs to  $q_0 = 0$ . Since the analysis of the CMB data yields  $\Omega_{k0}$  and the supernova data put a constraint on  $q_0$ .



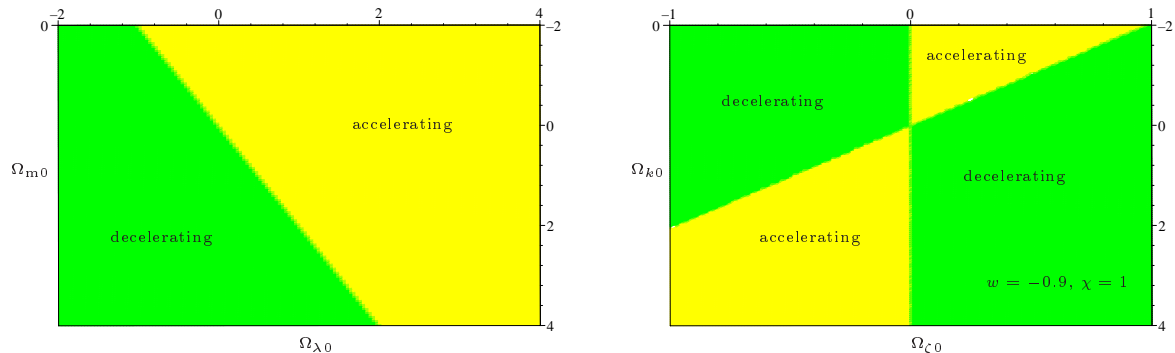


Figure 3.6: Sign of the deceleration factor  $q_0$  in the density parameter plane for the standard FLRW model (lhs) and for the Weyl-Cartan model (rhs).

### Other groups

As we have shown in sections 1.4.2 and 3.6, the magnitude-redshift relation depends on several assumptions. Especially its strong dependence on the underlying field equations renders it a useful tool to discriminate between different cosmological models. In tables 3.9 and 3.10 we collected the results of several other groups who used this relation within the FLRW as well as in non-standard models. It becomes clear from table 3.9 that in addition to the model dependence of the magnitude-redshift relation, the estimates for the cosmological parameters strongly depend on the data set used for fitting. Especially some of the early best-fit parameter sets, cf. S1 and G1 in table 3.9, e.g., correspond to unphysical models. The situation for the non-standard models listed in 3.10 is similar. As one infers from this table the parameters strongly depend on the underlying model and data set. Although it seems to be possible to describe the supernova data equally well within several of these scenarios, the main benefit of the cosmological standard model consists in its simplicity and its fit quality. Additionally, only a small number of cosmological tests have been worked out for all of the alternative models. Any serious competitor model has to pass the same cosmological tests as the FLRW model, cf. [93, 94, 95, 96, 100, 101, 102, 103]. It is noteworthy that nearly all groups come to the same result that a non-vanishing cosmological constant is inevitable for the description of the supernova data within the FLRW model. This conclusion is supported by our own results displayed in table 3.7.

### Outlook

Let us sum up and present an outlook before we investigate an interesting subcase of our model in the next section. In figure 3.7 we plotted the distance modulus versus the redshift up to  $z = 2$ . The upper curve on the lhs corresponds to the best-fit C2 within the Weyl-Cartan model, the other curves belong to the FLRW model. We infer that the supernovae at high redshift will appear dimmer within our model than in the FLRW case. The data point at  $z = 1.7$  corresponds to the farthest known supernova 1997ff

reported by Riess et al. in [125]. Despite its poor statistical significance this supernova seems to favor the best-fit FLRW model F13. Due to the large uncertainties we did not include 1997ff in our fitting procedure. Even the best-fit flat model F28 seems not to fit the data of 1997ff. A possible magnification of 1997ff by gravitational lensing was discussed by Mörtzell et al. in [148]. It is too early to make a definite statement at this point, one has to wait until more data at high redshift becomes available. As we can see from the rhs in figure 3.7, a survey at high redshifts, like SNAP [152, 153] e.g., should enable us to discriminate between the models C2 and F13.

In addition to the magnification due to gravitational lensing there is also an ongoing discussion about a possible dimming of the type Ia SNe via photon-axion oscillations, cf. [144]-[147]. Although such a mixing does not remove the need for a dark energy component it could in principle relax the bound on the equation of state of such a component, which has to be very close to the one of the cosmological constant in the standard model [131, 133, 138, 142].

One should clearly stress that our present model cannot be thought of as a serious competitor of the FLRW model, at least not for late stages of the universe. Of course the main objection is related to the material content, which is just a single component fluid with an equation of state similar to that of a cosmological constant. Another objection is connected with the fact that our model is limited to a specific redshift interval for certain parameter combinations. This becomes clear if one substitutes the best-fit parameters from table 3.8 into the expression for the expansion rate into equation (3.83). Since there seem to be no parameters which yield a positive expansion rate even at intermediate redshifts one has to replace the model, or at least the simple equation of state, guaranteeing compatibility with observations. Since this is not desirable we investigate a promising modification of the model in the next section.

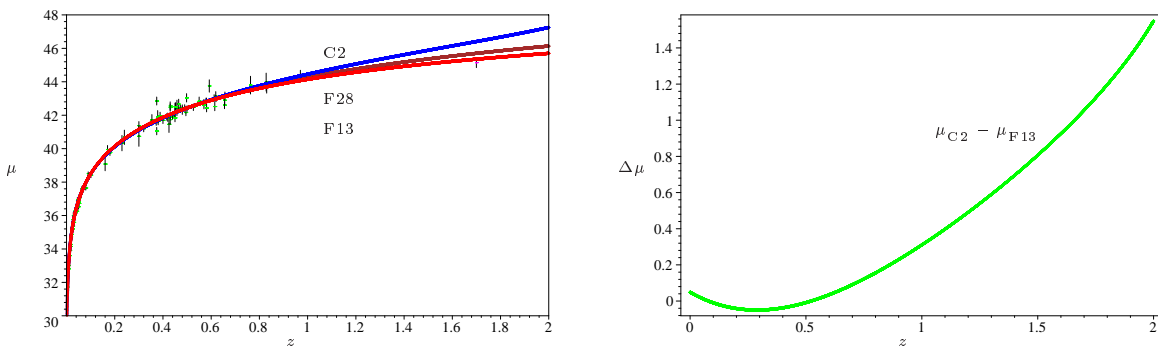


Figure 3.7: On the lhs we plotted the distance modulus versus the redshift for the best-fit models F13, F28, and C2 up to  $z = 2$ . As one can see from the rhs the difference between both models grows with the redshift.

### 3.9 Alternative approach

In the following we constrain our model to a certain parameter choice in the Lagrangian (3.3) right from the beginning. As becomes clear from the set of field equations, cf. also appendix E.2, the choice  $a_4 = -a_6$  leads to a very simple set of equations. Equation (3.49) is identically fulfilled and the rest of the field equations becomes equivalent to eqs. (1.13)-(1.14). The field equations are now given by

$$\left(\frac{\dot{S}}{S}\right)^2 + \frac{k}{S^2} = \frac{\kappa}{3\chi} \left( \mu - 4c \left(\frac{\zeta}{S}\right)^2 \right), \quad (3.91)$$

$$2\frac{\ddot{S}}{S} + \left(\frac{\dot{S}}{S}\right)^2 + \frac{k}{S^2} = -\frac{\kappa}{\chi} \left( p - 4c \left(\frac{\zeta}{S}\right)^2 \right). \quad (3.92)$$

These are the ordinary Friedmann equations with an additional contribution to the energy density on the rhs. The only change is due to the Noether identity, cf. eq. (3.50), which is now given by

$$\frac{d}{dt} (\mu S^4 - 8c (S\zeta)^2) + 4c S^2 \frac{d\zeta^2}{dt} = \frac{1}{4} \frac{dS^4}{dt} (\mu - 3p). \quad (3.93)$$

We assume that the equation of state is of the form  $p = w\mu$  and the scaling behavior of the energy density is the same as in the FLRW case, i.e.  $\mu \sim S^{-3(1+w)}$ . With this ansatz equation (3.93) has two solutions

$$\zeta \equiv 0, \quad \text{and} \quad \zeta = \frac{\iota}{S^2}. \quad (3.94)$$

The first solution leads to the standard FLRW scenario with vanishing cosmological constant. The second solution is of greater interest since it leads to the Weyl 1-form

$$Q = \frac{\iota}{S^3} dt, \quad (3.95)$$

which tends to zero as the universe expands. Note the change in the scaling behavior of  $\zeta$  in contrast to the solution for  $a_4 \neq -a_6$ .

#### Magnitude-redshift relation

The field equations in (3.91) and (3.92) are the usual Friedmann equations with an additional contribution to the energy and pressure from the dilation current. Because of this similarity we apply the procedure outlined in section 1.4 in order to derive the magnitude-redshift relation for this model. Substituting the solution for  $\zeta$  into the field equations (3.91), (3.92), and defining  $\varsigma := -\frac{4\kappa c}{3\chi}$  we have

$$H^2 + \frac{k}{S^2} = \frac{\kappa}{3\chi} \mu + \varsigma \frac{\iota^2}{S^6} \quad \Rightarrow \quad \Omega_k + \Omega_w + \Omega_\zeta = 1. \quad (3.96)$$

Here we introduced the usual density parameters  $\Omega_k = -\frac{k}{H^2 S^2}$ ,  $\Omega_w := \frac{\kappa}{3\chi H^2} \mu$ , and  $\Omega_\zeta := \varsigma \frac{\iota^2}{S^6 H^2}$ . In contrast to the model with  $a_4 \neq -a_6$  presented in section 3.4, we now have a simple relation between the density parameters, similar to the FLRW model, cf. equation (1.36). The Hubble rate is given in terms of the density parameters

$$\begin{aligned} H^2 &= \frac{\kappa}{3\chi} \mu - \frac{k}{S^2} + \varsigma \frac{\iota^2}{S^6} \\ &= H_0^2 \left[ \Omega_{w0} (1+z)^{3(1+w)} + \Omega_{k0} (1+z)^2 + \Omega_{\zeta0} (1+z)^6 \right] \\ &\stackrel{(3.96)}{=} H_0^2 (1+z)^2 \left\{ \Omega_{w0} [(1+z)^{1+3w} - 1] + \Omega_{\zeta0} [(1+z)^4 - 1] + 1 \right\}. \end{aligned} \quad (3.97)$$

The luminosity distance becomes

$$d_{\text{luminosity}} = S_0 (1+z) \Theta \left[ (H_0 S_0)^{-1} \int_0^z F[\tilde{z}] d\tilde{z} \right], \quad (3.98)$$

with  $F[\tilde{z}] := (1+\tilde{z})^{-1} \left\{ \Omega_{w0} [(1+\tilde{z})^{1+3w} - 1] + \Omega_{\zeta0} [(1+\tilde{z})^4 - 1] + 1 \right\}^{-\frac{1}{2}}$  and the function  $\Theta[x]$  as defined in eq. (1.49). We end up with

$$\begin{aligned} &d_{\text{luminosity}}(z, H_0, \Omega_{w0}, \Omega_{\zeta0}, w) \\ &= \frac{(1+z)}{H_0 \sqrt{|1 - \Omega_{w0} - \Omega_{\zeta0}|}} \Theta \left[ \sqrt{|1 - \Omega_{w0} - \Omega_{\zeta0}|} \int_0^z F[\tilde{z}] d\tilde{z} \right]. \end{aligned} \quad (3.99)$$

The magnitude-redshift relation is given by the usual expression, i.e.

$$m(z, H_0, \Omega_{w0}, \Omega_{\zeta0}, w, M) = M + 5 \log d_{\text{luminosity}}(z, H_0, \Omega_{w0}, \Omega_{\zeta0}, w) + 25. \quad (3.100)$$

### Deceleration parameter

One can easily calculate the deceleration parameter (1.59) for this model from (3.97). In case of a model which contains only ordinary matter with  $w = 0$  and the additional contribution from  $\iota$  the deceleration parameter becomes

$$q = \frac{\Omega_{m0} (1+z) + 4\Omega_{\zeta0} (1+z)^4}{2(\Omega_{\zeta0} [(1+z)^4 - 1] + \Omega_{m0} z + 1)}. \quad (3.101)$$

### Fitting method and results

Let us perform a  $\chi^2$ -minimization as described in section 3.7.2. In order to speed up the determination of the best-fit parameters of (3.100) we made use of the downhill simplex method of Nelder and Mead [35, 40]. A test of our implementation of this method can be found in appendix D. The confidence contours for this model are displayed on the upper lhs in figure 3.10 for a fixed value of  $H_0$ . In figure 3.8 we plotted the magnitude-redshift relation and the function  $(H/H_0)^2$  for the two best-fit models X1 and X2 from table 3.11. Note that both sets lead to a model which currently undergoes

an accelerating phase of expansion. The overall best-fit model X1 is clearly unphysical due to its negative value for  $\Omega_{m0}$ . If we allow only for positive values of  $\Omega_{m0}$  we arrive at the model X2, which slightly worsens the fit but still lies within the 95.4% confidence limit. As becomes clear from the plot on the lower rhs in figure 3.8, the model X2 is only valid up to a redshift of approximately  $z_{\max} \approx 1.54$ . Since this limit is in disagreement with the direct observation of high-redshifted objects, one has to discard the model. We conclude that the SN Ia data seem to exclude a simple model which encompasses only ordinary matter  $\Omega_{m0}$  and an additional contribution from the dilation current in form of  $\Omega_{\zeta0}$ . This statement is only valid for the ansatz (3.45) for the Weyl 1-form, because this assumption leads to the  $z^6$  scaling behavior of the  $\Omega_{\zeta0}$  term in the equation for the expansion rate (3.97). In order to describe the data one could introduce the usual cosmological constant, which we did not include in our Lagrangian (3.3). The introduction of this constant would result in an additional term in the expansion rate which redshifts with  $z^2$ . We will learn more about this possibility in section 3.10.2. In the following we shortly present two non-Riemannian cosmological models, which were proposed independently by two different groups. These models will turn out to be compatible with our one.

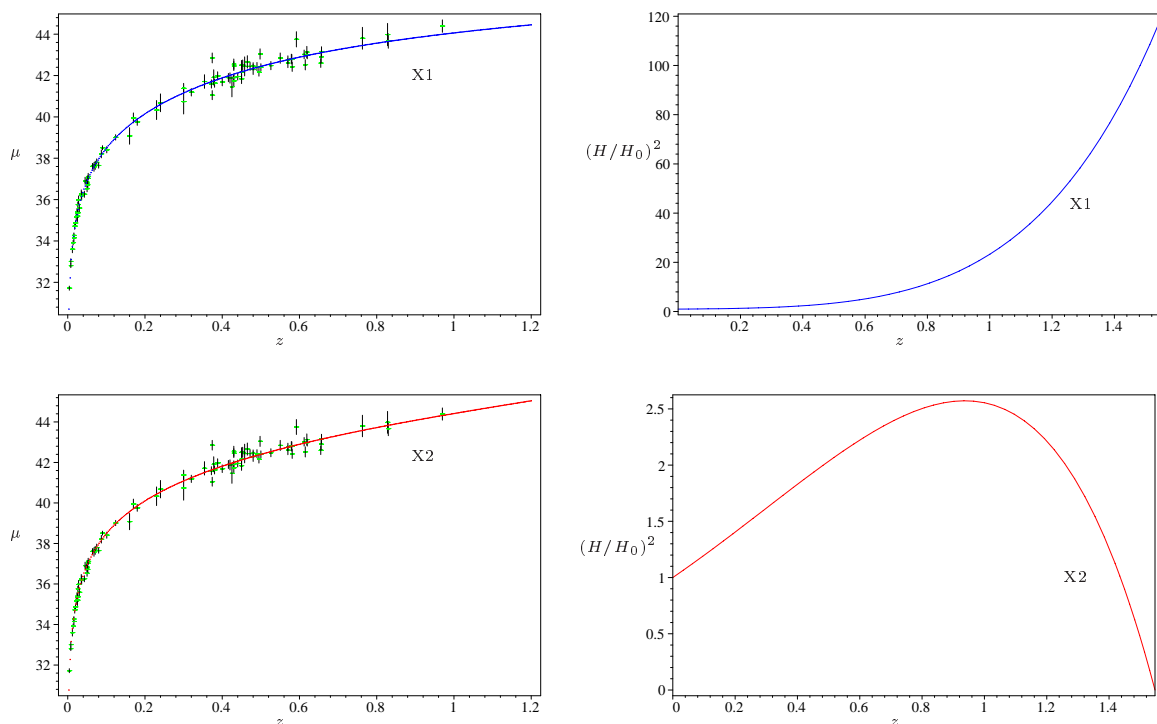


Figure 3.8: In the upper row we plotted the distance modulus  $\mu$  and the expansion rate  $(H/H_0)^2$  for the overall best-fit X1 from table 3.11. In the lower row we displayed  $\mu$  and  $(H/H_0)^2$  for the best-fit with positive  $\Omega_{m0}$ , i.e. X2 from table 3.11. As becomes clear from the picture at the lower rhs the maximum redshift for the model X2 is approximately given by  $z_{\max} \approx 1.54$ .

Table 3.11: Best-fit parameters for the Weyl-Cartan model with  $a_4 = -a_6$ .  $[H_0] = \text{km s}^{-1} \text{Mpc}^{-1}$ .

Symbol	$H_0$	$\Omega_{m0}$	$\Omega_{\zeta 0}$	$\chi^2$	$\chi_\nu^2$	$q_0$
X1	65.07	-3.405	0.548	134.45	1.51	-0.606
X2	63.26	0.008	-0.024	139.04	1.56	-0.044

## 3.10 Other models

### 3.10.1 Triplet model of Obukhov et al.

In [74] Obukhov et al. considered a cosmological model within the triplet regime of MAG, cf. section 2.3. In contrast to the vacuum case, which in general leads to the field equations displayed in (2.20)-(2.21), they considered a dilation hyperfluid model with vanishing spin-current. In addition, only a constrained version of the Lagrangian (2.15) was investigated, where<sup>7</sup>

$$\rho = 1, \quad \lambda = 0, \quad a_1, \dots, a_3 = 0, \quad b_{1,2,3,5} = 0, \quad c_2, \dots, c_4 = 0. \quad (3.102)$$

Using the usual Robertson-Walker line element, cf. eq. (1.3), the set of field equations, cf. eqs. (9.8) and (9.9) in [74], is given by

$$\left(\frac{\dot{S}}{S}\right)^2 + \frac{k}{S^2} = \frac{\kappa}{3} \left[ \mu + \frac{\kappa}{48a_0} \left(1 - \frac{3a_0}{b_4}\right) \frac{\psi^2}{S^6} \right], \quad (3.103)$$

$$2\frac{\ddot{S}}{S} + \left(\frac{\dot{S}}{S}\right)^2 + \frac{k}{S^2} = -\kappa \left[ p + \frac{\kappa}{48a_0} \left(1 - \frac{3a_0}{b_4}\right) \frac{\psi^2}{S^6} \right]. \quad (3.104)$$

Here  $a_0$  and  $b_4$  are the coupling constants of the triplet Lagrangian in (2.15) and  $\psi$  denotes an integration constant which enters the Weyl 1-form<sup>8</sup>

$$Q = -\frac{\kappa\psi}{8b_4} S^{-3} dt. \quad (3.105)$$

Defining a new constant  $v := \frac{\kappa^2}{144a_0} \left(1 - \frac{3a_0}{b_4}\right)$  we rewrite (3.103) according to

$$1 + \frac{k}{S^2 H^2} = \frac{\kappa}{3H^2} \mu + v \frac{\psi^2}{H^2 S^6} \quad \Rightarrow \quad \Omega_k + \Omega_w + \Omega_\psi = 1. \quad (3.106)$$

Here we introduced the density parameters  $\Omega_k := -\frac{k}{H^2 S^2}$ ,  $\Omega_w := \frac{\kappa}{3H^2} \mu$ ,  $\Omega_\psi := v \frac{\psi^2}{H^2 S^6}$  in the last step. Note that the coupling constants in this model and the ones introduced

<sup>7</sup>Note that also in this model the usual cosmological constant is set to zero.

<sup>8</sup>Be aware that we changed some of the variable names from [74] in order to avoid confusion with our notation.

in section 3.9 have different dimensions. Hence this model yields the same luminosity distance and magnitude-redshift relation as our Weyl-Cartan model from section 3.9. This is an interesting result since we derived exactly the same field equation from a very different approach. Of course all the numerical results from section 3.9 are also valid for this model.

### 3.10.2 Weyl-Cartan model of Babourova et al.

Additionally, one can show that the field equations of the models discussed in the previous sections 3.9 and 3.10.1 are equivalent to the field equations recently found by Babourova and Frolov in [72]. One can simply transform their field equation (7.1) into equation (3.103), by means of the following substitutions<sup>9</sup>:

$$\begin{aligned} a \rightarrow S, \quad \varepsilon = \varepsilon_\gamma a^{-3(1+\gamma)} &\rightarrow \mu, \quad \varepsilon_v \rightarrow 0, \quad \varepsilon \rightarrow \kappa, \quad \gamma \rightarrow w, \\ \frac{\alpha}{4\lambda^2 m^4} &\rightarrow \frac{3a_0 - b_4}{48a_0 b_4}, \quad JN \rightarrow \psi. \end{aligned} \quad (3.107)$$

Hence the results found in the previous sections are also valid for this model and place a quantitative limit on the model parameters. The solution for the Weyl 1-form is the same as in (3.105). Using the notation from (3.107), it is given by  $Q = -\frac{\varepsilon}{2\lambda m^2} \frac{JN}{a^3} dt$ . The choice  $\varepsilon_v = 0$  corresponds to a vanishing cosmological constant like in equation (3.103). Babourova and Frolov explicitly allow for a cosmological constant. This corresponds to an additional term  $-\lambda/3$  on the lhs of (3.103). Of course, such a term would alter the result for the magnitude-redshift relation. Defining the density parameter  $\Omega_\lambda := \frac{\lambda}{3H^2}$  as usual, the relation between the density parameters turns into  $\Omega_k + \Omega_w + \Omega_\psi + \Omega_\lambda = 1$ . Subsequently, equation (3.97) yields

$$H^2 = H_0^2 (1+z)^2 \left\{ \Omega_{w0} [(1+z)^{1+3w} - 1] + \Omega_{\psi0} [(1+z)^4 - 1] + \Omega_{\lambda0} [(1+z)^{-2} - 1] + 1 \right\}, \quad (3.108)$$

and the luminosity distance becomes

$$\begin{aligned} d_{\text{luminosity}}(z, H_0, \Omega_{w0}, \Omega_{\psi0}, \Omega_{\lambda0}, w) \\ = \frac{(1+z)}{H_0 \sqrt{|1 - \Omega_{w0} - \Omega_{\psi0} - \Omega_{\lambda0}|}} \Theta \left[ \sqrt{|1 - \Omega_{w0} - \Omega_{\psi0} - \Omega_{\lambda0}|} \int_0^z F[\tilde{z}] d\tilde{z} \right]. \end{aligned} \quad (3.109)$$

Here  $F[\tilde{z}] := H/H_0$  with the  $H$  from equation (3.108). For ordinary matter with  $w = 0$  the deceleration parameter is given by

$$q = \frac{\Omega_m (1+z)^3 + 4\Omega_\psi (1+z)^6 - 2\Omega_\lambda}{2\Omega_m z (1+z)^2 + 2(1+z)^2 - 2\Omega_\lambda z (2+z) + 2\Omega_\psi z \sum_{i=2}^5 (1+z)^i}. \quad (3.110)$$

In case the cosmological constant vanishes this result is compatible with (3.101). Hence we end up with three equivalent models which were all derived independently by different authors.

---

<sup>9</sup>Note that  $\alpha$ ,  $\lambda$ , and  $m$  are related to the coupling constants in the Lagrangian of Babourova et al., cf. eqs. (5.17) and (6.8) in [72].

### 3.10.3 Numerical results

Table 3.12 summarizes the best-fits found by us for a model which encompasses contributions from ordinary matter  $\Omega_{m0}$ , the triplet field  $\Omega_{\psi0}$ , and an additional cosmological constant  $\Omega_{\lambda0}$ . The overall best-fit L2 has a very low limiting redshift as depicted in figure 3.9. If we confine ourselves to positive values of  $\Omega_{\psi0}$  we arrive at the fit L1 which has only a slightly higher  $\chi^2$  than L2. Note that the density parameters for ordinary matter and the cosmological constant are very close to their values within the best-fit F13 for the FLRW model from table 3.7. Also in this model the universe is presently undergoing an accelerated phase of expansion with a deceleration factor which is of the same order of magnitude as in the FLRW case. In figure 3.10 we plotted the confidence regions for different parameter plane slices containing the L1 fit. The contours on the upper and lower rhs of figure 3.10 allow us to place an upper bound on the density parameter of the triplet field, i.e.  $\Omega_{\psi0} < 0.16$ .

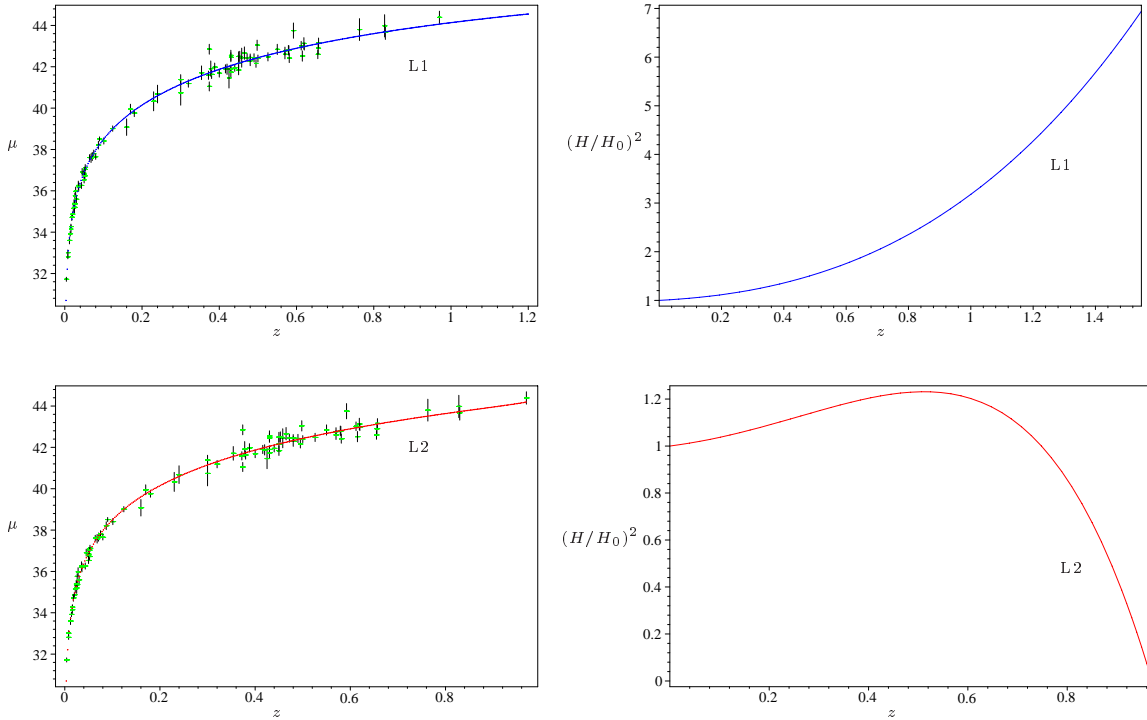


Figure 3.9: In the upper row we plotted the distance modulus  $\mu$  and the expansion rate  $(H/H_0)^2$  for the best-fit with positive density parameters, i.e. L1 from table 3.12. In the lower row we displayed  $\mu$  and  $(H/H_0)^2$  for the overall best-fit L2. As becomes clear from the picture at the lower rhs the maximum redshift for the model L2 is approximately given by  $z_{\max} \approx 0.97$ . Hence this model can be clearly excluded from further considerations.

The fit L1 leads to an age of the universe of about 13.2 Gyrs. This is slightly lower than the age of the universe in the FLRW model, which predicts 13.8 Gyrs in case of



Table 3.12: Best-fit parameters for the Weyl-Cartan model with  $a_4 = -a_6$  and an additional cosmological constant.  $[H_0] = \text{km s}^{-1}\text{Mpc}^{-1}$ .

Symbol	$H_0$	$\Omega_{m0}$	$\Omega_{\lambda0}$	$\Omega_{\psi0}$	$\chi^2$	$\chi^2_{\nu}$	$q_0$
L1	65.31	0.653	1.168	0.001	134.48	1.52	-0.839
L2	65.22	1.365	1.362	-0.093	133.97	1.52	-0.865

F13 and 14.6 Gyrs for the flat scenario F28, but still compatible with the age estimates from nucleochronocosmology which range from 11 to 15 Gyrs [157, 158].

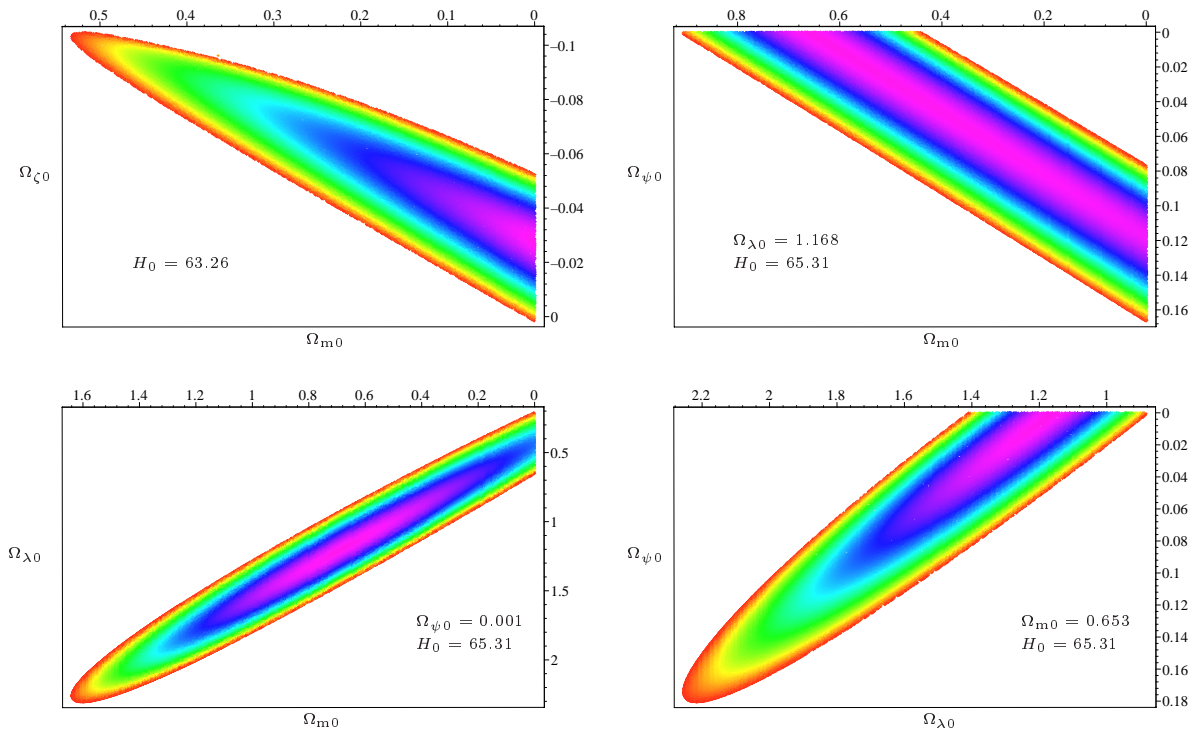


Figure 3.10: In the above figures we plotted the contour lines for parameter slices which contain the best-fits X2 and L1 from table 3.11 and table 3.12. The plot on the upper lhs corresponds to the fit X2, the other plots belong to the model L1 which encompasses an additional contribution from the cosmological constant. The outer boundaries correspond to the 95.4% confidence level.

## 3.11 Nucleosynthesis

In this section we work out the bounds from primordial nucleosynthesis on our Weyl-Cartan model. We focus on the special case in which  $\zeta = \zeta(t)$ . We are primarily interested in the effects due to the modified expansion rate of our new model. One

might also investigate the question of whether there are observable effects caused by modifications of the interface between the gravitational sector and the model of particle physics, in other words, the coupling of the new geometrical quantities to different particle species. In fact such an effect on BBN was already estimated in [205] for a model with torsion, which couples to the spin of particles. These estimates were based on the cross-section calculations for a helicity flip of the neutrino performed in [204]. The main conclusion of [205] is that the production rate of flipped neutrinos is much too low in order to affect nucleosynthesis in a significant way. Since these calculations were performed for a low-energy action from string theory it remains an open issue to calculate these rates for a more general type of Lagrangian, like for the one in equation (2.11). Of course such an investigation would require the knowledge of an Dirac-type matter field equation in MAG, which is currently not available [51]. In the following we solely concentrate on effects which are directly related to changes of the gravitational field equations.

### 3.11.1 Temperature of neutrinos and photons

One crucial point in the derivation of the  ${}^4\text{He}$  abundance is the relation between the photon and neutrino temperature, which indirectly influences the capture time via the time-temperature relation (1.130). Let us briefly sketch the procedure which leads to the different temperatures of the neutrinos and the photons within the standard model in order to asses if there is a modification of this relation within the Weyl-Cartan model. Note that the following derivation is only valid in equilibrium. However, the decoupling of the neutrinos and the succeeding annihilation of the electrons is surely not an equilibrium process. Hence the upcoming derivation should be viewed as a first order estimate. In [236] it was shown that non-equilibrium effects lead to corrections of the helium abundance at the  $10^{-4}$  level, which surely do not affect our simple estimate for  $Y_{4\text{He}}$ . From the usual expression for the entropy  $\mathcal{S}$  from thermodynamics, i.e.

$$d\mathcal{S}(V, T) = \frac{1}{T} [d(\mu(T) V) + p(T) dV] = \frac{1}{T} \left[ V \frac{\partial \mu}{\partial T} dT + (\mu + p) dV \right] \quad (3.111)$$

we can infer, by comparing the coefficients with  $d\mathcal{S}(V, T) = \frac{\partial \mathcal{S}}{\partial T} dT + \frac{\partial \mathcal{S}}{\partial V} dV$ , that

$$\frac{\partial \mathcal{S}}{\partial V} = \frac{\mu + p}{T}, \quad \text{and} \quad \frac{\partial \mathcal{S}}{\partial T} = \frac{V}{T} \frac{\partial \mu}{\partial T}. \quad (3.112)$$

Since the partial derivatives commute we have

$$\begin{aligned} \frac{\partial^2 \mathcal{S}}{\partial V \partial T} &= \frac{\partial}{\partial T} \left( \frac{\mu + p}{T} \right) = \frac{\partial}{\partial V} \left( \frac{V}{T} \frac{\partial \mu}{\partial T} \right) \\ &\Leftrightarrow \frac{\partial p}{\partial T} = \frac{1}{T} (\mu + p). \end{aligned} \quad (3.113)$$

Substitution of (3.113) into eq. (3.111) yields

$$d\mathcal{S} = \frac{V}{T} d(\mu + p) \quad \rightarrow \quad \mathcal{S}(V, T) = \frac{V}{T} [\mu(T) + p(T)]. \quad (3.114)$$

Hence we obtain an expression for the entropy in terms of the pressure and the energy density. Comparison of this result with the Noether identity of the FLRW model, i.e. the equation on the lhs in (1.16), yields

$$\dot{\mu}S \stackrel{\text{GR}}{=} -3\dot{S}(\mu + p) \Leftrightarrow S^3 \frac{dp}{dt} = \frac{d}{dt} [S^3(\mu + p)]. \quad (3.115)$$

Rewriting the expression for the pressure (3.113)

$$\frac{\partial p}{\partial t} = \frac{dT}{dt} \frac{1}{T} (\mu + p) = \frac{\dot{T}}{T} (\mu + p), \quad (3.116)$$

and substituting this equation into the lhs of (3.115) we obtain

$$S^3 \frac{\dot{T}}{T} (\mu + p) = \frac{d}{dt} [S^3(\mu + p)] \Rightarrow \frac{d}{dt} \left[ \frac{S^3}{T} (\mu + p) \right] = 0. \quad (3.117)$$

Thus, we found a conserved quantity which, after comparison with eq. (3.114), could be termed entropy provided we identify the volume  $V$  with  $S^3$ . Let us define the so-called entropy density  $s := \mathcal{S}/V$ . This density can be written in terms of the temperature by using the expression for the energy density (1.68)

$$\begin{aligned} s &:= \frac{\mathcal{S}}{V} \stackrel{(3.114)}{=} \frac{1}{T} [\mu + p] \stackrel{p=\frac{1}{3}\mu}{=} \frac{4}{3T} \mu \\ &\stackrel{(1.68)}{=} \frac{2\pi^2}{45} T^3 \left( \frac{7}{8} \sum_{i=\text{fermions}} g_{\text{Fi}} + \sum_{i=\text{bosons}} g_{\text{Bi}} \right) = \frac{2\pi^2}{45} T^3 g_{\text{total}}(T). \end{aligned} \quad (3.118)$$

Equating of the conserved quantity  $sV$  before and after  $e^+e^-$  annihilation yields

$$\begin{aligned} (sV)|_{\text{before}} = (sV)|_{\text{after}} &\Leftrightarrow \left( \frac{7}{8} \times 2 \times 2 + 2 \right) T^3 S^3|_{\text{before}} = 2 T^3 S^3|_{\text{after}} \\ &\Leftrightarrow \left( \frac{11}{4} \right)^{\frac{1}{3}} TS|_{\text{before}} = TS|_{\text{after}}. \end{aligned} \quad (3.119)$$

Since the neutrinos decouple from the plasma before electrons and positrons annihilate they do not benefit from the change in the entropy, i.e., the entropy for the neutrino subsystem is conserved separately. Hence the temperature of the photons and neutrinos differ by the numerical factor in equation (3.119), which finally leads to  $T_\gamma = \left(\frac{11}{4}\right)^{\frac{1}{3}} T_\nu$ .

Let us come back to the question posed at the beginning of this section, i.e. is the relation between  $T_\gamma$  and  $T_\nu$  still valid within an alternative model? The general answer to this question is *no*. The dependence on the underlying cosmological model is encoded in the equation inferred from the Noether identity in eq. (3.115). As we have seen in the previous sections on alternative models, the Noether identity is not necessarily of the same form as in the FLRW model, cf. equations (3.34)–(3.35), (3.59), and (3.93). Hence one has to redo the above calculation for every non-standard model. Nevertheless there is hope in case of the alternative Weyl-Cartan model with  $a_4 = -a_6$  for which

the Noether identity is given by (3.93). Using the solution for the function  $\zeta = \iota/S^2$ , equation (3.93) can be transformed into

$$\frac{d}{dt}(\mu S^4) = \frac{1}{4} \frac{dS^4}{dt} (\mu - 3p) \quad \Leftrightarrow \quad \dot{\mu} S = -3\dot{S} (\mu + p), \quad (3.120)$$

which is identical with the FLRW result in equation (3.115). Hence for this special choice of  $\zeta$ , which is the one investigated by us in the preceding sections, the above derivation for the relation between the temperatures of photons and neutrinos remains valid.

### 3.11.2 Distribution functions

Let us recall that in a homogeneous and isotropic space, i.e.  $f(q, t) \rightarrow f(E, t)$ , and with  $q^\alpha = (E, q^i)$  the Boltzmann equation took the following form

$$\left( E \frac{\partial}{\partial t} - \Gamma^0_{\alpha\beta} q^\alpha q^\beta \frac{\partial}{\partial E} \right) f(E, t) = 0. \quad (3.121)$$

In contrast to (1.97) the connection in (3.121) is now given by the one for the Weyl-Cartan model as displayed in appendix E.3.2. Hence equation (3.121) turns into

$$\left( E \frac{\partial}{\partial t} - \left( H g_{ij} q^i q^j + \frac{\zeta}{2S} g_{\alpha\beta} q^\alpha q^\beta \right) \frac{\partial}{\partial E} \right) f(E, t) = 0. \quad (3.122)$$

Here the function  $\zeta = \zeta(t)$  is that from the special ansatz for the Weyl 1-form made in (3.45). Hence, for a massless species we end up with

$$\left( \frac{\partial}{\partial t} - H E \frac{\partial}{\partial E} - \frac{\zeta}{S} E \frac{\partial}{\partial E} \right) f(E, t) = 0. \quad (3.123)$$

Of course the last term has to be small if we still want to use the distribution function from section 1.5. From an observational point of view one has to keep in mind the FIRAS result, which strictly limits the spectrum to a perfect blackbody, thereby placing a strong bound on the contribution of the last term.

### 3.11.3 ${}^4\text{He}$ abundance

As we have shown in detail in section 1.6 the neutron-to-baryon ratio for vanishing chemical potential is given by  $Y_n(y, Q, \tau, g_{\text{total}})$  as displayed in equation (1.118). Taking into account the neutron decay this ratio becomes  $\check{Y}_n = e^{-\frac{t_c}{\tau}} Y_n$ , cf. equation (1.128). Hence, the main modification due to an altered expansion rate can be ascribed to a change of the capture time  $t_c$ . In section 1.6 we have shown that the capture time is determined by the temperature at which the neutrons are captured within deuterium. We estimated the capture time to be of the order  $T_c \sim 0.1$  MeV.

In the following we assume that the universe has entered its radiation dominated epoch, hence the easiest way to take care of a modified expansion rate is to put limits on the spin degeneracy factor  $g_{\text{total}}$  in the equation for the expansion rate (1.114). A change of this parameter corresponds to a correction of the expansion rate due to the additional contribution from the dilation current to the energy density, cf. the rhs of equation (3.96). In order to keep things as clear as possible we briefly collect the crucial steps in the estimation of the helium abundance:

1. Determine the asymptotic value of neutron-to-proton ratio without the decay correction of the neutron, i.e. calculate  $Y_n(\infty, Q, \tau, g_{\text{total}})$  with the help of (1.118).
2. Derive the capture temperature  $T_c$  by estimating the onset of the deuterium formation.
3. Use the estimate for the capture temperature to derive the corresponding capture time  $t_c(T_c, g_{\text{total}})$  with the help of (1.130).
4. Calculate the  ${}^4\text{He}$  abundance via (1.136), i.e.  $Y_{4\text{He}}(g_{\text{total}}, \tau, \eta, m_n, m_p, m_D) = 2e^{-\frac{t_c(T_c, g_{\text{total}})}{\tau}} Y_n(\infty, Q, \tau, g_{\text{total}})$ .

Before we calculate the helium abundance let us comment on the second point in the above list, i.e. the estimation of the capture temperature  $T_c$ . In section 1.6 we made use of the condition  $X_D(\eta, m_n, m_p, m_D, Y_n(\infty)) \approx 1$  in combination with equation (1.135) to estimate the order of magnitude of  $T_c$ . Since this equation is based on the equilibrium expressions for neutron, proton, and deuterium number densities it leads to an underestimation of the capture temperature. Because the helium abundance is very sensitive to the capture temperature this condition should serve only as a rough estimate for  $T_c$ . In the following we will make use of the condition  $\tilde{X}_D \approx 1$  where  $\tilde{X}_D$  is given by<sup>10</sup>

$$\tilde{X}_D(T, \eta, m_n, m_p, m_D) := 1.116 \times 10^{13} e^{-1.44 \left(\frac{\varepsilon_D}{T}\right)^{\frac{1}{3}}} e^{\frac{\varepsilon_D}{T}} \left(\frac{\varepsilon_D}{T}\right)^{-\frac{17}{6}}, \quad (3.124)$$

which was derived by Bernstein et al. in eq. (3.40) of [193]. Figure 3.11 contains a comparison of the two conditions for different values of the baryon-to-photon ratio.

---

<sup>10</sup>We already made use of this condition in figure 1.9.

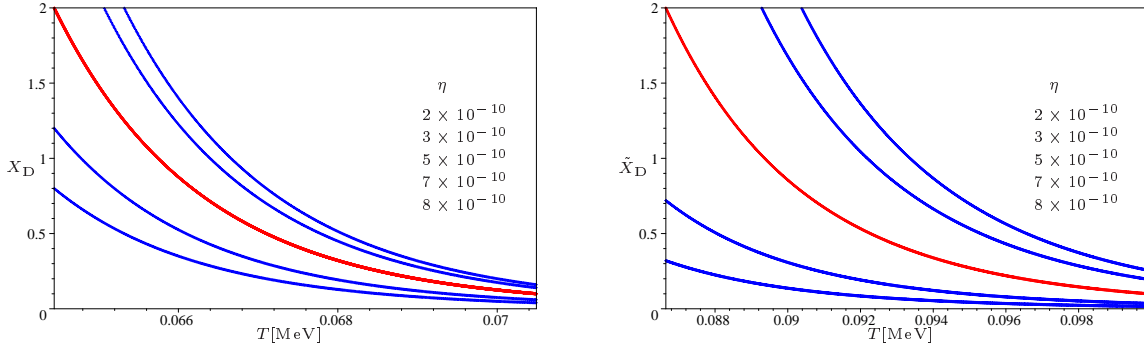


Figure 3.11: In the above figures we plotted  $X_D$  and  $\tilde{X}_D$  for different values of the baryon-to-photon ratio  $\eta$ . It becomes clear from the lhs that the equilibrium condition  $X_D \approx 1$  underestimates the capture temperature  $T_c$ . As explained in the text we will stick to the condition  $\tilde{X}_D \approx 1$  which was derived by Bernstein et al. in [193]. The corresponding plots of  $\tilde{X}_D$  are displayed on the rhs for different values of  $\eta$ . Note that the red line in both plots corresponds to  $\eta = 5 \times 10^{-10}$ .

Now we have everything at hand in order to calculate the helium abundance by means of the procedure described in 1-4. The results of this numerical calculation for different values of the baryon-to-photon ratio are displayed in figure 3.12 together with the experimental bounds from table 1.7 and table 1.8. Since the baryon-to-photon ratio is mainly fixed by the deuterium abundance, which we do not calculate here, we are going to use the rather broad interval  $[10^{-10}, 10^{-9}]$  for  $\eta$  in the following.

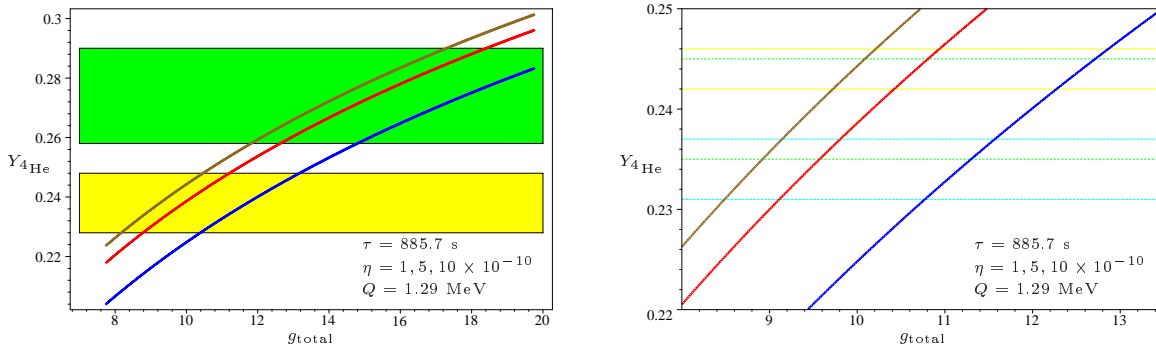


Figure 3.12: On the upper lhs we plotted the dependence of the  ${}^4\text{He}$  abundance on  $g_{\text{total}}$  for different values of baryon-to-photon ratio  $\eta$ . The upper line corresponds to  $\eta = 10^{-9}$  the lower one to  $10^{-10}$ . The boxes correspond to the observational limits from table 1.8. On the rhs we plotted  $Y_{4\text{He}}$  and the, partially overlapping, observational bounds  $Y_1, Y_2, Y_3$  from table 1.7. Note that the yellow region on the lhs incorporates all of the regions on the rhs.

Table 3.13:  ${}^4\text{He}$  abundance limits on  $\Omega_\psi$ .  $H_0 = 100 h \text{ km s}^{-1} \text{ Mpc}^{-1}$ .

Symbol	$\eta \times 10^{10}$	$\tilde{g}_{\text{total,min}}$	$\tilde{g}_{\text{total,max}}$	$\Omega_{\text{b}0} h^2$	$\Omega_{\psi 0,\text{min}} h^2 \times 10^{10}$	$\Omega_{\psi 0,\text{max}} h^2 \times 10^{10}$
H1	1	10.41	13.17	0.003663	-0.380592	2.708923
H2	2	9.67	12.29	0.007327	-1.081847	1.542633
H3	3	9.27	11.81	0.010990	-1.384456	0.991569
H4	4	8.99	11.47	0.014653	-1.565664	0.640499
H5	5	8.79	11.21	0.018317	-1.675158	0.393149
H6	6	8.63	11.01	0.021980	-1.752351	0.214910
H7	7	8.49	10.85	0.025643	-1.815078	0.080313
H8	8	8.37	10.71	0.029306	-1.863647	-0.031321
H9	9	8.27	10.59	0.032970	-1.898440	-0.122480
H10	10	8.19	10.47	0.036633	-1.919856	-0.209984

Let us come back to the parameters of the triplet model. In order to estimate the limit on  $\Omega_\psi$  via the helium abundance we can make use of the different expansion rates within FLRW and the triplet model. With  $\mu_\psi := \frac{3v}{\kappa} \frac{\psi^2}{S^6}$  and

$$H_{\text{FLRW}}^2 = \frac{\pi^2 \kappa}{90} g_{\text{total}} T^4 = \frac{\kappa}{3} \mu_{\text{r}}, \quad (3.125)$$

$$H_{\text{triplet}}^2 = \frac{\pi^2 \kappa}{90} \tilde{g}_{\text{total}} T^4 = \frac{\kappa}{3} (\mu_{\text{r}} + \mu_\psi), \quad (3.126)$$

we can derive the value of  $\mu_\psi$  from the upper limit on  $\tilde{g}_{\text{total}}$ , i.e.

$$\mu_{\psi,\text{BBN}} = \frac{\pi^2}{30} T_{\text{BBN}}^4 (\tilde{g}_{\text{total}} - g_{\text{total}}). \quad (3.127)$$

Hence the present day value of the  $\Omega_\psi$  density parameter is given by

$$\Omega_{\psi 0} = \frac{\mu_{\psi 0}}{\mu_{c 0}} = \frac{\mu_{\psi,\text{BBN}}}{\mu_{c 0}} \left( \frac{T_0}{T_{\text{BBN}}} \right)^6. \quad (3.128)$$

Of course we need to know the actual temperature of the species which carry dilation charges in order to obtain a numerical value for  $\Omega_{\psi 0}$ .

In table 3.13 we summarized the upper and lower bounds from observations on the degeneracy factor  $\tilde{g}_{\text{total}}$  for several values of the baryon-to-photon ratio within the range  $[10^{-10}, 10^{-9}]$ . The numerical value of the baryonic density parameter  $\Omega_{\text{b}}$  is fixed by the choice of the baryon-to-photon ratio  $\eta$  via<sup>11</sup>

$$\Omega_{\text{b}0} := \frac{\mu_{\text{b}0}}{\mu_{c 0}} = \frac{\kappa}{3H_0^2} \bar{m}_{\text{b}} n_{\text{b}0} = \frac{\kappa}{3H_0^2} \bar{m}_{\text{b}} n_{\gamma 0} \eta. \quad (3.129)$$

<sup>11</sup>Note that we used  $\bar{m}_{\text{b}} = m_{\text{n}} = 939.56 \text{ MeV}$  for the mean baryon mass.

Additionally, we calculated the bounds on  $\Omega_{\psi_0}$  with the help of (3.127) and (3.128). In the last step we assumed that the temperature  $T_0$  in (3.128) equals the photon temperature measured by FIRAS and the temperature at nucleosynthesis is given by the capture temperature estimated via (3.124). Hence, within our very broad range for  $\eta$  the product of the dilation density parameter  $\Omega_{\psi_0}$  and the parameter  $h$ , which characterizes the uncertainty in the determination of the Hubble rate, is limited to

$$\Omega_{\psi_0} h^2 \in [-1.91, 2.70] \times 10^{-10}. \quad (3.130)$$

### 3.11.4 Comparison with the precision estimate

Finally, let us compare our result with the fitting formula for the  ${}^4\text{He}$  abundance obtained by Lopez and Turner in [237] on the basis of their numerical nucleosynthesis calculation. The fitting formula for  $Y_{4\text{He}}^{\text{precision}}(\eta, \tau)$  provided in equation (43) of [237] depends on two parameters: (i) the neutron lifetime, and (ii) the baryon-to-photon ratio. It is valid for three neutrino species and for  $\eta \in [10^{-10}, 10^{-9}]$  and  $\tau \in [880, 890]$  s. In figure 3.13 we plotted their estimate together with our semi-analytical result within the usual interval for the baryon-to-photon ratio. We assumed that there are only the three standard neutrino species. The deviation of both estimates becomes smaller than 0.002 for intermediate values of  $\eta$ , see the rhs of figure 3.13. Hence, the semi-analytical method of Bernstein et al. seems to be still a good tool for estimating the primordial helium abundance.

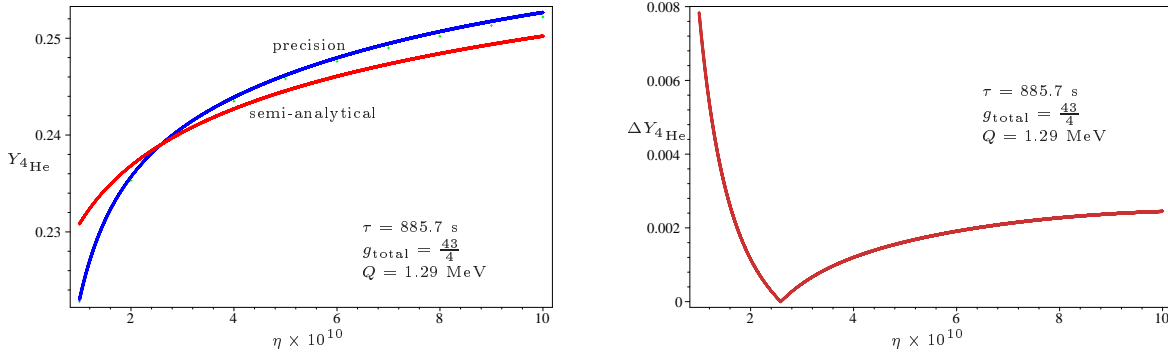


Figure 3.13: On the lhs we plotted in blue the helium abundance calculated from the fitting formula given by Lopez and Turner in eq. (43) of [237] for different values of the baryon-to-photon ratio  $\eta$ . Note that this fitting formula was derived from a numerical code which takes into account several higher order effects, cf. [237] for details. The red line corresponds to our semi-analytical calculation obtained by carrying out steps 1-4 from section 3.11. The green data points were generated by using the numerical code of Kawano [182, 183]. On the rhs we plotted the absolute difference between the semi-analytical and the precision estimate defined by  $\Delta Y_{4\text{He}} := \left| Y_{4\text{He}}^{\text{semi-analytical}} - Y_{4\text{He}}^{\text{precision}} \right|$ .



## 3.12 Summary

### 3.12.1 Combined constraints

Let us summarize our results concerning the alternative approach. On the theoretical side we were able to show that our Weyl-Cartan model has an interesting special case, which proved to be compatible with the models proposed by two other groups. The simplest case, i.e. a model which encompasses only ordinary matter  $\Omega_m$  and an additional contribution from the density parameter  $\Omega_\zeta$ , associated with the Weyl 1-form, is only compatible with the SN Ia data for negative values of the  $\Omega_\zeta$  parameter. Negative values of  $\Omega_\zeta$  enforce us to specify a maximum redshift  $z_{\max}$  at which the model has to be replaced by another, yet unknown, one. Since the best-fit leads to a rather small limiting redshift we switched to the case with an additional contribution from the cosmological constant in form of  $\Omega_\lambda$ . Within this ansatz we are able to describe the SN Ia data for positive  $\Omega_\psi$ , thereby removing the problem of a limiting redshift. In turn the data allow us to place an upper limit on the present day value of  $\Omega_\psi$  which must not account to more than 16% of the critical density. Since the new density parameter  $\Omega_\psi$  scales  $\sim z^6$ , this upper limit is not likely to be reached since it would lead to a dilation dominated phase at rather low-redshifts which would be in conflict with several other cosmological tests. Therefore we worked out the constraints on  $\Omega_\psi$  at the other end of the redshift scale by estimating its maximal contribution to the expansion rate at the time of primordial nucleosynthesis. As we have guessed before, the observed helium abundance puts very tight bounds on  $\Omega_{\psi 0}$ . Adopting our generous limit on  $\eta$ , we find that the upper bound on  $\Omega_{\psi 0}$  from nucleosynthesis lies approximately ten orders of magnitude below the bound inferred from the SN Ia. Hence, if one assumes that the model is valid from nucleosynthesis to our present epoch, the contribution from  $\Omega_{\psi 0}$  to the critical density lies even below the contribution from radiation [104]. Nevertheless both tests are consistent with each other what makes our model a viable candidate at both ends of the redshift scale accessible to current observations. To our knowledge this is the first time that a MAG based cosmological model was constrained by fitting to real data sets.

#### Possible extensions

Finally, let us note that the most pressing task concerning nucleosynthesis will be to modify one of the available numerical codes, because the semi-analytical calculation used by us does not place any constraints on the abundances of the other light elements. Especially the abundance of deuterium is of importance due to its sensitivity to the baryon-to-photon ratio. In our calculations we used the baryon-to-photon ratio as an input parameter rather than a fit parameter. Of course this dilutes its role as an estimator of the baryon density. In the view of recent CMB experiments nucleosynthesis is no longer the strongest test of the baryon density. In particular the analysis of the skymap measured by the WMAP satellite yields a very strong constraint on the combination  $\Omega_b h^2$ , cf. [178]. However, one has to check whether our result is compatible with the production of the other light elements.

### 3.12.2 The future

One of our main future goals will be to confront our model and other alternative scenarios with recent CMB measurements [175]–[181]. As mentioned before, the calculation of the CMB anisotropy spectrum depends on several mechanisms and input parameters. The list of different physical processes leading to temperature fluctuations in the CMB is long and ranges from intrinsic perturbations on the last-scattering surface to the scattering of photons in gas clouds on their way to the observer. We will not discuss these effects here, see [11, 163, 164], e.g., and the seminal works [161, 162]. In addition to the physical effects leading to CMB anisotropies one also has to take great care of gauge related questions [165, 166]. There exist several numerical codes for the calculation of the anisotropy spectrum within different gauges [167]–[170]. The precise determination of cosmological parameters from the anisotropy spectrum at all length scales requires the use of such codes [171, 172, 173]. Nevertheless it is possible to perform a simple order of magnitude estimate for some parameters.

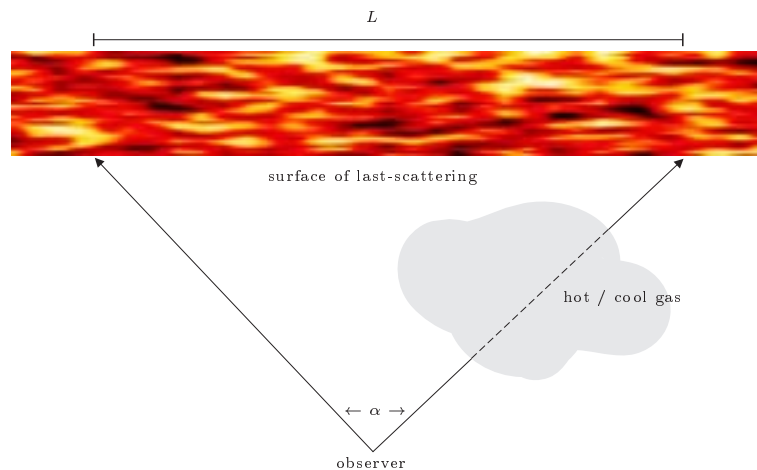


Figure 3.14: Schematic drawing of the last-scattering surface. An observer detects differences in the CMB temperature by comparing the photons coming from different directions separated by an angle  $\alpha$ . Different angles correspond to different scales on the last-scattering surface and depend on the underlying cosmological model. Such kind of differential measurements were performed by the DMR detector onboard of the COBE satellite.

In figure 3.14 we sketched the experimental setup for a CMB anisotropy measurement. In principle one performs a statistical analysis of the differential measurement of the photon temperature at different angular scales. The angle  $\alpha$  under which a given length scale  $L$  on the surface of last-scattering appears to us nowadays can be inferred from

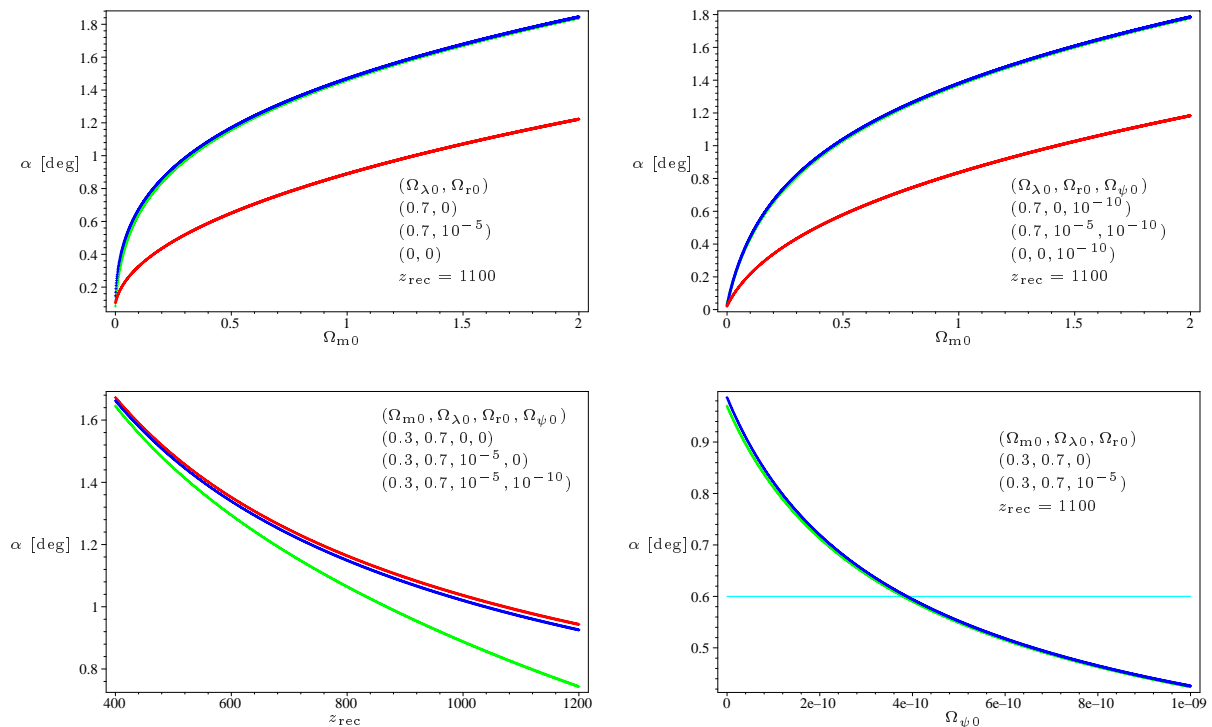


Figure 3.15: In the above plots we depicted the angle  $\alpha$  subtended by the Hubble radius at last scattering for different parameter combinations. The upper lhs corresponds to the FLRW model, and on the upper rhs the angle is plotted for the alternative Weyl-Cartan scenario. Note that we chose  $\Omega_{\psi_0}$  according to the limit inferred from nucleosynthesis. On the lower lhs we plotted the dependence of  $\alpha$  on the recombination redshift  $z_{\text{rec}}$  for both models. On the lower rhs the dependence of  $\alpha$  on  $\Omega_{\psi_0}$  is displayed. The horizontal line in this plot corresponds to the angular scale of the acoustic horizon as measured by WMAP. From the above plots it becomes clear that a contribution from radiation of the order  $10^{-5}$  does not significantly alter the resulting angle.

$$\alpha \approx \frac{L (1+z)^2}{d_{\text{luminosity}}}. \quad (3.131)$$

The size of a causally connected region is approximately the Hubble length  $H^{-1}$ . Hence (3.131), together with our results for the luminosity distance, enables us to calculate the angular scale of causally connected patches. The size of these regions is related to a feature within the CMB anisotropy spectrum, the so-called first acoustic peak. The position of the first peak depends on the scale of the sound horizon within the plasma at the time of decoupling. Since the angular scale corresponding to the first peak location has to be smaller than the angular scale of the Hubble horizon we can use it to place an upper bound on the  $\Omega_{\psi_0}$  density parameter of the Weyl-Cartan model. In figure 3.15 we

plotted the parameter dependence of  $\alpha$  for the FLRW and the alternative Weyl-Cartan model. The bound on  $\Omega_{\psi_0}$  for a model with  $\Omega_{m_0} = 0.3$  and  $\Omega_{\lambda_0} = 0.7$  can be read off from the plot at the lower rhs. Therein the horizontal line corresponds to the angular scale of the acoustic horizon as measured by the WMAP satellite (note that we made use of the relation  $\alpha \sim \frac{\pi}{\ell}$ ). This scale translates into an upper bound  $\Omega_{\psi_0} < 4 \times 10^{-10}$ . For the best-fit parameters  $\Omega_{m_0} = 0.653$  and  $\Omega_{\lambda_0} = 1.168$  of the model L1 from table 3.12 we obtain  $\Omega_{\psi_0} < 10^{-8}$ . Hence the CMB data puts a much more stringent constraint on the dilation density parameter than the SN Ia data. The bound on  $\Omega_{\psi_0}$  is compatible with our estimate from nucleosynthesis, cf. table 3.13. Therefore the Weyl-Cartan model with  $a_4 = -a_6$  represents a viable alternative cosmological model. It would be interesting to modify one of the existing numerical codes in order to calculate the full anisotropy spectrum within this model.

### 3.13 Dimensions

Table 3.14: Dimensions.

Quantities	1	Length
Gauge potentials	$[g_{\alpha\beta}], [\Gamma_{\alpha}^{\beta}]$	$[\vartheta^{\alpha}]$
Gauge field strengths	$[Q_{\alpha\beta}], [R_{\alpha\beta}]$	$[T^{\alpha}]$
Gauge field excitations	$[M^{\alpha\beta}], [H^{\alpha}_{\beta}]$	$[H_{\alpha}]^{-1}$
Gauge field currents	$[E^{\alpha}_{\beta}], [m^{\alpha\beta}]$	$[E_{\alpha}]^{-1}$
Matter currents	$[\Delta_{\alpha\beta}], [\sigma^{\alpha\beta}], [\tau_{\alpha\beta}]$	$[\Sigma_{\alpha}]^{-1}$
Coordinates	$[\theta], [\phi], [r]$	$[t]$
Coupling constants	$[\chi], [a_I], [b], [b_4]$	$[\kappa]^{\frac{1}{2}}, [c_I]^{-\frac{1}{2}}$
Functions	$[\xi], [\zeta], [\Omega_k], [\Omega_{\Lambda}], [\Omega_{\zeta}],$ $[\Omega_w], [G], [\Theta], [F], [\Omega_{\lambda}]$	$[\mu]^{-\frac{1}{4}}, [p_r]^{-\frac{1}{4}}, [p_t]^{-\frac{1}{4}}, [\Sigma_{\alpha\beta}]^{-\frac{1}{4}}$ $[S]$
Miscellany	$[z], [q], [m], [M],$ $[\mathcal{M}], [\mu], [\mathcal{S}], [\alpha]$	$[d_{\text{luminosity}}], [s]^{-\frac{1}{3}}, [L]$
Constants	$[k], [w], [\zeta], [\psi]$	$[\Xi]^{-\frac{1}{4}}, [\Lambda]^{-\frac{1}{2}}, [\varkappa_w]^{\frac{1}{-4+3(1+w)}},$ $[\lambda]^{-\frac{1}{2}}, [v]^{\frac{1}{4}}$
eq. (3.63)		$[\varkappa_1], [\varkappa_2]$
eq. (3.70)		$[l]$
eq. (3.73)		$[\varkappa_3]^{-\frac{1}{2}}$
eq. (3.74)		$[\varkappa_1]^{\frac{1}{2}}, [\varkappa_2]$
eq. (3.75)		$[\varkappa_1], [\varkappa_2]$
eq. (3.94)		$[l]^{\frac{1}{2}}$

# Appendix A

## Conventions and identities

### A.1 Exterior calculus and the hodge dual

For two differential forms  $\lambda \in \Lambda^p, \nu \in \Lambda^q$ , we define the exterior multiplication as follows,

$$\begin{aligned} \wedge : \quad \Lambda^p \times \Lambda^q &\longrightarrow \Lambda^{p+q} \\ \lambda \wedge \nu (v_1, \dots, v_{p+q}) &:= \frac{(p+q)!}{p!q!} \lambda(v_{[1}, \dots, v_p) \cdot \nu(v_{p+1}, \dots, v_{p+q}]) \\ &\stackrel{\text{alternatively}}{=} \frac{1}{p!q!} \sum_{\pi} \text{sgn}(\pi) \cdot \lambda(v_{\pi(1)}, \dots, v_{\pi(p)}) \cdot \nu(v_{\pi(p+1)}, \dots, v_{\pi(p+q)}), \end{aligned}$$

which, in case of  $\omega \in \Lambda^r, \mu \in \Lambda^p, a \in R$ , yields the properties:

$$(\lambda + \mu) \wedge \nu = \mu \wedge \nu + \lambda \wedge \nu, \quad (\text{A.1})$$

$$(a\lambda) \wedge \nu = \lambda \wedge (a\nu) = a(\lambda \wedge \nu), \quad (\text{A.2})$$

$$(\lambda \wedge \nu) \wedge \omega = \lambda \wedge (\nu \wedge \omega), \quad (\text{A.3})$$

$$\lambda \wedge \nu = (-1)^{pq} \nu \wedge \lambda. \quad (\text{A.4})$$

For elements of the underlying vector space  $v \in V$  we define the interior multiplication of a vector with a form  $\lambda \in \Lambda^p, p > 0, \forall u_1, \dots, u_{p-1} \in V$  as:

$$\begin{aligned} \lrcorner : \quad \Lambda^p &\longrightarrow \Lambda^{p-1} \\ v \lrcorner \lambda(u_1, \dots, u_{p-1}) &:= \lambda(v, u_1, \dots, u_{p-1}). \end{aligned}$$

For  $p = 0$  we define  $v \lrcorner \lambda := 0$ . For  $\mu \in \Lambda^p, \nu \in \Lambda^q, v, u \in V, a \in R$ , the following properties follow immediately:

$$v \lrcorner (\lambda + \mu) = v \lrcorner \lambda + v \lrcorner \mu, \quad (\text{A.5})$$

$$(v + u) \lrcorner \lambda = v \lrcorner \lambda + u \lrcorner \lambda, \quad (\text{A.6})$$

$$(av) \lrcorner \lambda = a(v \lrcorner \lambda), \quad (\text{A.7})$$

$$v \lrcorner u \lrcorner \lambda = -u \lrcorner v \lrcorner \lambda, \quad (\text{A.8})$$

$$v \lrcorner (\lambda \wedge \nu) = (v \lrcorner \lambda) \wedge \nu + (-1)^p \lambda \wedge (v \lrcorner \nu). \quad (\text{A.9})$$

Note that for a frame  $e_\alpha$  dual to the coframe  $\vartheta^\beta$

$$e_\alpha \rfloor \vartheta^\beta = \vartheta^\beta(e_\alpha) = \delta_\alpha^\beta. \quad (\text{A.10})$$

If a metric  $g$  and a coframe are given, we define

$$g = g_{\alpha\beta} \vartheta^\alpha \otimes \vartheta^\beta, \quad (\text{A.11})$$

$$g^{\alpha\beta} g_{\beta\gamma} = \delta_\gamma^\alpha. \quad (\text{A.12})$$

The generalized Kronecker-symbol shall be given by

$$\delta_{\alpha\beta\dots}^{\mu\nu\dots} := \begin{cases} sgn(\pi) & \text{if there exists a permutation } \pi \text{ with } \pi(\alpha\beta\dots) = (\mu\nu\dots) \\ 0 & \text{else} \end{cases}, \quad (\text{A.13})$$

and the components of the  $\epsilon$ -tensor by

$$\epsilon_{\alpha_1\dots\alpha_n} := \delta_{\alpha_1\dots\alpha_n}^{1\dots n}, \quad (\text{A.14})$$

$$\epsilon^{\alpha_1\dots\alpha_n} := \delta_{1\dots n}^{\alpha_1\dots\alpha_n}. \quad (\text{A.15})$$

Hence, the indices of the  $\epsilon$ -tensor are *not* raised by a metric tensor. It follows

$$\epsilon_{12\dots n} = +1 \quad , \quad \epsilon^{12\dots n} = +1 \quad , \quad \epsilon_{\alpha_1\dots\alpha_n} \epsilon^{\beta_1\dots\beta_n} := \delta_{\alpha_1\dots\alpha_n}^{\beta_1\dots\beta_n}. \quad (\text{A.16})$$

Given a metric  $g$ , we define the Hodge dual of a  $p$ -form  $\lambda$  in  $n$ -dimensional space ( $p \leq n$ ) as

$$\begin{aligned} * & : \Lambda^p \longrightarrow \Lambda^{n-p} \\ * \lambda & := \frac{\sqrt{\det(g)}}{(n-p)! p!} \lambda^{\alpha_1\dots\alpha_p} \epsilon_{\alpha_1\dots\alpha_n} \vartheta^{\alpha_{p+1}} \wedge \dots \wedge \vartheta^{\alpha_n}. \end{aligned}$$

Let  $\lambda$  and  $\phi$  be  $p$ -forms,  $a \in R$ ,  $n$  the dimension of the space, and 'ind' denote the number of minus signs in the diagonal form of the metric, then the following identities hold:

$$*(\lambda + \phi) = *\lambda + *\phi, \quad (\text{A.17})$$

$$*(a\lambda) = a *\lambda, \quad (\text{A.18})$$

$$**\lambda = (-1)^{p(n-p)+\text{ind}} \lambda, \quad (\text{A.19})$$

$$*\lambda \wedge \phi = *\phi \wedge \lambda, \quad (\text{A.20})$$

$$e_\alpha \rfloor *\lambda = *(\lambda \wedge \vartheta_\alpha), \quad (\text{A.21})$$

$$*(e_\alpha \rfloor \lambda) = (-1)^{p-1} \vartheta_\alpha \wedge *\lambda, \quad (\text{A.22})$$

$$\vartheta^\alpha \wedge (e_\alpha \rfloor \lambda) = p\lambda, \quad (\text{A.23})$$

$$e_\beta \rfloor *(\vartheta^\alpha \wedge \dots \wedge \vartheta^{\alpha_p}) = *(\vartheta^{\alpha_1} \wedge \dots \wedge \vartheta^{\alpha_p} \wedge \vartheta_\beta), \quad (\text{A.24})$$

$$\begin{aligned} \vartheta^\mu \wedge *(\vartheta^{\alpha_1} \wedge \dots \wedge \vartheta^{\alpha_p}) &= \sum_{i=1}^p (-1)^{p-i} g^{\mu\alpha_i} *(\vartheta^{\alpha_1} \wedge \dots \\ &\quad \wedge \vartheta^{\alpha_{i-1}} \wedge \vartheta^{\alpha_{i+1}} \wedge \dots \wedge \vartheta^{\alpha_p}), \end{aligned} \quad (\text{A.25})$$

$$e_\alpha \rfloor \lambda = (-1)^{n(p+1)+\text{ind}} *(\vartheta_\alpha \wedge *\lambda), \quad (\text{A.26})$$

$$*(e_\alpha \rfloor *\lambda) = (-1)^{(n+1)(p+1)+\text{ind}} (\lambda \wedge \vartheta_\alpha). \quad (\text{A.27})$$

In a 4-dimensional vector space  $V$  with volume 4-form  $\eta$  and metric  $g$  we may define

$$\eta_\alpha = e_\alpha \rfloor \eta, \quad \eta_{\alpha\beta} = e_\beta \rfloor \eta_\alpha, \quad \eta_{\alpha\beta\gamma} = e_\gamma \rfloor \eta_{\alpha\beta}, \quad (\text{A.28})$$

with the following properties:

$$\eta_\alpha = \star \vartheta_\alpha, \quad (\text{A.29})$$

$$\eta_{\alpha\beta} = \star(\vartheta_\alpha \wedge \vartheta_\beta), \quad (\text{A.30})$$

$$\eta_{\alpha\beta\gamma} = \star(\vartheta_\alpha \wedge \vartheta_\beta \wedge \vartheta_\gamma), \quad (\text{A.31})$$

$$e_\delta \rfloor \eta_{\alpha\beta\gamma} = \eta_{\alpha\beta\gamma\delta} = \star(\vartheta_\alpha \wedge \vartheta_\beta \wedge \vartheta_\gamma \wedge \vartheta_\delta). \quad (\text{A.32})$$

Alternatively, without a metric

$$\eta_{\alpha_1 \dots \alpha_p} = e_{\alpha_p} \rfloor e_{\alpha_{p-1}} \rfloor \dots e_{\alpha_1} \rfloor (\epsilon_{\beta\gamma\mu\nu} \vartheta^\beta \wedge \vartheta^\gamma \wedge \vartheta^\mu \wedge \vartheta^\nu). \quad (\text{A.33})$$

## A.2 Identities

The field strengths nonmetricity  $Q_{\alpha\beta}$ , torsion  $T^\alpha$ , and curvature  $R_\alpha{}^\beta$  obey the following Bianchi identities:

$$DQ_{\alpha\beta} = 2R_{(\alpha}{}^\gamma g_{\beta)\gamma}, \quad (\text{A.34})$$

$$DT^\alpha = R_\gamma{}^\alpha \wedge \vartheta^\gamma, \quad (\text{A.35})$$

$$DR_\alpha{}^\beta = 0. \quad (\text{A.36})$$

In a 4-dimensional space with  $Q := \frac{1}{4}Q_\gamma{}^\gamma$  the covariant derivatives of the  $\eta$ -basis can be written as:

$$D\eta_{\alpha_1} = -2Q \wedge \eta_{\alpha_1} + T^\beta \wedge \eta_{\alpha_1\beta}, \quad (\text{A.37})$$

$$D\eta_{\alpha_1\alpha_2} = -2Q \wedge \eta_{\alpha_1\alpha_2} + T^\beta \wedge \eta_{\alpha_1\alpha_2\beta}, \quad (\text{A.38})$$

⋮

$$D\eta_{\alpha_1\dots\alpha_4} = -2Q \wedge \eta_{\alpha_1\dots\alpha_4}. \quad (\text{A.39})$$





# Appendix B

## Units and numbers

### B.1 Units

In this work we make use of natural units, i.e.  $\hbar = k_B = c = 1$ . With this choice there is only the unit length for different physical quantities as depicted table B.1. The units for the quantities introduced in each chapter are summarized in a table at the end of the corresponding chapter (cf. section 1.8, p. 50, section 2.5, p. 59, and section 3.13, p. 106). The units of the operators which were introduced in appendix A can be read off from table B.2. In numerical calculations we always make use of the SI system of units, if not stated otherwise within the text. The corresponding SI definitions for different physical quantities are summarized in table B.3.

Table B.1: Natural units .

[energy]	[mass]	[time]	[length]	[temperature]
$\text{length}^{-1}$	$\text{length}^{-1}$	length	length	$\text{length}^{-1}$

Table B.2: Operators and natural units.

Operator	1	Length
hodge dual ( $n$ dimension of the spacetime, $p$ degree of the form)		$[*]_{n-2p}^{-1}$
exterior derivative	$[d]$	
inner product	$[ ]$	
outer product	$[\wedge]$	

Table B.3: SI system of units.

Physical quantity	Name	Symbol		
length	meter	m		
mass	kilogram	kg		
time	second	s		
electric current	ampere	A		
thermodynamic temperature	kelvin	K		
amount of substance	mole	mol		
luminous intensity	candela	cd		
Derived units			Comb. unit	Basis units
frequency	hertz	Hz		$s^{-1}$
energy	joule	J		$kg\ m^2\ s^{-2}$
force	newton	N	$J\ m^{-1}$	$kg\ m\ s^{-2}$
power	watt	W	$J\ s^{-1}$	$kg\ m^2\ s^{-3}$
pressure	pascal	Pa	$J\ m^{-3}$	$kg\ m^{-1}\ s^{-2}$
plane angle	radian	rad		$m\ m^{-1}$
solid angle	steradian	sr		$m^2\ m^{-2}$
electric charge	coulomb	C		A s
electric potential	volt	V	$J\ s^{-1}\ A^{-1}$	$kg\ m^2\ s^{-3}\ A^{-1}$
electric resistance	ohm	$\Omega$	$J\ s^{-1}\ A^{-2}$	$kg\ m^2\ s^{-3}\ A^{-2}$
electric capacity	farad	F	$J^{-1}\ s^2\ A^2$	$kg^{-1}\ m^{-2}\ s^4\ A^2$
electric conductance	siemens	S	$J^{-1}\ s\ A^2$	$kg^{-1}\ m^{-2}\ s^3\ A^2$
magnetic flux	weber	Wb	$J\ A^{-1}$	$kg\ m^2\ s^{-2}\ A^{-1}$
inductance	henry	H	$J\ A^{-2}$	$kg\ m^2\ s^{-2}\ A^{-2}$
magnetic flux density	tesla	T	$J\ A^{-1}\ m^{-2}$	$kg\ s^{-2}\ A^{-1}$
luminous flux	lumen	lm	cd sr	cd
illuminance	lux	lx	lm $m^{-2}$	cd $m^{-2}$
activity	becquerel	Bq		$s^{-1}$
absorbed dose	gray	Gr	$J\ kg^{-1}$	$m^2\ s^{-2}$
dose equivalent	sievert	Sv	$J\ kg^{-1}$	$m^2\ s^{-2}$

## B.2 Constants

This section contains a collection of the numerical values of the constants used for numerical calculations within this work. Table B.4 contains a collection of the fundamental constants and their numerical value in SI units. Note that we rounded the last digit, these values are compatible with [1] and, with exception of  $G$ , with [84, 85]. Note the uncertainty in the last digit of  $G = 6.673(10)\ m^3\ kg^{-1}\ s^{-2}$  after [85]. Some authors make use of cgs units, hence we quoted the numerical values for the fundamental constants in table B.5. Table B.6 contains the numerical values of the Planck quantities in SI units.

Since some authors use so-called reduced quantities with  $G \rightarrow 8\pi G$ , see [11] e.g., we compiled their numerical values in table B.7. Table B.8 represents an useful collection of conversion factors and mnemonics. Note that the choice of the gravitational coupling constant depends on whether one chooses  $\mu$  to be a mass or energy density. In any case the relation  $[\kappa\mu] = \text{m}^{-2}$  has to hold. Thus, for  $[\mu] = \text{kg m}^{-3}$ , i.e. a mass density we choose  $\kappa$  from below. For  $[\mu] = \text{kg m}^{-1} \text{s}^{-2}$ , i.e. a energy density we choose  $\tilde{\kappa}$ .

Table B.4: Fundamental constants in SI units.

Fundamental constants	Symbol	SI value	Unit SI	Comb. unit
Planck's constant	$h$	$6.6261 \times 10^{-34}$	$\text{m}^2 \text{kg s}^{-1}$	J s
	$\hbar$	$1.0546 \times 10^{-34}$	$\text{m}^2 \text{kg s}^{-1}$	J s
Speed of light	$c$	$2.9979 \times 10^8$	$\text{m s}^{-1}$	
Boltzmann's constant	$k_B$	$1.3807 \times 10^{-23}$	$\text{m}^2 \text{kg s}^{-2} \text{K}^{-1}$	J K <sup>-1</sup>
Newton's constant	$G$	$6.6720 \times 10^{-11}$	$\text{m}^3 \text{kg}^{-1} \text{s}^{-2}$	N m <sup>2</sup> kg <sup>-2</sup>
Electron charge	$e$	$1.6022 \times 10^{-19}$	A s	C

Table B.5: Fundamental constants in cgs units.

Fundamental constants	Symbol	CGS value	Unit cgs
Planck's constant	$h$	$6.6261 \times 10^{-27}$	$\text{cm}^2 \text{g s}^{-1}$
	$\hbar$	$1.0546 \times 10^{-27}$	$\text{cm}^2 \text{g s}^{-1}$
Speed of light	$c$	$2.9979 \times 10^{10}$	$\text{cm s}^{-1}$
Boltzmann's constant	$k_B$	$1.3807 \times 10^{-16}$	$\text{erg K}^{-1}$
Newton's constant	$G$	$6.6720 \times 10^{-8}$	$\text{cm}^3 \text{g}^{-1} \text{s}^{-2}$
Electron charge	$e$	$4.8032 \times 10^{-10}$	esu

Table B.6: Planck quantities.

Planck quantities	Symbol/Definition	Numerical value SI	Unit SI
Planck energy	$E_{\text{Pl}} := \sqrt{\frac{\hbar c^5}{G}}$	$= 1.9564 \times 10^9$	$\text{kg m}^2 \text{s}^{-2}$
Planck mass	$m_{\text{Pl}} := \sqrt{\frac{\hbar c}{G}}$	$= 2.1768 \times 10^{-8}$	kg
Planck length	$l_{\text{Pl}} := \sqrt{\frac{\hbar G}{c^3}}$	$= 1.6160 \times 10^{-35}$	m
Planck time	$t_{\text{Pl}} := \sqrt{\frac{\hbar G}{c^5}}$	$= 5.3904 \times 10^{-44}$	s
Planck density	$\mu_{\text{Pl}} := \frac{c^5}{\hbar G^2}$	$= 5.1580 \times 10^{96}$	$\text{kg m}^{-3}$

Table B.7: Reduced Planck quantities.

Reduced Planck quant.	Symbol/Definition	Num. value SI	Unit SI
Reduced Planck energy	$\tilde{E}_{\text{Pl}} := \sqrt{\frac{\hbar c^3}{\kappa}} = \sqrt{\frac{\hbar c}{\tilde{\kappa}}}$	$= 3.9024 \times 10^8$	$\text{kg m}^2 \text{s}^{-2}$
Reduced Planck mass	$\tilde{m}_{\text{Pl}} := \sqrt{\frac{\hbar}{\kappa c}} = \sqrt{\frac{\hbar}{\tilde{\kappa} c^3}}$	$= 4.3421 \times 10^{-9}$	kg
Reduced Planck length	$\tilde{l}_{\text{Pl}} := \sqrt{\frac{\hbar \kappa}{c}} = \sqrt{\hbar \tilde{\kappa} c}$	$= 8.1015 \times 10^{-35}$	m
Reduced Planck time	$\tilde{t}_{\text{Pl}} := \sqrt{\frac{\hbar \kappa}{c^3}} = \sqrt{\frac{\hbar \tilde{\kappa}}{c}}$	$= 2.7023 \times 10^{-43}$	s
Reduced Planck density	$\tilde{\mu}_{\text{Pl}} := \frac{c}{\hbar \kappa^2} = (c^3 \hbar \tilde{\kappa}^2)^{-1}$	$= 8.1659 \times 10^{93}$	$\text{kg m}^{-3}$

Table B.8: Conversion factors, constants, and mnemonics.

Conversion factors	Numerical value SI	Unit SI	Natural Unit
Energy	$1.6021 \times 10^{-10}$	$\text{kg m}^2 \text{s}^{-2}$	GeV
Mass	$1.7827 \times 10^{-27}$	kg	$\text{GeV } c^{-2}$
Length	$1.9732 \times 10^{-16}$	m	$\text{GeV}^{-1} \hbar c$
Time	$6.5821 \times 10^{-25}$	s	$\text{GeV}^{-1} \hbar$
Temperature	$1.1605 \times 10^{13}$	K	$\text{GeV } k_{\text{B}}^{-1}$
<b>Mnemonics</b>	1 eV $\sim$		
Mass	$1.7827 \times 10^{-36}$	kg	
Length	$1.9732 \times 10^{-25}$	m	
Time	$6.5821 \times 10^{-34}$	s	
Temperature	$1.1605 \times 10^4$	K	
<b>Non SI unit</b>			
1 eV	$1.6022 \times 10^{-19}$	$\text{m}^2 \text{kg s}^{-2}$	
1 pc	$3.0856 \times 10^{16}$	m	
1 ly = $\frac{1 \text{ pc}}{3.2615}$	$9.4634 \times 10^{15}$	m	
<b>Constants</b>			
$H_0 := 100h \text{ km s}^{-1} \text{Mpc}^{-1}$	$3.2399h \times 10^{-18}$	$\text{s}^{-1}$	
$\mu_{\text{c0}} := 3H_0^2/8\pi G$	$1.8779h^2 \times 10^{-26}$	$\text{kg m}^{-3}$	
$\kappa := \frac{8\pi G}{c^2}$	$1.8657 \times 10^{-26}$	$\text{m kg}^{-1}$	
$\tilde{\kappa} := \frac{8\pi G}{c^4}$	$2.0759 \times 10^{-43}$	$\text{s}^2 \text{m}^{-1} \text{kg}^{-1}$	
	<b>Numerical value</b>	<b>Natural unit</b>	
$H_0$	$2.1325h \times 10^{-42}$	GeV	
$\mu_{\text{c0}}$	$8.0938h^2 \times 10^{-47}$	$\text{GeV}^4$	
$m_{\text{Pl}}$	$1.2210 \times 10^{19}$	GeV	
$l_{\text{Pl}}$	$8.1895 \times 10^{-20}$	$\text{GeV}^{-1}$	
$t_{\text{Pl}}$	$8.1895 \times 10^{-20}$	$\text{GeV}^{-1}$	
$\mu_{\text{Pl}}$	$2.2231 \times 10^{76}$	$\text{GeV}^4$	

## B.3 Elementary particles and electromagnetic spectrum

Table B.9: Elementary particles (leptons &amp; quarks).

Charge [ $q_e$ ]	0	-1	$\frac{2}{3}$	$-\frac{1}{3}$
	$\nu_e$	$e$	$u$	$d$
Mass	< 3 eV	0.51 MeV	1.5 – 4.5 MeV	5 – 8.5 MeV
	$\nu_\mu$	$\mu$	$c$	$s$
Mass	< 0.19 MeV	105.65 MeV	1.0 – 1.4 GeV	80 – 155 MeV
	$\nu_\tau$	$\tau$	$t$	$b$
Mass	< 18.2 MeV	1.77 GeV	169.8 – 188.5 GeV	4.0 – 4.5 GeV

Table B.10: Electromagnetic spectrum.

Name	Wavelengths [m]	Frequency [Hz]	Photon energy [eV]
Radio	$10^3 - 0.3$	$10^5 - 10^9$	$10^{-10} - 10^{-6}$
Microwave	$0.3 - 10^{-3}$	$10^9 - 3 \times 10^{11}$	$10^{-6} - 10^{-3}$
Infrared far	$10^{-3} - 3 \times 10^{-5}$	$3 \times 10^{11} - 4 \times 10^{14}$	$10^{-3} - 10^{-1}$
middle	$3 \times 10^{-5} - 3 \times 10^{-6}$		
near	$3 \times 10^{-6} - 7.8 \times 10^{-7}$		
Visible	$7.8 \times 10^{-7} - 3.8 \times 10^{-7}$	$4 \times 10^{14} - 8 \times 10^{14}$	$10^{-1} - 10$
Ultraviolet	$3.8 \times 10^{-7} - 6 \times 10^{-10}$	$8 \times 10^{14} - 5 \times 10^{17}$	$10 - 10^3$
X-rays	$10^{-9} - 6 \times 10^{-12}$	$3 \times 10^{17} - 5 \times 10^{19}$	$10^3 - 10^5$
$\gamma$ -rays	$10^{-10} - 10^{-14}$	$3 \times 10^{18} - 3 \times 10^{22}$	$10^4 - 10^8$

Table B.11: Bosons and Hadrons (= Mesons + Baryons).

	Name	Symbol	Interaction	Mass	Charge [ $q_e$ ]	Spin		
<b>Bosons</b>	Photon	$\gamma$	electromagnetic	$< 2 \times 10^{-16}$ eV	$< 5 \times 10^{-30}$	1		
	Graviton	$g$	gravitational	0	0	2		
	Gluons	$g_{i=1..8}$	strong	n.d.	0	1		
	W-Boson	$W^\pm$	weak (charged curr.)	80.4 GeV	$\pm 1$	1		
	Z-Boson	Z	weak (neutral curr.)	91.1 GeV	0	1		
	Higgs	$H^0$		$> 114.3$ GeV				
		$H^\pm$		$> 71.5$ GeV				
<b>Composition</b>								
<b>Mesons</b>  <i>(<math>q_i\bar{q}_j</math>)</i>	$\pi$ -Meson	$\pi^0$	$(u\bar{u}, d\bar{d})$	134.9 MeV	264	0	$8.4 \times 10^{-17}$	
		$\pi^\pm$	$(u\bar{d}, d\bar{u})$	139.5 MeV	273	$\pm 1$	$2.60 \times 10^{-8}$	
	K-Meson	$K^\pm$	$(u\bar{s}, s\bar{u})$	493.6 MeV	967	$\pm 1$	$1.23 \times 10^{-8}$	
		$K^0$	$(d\bar{s}, s\bar{d})$	497.6 MeV	974	0	$0.89 \times 10^{-10}$	
	$\eta$ -Meson	$\eta$	$(u\bar{u}, d\bar{d})$	547.3 MeV	1072	0		
	$\rho$ -Meson	$\rho^0$	$(u\bar{d}, d\bar{u}, u\bar{u}, d\bar{d})$	769.3 MeV	1468	0		
		$\rho^\pm$		769.3 MeV	1468	$\pm 1$		
	$\omega$ -Meson	$\omega^0$	$(u\bar{u}, d\bar{d})$	782.5 MeV	1530	$\pm 1$		
	<b>Baryons</b>  <i>(<math>q_iq_jq_k</math>)</i>	Proton	$p$	$(uud)$	938.27 MeV	1836	$\pm 1$	$> 1.6 \times 10^{25}$ yr
		Neutron	$n$	$(udd)$	939.56 MeV	1839	0	885.7
$\Lambda$ -Hyperon		$\Lambda^0$	$(uds)$	1115.6 MeV	2183	0	$2.63 \times 10^{-10}$	
$\Sigma$ -Hyperon		$\Sigma^+$	$(uus)$	1189.3 MeV	2328	1	$0.80 \times 10^{-10}$	
		$\Sigma^0$	$(uds)$	1192.6 MeV	2332	0	$7.4 \times 10^{-20}$	
		$\Sigma^-$	$(dds)$	1197.4 MeV	2341	-1	$1.47 \times 10^{-10}$	
$\Xi$ -Hyperon		$\Xi^0$	$(uss)$	1314.8 MeV	2566	0	$2.90 \times 10^{-10}$	
		$\Xi^-$	$(dss)$	1321.3 MeV	2582	-1	$1.63 \times 10^{-10}$	

# Appendix C

## Decompositions

### C.1 Decomposing the curvature 2-form

Decomposition of the curvature 2-form  $R_\alpha{}^\beta$  into symmetric and antisymmetric part yields

$$R_\alpha{}^\beta = W_\alpha{}^\beta + Z_\alpha{}^\beta = d\Gamma_\alpha{}^\beta - \Gamma_\alpha{}^\gamma \wedge \Gamma_\gamma{}^\beta, \quad (\text{C.1})$$

where  $W_{\alpha\beta} = R_{[\alpha\beta]}$  is called the rotational curvature and  $Z_{\alpha\beta} = R_{(\alpha\beta)}$  strain curvature. The irreducible decomposition (cf. [44, 48]) of the rotational curvature  $W_{\alpha\beta}$ , reads

$$\begin{aligned} W_{\alpha\beta} &= {}^{(1)}W_{\alpha\beta} + {}^{(2)}W_{\alpha\beta} + {}^{(3)}W_{\alpha\beta} + {}^{(4)}W_{\alpha\beta} + {}^{(5)}W_{\alpha\beta} + {}^{(6)}W_{\alpha\beta} \\ &\sim \text{weyl} + \text{paircom} + \text{pscalar} + \text{ricsymf} + \text{ricanti} + \text{scalar} \\ &\sim 10 + 9 + 1 + 9 + 6 + 1. \end{aligned} \quad (\text{C.2})$$

Note that here and in the following the number of independent components corresponds to spacetimes with dimension  $n = 4$ . We define the *contracted* quantities by means of the frame  $e_\alpha$ , coframe  $\vartheta^\alpha$  and the hodge star  $*$  as follows:

$$W^\alpha := e_\beta \rfloor W^{\alpha\beta}, \quad (\text{C.3})$$

$$W := e_\alpha \rfloor W^\alpha, \quad (\text{C.4})$$

$$X^\alpha := *(W^{\beta\alpha} \wedge \vartheta_\beta), \quad (\text{C.5})$$

$$X := e_\alpha \rfloor X^\alpha. \quad (\text{C.6})$$

Further decomposition leads to

$$\Psi_\alpha := X_\alpha - \frac{1}{4}\vartheta_\alpha \wedge X - \frac{1}{2}e_\alpha \rfloor (\vartheta^\beta \wedge X_\beta), \quad (\text{C.7})$$

$$\Phi_\alpha := W_\alpha - \frac{1}{4}W\vartheta_\alpha - \frac{1}{2}e_\alpha \rfloor (\vartheta^\beta \wedge W_\beta). \quad (\text{C.8})$$

Using these definitions, the irreducible pieces of the rotational curvature  $W_{\alpha\beta}$  read

$${}^{(1)}W_{\alpha\beta} = W_{\alpha\beta} - \sum_{I=2}^6 {}^{(I)}W_{\alpha\beta}, \quad (\text{C.9})$$

$${}^{(2)}W_{\alpha\beta} = - *(\vartheta_{[\alpha} \wedge \Psi_{\beta]}), \quad (\text{C.10})$$

$${}^{(3)}W_{\alpha\beta} = -\frac{1}{12} *(X \wedge \vartheta_{\alpha} \wedge \vartheta_{\beta}), \quad (\text{C.11})$$

$${}^{(4)}W_{\alpha\beta} = -\vartheta_{[\alpha} \wedge \Phi_{\beta]}, \quad (\text{C.12})$$

$${}^{(5)}W_{\alpha\beta} = -\frac{1}{2} \vartheta_{[\alpha} \wedge e_{\beta]} \rfloor (\vartheta^{\gamma} \wedge W_{\gamma}), \quad (\text{C.13})$$

$${}^{(6)}W_{\alpha\beta} = -\frac{1}{12} W \vartheta_{\alpha} \wedge \vartheta_{\beta}. \quad (\text{C.14})$$

We now proceed by splitting up the strain curvature  $Z_{\alpha\beta}$  into its tracefree (or shear) and trace (or dilation) part. After that we will perform an even finer decomposition into its irreducible pieces.

$$Z_{\alpha\beta} := \mathcal{Z}_{\alpha\beta} + \frac{1}{4} g_{\alpha\beta} Z, \quad (\text{C.15})$$

$$Z := Z_{\alpha}{}^{\alpha}, \quad \mathcal{Z}_{\alpha} := e^{\beta} \rfloor \mathcal{Z}_{\alpha\beta}, \quad (\text{C.16})$$

$$\Delta := \frac{1}{2} (\vartheta^{\alpha} \wedge \mathcal{Z}_{\alpha}), \quad Y_{\alpha} := *(\mathcal{Z}_{\alpha\beta} \wedge \vartheta^{\beta}), \quad (\text{C.17})$$

$$\Xi_{\alpha} := \mathcal{Z}_{\alpha} - \frac{1}{2} e_{\alpha} \rfloor (\vartheta^{\gamma} \wedge \mathcal{Z}_{\gamma}), \quad \Upsilon_{\alpha} := Y_{\alpha} - \frac{1}{2} e_{\alpha} \rfloor (\vartheta^{\gamma} \wedge Y_{\gamma}). \quad (\text{C.18})$$

With these definitions the irreducible decomposition of  $Z_{\alpha\beta}$  may be written as

$$\begin{aligned} Z_{\alpha\beta} &= {}^{(1)}Z_{\alpha\beta} + {}^{(2)}Z_{\alpha\beta} + {}^{(3)}Z_{\alpha\beta} + {}^{(4)}Z_{\alpha\beta} + {}^{(5)}Z_{\alpha\beta} \\ &\sim \text{zcurvone} + \text{zcurvtwo} + \text{zcurvthree} + \text{dilcurv} + \text{zcurvfive} \\ &\sim 30 + 9 + 6 + 6 + 9, \end{aligned} \quad (\text{C.19})$$

where

$${}^{(1)}Z_{\alpha\beta} = Z_{\alpha\beta} - \sum_{I=2}^5 {}^{(I)}Z_{\alpha\beta}, \quad (\text{C.20})$$

$${}^{(2)}Z_{\alpha\beta} = -\frac{1}{4} *[\vartheta_{(\alpha} \wedge \Upsilon_{\beta)}], \quad (\text{C.21})$$

$${}^{(3)}Z_{\alpha\beta} = \frac{1}{6} [2\vartheta_{(\alpha} \wedge (e_{\beta)} \rfloor \Delta) - g_{\alpha\beta} \Delta], \quad (\text{C.22})$$

$${}^{(4)}Z_{\alpha\beta} = \frac{1}{4} g_{\alpha\beta} Z, \quad (\text{C.23})$$

$${}^{(5)}Z_{\alpha\beta} = \frac{1}{4} \vartheta_{(\alpha} \wedge \Xi_{\beta)}. \quad (\text{C.24})$$



In Riemannian spaces  ${}^{(2)}W_{\alpha\beta} = {}^{(3)}W_{\alpha\beta} = {}^{(5)}W_{\alpha\beta} = Z_{\alpha\beta} = 0$  holds. In order to distinguish the more general MAG from the Riemannian case, we denote the Riemannian curvature 2-form by  $\tilde{R}_{\alpha\beta}$ , thus we arrive at

$$\begin{aligned}\tilde{R}_{\alpha\beta} &= {}^{(1)}\tilde{R}_{\alpha\beta} + {}^{(4)}\tilde{R}_{\alpha\beta} + {}^{(6)}\tilde{R}_{\alpha\beta} \\ &\sim \text{weyl} + \text{fourcurv} + \text{sixcurv}\end{aligned}\tag{C.25}$$

$$\sim 10 + 9 + 1,\tag{C.26}$$

where

$$\tilde{R}_\alpha = e_\beta \rfloor \tilde{R}_\alpha{}^\beta,\tag{C.27}$$

$$\tilde{R} = e_\alpha \rfloor \tilde{R}^\alpha,\tag{C.28}$$

$$\tilde{R}_\alpha^\alpha = \tilde{R}_\alpha - \frac{1}{4}\tilde{R}\vartheta_\alpha,\tag{C.29}$$

$${}^{(4)}\tilde{R}_{\alpha\beta} = -\vartheta_{[\alpha} \wedge \tilde{R}_{\beta]}^\alpha,\tag{C.30}$$

$${}^{(6)}\tilde{R}_{\alpha\beta} = -\frac{1}{12}\tilde{R}\vartheta_\alpha \wedge \vartheta_\beta,\tag{C.31}$$

$$C_{\alpha\beta} = \tilde{R}_{\alpha\beta} - {}^{(4)}\tilde{R}_{\alpha\beta} - {}^{(6)}\tilde{R}_{\alpha\beta} = {}^{(1)}\tilde{R}_{\alpha\beta},\tag{C.32}$$

$${}^+C_{\alpha\beta} = \frac{1}{2}(C_{\alpha\beta} + i^*C_{\alpha\beta}).\tag{C.33}$$

Here  ${}^+C_{\alpha\beta}$  denotes the selfdual Weyl (or conformal) 2-form.

## C.2 Decomposing the torsion 2-form

Decomposing the torsion 2-form into its three irreducible parts yields:

$$\begin{aligned}T^\alpha &= {}^{(1)}T^\alpha + {}^{(2)}T^\alpha + {}^{(3)}T^\alpha \\ &\sim \text{tentor} + \text{trator} + \text{axitor} \\ &\sim 16 + 4 + 4,\end{aligned}\tag{C.34}$$

where

$${}^{(1)}T^\alpha = T^\alpha - {}^{(2)}T^\alpha - {}^{(3)}T^\alpha,\tag{C.35}$$

$${}^{(2)}T^\alpha = \frac{1}{3}\vartheta^\alpha \wedge (e_\beta \rfloor T^\beta),\tag{C.36}$$

$${}^{(3)}T^\alpha = \frac{1}{3}e^\alpha \rfloor (\vartheta_\beta \wedge T^\beta).\tag{C.37}$$

## C.3 Decomposing the nonmetricity 1-form

Decomposing the nonmetricity 1-form into its four irreducible parts yields:

$$\begin{aligned}Q_{\alpha\beta} &= {}^{(1)}Q_{\alpha\beta} + {}^{(2)}Q_{\alpha\beta} + {}^{(3)}Q_{\alpha\beta} + {}^{(4)}Q_{\alpha\beta} \\ &\sim \text{trinom} + \text{binom} + \text{vecnom} + \text{conom} \\ &\sim 16 + 16 + 4 + 4.\end{aligned}\tag{C.38}$$

Using the following definitions

$$Q := \frac{1}{4}Q_\alpha{}^\alpha, \quad (\text{C.39})$$

$$\mathcal{Q}_{\alpha\beta} := Q_{\alpha\beta} - Qg_{\alpha\beta}, \quad (\text{C.40})$$

$$\Lambda_\alpha := e^\beta \rfloor \mathcal{Q}_{\alpha\beta}, \quad (\text{C.41})$$

$$\Lambda := \Lambda_\alpha \vartheta^\alpha, \quad (\text{C.42})$$

$$\Theta_\alpha := \star(\mathcal{Q}_{\alpha\beta} \wedge \vartheta^\beta), \quad (\text{C.43})$$

$$\Theta := \vartheta^\alpha \wedge \Theta_\alpha, \quad (\text{C.44})$$

$$\Omega_\alpha := \Theta_\alpha - \frac{1}{3}e_\alpha \rfloor \Theta, \quad (\text{C.45})$$

we can explicitly write down the single parts:

$${}^{(1)}Q_{\alpha\beta} = Q_{\alpha\beta} - \sum_{I=2}^4 {}^{(I)}Q_{\alpha\beta}, \quad (\text{C.46})$$

$${}^{(2)}Q_{\alpha\beta} = \frac{2}{3} \star(\vartheta_{(\alpha} \wedge \Omega_{\beta)}), \quad (\text{C.47})$$

$${}^{(3)}Q_{\alpha\beta} = \frac{4}{9} \left( \vartheta_{(\beta} \Lambda_{\alpha)} - \frac{1}{4}g_{\alpha\beta} \Lambda \right), \quad (\text{C.48})$$

$${}^{(4)}Q_{\alpha\beta} = g_{\alpha\beta} Q. \quad (\text{C.49})$$

## C.4 Decomposition of the linear connection

We display the linear connection  $\Gamma_{\alpha\beta}$  of MAG expressed in terms of the metric  $g_{\alpha\beta}$ , coframe  $\vartheta^\alpha$ , torsion  $T^\alpha$ , and nonmetricity  $Q_{\alpha\beta}$ . As we will see in appendix D.1.1, this representation becomes necessary if we start by making an ansatz for torsion and nonmetricity and then subsequently compute all other geometric properties from  $\Gamma_{\alpha\beta}$  by machine. We start with the definition of the so called anholonomy 2-form

$$C^\beta := d\vartheta^\beta. \quad (\text{C.50})$$

As shown in section 3.10 of [44] the following equations hold

$$\Gamma_{(\alpha\beta)} = \frac{1}{2}(dg_{\alpha\beta} + Q_{\alpha\beta}), \quad (\text{C.51})$$

$$\Gamma_{\beta\alpha} \wedge \vartheta^\beta = T_\alpha - C_\alpha := \Phi_\alpha, \quad (\text{C.52})$$

$$\Gamma_{\alpha\beta} = e_{[\alpha} \rfloor \Phi_{\beta]} - \frac{1}{2}(e_\alpha \rfloor e_\beta \rfloor \Phi_\gamma) \vartheta^\gamma + \Gamma_{(\alpha\beta)} + (e_\beta \rfloor \Gamma_{(\alpha\gamma)} - e_\alpha \rfloor \Gamma_{(\beta\gamma)}) \vartheta^\gamma. \quad (\text{C.53})$$

This set of equations leads to the following expression for the connection:

$$\begin{aligned} \Gamma_{\alpha\beta} &= \frac{1}{2}dg_{\alpha\beta} + (e_{[\alpha} \rfloor dg_{\beta]\gamma}) \vartheta^\gamma + e_{[\alpha} \rfloor C_{\beta]} - \frac{1}{2}(e_\alpha \rfloor e_\beta \rfloor C_\gamma) \vartheta^\gamma \\ &\quad - e_{[\alpha} \rfloor T_{\beta]} + \frac{1}{2}(e_\alpha \rfloor e_\beta \rfloor T_\gamma) \vartheta^\gamma + \frac{1}{2}Q_{\alpha\beta} + (e_{[\alpha} \rfloor Q_{\beta]\gamma}) \vartheta^\gamma \end{aligned} \quad (\text{C.54})$$

$$= \Gamma_{\alpha\beta}^{\{\}} - e_{[\alpha} \rfloor T_{\beta]} + \frac{1}{2}(e_\alpha \rfloor e_\beta \rfloor T_\gamma) \vartheta^\gamma + \frac{1}{2}Q_{\alpha\beta} + (e_{[\alpha} \rfloor Q_{\beta]\gamma}) \vartheta^\gamma. \quad (\text{C.55})$$

# Appendix D

## Computer stuff

Throughout this work we made extensive use of the common computer algebra systems `Reduce` 3.7 and `Maple` 5.1/7.0/8.0, cf. figure D.1. In some special cases we also used `Mathematica` 4.1 to perform cross-checks. For a general introduction into `Reduce` and `Mathematica` see [30]–[34]. For the use of computer algebra systems in gravity see [29, 42, 43], e.g. The documentation of the popular `GRTensor II` package can be found in [41]. Due to limited space we display only some of the `Reduce` routines in this appendix. However, all files can be requested from the author via email ([dp@thp.uni-koeln.de](mailto:dp@thp.uni-koeln.de)).

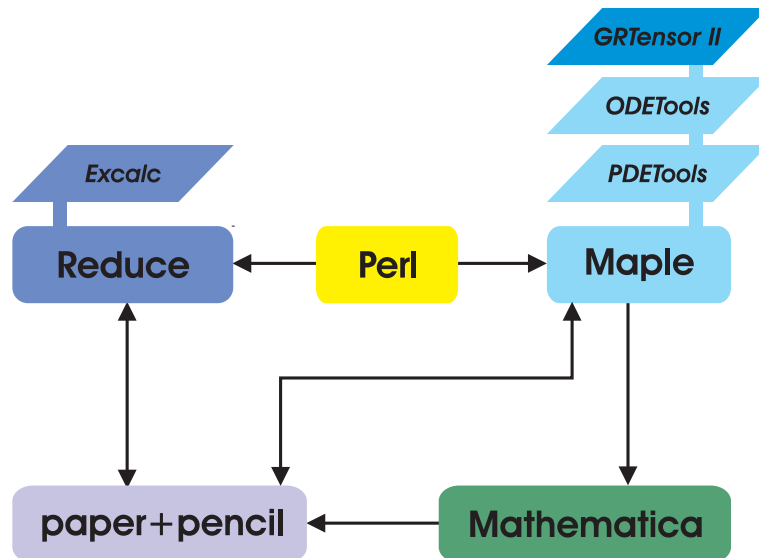


Figure D.1: Schematic drawing of the different computer algebra systems used throughout this thesis. The arrows symbolize the data exchange between the systems. When searching for exact solutions one starts, in most cases, at the lower left corner of the diagram performing several *iterations* clockwise.

Figure D.2 contains a test of our implementation of the downhill simplex method of Nelder and Mead [35, 40]. We used this method in our search for the best-fit parameters in section 3.9.

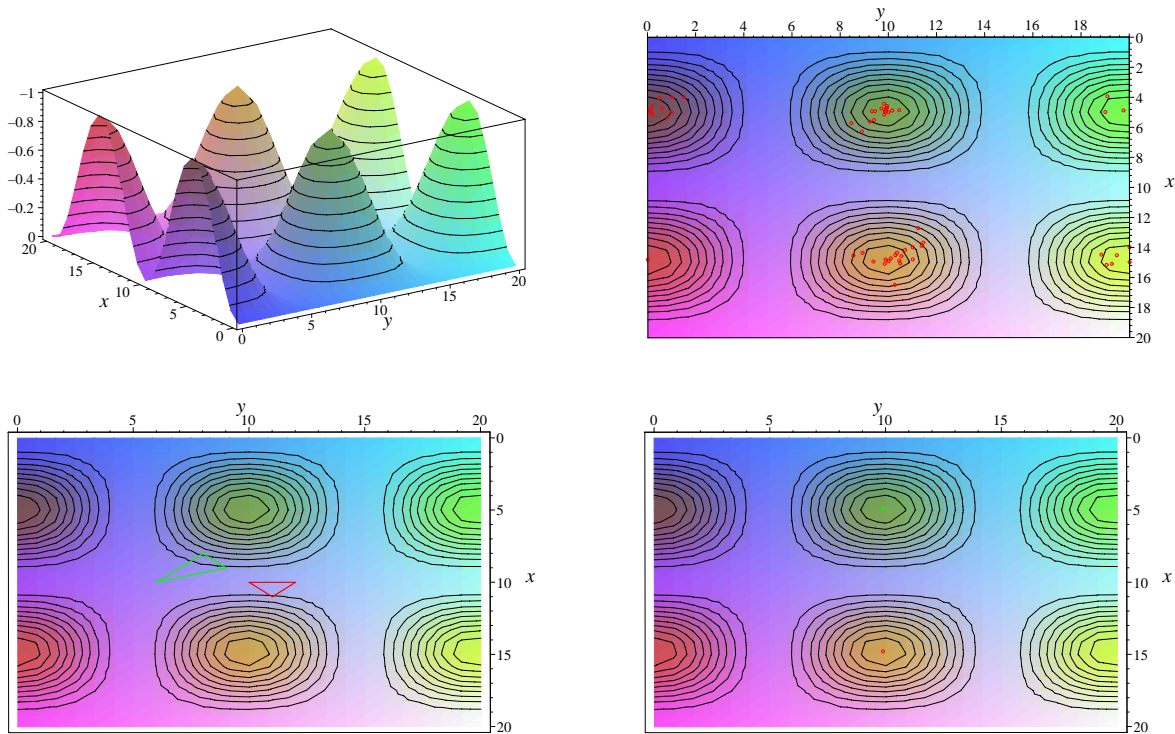


Figure D.2: Test of the downhill simplex implementation of Nelder and Mead [35, 40]. On the top lhs a test function is plotted. The second row shows how an initial green and red simplex *fall* into the minima after sufficiently many iterations. The top rhs figure shows the result for a random distribution of 100 simplices after 100 iterations (all drawn in red).

## D.1 General routines

### D.1.1 Decomposition routines

```

%
% magdec
%
% Dirk Puetzfeld
%
% decomposition routines used in MAG cf. notation in
% Socorro et al. Comp. Phys. Comm. 115 gr-qc/9804068
% and Hehl et al. Phys. Rep. 1995 258 1+2.
%
% Last update: 2002-12-12 by dp
%
% List of the included routines:
%
% decomposeRotationalCurvature tested.
% decomposeStrainCurvature tested.
% decomposeTorsion tested.
% decomposeNonmetricity tested.
% checkStrainCurvature tested.
% checkRotationalCurvature tested.

```

```

% checkTorsion tested.
% checkNonmetricity tested.
% displayStrainCurvature tested.
% displayRotationalCurvature tested.
% displayTorsion tested.
% displayNonmetricity tested.
%

let calculateConnectionCurvature=begin

write "calculating connection and curvature..."$

%
% Calculation of the connection and curvature
%
% needs: coframe o(a), frame e(a), metric g(a,b),
%         torsion2(a) , nonmetricity nonmet1(a,b)
%

pform conn1(a,b)=1,{anhol2(a),curv2(a,b)}=2$

anhol2(a)      := d o(a)$

conn1(-a,-b)   := (1/2) * d g(-a,-b) +(1/2) * (e(-a) _| (d g(-b,-c)) - e(-b) _| (d g(-a,-c))) * o(c)
               + (1/2) * (e(-a) _| anhol2(-b) - e(-b) _| anhol2(-a))
               - (1/2) * (e(-a) _| (e(-b) _| anhol2(-c))) * o(c)
               - (1/2) * (e(-a) _| torsion2(-b) - e(-b) _| torsion2(-a))
               + (1/2) * (e(-a) _| (e(-b) _| torsion2(-c))) * o(c) + (1/2) * nonmet1(-a,-b)
               + (1/2) * (e(-a) _| nonmet1(-b,-c) - e(-b) _| nonmet1(-a,-c)) * o(c)$

curv2(-a,b) := d conn1(-a,b) - conn1(-a,c) ^ conn1(-c,b)$

end$

let decomposeRotationalCurvature=begin

write "decomposing rotational curvature..."$

%
% Decomposition of the rotational curvature
%
% needs: coframe o(a), frame e(a), metric g(a,b), curv2(a,b)
%

pform {wzero,xzero}=0,
      {wone1(a),xone1(a),psi1(a),phi1(a)}=1,
      {w2(a,b),paircom2(a,b),pscalar2(a,b),ricsymf2(a,b),
       ricanti2(a,b),scalar2(a,b),weyl2(a,b),sdweyl2(a,b)}=2$

w2(-a,-b)    := (1/2) * (curv2(-a,-b) - curv2(-b,-a))$
wone1(a)     := e(-b) _| w2(a,b)$
wzero       := e(-b) _| wone1(b)$
xone1(a)    := #(w2(b,a) ^ o(-b))$
xzero      := e(-a) _| xone1(a)$
psi1(-a)    := xone1(-a) - (1/4) * o(-a) ^ xzero - (1/2) * e(-a) _| (o(b) ^ xone1(-b))$
phi1(-a)    := wone1(-a) - (1/4) * o(-a) * wzero - (1/2) * e(-a) _| (o(b) ^ wone1(-b))$

paircom2(-a,-b) := -(1/2) * #(o(-a) ^ psi1(-b) - o(-b) ^ psi1(-a))$
pscalar2(-a,-b) := -(1/12) * #(xzero ^ o(-a) ^ o(-b))$
ricsymf2(-a,-b) := -(1/2) * (o(-a) ^ phi1(-b) - o(-b) ^ phi1(-a))$
ricanti2(-a,-b) := -(1/4) * (o(-a) ^ (e(-b) _| (o(c) ^ wone1(-c))) - o(-b) ^ (e(-a) _| (o(c) ^ wone1(-c))))$
scalar2(-a,-b)  := -(1/12) * wzero * o(-a) ^ o(-b)$
weyl2(-a,-b)   := w2(-a,-b) - paircom2(-a,-b) - pscalar2(-a,-b) - ricsymf2(-a,-b)
               - ricanti2(-a,-b) - scalar2(-a,-b)$
sdweyl2(-a,-b) := (1/2) * (weyl2(-a,-b) - i * #weyl2(-a,-b))$

```

```

% clear wzero,xzero,wone1(a),xone1(a),psi1(a),phi1(a)$

end$

let decomposeStrainCurvature = begin

write "decomposing symmetric curvature..."$

%
% Decomposition of the strain curvature
%
% needs: coframe o(a), frame e(a), metric g(a,b), curv2(a,b)
%

pform {ztracef1(a),yy1(a),xi1(a),upsilon1(a)}=1,
      {z2(a,b),ztracef2(a,b),delta2,zcurvone2(a,b),zcurvtwo2(a,b),
       zcurvthree2(a,b),dilcurv2(a,b),zcurvfive2(a,b)}=2$

z2(-a,-b)      := (1/2) * (curv2(-a,-b) + curv2(-b,-a))$
ztracef2(-a,-b) := z2(-a,-b) - (1/4) * g(-a,-b) * z2(-c,c)$
ztracef1(-a)   := e(b) _| ztracef2(-a,-b)$
delta2         := (1/2) * o(a) ^ ztracef1(-a)$
yy1(-a)       := #(ztracef2(-a,-b) ^ o(b))$
xi1(-a)       := ztracef1(-a) - (1/2) * e(-a) _| (o(c) ^ ztracef1(-c))$
upsilon1(-a)  := yy1(-a) - (1/2) * e(-a) _| (o(c) ^ yy1(-c))$

zcurvtwo2(-a,-b) := -(1/4) * #(o(-a) ^ upsilon1(-b) + o(-b) ^ upsilon1(-a))$
zcurvthree2(-a,-b) := -(1/6) * (2 * (o(-a) ^ (e(-b) _| delta2) + o(-b) ^ (e(-a) _| delta2)) - 2 * g(-a,-b) * delta2)$
dilcurv2(-a,-b)  := (1/4) * g(-a,-b) * z2(-c,c)$
zcurvfive2(-a,-b) := (1/4) * (o(-a) ^ xi1(-b) + o(-b) ^ xi1(-a))$
zcurvone2(-a,-b) := z2(-a,-b) - zcurvtwo2(-a,-b) - zcurvthree2(-a,-b) - dilcurv2(-a,-b) - zcurvfive2(-a,-b)$

% clear ztracef1(a),yy1(a),xi1(a),upsilon1(a),ztracef2(a,b),delta2$

end$

let decomposeTorsion = begin

write "decomposing torsion..."$

%
% Decomposition of the torsion
%
% needs: coframe o(a), frame e(a), metric g(a,b), torsion2(a)
%

pform {tantor2(a),trator2(a),axitor2(a)}=2$

trator2(a) := (1/3) * o(a) ^ (e(-b) _| torsion2(b))$
axitor2(a) := (1/3) * e(a) _| (o(-b) ^ torsion2(b))$
tantor2(a) := torsion2(a) - trator2(a) - axitor2(a)$

end$

let decomposeNonmetricity = begin

write "decomposing nonmetricity..."$

%
% Decomposition of the nonmetricity
%
% needs: coframe o(a), frame e(a), metric g(a,b), nonmet1(a,b)
%

pform lamzero(a)=0,
      {weylcovector1,nomtracefree1(a,b),lamone1,binom1(a,b),

```

```

    vecnom1(a,b),trinom1(a,b),conom1(a,b)]=1,
    {thetatwo2(a),omega2(a)}=2,
    thetathree3=3$

weylcovector1      := nonmet1(-c,c) / 4$
nomtracefree1(-a,-b) := nonmet1(-a,-b) - g(-a,-b) * weylcovector1$
lamzero(-a)        := e(b) _| nomtracefree1(-a,-b)$
lamone1            := lamzero(-a) * o(a)$
thetatwo2(-a)      := #(nomtracefree1(-a,-b) ^ o(b))$
thetathree3        := o(a) ^ thetatwo2(-a)$
omega2(-a)          := thetatwo2(-a) - (1/3) * e(-a) _| thetathree3$

binom1(-a,-b)      := (1/3) * #(o(-a) ^ omega2(-b) + o(-b) ^ omega2(-a))$
vecnom1(-a,-b)     := (4/9) * ((o(-b) * lamzero(-a) + o(-a) * lamzero(-b)) / 2 - g(-a,-b) * lamone1/4)$
conom1(-a,-b)      := g(-a,-b) * weylcovector1$
trinom1(-a,-b)     := nonmet1(-a,-b) - binom1(-a,-b) - vecnom1(-a,-b) - conom1(-a,-b)$

%clear lamzero(a),nomtracefree1(a,b),lamone1,thetatwo2(a),omega2(a),thetathree3$

end$

let checkStrainCurvature = begin

write "test if decomposition of the strain curvature works..."$

%
% Checks consistency of the strain curvature decomposition
%
% needs: z2(-a,-b), zcurvone2(-a,-b), zcurvtwo2(-a,-b),
%        zcurvthree2(-a,-b), dilcurv2(-a,-b), zcurvfive2(-a,-b)
%

pform hilf1(a,b)=2$

hilf1(-a,-b) := z2(-a,-b) - zcurvone2(-a,-b) - zcurvtwo2(-a,-b) - zcurvthree2(-a,-b)
              - dilcurv2(-a,-b) - zcurvfive2(-a,-b)$

hilf2:=0$

for zaehler1:=0:3 do <<
  for zaehler2:=0:3 do <<
    if hilf1(-zaehler1,-zaehler2) neq 0 then hilf2:=hilf2+1$
  >>
>>

if hilf2 = 0 then write "decomposition ok..." else write "something is wrong..."$

clear hilf1,hilf2,zaehler1,zaehler2$

end$

let checkRotationalCurvature = begin

write "test if decomposition of the rotational curvature works:"$

%
% Checks consistency of the rotational curvature decomposition
%
% needs: w2(-a,-b), paircom2(-a,-b), pscalar2(-a,-b),
%        ricsymf2(-a,-b), ricanti2(-a,-b), scalar2(-a,-b), weyl2(-a,-b)
%

pform hilf1(a,b)=2$

hilf1(-a,-b):=w2(-a,-b) - paircom2(-a,-b) - pscalar2(-a,-b) - ricsymf2(-a,-b)

```

```

- ricanti2(-a,-b) - scalar2(-a,-b) - weyl2(-a,-b)$

hilf2:=0$

for zaehler1:=0:3 do <<
  for zaehler2:=0:3 do <<
    if hilf1(-zaehler1,-zaehler2) neq 0 then hilf2:=hilf2+1$
  >>;
>>;

if hilf2 = 0 then write "decomposition ok..." else write "something is wrong..."$

clear hilf1,hilf2,zaehler1,zaehler2$

end$

let checkTorsion = begin

write "test if decomposition of the torsion works:"$

%
% Checks consistency of the torsion decomposition
%
% needs: torsion2(a), tentor2(a), trator2(a), axitor2(a)
%

pform hilf1(a)=2$

hilf1(a) := torsion2(a) - tentor2(a) - trator2(a) - axitor2(a)$

hilf2 := 0$

for zaehler1:=0:3 do <<
  if hilf1(zaehler1) neq 0 then hilf2:=hilf2+1$
>>;

if hilf2 = 0 then write "decomposition ok..." else write "something is wrong..."$

clear hilf1,hilf2,zaehler1$

end$

let checkNonmetricity = begin

write "test if decomposition of the nonmetricity works:"$

%
% Checks consistency of the torsion decomposition
%
% needs: nonmet1(-a,-b), trinom1(-a,-b), binom1(-a,-b)
%          vecnom1(-a,-b), conom1(-a,-b)
%

pform hilf1(a,b)=1$

hilf1(-a,-b) := nonmet1(-a,-b)- trinom1(-a,-b) - binom1(-a,-b) - vecnom1(-a,-b) - conom1(-a,-b)$

hilf2 := 0$

for zaehler1:=0:3 do <<
  for zaehler2:=0:3 do <<
    if hilf1(-zaehler1,-zaehler2) neq 0 then hilf2:=hilf2+1$
  >>;
>>;

if hilf2 = 0 then write "decomposition ok..." else write "something is wrong..."$

```



```

clear hilf1,hilf2,zaehler1,zaehler2$

end$

let displayStrainCurvature = begin

write "the irreducible pieces of the strain curvature read..."$

%
% Displays the irreducible pieces of the strain curvature
%
% needs: zcurvone2(-a,-b), zcurvtwo2(-a,-b), zcurvthree2(-a,-b),
%         dilcurv2(-a,-b), zcurvfive2(-a,-b)
%

% recalculate pieces

zcurvone2(-a,-b)$
zcurvtwo2(-a,-b)$
zcurvthree2(-a,-b)$
dilcurv2(-a,-b)$
zcurvfive2(-a,-b)$

% display pieces

write "zcurvone2(-a,-b):"$ write zcurvone2(-a,-b)$
write "zcurvtwo2(-a,-b):"$ write zcurvtwo2(-a,-b)$
write "zcurvthree2(-a,-b):"$ write zcurvthree2(-a,-b)$
write "dilcurv2(-a,-b):"$ write dilcurv2(-a,-b)$
write "zcurvfive2(-a,-b):"$ write zcurvfive2(-a,-b)$

end$

let displayRotationalCurvature = begin

write "irreducible pieces of the rotational curvature"$

%
% Displays the irreducible pieces of the rotational curvature
%
%
% needs: paircom2(-a,-b), pscalar2(-a,-b), ricsymf2(-a,-b),
%         ricanti2(-a,-b), scalar2(-a,-b), weyl2(-a,-b)
%

% recalculate pieces

paircom2(-a,-b)$
pscalar2(-a,-b)$
ricsymf2(-a,-b)$
ricanti2(-a,-b)$
scalar2(-a,-b)$
weyl2(-a,-b)$

% display pieces

write "paircom2:"$ write paircom2(-a,-b)$
write "pscalar2:"$ write pscalar2(-a,-b)$
write "ricsymf2:"$ write ricsymf2(-a,-b)$
write "ricanti2:"$ write ricanti2(-a,-b)$
write "scalar2:"$ write scalar2(-a,-b)$
write "weyl2:"$ write weyl2(-a,-b)$

end$

```

```

let displayTorsion = begin

write "irreducible pieces of the torsion"$

%
% Displays irreducible pieces of the torsion
%
% needs: tentor2(a), trator2(a), axitor2(a)
%

% recalculate pieces

tentor2(a)$
trator2(a)$
axitor2(a)$

% display pieces

write "tentor2(a):"$ write tentor2(a)$
write "trator2(a):"$ write trator2(a)$
write "axitor2(a):"$ write axitor2(a)$

end$

let displayNonmetricity = begin

write "irreducible pieces of the nonmetricity"$

%
% Displays the irreducible pieces of the nonmetricity
%
% needs: trinom1(-a,-b), binom1(-a,-b), vecnom1(-a,-b), conom1(-a,-b)
%

% recalculate pieces

trinom1(-a,-b)$
binom1(-a,-b)$
vecnom1(-a,-b)$
conom1(-a,-b)$

% display pieces

write "trinom1(-a,-b)"$ write trinom1(-a,-b)$
write "binom1(-a,-b)"$ write binom1(-a,-b)$
write "vecnom1(-a,-b)"$ write vecnom1(-a,-b)$
write "conom1(-a,-b)"$ write conom1(-a,-b)$

end$

$end$

```

## D.1.2 Noether identities

```

%
% General form of the Noether identities
%
% Dirk Puetzfeld
%
% needs: mhypermom3(a,b),menenergy3(a),mstress4(a,b)
%
% Last update: 2002-12-12 by dp
%

let NoetherIdentities=begin

```

```

pform {nfirst4(a),nsecond4(a,b)}=4$

pform {Dmenergy4(a),Dmhypermom4(a,b)}=4$

Dmenergy4(-a) := d menergy3(-a) - conn1(-a,b) ^ menergy3(-b)$
Dmhypermom4(a,-b) := d mhypermom3(a,-b) + conn1(-c,a) ^ mhypermom3(c,-b) - conn1(-b,c) ^ mhypermom3(a,-c)$
nfirst4(-a) := Dmenergy4(-a) - (e(-a) _| torsion2(b)) ^ menergy3(-b) + (1/2) * (e(-a)
_ | nonmet1(-b,-c)) * mstress4(b,c) - (e(-a) _| curv2(-b,c)) ^ mhypermom3(b,-c)$
nsecond4(a,-b) := Dmhypermom4(a,-b) - g(-b,-c) * mstress4(a,c) + o(a) ^ menergy3(-b)$

end$

let displayFieldEquations=begin

write "MAG field equations:"$
write "first:"$
write first3(-a)-menergy3(-a);
write "second:"$
write second3(-a,-b)-mhypermom3(-a,-b);

end$

let displayNoetherIdentities=begin

write "Noether identities:"$
write "nfirst:"$
write nfirst4(-a)$
write "nsecond:"$
write nsecond4(-a,-b)$

end$

$end$

```

### D.1.3 Triplet ansatz in vacuum

```

% triplet_vacuum
%
% Dirk Puetzfeld
%
% Implements the triplet ansatz Lagrangian
% and calculates the gauge field excitation
% and the corresponding field equations
% for the vacuum case.
%
% last update: 2003-01-19 by dp
%

let TripletExcitationsLagrangian=begin

pform {htr2(a),hrot2(a,b)}=2,
      {energy3(a),hypermom3(a,b),capm3(a,b)}=3,
      {lagone4,lagtwo4,lagthree4,lagfour4,lagfive4,lagsix4,lag4}=4$

% strong represents the strong coupling constant
% kappa represents the weak coupling constant

htr2(-a) := -(1/kappa) * #(aa1 * tentor2(-a) + aa2 * trator2(-a) + aa3 * axitor2(-a)
+ (cc2 * binom1(-a,-b) + cc3 * vecnom1(-a,-b) + cc4 * conom1(-a,-b)) ^ o(b))$
hrot2(a,-b) := (aa0/(2*kappa)) * eta2(a,-b) + (zz4/strong) * (# dilcurv2(a,-b))$
capm3(a,b) := -(2/kappa) * ( #(bb1 * trinom1(a,b) + bb2 * binom1(a,b)
+ bb3 * vecnom1(a,b) + bb4 * conom1(a,b)) + (1/4) *
bb5 * (o(a) ^ #(weylcovector1 ^ o(b)) + o(b) ^ #(weylcovector1 ^ o(a))
- (1/2) * g(a,b) * #(3 * weylcovector1 + lamone1))

```

```

+ (1/2) * cc2 * (o(a) ^ # tensor2(b) + o(b) ^ # tensor2(a))
+ (1/2) * cc3 * (o(a) ^ # trator2(b) + o(b) ^ # trator2(a))
+ (1/4) * (cc3 - cc4) * g(a,b) * # (e(-c) _| torsion2(c))$

lagone4 := (1 / (2*kappa)) * (-aa0 * curv2(a,b) ^ eta2(-a,-b) - 2 * lamda * eta4)$
lagtwo4 := (1 / (2*kappa)) * torsion2(a) ^ # (aa1 * tentor2(-a) + aa2 * trator2(-a) + aa3 * axitor2(-a))$
lagthree4 := (1 / kappa) * (cc2 * binom1(-a,-b) + cc3 * vecnom1(-a,-b)
+ cc4 * conom1(-a,-b)) ^ o(a) ^ # torsion2(b)$
lagfour4 := (1 / (2*kappa)) * nonmet1(-a,-b) ^ # (bb1 * trinom1(a,b) + bb2 * binom1(a,b)
+ bb3 * vecnom1(a,b) + bb4 * conom1(a,b)) $
lagfive4 := -(zz4 / (2*strong)) * curv2(a,b) ^ (# dilcurv2(-a,-b))$
lagsix4 := (bb5 / (2*kappa)) * (vecnom1(-a,-c) ^ o(a) ^ # (conom1(b,c) ^ o(-b)))$
lag4 := lagone4 + lagtwo4 + lagthree4 + lagfour4 + lagfive4 + lagsix4$

write "m**2=0 equals:"$

32 * bb4 * aa2 * bb3 - 12 * aa0 * aa2 * bb3 - 64 * bb4 * aa0 * bb3 - 24 * bb3 * cc4**2
- 48 * bb3 * cc4 * aa0 - 32 * bb4 * aa0**2 - 24 * bb4 * cc3**2 + 9 * aa2 * bb5 * aa0
- 6 * aa2 * aa0**2 + 9 * aa0 * cc3**2 - 48 * bb4 * cc3 * aa0 + 4 * bb4 * aa2 * aa0
-24 * aa0**2 * cc4 + 9 * aa0 * bb5**2 - (9/2) * aa2 * bb5**2 - 3 * aa0 * cc4**2
+ 18 * cc3 * cc4 * bb5 - 18 * cc3 * cc4 * aa0 + 18 * cc3 * aa0 * bb5 +18 * aa0 * cc4 * bb5:=0;

end$

let FieldEquations=begin

pform {first3(a),second3(a,b),Dhtr3(a),Dhrot3(a,b)}=3$

Dhtr3(-a) := d htr2(-a) - conn1(-a,b) ^ htr2(-b)$
Dhrot3(a,-b) := d hrot2(a,-b) + conn1(-c,a) ^ hrot2(c,-b) - conn1(-b,c) ^ hrot2(a,-c)$
energy3(-a) := e(-a) _| lag4 + (e(-a) _| torsion2(b)) ^ htr2(-b) + (e(-a) _| curv2(-b,c)) ^ hrot2(b,-c)
+ (1/2) * (e(-a) _| nonmet1(-b,-c)) * capm3(b,c)$
hypermom3(a,-b) := -o(a) ^ htr2(-b) - capm3(a,-b)$

%
% note that maxenergy3 may vanish
%

%first3(-a):= Dhtr3(-a) - energy3(-a) - maxenergy3(-a)$

first3(-a):= Dhtr3(-a) - energy3(-a)$

second3(-a,-b):= Dhrot3(-a,-b) - hypermom3(-a,-b)$

end$

$end$

```

### D.1.4 Extended Weyl-Cartan Lagrangian ( $V_1 = \sum_{I=1}^4 c_I {}^{(I)}Q_{\alpha\beta} \wedge \star Q^{\beta\alpha}$ )

```

%
% Implements the Lagrangian of the extended Weyl-Cartan model
% and calculates the gauge field excitation and the corresponding
% field equations on the basis of the magdec decomposition.
%
% Dirk Puetzfeld
%
% Last update: 2002-12-12 by dp
%

let AddQuadNonmetricityExcitationsLagrangian=begin

```

```

pform {htr2(a),hrot2(a,b)}=2,
      {energy3(a),hypermom3(a,b),capm3(a,b)}=3,
      {lagone4,lagtwo4,lagthree4,lagfour4,lagfive4,lagsix4,lag4}=4$

% strong represents the strong coupling constant
% kappa represents the weak coupling constant

htr2(-a) := 0$

hrot2(a,-b) := -(chi / (2*kappa)) * eta2(-b,a) - 2 * aa1 * (# weyl2(-b,a)) - 2 * aa2 * (# paircom2(-b,a))
              - 2 * aa3 * (# pscalar2(-b,a)) - 2 * aa4 * (# ricsymf2(-b,a)) - 2 * aa5 * (# ricanti2(-b,a))
              - 2 * aa6 * (# scalar2(-b,a)) - (bb/2) * g(a,-c) * g(c,-b) * (# curv2(-j,j))$

capm3(a,b) := -4 * cc * (# nonmet1(b,a))$
lagone4 := (chi / (2*kappa)) * curv2(-a,b) ^ eta2(-b,a)$
lagtwo4 := aa1 * weyl2(-a,b) ^ (# curv2(-b,a)) + aa2 * paircom2(-a,b) ^ (# curv2(-b,a))
              + aa3 * pscalar2(-a,b) ^ (# curv2(-b,a)) + aa4 * ricsymf2(-a,b) ^ (# curv2(-b,a))
              + aa5 * ricanti2(-a,b) ^ (# curv2(-b,a)) + aa6 * scalar2(-a,b) ^ (# curv2(-b,a))$
lagthree4 := (bb/2) * (curv2(-a,-b) ^ (# curv2(b,a)) + curv2(-b,-a) ^ (# curv2(b,a)))$
lagfour4 := cc * (nonmet1(-a,-b) ^ (# nonmet1(b,a)))$
lag4 := lagone4+lagtwo4+lagthree4+lagfour4$

%clear lagone4,lagtwo4,lagthree4,lagfour4,lagfive4,lagsix4$

end$

let FieldEquations=begin

pform {first3(a),second3(a,b),Dhtr3(a),Dhrot3(a,b)}=3$

Dhtr3(-a) := d htr2(-a) - conn1(-a,b) ^ htr2(-b)$
Dhrot3(a,-b) := d hrot2(a,-b) + conn1(-c,a) ^ hrot2(c,-b) - conn1(-b,c) ^ hrot2(a,-c)$
energy3(-a) := e(-a) _| lag4 + (e(-a) _| torsion2(b)) ^ htr2(-b) + (e(-a) _| curv2(-b,c)) ^ hrot2(b,-c)
              + (1/2) * (e(-a) _| nonmet1(-b,-c)) * capm3(b,c)$
hypermom3(a,-b) := -o(a) ^ htr2(-b) - g(-b,-c) * capm3(a,c)$
first3(-a) := Dhtr3(-a) - energy3(-a)$
second3(-a,-b) := Dhrot3(-a,-b) - hypermom3(-a,-b)$

end$

$end$

```

## D.2 Cosmology

### D.2.1 Standard model

```

%
% Standard cosmology with Robertson-Walker metric and ideal fluid
%
%
% last update: 2003-01-11 by dp
%

on gc; on ezgcd;

out "robertson_walker.reo";

showtime;

load_package excalc$

pform ss=0$

```

```

fdomain ss=ss(t);

% Coordinates (t,r,theta,phi)

coframe o(0)=d t,
        o(1)=ss * (1-kk * r**2)**(-1/2) * d r,
        o(2)=ss * r * d theta,
        o(3)=ss * r * sin(theta) * d phi
with

metric g= - o(0) * o(0) + o(1) * o(1) + o(2) * o(2) + o(3) * o(3)$

frame e$

on nero;

riemannconx chris1 $

chris1(-a,b) := chris1(b,-a)$

pform curv2(a,b)=2$

curv2(-a,b) := d chris1(-a,b) + chris1(-c,b) ^ chris1(-a,c)$

pform ricci1(a)=1$

pform rscalar=0$

ricci1(a) := e(-b) _| curv2(a,b)$
rscalar := e(-a) _| ricci1(a)$

pform tfricci1(a)=1$

pform {fourcurv2(a,b),sixcurv2(a,b),weylc2(a,b),sdweylc2(a,b),cotton2(a)}=2$

tfricci1(-a) := ricci1(-a) - (1/4) * rscalar * o(-a)$
fourcurv2(-a,-b) := - (1/2) * (o(-a) ^ tfricci1(-b) - o(-b) ^ tfricci1(-a))$
sixcurv2(-a,-b) := - (1/12) * rscalar * o(-a) ^ o(-b)$
weylc2(-a,-b) := curv2(-a,-b) - fourcurv2(-a,-b) - sixcurv2(-a,-b)$
sdweylc2(a,b) := (1/2) * (weylc2(a,b) + i * #weylc2(a,b))$

pform eta0(a,b,c,d)=0,eta1(a,b,c)=1,eta2(a,b)=2,eta3(a)=3,eta4=4$

eta4 := # 1 $
eta3(a) := e(a) _| eta4 $
eta2(a,b) := e(b) _| eta3(a) $
eta1(a,b,c) := e(c) _| eta2(a,b) $
eta0(a,b,c,d) := e(d) _| eta1(a,b,c) $

off nat$

pform fluidenergy3(-a)=3$

pform fluid_components0(-a,-b)=0$

pform {mue,pp}=0$

fdomain mue=mue(t),pp=pp(t)$

pform uu(a)=0$

uu(0):=1;uu(1):=0;uu(2):=0;uu(3):=0;

fluid_components0(a,b) := (mue+pp) * uu(a) * uu(b) + pp * g(a,b);
fluidenergy3(-a) := fluid_components0(-a,-b) * eta3(b);

```

```

write "Einstein field equation with cosmological constant:"$

pform gleichung(-a)=3;

gleichung(-a) := eta1(-a,-b,-c) ^ curv2(b,c) + 2 * lamda * eta3(-a) - 2 * kappa *fluidenergy3(-a);

pform {nfirst4(a),Dmenergy4(a)}=4$

Dmenergy4(-a) := d fluidenergy3(-a) - chris1(-a,b) ^ fluidenergy3(-b)$
nfirst4(-a)   := Dmenergy4(-a)$

write "First Noether identity:"$

nfirst4(-a);

write "Curvature invariant:"$

write (# (curv2(a,b) ^ (# curv2(-a,-b))))$

showtime;

shut "robertson_walker.reo";

end$

bye;

```

## D.2.2 Extended Weyl-Cartan model

```

%
% A cosmological model in Weyl-Cartan spacetime
%
%
% Dirk Puetzfeld
%
% last update 2003-01-14 by dp
%
%
% In this file we perform some of the calculations for the
% Weyl-Cartan model presented in CQG 19 (2002) 3363-3280.
%
% Note in the Weyl-Cartan spacetime (Y4) the nonmetricity
% is related to the so called Weyl 1-form, i.e. only the
% trace part survives
%
% Additionally the symmetric part of the curvature turns
% out to be proportional to the derivative of the Weyl 1-form.
%
% Note: Note that there are several switches an commented
%       areas which have to selected. Be sure to select
%       the correct branch for omega.
%
% Needs: magdec
%       extweyl_lagrangian
%

showtime;

on gc; on ezgcd; on nero;

out "weyl_quad_nonmet.reo";

load_package excalc$

```

```

pform ss=0$
fdomain ss=ss(t);

% Coordinates (t,r,theta,phi)

coframe o(0)=d t,
      o(1)=(1 - kk * r**2)**(-1/2) * ss * d r,
      o(2)=ss * r * d theta,
      o(3)=ss * r * sin(theta) * d phi
with

metric g=o(0)*o(0) - o(1)*o(1) - o(2)*o(2) - o(3)*o(3)$

frame e$

write "components of the metric:"$
write g(-a,-b);

% Ansatz for omega entering the definition of torsion and nonmetricity

on nero;

pform omegal=1 $

% SWITCHES !
%
% ansatz_switch : 1 -> xi=xi(t,r)
%                2 -> xi=xi(t)
%
%
% simplification_switch : 1 -> simplifications belonging to ansatz 1
%                          2 -> ppt:=ppr
%
% equation_of_state_switch : 1 -> vacuum ppr:=-mue
%                             2 -> radiation ppr:=(1/3) * mue
%                             3 -> matter ppr:=0
%                             4 -> parametrized 1: ppr:=ww(t) * mue(t)
%                               with xif=iota/S ansatz
%                             5 -> parametrized 2: ppr:=ww(t) * mue(t)
%
%
%
ansatz_switch      := 2;
simplification_switch := 2;
equation_of_state_switch := 4;

write "Selecting explicit omegal:";

pform xif=0$

if ansatz_switch=1 then <<
  write "Choosing domain of xi=xi(t,r)...";
  fdomain xif=xif(t,r)$
>>;

if ansatz_switch=2 then <<
  write "Choosing domain of xi=xi(t)...";
  fdomain xif=xif(t)$
>>;

omegal := (xif/ss) * o(0);

% Computation of the torsion and nonmetricity

pform torsion2(a)=2,nonmet1(a,b)=1$

```



```

nonmet1(a,b) := g(a,b) * omega1$
torsion2(a) := (1/2) * omega1 ^ o(a)$

% Computation of the curvature and eta basis

pform eta0(a,b,c,d)=0,eta1(a,b,c)=1,eta2(a,b)=2,eta3(a)=3,eta4=4$

eta4 := # 1$
eta3(a) := e(a) _| eta4$
eta2(a,b) := e(b) _| eta3(a)$
eta1(a,b,c) := e(c) _| eta2(a,b)$
eta0(a,b,c,d) := e(d) _| eta1(a,b,c)$

pform menergy3(-a)=3$

pform fluid_components0(-a,-b)=0$

pform {mue,ppr,ppt}=0$

fdomain mue=mue(t),ppr=ppr(t),ppt=ppt(t)$

fluid_components0(0,0):=mue;fluid_components0(0,1):=0;fluid_components0(0,2):=0;fluid_components0(0,3):=0;
fluid_components0(1,0):=0;fluid_components0(1,1):=ppr;fluid_components0(1,2):=0;fluid_components0(1,3):=0;
fluid_components0(2,0):=0;fluid_components0(2,1):=0;fluid_components0(2,2):=ppt;fluid_components0(2,3):=0;
fluid_components0(3,0):=0;fluid_components0(3,1):=0;fluid_components0(3,2):=0;fluid_components0(3,3):=ppt;

menergy3(-a) := fluid_components0(-a,-b) * eta3(b);

in "magdec"$

calculateConnectionCurvature$
decomposeRotationalCurvature$
decomposeStrainCurvature$
decomposeTorsion$
decomposeNonmetricity$
checkStrainCurvature$
checkRotationalCurvature$
checkTorsion$
checkNonmetricity$

write "Geometrical quantities:";

off nat;

write ricsymf2(a,b);
write scalar2(a,b);
write dilcurv2(a,b);

displayStrainCurvature;
displayRotationalCurvature;
displayTorsion;
displayNonmetricity;

on nat;

write "Check if decomposition of the symmetric part of the curvature (strain curvature) equals d omega:"$

zcurvone2(-a,-b) + zcurvtwo2(-a,-b) + zcurvthree2(-a,-b) + dilcurv2(-a,-b)
+ zcurvfive2(-a,-b) - (1/2) * g(-a,-b) * d omega1;

in "extweyl_lagrangian"$

AddQuadNonmetricityExcitationsLagrangian$
FieldEquations$

pform mhypermom3(a,b)=3$

```

```

write "Matter-hypermomentum calculated from nonmetricity:"$
off nat;
write mhypermom3(-a,-b) := -(1/4) * g(-a,-b) * (bb * (d (# (d nonmet1(c,-c))))
+ cc * g(-m,-n) * ( #(g(n,m) * nonmet1(c,-c))));
pform mstress4(a,b)=4$
write "Metric stress-energy:"$
write mstress4(-a,-b) := -(1/4) * g(-a,-b) * (d hypermom3(c,-c))
+ (1/2) * (o(-a) ^ menergy3(-b) + o(-b) ^ menergy3(-a))$
in "noether"$
NoetherIdentities$
off nero;on exp;off nat;
displayFieldEquations$
displayNoetherIdentities$
write "Connection 1-form:";
on nero;
write conn1(-a,-b);
write e(a) _| conn1(-b,-c);
write "Noether identity rewritten by Obukhov cf. gr-qc/9604047 eq. (52)";
riemannconx chris1 $
chris1(-a,b):=chris1(b,-a)$
pform nonriemconn1(-a,-b)=1$
nonriemconn1(-a,-b):=conn1(-a,-b) - chris1(-a,-b);
write "Non-Riemannian parts of eq. (52):";
pform nonriemnoetherlhs4(-a)=4$
nonriemnoetherlhs4(-a) := d (mhypermom3(b,c) * (e(-a) _| nonriemconn1(-b,-c)))
- chris1(-a,d) ^ (mhypermom3(b,c) * (e(-d) _| nonriemconn1(-b,-c)))
+ mhypermom3(b,c) ^ (e(-a) _| nonriemconn1(-b,-c));
on nat;
write "Hodge dual of the cov. derivative of the hypermomentum (check hyperfluid relation)";
off nat;
pform dmhyper0(-a,-b)=0;
write dmhyper0(a,-b) := #(d mhypermom3(a,-b) + conn1(a,-c) ^ mhypermom3(c,-b));
write "Check if last term in (3.28) of Obukhov vanishes";
off nero;
write g(-c,-a) * dmhyper0(c,-b) - g(-c,-b) * dmhyper0(c,-a);

```

```

write "Check mstress symmetry"$

write mstress4(-a,-b) - mstress4(-b,-a);

off nero;

if simplification_switch=2 then <<

write "Radial and tangential stresses are equal for xi=xi(t)";

ppt:=ppr;

if equation_of_state_switch=1 then <<
  write "Vacuum equation of state:";
  ppr := - mue;
  write "Mue expressed via xi:";
  write mue := - 2 * cc * (xif / ss)**2;

>>;

if equation_of_state_switch=2 then <<
  write "Radiative equation of state:";
  ppr := (1/3) * mue;
  write "relation for xif from (1.60)";
  write 8 * cc * (xif / ss)**2 := 0;

>>;

if equation_of_state_switch=3 then <<
  write "Matter dominated equation of state:";
  ppr := 0;
  write "Relation between mue and xif:";
  write mue := -8 * cc * (xif / ss)**2;

>>;

if equation_of_state_switch=4 then <<
  write "Parametrized equation of state:";
  pform ww=0;
  fdomain ww=ww(t);
  ppr := ww * mue;
  write "Relation between mue and xif:";
  write mue := -8 * cc / (1 - 3 * ww) * (xif / ss)**2;

>>;

if equation_of_state_switch=5 then <<
  write "Parametrized equation of state:";
  pform ww=0;
  fdomain ww=ww(t);
  ppr := ww * mue;
  write "Relation between mue and xif:";
  write mue := -8 * cc / (1 - 3 * ww) * (xif / ss)**2;

>>;

on nero;
displayFieldEquations$
displayNoetherIdentities$

% Vacuum solution

if equation_of_state_switch=1 then <<
  write "Noether identity yields relation between xi(t) and S(t)";
  write xif := iota / ss;

>>;

if equation_of_state_switch=2 then <<
  write "Noether identity yields relation between mue(t) and S(t)";
  write mue := iota / ss**4;

```

```

>>;

if equation_of_state_switch=3 then <<
  write "Noether identity yields relation between xi(t) and S(t):";
  write xif := iota / ss;
>>;

if equation_of_state_switch=4 then <<
  write "Noether identity yields relation between xi(t) and S(t):";
  write xif := iota / ss;
>>;

if equation_of_state_switch=5 then <<
  write "Noether identity yields relation between ww(t), xi(t), and S(t):";
  write ww:=(xif**2 * ss**2 * ccc3-1)/(xif**2 * ss**2 * ccc3 - 3);
>>;

displayFieldEquations$
displayNoetherIdentities$

on nat;
write "Curvature, torsion, and nonmetricity before insertion of an explicit solution for S(t):";
off nat;

displayStrainCurvature$
displayRotationalCurvature$
displayTorsion$
displayNonmetricity$

on nat;
write "Solution for scale factor S(t) (does not depend on equation of state!):";
off nat;

%
% SWITCH !
% Be sure to select kk in the appropriate way
%

%write kk:=0; write "k=0:";

write "kk<>0:";

write test_switch:=0;

if kk=0 then <<
  write "Solution for k=0:";
  %write ss:= ccc1 * (2 * (t + ccc2) / ccc1)**(1/2);
  %write ss:=-ccc1 * (2 * (t + ccc2) / ccc1)**(1/2);
  %write ss:= ccc1;

% Coupling constants concerning vacuum solution

  if equation_of_state_switch=1 then <<

    if test_switch=1 then <<
      write "Test if direct selection of ccc1 leads to the same results:";
      write ccc1 := (iota/chi) * (-2 * chi * cc * kappa)**(1/2);
    %Solution for ccc1 holds for both signs
      %write ccc1 := -(iota / chi) * (-2 * chi * cc * kappa)**(1/2);
      >>;
    >>;

% Coupling constants concerning radiative solution

  if equation_of_state_switch=2 then <<
    % Noether identity yields solution for xi(t)

```

```

    %write xif := ccc3 / (ccc2 + t); % + branch
    %write xif := ccc3 / ss**2; % - branch
    write xif :=-ccc3;
  >>;
>>;

if kk neq 0 then <<
  write "Solution for k<>0:";
  %write ss :=-((-kk*(ccc2**2 * kk**2 - ccc1 + t**2 * kk**2 + 2 * t * kk**2 * ccc2))**(1/2))/kk;
  write ss := (-kk*(ccc2**2 * kk**2 - ccc1 + t**2 * kk**2 + 2 * t * kk**2 * ccc2))**(1/2)/kk;

% coupling constants concerning vacuum solution

  if equation_of_state_switch=1 then <<
    if test_switch=1 then <<
      write "Test if direct selection of ccc1 leads to the same results:";
      % Solution or ccc1 is valid for both signs
      write ccc1 := -2 * cc * iota**2 * kappa / chi;
    >>;
  >>;

  if equation_of_state_switch=2 then <<
    write xif := ccc3 / (kk**2 * (ccc2 + t)**2 - ccc1); % + branch and - branch
  >>;

>>;

displayFieldEquations$
displayNoetherIdentities$

if equation_of_state_switch=1 then <<

  if kk=0 then <<
    write "Choose ccc1 in order to fulfill the the field equations (for k=0):";
    write ccc1:= (iota / chi) * (-2 * chi * cc * kappa)**(1/2);
  >>;

  if kk neq 0 then <<
    write "Choose ccc1 in order to fulfill the the field equations (for k<>0):";
    write ccc1:= -2 * cc * iota**2 * kappa / chi;
  >>;

>>;

if equation_of_state_switch=2 then <<

  if kk=0 then <<
    write "Choose ccc1 in order to fulfill the the field equations (for k=0):";
    write ccc3 :=0; write iota:=0; % for constant xi
  >>;

  if kk neq 0 then <<
    write "Choose ccc1 and ccc3 in order to fulfill the the field equations (for k<>0):";
    write ccc3 :=0; write ccc1 := (1/3) * (iota * kappa / chi); % + branch and - branch
  >>;

>>;

if equation_of_state_switch=3 then <<

  if kk=0 then <<
    write "Choose ccc1 in order to fulfill the the field equations (for k=0):";
    %write ccc1 := 2 * (-chi * cc * kappa)**(1/2) * (iota / chi); % + branch and - branch
    %write ccc1 := -2 * (-chi * cc * kappa)**(1/2) * (iota / chi); % + branch and - branch
    write cc := 0; % const branch
    %write iota :=0; % const branch

```

```

>>;

if kk neq 0 then <<
  write "Choose ccc1 in order to fulfill the the field equations (for k<>0):";
  write ccc1 := -4 * cc * iota**2 * kappa / chi; % + branch and - branch
>>;

>>;

if equation_of_state_switch=4 then <<

  if kk=0 then <<
    % Solution for S=const
    %write solve((12 * cc * iota**2 * (ww - 1)) / (ccc1**4 * (3 * ww - 1))=0,ww);
    %write ww := 1;

    % Solution for S=+/- branch
    write solve((3 * (4 * cc * iota**2 * kappa * ww - 4 * cc * iota**2 * kappa
      + 3 * ccc1**2 * chi * ww - ccc1**2 * chi)) / (4 * ccc1**2 * kappa * (3 * ccc2**2 * ww
      - ccc2**2 + 6*ccc2*t*ww - 2*ccc2*t + 3*t**2*ww - t**2))=0,ww);
    write ww := (4 * cc * iota**2 * kappa + ccc1**2 * chi) / (4 * cc * iota**2 * kappa + 3 * ccc1**2 * chi);
  >>;

  if kk neq 0 then <<
    write "Choice for w(t) in order to fulfill first Noether identity:";
    write solve((-24 * @(ww,t) * cc * iota**2 * kk**2) / (9 * ccc1**2 * ww**2 - 6 * ccc1**2*ww + ccc1**2
      -18 * ccc1 * ccc2**2 * kk**2 * ww**2 + 12 * ccc1 * ccc2**2 * kk**2 * ww
      -2 * ccc1 * ccc2**2 * kk**2 - 36 * ccc1 * ccc2 * kk**2 * t * ww**2
      +24 * ccc1 * ccc2 * kk**2 * t * ww - 4 * ccc1 * ccc2 * kk**2 * t
      -18 * ccc1 * kk**2 * t**2 * ww**2 + 12 * ccc1 * kk**2 * t**2 * ww
      -2 * ccc1 * kk**2 * t**2 + 9 * ccc2**4 * kk**4 * ww**2 - 6 * ccc2**4 * kk**4 * ww
      + ccc2**4 * kk**4 + 36 * ccc2**3 * kk**4 * t * ww**2 - 24 * ccc2**3 * kk**4 * t * ww
      + 4 * ccc2**3 * kk**4 * t + 54 * ccc2**2 * kk**4 * t**2 * ww**2
      - 36 * ccc2**2 * kk**4 * t**2 * ww + 6 * ccc2**2 * kk**4 * t**2
      + 36 * ccc2 * kk**4 * t**3 * ww**2 - 24 * ccc2 * kk**4 * t**3 * ww
      + 4 * ccc2 * kk**4 * t**3 + 9 * kk**4 * t**4 * ww**2 - 6 * kk**4 * t**4 * ww
      + kk**4 * t**4)=0,ww);
    write "Choice for w(t) in order to fulfill frist3(-0) field equation:";
    write solve((3 * kk**2 * (4 * cc * iota**2 * kappa * ww - 4 * cc * iota**2 * kappa
      + 3 * ccc1 * chi * ww - ccc1 * chi)) / (kappa * (3 * ccc1**2 * ww - ccc1**2
      - 6 * ccc1 * ccc2**2 * kk**2 * ww + 2 * ccc1 * ccc2**2 * kk**2
      - 12 * ccc1 * ccc2 * kk**2 * t * ww + 4 * ccc1 * ccc2 * kk**2 * t
      - 6 * ccc1 * kk**2 * t**2 * ww + 2 * ccc1 * kk**2 * t**2
      + 3 * ccc2**4 * kk**4 * ww - ccc2**4 * kk**4 + 12 * ccc2**3 * kk**4 * t * ww
      - 4 * ccc2**3 * kk**4 * t + 18 * ccc2**2 * kk**4 * t**2 * ww
      - 6 * ccc2**2 * kk**4 * t**2 + 12 * ccc2 * kk**4 * t**3 * ww
      - 4 * ccc2 * kk**4 * t**3 + 3 * kk**4 * t**4 * ww - kk**4 * t**4))=0,ww);
    write "Choice for w(t) in order to fulfill frist3(-1) field equation:";
    write solve((kk**2 * (4 * cc * iota**2 * kappa * ww - 4 * cc * iota**2 * kappa
      + 3 * ccc1 * chi * ww - ccc1 * chi)) / (kappa * (3 * ccc1**2 * ww - ccc1**2
      - 6 * ccc1 * ccc2**2 * kk**2 * ww + 2 * ccc1 * ccc2**2 * kk**2
      - 12 * ccc1 * ccc2 * kk**2 * t * ww + 4 * ccc1 * ccc2 * kk**2 * t
      - 6 * ccc1 * kk**2 * t**2 * ww + 2 * ccc1 * kk**2 * t**2 + 3 * ccc2**4 * kk**4 * ww
      - ccc2**4 * kk**4 + 12 * ccc2**3 * kk**4 * t * ww - 4 * ccc2**3 * kk**4 * t
      + 18 * ccc2**2 * kk**4 * t**2 * ww - 6 * ccc2**2 * kk**4 * t**2
      + 12 * ccc2 * kk**4 * t**3 * ww - 4 * ccc2 * kk**4 * t**3 + 3 * kk**4 * t**4 * ww
      - kk**4 * t**4))=0,ww);
    % Solution for S=+/- branch
    on nat;
    write "Of course we make the following ansatz which fulfills all of the three conditions from above:";
    off nat;
    write ww := (4 * cc * iota**2 * kappa + ccc1 * chi) / (4 * cc * iota**2 * kappa + 3 * ccc1 * chi);
  >>;

>>;

```

```

if equation_of_state_switch=5 then <<

  if kk=0 then <<
    % Solution for S=const
    % write cc := 0;
    % Solution for S=+/- branch
    write ccc3 := -4 * cc * kappa / (ccc1**2 * chi);
  >>;

  if kk neq 0 then <<
    % Solution for S=+/- branch
    write ccc3 := - 4 * cc * kappa / (ccc1 * chi);
  >>;

>>;

>>; % End of branch concerning the ansatz xi=xi(t)

displayFieldEquations$
displayNoetherIdentities$

write "Final form of the function xi:"; write xif;
write "Final form of the energy-density now reads:"; write mue;
write "Final form of the matter quantities:";
write "mstress4(-a,-b)"; write mstress4(-a,-b);
write "mhypermom3(-a,-b)"; write mhypermom3(-a,-b);
write "menergy3(-a)"; write menergy3(-a);
write "Final form of the geometrical quantities:";
displayStrainCurvature;
displayRotationalCurvature;
displayTorsion;
displayNonmetricity;
write nonriemnoetherlhs4(-a);

showtime;

shut "weyl_quad_nonmet.reo";

out "field_xi_t_r_dt.reo";
write first3(-a)-menergy3(-a)$
write second3(-a,-b)-mhypermom3(-a,-b)$
shut "field_xi_t_r_dt.reo";

out "noether_xi_t_r_dt.reo";
write nfirst4(-a)$
write nsecond4(-a,-b)$
shut "noether_xi_t_r_dt.reo";

if ansatz_switch=1 then <<
  out "curvature_torsion_nonmet_xi_t_r.reo";
  on nero;
  displayStrainCurvature$
  displayRotationalCurvature$
  displayTorsion$
  displayNonmetricity$
  shut "curvature_torsion_nonmet_xi_t_r.reo";
>>;

if ansatz_switch=2 then <<
  out "curvature_torsion_nonmet_xi_t.reo";
  on nero;
  displayStrainCurvature$
  displayRotationalCurvature$
  displayTorsion$

```

```
displayNonmetricity$  
  shut "curvature_torsion_nonmet_xi_t.reo";  
>>  
  
end$  
  
bye;
```



# Appendix E

## Miscellany

### E.1 Field equations and Noether identities for $\xi = \xi(t, r)$ using computer algebra

#### Field equations

$$\begin{aligned} -3\ddot{S}^2 a_4 \kappa S^2 - 3\ddot{S}^2 a_6 \kappa S^2 + 3\dot{S}^4 a_4 \kappa + 3\dot{S}^4 a_6 \kappa + 6\dot{S}^2 a_4 \kappa k + 6\dot{S}^2 a_6 \kappa k + 3\dot{S}^2 \chi S^2 \\ + \xi_{,r}^2 b \kappa k r^2 - \xi_{,r}^2 b \kappa + 3a_4 \kappa k^2 + 3a_6 \kappa k^2 + 4c \kappa S^2 \xi^2 + 3\chi k S^2 - \kappa \mu S^4 = 0 \end{aligned} \quad (\text{E.1})$$

$$\begin{aligned} -\ddot{S}^2 a_4 \kappa S^2 - \ddot{S}^2 a_6 \kappa S^2 - 2\ddot{S} \chi S^3 + \dot{S}^4 a_4 \kappa + \dot{S}^4 a_6 \kappa + 2\dot{S}^2 a_4 \kappa k + 2\dot{S}^2 a_6 \kappa k - \dot{S}^2 \chi S^2 \\ - \xi_{,r}^2 b \kappa k r^2 + \xi_{,r}^2 b \kappa + a_4 \kappa k^2 + a_6 \kappa k^2 + 4c \kappa S^2 \xi^2 - \chi k S^2 - \kappa p_r S^4 = 0 \end{aligned} \quad (\text{E.2})$$

$$\begin{aligned} \ddot{S}^2 a_4 \kappa S^2 + \ddot{S}^2 a_6 \kappa S^2 + 2\ddot{S} \chi S^3 - \dot{S}^4 a_4 \kappa - \dot{S}^4 a_6 \kappa - 2\dot{S}^2 a_4 \kappa k - 2\dot{S}^2 a_6 \kappa k + \dot{S}^2 \chi S^2 \\ - \xi_{,r}^2 b \kappa k r^2 + \xi_{,r}^2 b \kappa - a_4 \kappa k^2 - a_6 \kappa k^2 - 4c \kappa S^2 \xi^2 + \chi k S^2 + \kappa p_t S^4 = 0 \end{aligned} \quad (\text{E.3})$$

$$\begin{aligned} \ddot{S} a_4 S^2 + \ddot{S} a_6 S^2 + \ddot{S} \dot{S} a_4 S + \ddot{S} \dot{S} a_6 S - 2\dot{S}^3 a_4 - 2\dot{S}^3 a_6 - 2\dot{S} a_4 k - 2\dot{S} a_6 k = 0 \end{aligned} \quad (\text{E.4})$$

#### Noether identities

$$\begin{aligned} \dot{\mu} S^4 - 16\dot{S} c S \xi^2 + 3\dot{S} \mu S^3 + \dot{S} p_r S^3 + 2\dot{S} p_t S^3 - 2\xi_{,rt} \xi_{,r} b \kappa r^2 + 2\xi_{,rt} \xi_{,r} b - 8\xi_{,t} c S^2 \xi = 0 \end{aligned} \quad (\text{E.5})$$

$$\begin{aligned} -\xi_{,rr} \xi_{,r} b \kappa r^3 + \xi_{,rr} \xi_{,r} b r - 3\xi_{,r}^2 b \kappa r^2 + 2\xi_{,r}^2 b + 4\xi_{,r} c r S^2 \xi - p_r S^4 + p_t S^4 = 0 \end{aligned} \quad (\text{E.6})$$

## E.2 Field equations and Noether identities for $\zeta = \zeta(t)$ using computer algebra

### Field equations

$$0 = -3\ddot{S}^2 a_4 \kappa S^2 - 3\ddot{S}^2 a_6 \kappa S^2 + 3\dot{S}^4 a_4 \kappa + 3\dot{S}^4 a_6 \kappa + 6\dot{S}^2 a_4 \kappa k + 6\dot{S}^2 a_6 \kappa k + 3\dot{S}^2 \chi S^2 + 3a_4 \kappa k^2 + 3a_6 \kappa k^2 + 4c\kappa S^2 \zeta^2 + 3\chi k S^2 - \kappa \mu S^4 \quad (\text{E.7})$$

$$0 = -\ddot{S}^2 a_4 \kappa S^2 - \ddot{S}^2 a_6 \kappa S^2 - 2\ddot{S} \chi S^3 + \dot{S}^4 a_4 \kappa + \dot{S}^4 a_6 \kappa + 2\dot{S}^2 a_4 \kappa k + 2\dot{S}^2 a_6 \kappa k - \dot{S}^2 \chi S^2 + a_4 \kappa k^2 + a_6 \kappa k^2 + 4c\kappa S^2 \zeta^2 - \chi k S^2 - \kappa p_r S^4 \quad (\text{E.8})$$

$$0 = \ddot{S}^2 a_4 \kappa S^2 + \ddot{S}^2 a_6 \kappa S^2 + 2\ddot{S} \chi S^3 - \dot{S}^4 a_4 \kappa - \dot{S}^4 a_6 \kappa - 2\dot{S}^2 a_4 \kappa k - 2\dot{S}^2 a_6 \kappa k + \dot{S}^2 \chi S^2 - a_4 \kappa k^2 - a_6 \kappa k^2 - 4c\kappa S^2 \zeta^2 + \chi k S^2 + \kappa p_t S^4 \quad (\text{E.9})$$

$$0 = \ddot{S} a_4 S^2 + \ddot{S} a_6 S^2 + \ddot{S} \dot{S} a_4 S + \ddot{S} \dot{S} a_6 S - 2\dot{S}^3 a_4 - 2\dot{S}^3 a_6 - 2\dot{S} a_4 k - 2\dot{S} a_6 k \quad (\text{E.10})$$

### Noether identities

$$0 = \dot{\mu} S^3 - 16\dot{S} c \zeta^2 + 3\dot{S} \mu S^2 + \dot{S} p_r S^2 + 2\dot{S} p_t S^2 - 8\zeta_{,t} c S \zeta \quad (\text{E.11})$$

$$0 = -p_r + p_t \quad (\text{E.12})$$

## E.3 Robertson-Walker metric

In the following we collect some basic results for the Robertson-Walker metric which are used throughout the work. Coordinates are labeled from  $x^\alpha = (t, r, \theta, \phi)$  with signature is  $(-, +, +, +)$ .

### E.3.1 Riemannian connection

Calculated with GrTensor II 1.79 (R4) (metric rwk) and Reduce 3.7:

$$\begin{aligned} \Gamma^1_{10} &= \Gamma^2_{20} = \Gamma^3_{30} = -\Gamma^1_{01} = -\Gamma^2_{02} = -\Gamma^3_{03} = -\frac{\dot{S}}{S}, \\ \Gamma^2_{21} &= \Gamma^3_{31} = -\Gamma^2_{12} = -\Gamma^3_{13} = -\frac{1}{r}, \\ \Gamma^0_{11} &= \frac{S\dot{S}}{kr^2 - 1}, \quad \Gamma^1_{11} = -\frac{kr}{kr^2 - 1}, \\ \Gamma^0_{22} &= -S\dot{S}r^2, \quad \Gamma^0_{33} = -S\dot{S}r^2 \sin^2 \theta, \\ \Gamma^1_{22} &= (1 - kr^2) r, \quad \Gamma^1_{33} = (1 - kr^2) r \sin^2 \theta, \\ \Gamma^2_{23} &= -\Gamma^2_{32} = -\frac{\cos \theta}{\sin \theta}, \quad \Gamma^2_{33} = \sin \theta \cos \theta. \end{aligned} \quad (\text{E.13})$$

### E.3.2 Weyl-Cartan connection

Calculated with Reduce 3.7 for the special case  $\xi \rightarrow \zeta$ :

$$\begin{aligned}
\Gamma^0_{00} &= \frac{\zeta}{2S}, \quad \Gamma^1_{10} = \Gamma^2_{20} = \Gamma^3_{30} = -\Gamma^1_{01} = -\Gamma^2_{02} = -\Gamma^3_{03} = -\frac{\dot{S}}{S}, \\
\Gamma^0_{11} &= \frac{S(2\dot{S} + \zeta)}{2(kr^2 - 1)}, \quad \Gamma^1_{11} = -\frac{kr}{kr^2 - 1}, \quad \Gamma^0_{22} = -\frac{r^2 S}{2}(2\dot{S} + \zeta), \\
\Gamma^1_{22} &= r(1 - kr^2), \quad \Gamma^2_{21} = \Gamma^3_{31} = -\Gamma^2_{12} = -\Gamma^3_{13} = -\frac{1}{r}, \\
\Gamma^2_{33} &= \cos\theta \sin\theta, \quad \Gamma^3_{23} = \frac{\cos\theta}{\sin\theta}, \\
\Gamma^0_{33} &= -\frac{\sin^2\theta r^2 S}{2}(2\dot{S} + \zeta), \quad \Gamma^1_{33} = \sin^2\theta r(1 - kr^2).
\end{aligned} \tag{E.14}$$

## E.4 SN Ia data set

In table E.1 we display the SN Ia set for fitting as provided by Y. Wang. Note that  $\sigma_{mz}$  is calculated iteratively via (3.89). The displayed values for  $\sigma_{mz}$  correspond to the standard FLRW model with  $(\Omega_{m0} = 0.3, \Omega_{\lambda0} = 0.7, H_0 = 65 \frac{\text{km}}{\text{s Mpc}})$ .

Table E.1: SN Ia data set for fitting.

SN name	$z$	$\mu_0$	$\sigma_{\mu_0}$	$\sigma_z$	$\sigma_{mz}$
1996E	0.43	41.74	0.28	200.0	0.003998
1996H	0.62	42.98	0.17	200.0	0.002841
1996I	0.57	42.76	0.19	2500.0	0.038438
1996J	0.30	41.38	0.24	200.0	0.005570
1996K	0.38	41.63	0.20	2500.0	0.056023
1996U	0.43	42.55	0.25	200.0	0.003998
1997ce	0.44	41.95	0.17	2500.0	0.048929
1997cj	0.50	42.40	0.17	2500.0	0.043451
1997ck	0.97	44.39	0.30	200.0	0.001845
1995K	0.48	42.45	0.17	200.0	0.003611
1995ao	0.30	40.74	0.60	200.0	0.005570
1995ap	0.23	40.33	0.46	2500.0	0.088889
1996R	0.16	39.08	0.40	200.0	0.009948
1996T	0.24	40.68	0.43	200.0	0.006838
1997I	0.17	39.95	0.24	200.0	0.009403

SN name	$z$	$\mu_0$	$\sigma_{\mu_0}$	$\sigma_z$	$\sigma_{mz}$
1997ap	0.83	43.67	0.35	2500.0	0.026861
1992bo	0.018	34.72	0.16	200.0	0.081575
1992bc	0.020	34.87	0.11	200.0	0.073523
1992aq	0.101	38.41	0.15	200.0	0.015313
1992ae	0.075	37.80	0.17	200.0	0.020322
1992P	0.026	35.76	0.13	200.0	0.056798
1990af	0.050	36.53	0.15	200.0	0.030017
1994M	0.024	35.39	0.18	200.0	0.061445
1994S	0.016	34.27	0.12	200.0	0.091638
1994T	0.036	36.19	0.21	200.0	0.041306
1995D	0.008	33.01	0.13	200.0	0.182192
1995E	0.012	33.60	0.17	200.0	0.121825
1995ac	0.049	36.85	0.13	200.0	0.030610
1995ak	0.022	35.15	0.16	200.0	0.066935
1995bd	0.016	34.15	0.19	200.0	0.091638
1996C	0.028	35.98	0.20	200.0	0.052815
1996ab	0.124	39.01	0.13	200.0	0.012622
1992ag	0.026	35.37	0.23	200.0	0.056798
1992al	0.014	33.92	0.11	200.0	0.104576
1992bg	0.035	36.26	0.21	200.0	0.042457
1992bh	0.045	36.91	0.17	200.0	0.033244
1992bl	0.043	36.26	0.15	200.0	0.034744
1992bp	0.080	37.65	0.13	200.0	0.019108
1992br	0.087	38.21	0.19	200.0	0.017641
1992bs	0.064	37.61	0.14	200.0	0.023658
1993H	0.025	35.20	0.26	200.0	0.059029
1993O	0.052	37.03	0.12	200.0	0.028899
1993ag	0.050	36.80	0.17	200.0	0.030017
1994U	0.004	31.72	0.10	200.0	0.363282
1997bp	0.008	32.81	0.10	200.0	0.182192
1996V	0.025	35.35	0.17	200.0	0.059029
1994C	0.052	36.72	0.15	200.0	0.028899
1995M	0.053	37.12	0.15	200.0	0.028372
1995ae	0.068	37.58	0.21	200.0	0.022321
1994B	0.090	38.51	0.10	200.0	0.017082
1992bi	0.458	42.44	0.46	300.0	0.005657
1994F	0.354	41.71	0.33	300.0	0.007176
1994G	0.425	41.46	0.49	300.0	0.006063
1994H	0.374	41.05	0.22	300.0	0.006822

SN name	$z$	$\mu_0$	$\sigma_{\mu_0}$	$\sigma_z$	$\sigma_{mz}$
1994al	0.420	41.88	0.25	300.0	0.006130
1994am	0.372	41.59	0.20	300.0	0.006856
1994an	0.378	41.91	0.37	300.0	0.006755
1995aq	0.453	42.50	0.25	300.0	0.005715
1995ar	0.465	42.66	0.30	1500.0	0.027891
1995as	0.498	43.04	0.25	300.0	0.005234
1995at	0.655	42.60	0.21	300.0	0.004045
1995aw	0.400	41.69	0.19	9000.0	0.192365
1995ax	0.615	42.52	0.25	300.0	0.004294
1995ay	0.480	42.29	0.24	300.0	0.005416
1995az	0.450	41.84	0.23	300.0	0.005750
1995ba	0.388	41.98	0.20	300.0	0.006595
1996cf	0.570	42.60	0.22	3000.0	0.046126
1996cg	0.490	42.43	0.20	3000.0	0.053132
1996ci	0.495	42.16	0.19	300.0	0.005263
1996ck	0.656	42.90	0.28	300.0	0.004039
1996cl	0.828	43.98	0.54	300.0	0.003231
1996cm	0.450	42.50	0.23	3000.0	0.057505
1996cn	0.430	42.46	0.22	3000.0	0.059977
1997F	0.580	42.79	0.23	300.0	0.004538
1997G	0.763	43.80	0.53	300.0	0.003496
1997H	0.526	42.48	0.20	300.0	0.004973
1997J	0.619	43.13	0.28	300.0	0.004268
1997K	0.592	43.75	0.37	300.0	0.004451
1997L	0.550	42.84	0.25	3000.0	0.047698
1997N	0.180	39.76	0.17	300.0	0.013376
1997O	0.374	42.85	0.24	300.0	0.006822
1997P	0.472	42.44	0.19	300.0	0.005501
1997Q	0.430	41.90	0.18	3000.0	0.059977
1997R	0.657	43.16	0.23	300.0	0.004034
1997S	0.612	43.02	0.21	300.0	0.004314
1997ac	0.320	41.19	0.18	3000.0	0.078741
1997af	0.579	42.81	0.22	300.0	0.004545
1997ai	0.450	42.16	0.30	3000.0	0.057505
1997aj	0.581	42.42	0.22	300.0	0.004530
1997am	0.416	41.90	0.20	300.0	0.006184
1990O	0.030	35.59	0.20	600.0	0.148089
1993B	0.071	37.66	0.20	600.0	0.064248

## E.5 Symmetric tracefree part of the second field equation

In this appendix we provide a short derivation of the symmetric tracefree part of the second field equation as displayed in equation (3.15). Although we did not use this explicit form of the second field equation in our CA programs, it might become handy in future calculations. In the following we make use of the gauge field excitations (3.5)–(3.9), which were derived from our Lagrangian in (3.3). The symmetric part of the second MAG field equation becomes

$$\begin{aligned}
& g_{\gamma(\alpha}DH^{\gamma}_{\beta)} - g_{\gamma(\alpha}E^{\gamma}_{\beta)} \\
= & g_{\gamma(\alpha}D \left( -\frac{\chi}{2\kappa}\eta^{\gamma}_{\beta)} - 2 \sum_{I=1}^6 a_I {}^{\star(I)}W^{\gamma}_{\beta)} - \frac{b}{2} {}^{\star} \left( \delta^{\gamma}_{\beta)} R^{\nu}_{\nu} \right) \right) - cg_{\alpha\beta} {}^{\star}Q^{\gamma}_{\gamma} \\
\stackrel{(A.38)}{=} & \frac{\chi}{2\kappa}Q_{(\alpha}{}^{\gamma} \wedge \eta_{\gamma|\beta)} - g_{\gamma(\alpha}D \left( 2 \sum_{I=1}^6 a_I {}^{\star(I)}W^{\gamma}_{\beta)} + \frac{b}{2} {}^{\star} \left( \delta^{\gamma}_{\beta)} R^{\nu}_{\nu} \right) \right) - cg_{\alpha\beta} {}^{\star}Q^{\gamma}_{\gamma} \\
= & \frac{\chi}{2\kappa}Q_{(\alpha}{}^{\gamma} \wedge \eta_{\gamma|\beta)} - \frac{b}{2}g_{\alpha\beta}d {}^{\star}R^{\gamma}_{\gamma} - 2 \sum_{I=1}^6 a_I g_{\gamma(\alpha}D {}^{\star(I)}W^{\gamma}_{\beta)} - cg_{\alpha\beta} {}^{\star}Q^{\gamma}_{\gamma}.
\end{aligned} \tag{E.15}$$

The trace part is given by

$$\begin{aligned}
dH^{\gamma}_{\gamma} - E^{\gamma}_{\gamma} &= d \left( -\frac{\chi}{2\kappa}\eta^{\gamma}_{\gamma} - 2b {}^{\star}R^{\gamma}_{\gamma} \right) - cg_{\gamma\mu} {}^{\star} \left( g^{\gamma\mu}Q^{\alpha}_{\alpha} \right) \\
&= -2bd {}^{\star}R^{\gamma}_{\gamma} - 4c {}^{\star}Q^{\gamma}_{\gamma}.
\end{aligned} \tag{E.16}$$

Hence the symmetric tracefree part of the second field equation is given by

$$\begin{aligned}
& g_{\gamma(\alpha}DH^{\gamma}_{\beta)} - g_{\gamma(\alpha}E^{\gamma}_{\beta)} - \frac{1}{4}g_{\alpha\beta}DH^{\gamma}_{\gamma} + \frac{1}{4}g_{\alpha\beta}E^{\gamma}_{\gamma} \\
= & \frac{\chi}{2\kappa}Q_{(\alpha}{}^{\gamma} \wedge \eta_{\gamma|\beta)} - 2 \sum_{I=1}^6 a_I g_{\gamma(\alpha}D {}^{\star(I)}W^{\gamma}_{\beta)}.
\end{aligned} \tag{E.17}$$

In a Weyl-Cartan spacetime  $Q_{\alpha\beta} := \frac{1}{4}g_{\alpha\beta}Q^{\gamma}_{\gamma}$ . Therefore the first term in the last equation vanishes, yielding

$$-2 \sum_{I=1}^6 a_I g_{\gamma(\alpha}D {}^{\star(I)}W^{\gamma}_{\beta)} \stackrel{\text{WC}}{=} \mathring{\Delta}^{\text{WC}}_{(\alpha\beta)}, \tag{E.18}$$

where  $\mathring{\Delta}^{\text{WC}}_{(\alpha\beta)} := \Delta_{(\alpha\beta)} - \frac{1}{4}g_{\alpha\beta}\Delta^{\gamma}_{\gamma}$  represents the shear current. Additionally, the  $a_6$  term can be rewritten with the help of formula (A.38). With

$${}^{(6)}W_{\alpha\beta} := -\frac{1}{12}W \vartheta_{\alpha} \wedge \vartheta_{\beta}, \tag{E.19}$$

we obtain

$$g_{\gamma(\alpha} D^{\star(6)} W^{\gamma}_{\beta)} \stackrel{(A.38)}{=} \frac{1}{12} W Q_{(\alpha}{}^{\mu} \wedge \eta^{\mu}{}_{|\beta)} \stackrel{\text{WC}}{=} 0. \quad (\text{E.20})$$

Hence in a Weyl-Cartan spacetime the  $a_6$  term drops from the sum in (E.21). Therefore the symmetric tracefree part is given by

$$-2 \sum_{I=1}^5 a_I g_{\gamma(\alpha} D^{\star(I)} W^{\gamma}_{\beta)} \stackrel{\text{WC}}{=} \mathcal{A}_{(\alpha\beta)}. \quad (\text{E.21})$$





# Bibliography

## [Textbooks & Monographs]

- [1] E.W. Kolb, Michael S. Turner: *The early universe*. Addison-Wesley, Redwood City (1990)
- [2] J.A. Peacock: *Cosmological physics*. Cambridge University Press, Cambridge (1999)
- [3] P.J.E. Peebles: *Principles of physical cosmology*. Princeton University Press, Princeton (1993)
- [4] G. Börner: *The early universe – Facts and fiction*. Springer, Berlin, 3rd edition (1993)
- [5] H. Goenner: *Einführung in die Kosmologie*. Spektrum Akademischer Verlag, Heidelberg (1994)
- [6] E.W. Kolb, Michael S. Turner eds.: *The early universe - Reprints*. Addison-Wesley, Redwood City (1988)
- [7] G.B. Field (ed.), H. Arp, J.N. Bahcall: *The redshift controversy*. W.A. Benjamin, Reading (1973)
- [8] M. Rowan-Robinson: *The cosmological distance ladder*. W.H. Freeman, New York (1985)
- [9] E.R. Harrison: *Cosmology - the science of the universe*. Cambridge University Press, Cambridge, 2nd edition (2000)
- [10] T. Padmanabhan: *Structure formation in the universe*. Cambridge University Press, Cambridge, reprinted edition (1995)
- [11] A.R. Liddle, D.H. Lyth: *Cosmological inflation and large-scale structure*. Cambridge University Press, Cambridge (2000)
- [12] T. Padmanabhan: *Theoretical astrophysics Volume I: Astrophysical processes*. Cambridge University Press, Cambridge (2000)
- [13] T. Padmanabhan: *Theoretical astrophysics Volume II: Stars and stellar systems*. Cambridge University Press, Cambridge (2001)

- [14] A.D. Linde: *Inflation and quantum cosmology*. Academic Press, Boston (1990)
- [15] A.D. Linde: *Elementarteilchen und inflationärer Kosmos: zur gegenwärtigen Theorienbildung*. Spektrum Akademischer Verlag, Heidelberg (1993)
- [16] P.J.E. Peebles: *The large-scale structure of the universe*. Princeton University Press, Princeton (1980)
- [17] P. Coles, G.F.R. Ellis: *Is the universe open or closed?* Cambridge University Press, Cambridge (1997)
- [18] J.C. Niemeyer, J.W. Truran (eds.): *Type Ia supernovae: Theory and cosmology*. Cambridge University Press, Cambridge (2000)
- [19] F. Hoyle, G. Burbidge, J.V. Narlikar: *A different approach to cosmology*. Cambridge University Press, Cambridge (2000)
- [20] B.E. Pagel: *Nucleosynthesis and chemical evolution of galaxies*. Cambridge University Press, Cambridge (1997)
- [21] M.L. Lachièze-Rey, E. Gunzig: *The cosmological background radiation - Echo of the early universe*. Cambridge University Press, Cambridge (1999)
- [22] R. d'Inverno: *Einführung in die Relativitätstheorie*. VCH, Weinheim (1995)
- [23] H. Stephani: *Allgemeine Relativitätstheorie*. Deutscher Verlag der Wissenschaften, Berlin, 3rd edition (1988)
- [24] S. Weinberg: *Gravitation and cosmology*. Wiley, New York (1972)
- [25] D. Kramer, H. Stephani, E. Herlt, M. MacCallum: *Exact solutions of Einstein's field equations*. Cambridge University Press, Cambridge (1980)
- [26] C.W. Misner, K.S. Thorne, J.A. Wheeler: *Gravitation*. Freeman, San Francisco (1973)
- [27] C. Lämmerzahl, C.W.F. Everitt, F.W. Hehl (eds.): *Gyros, clocks, interferometers . . . : Testing relativistic gravity in space* Springer, Berlin, Lecture notes in physics: Vol. 562 (2001)
- [28] C.M. Will: *Theory and experiment in gravitational physics*. Cambridge University Press, Cambridge (1993)
- [29] F.W. Hehl, R.A. Puntigam, H. Ruder (Eds.): *Relativity and scientific computing: computer algebra, numerics, visualization*. Springer-Verlag, Berlin (1986)
- [30] Hehl, Winkelmann, Meyer: *Reduce*. Springer-Verlag, Berlin, 2nd edition, (1993)
- [31] A.C. Hearn: *Reduce User's and Contributed Packages Manual Version 3.7* (1999)

- [32] J. Ueberberg: *Einführung in die Computeralgebra mit Reduce*. BI Wissenschaftsverlag, Mannheim (1992)
- [33] M. Kofler: *Mathematica - Einführung, Anwendung, Referenz*. Addison Wesley Longman, Bonn, 3rd edition (1998)
- [34] M.L. Herrmann: *Mathematica - Eine beispielorientierte Einführung*. Addison Wesley Longman, Bonn (1997)
- [35] W.H. Press, S.A. Teukolsky, W.T. Vetterling, B.P. Flannery: *Numerical recipes in C - The Art of scientific computing*. Cambridge University Press, Cambridge, 2nd edition (1992)
- [36] P.R. Bevington: *Data reduction and error analysis for the physical sciences*. McGraw-Hill, New York, 2nd edition (1992)
- [37] B.R. Martin: *Statistics for physicists*. Academic Press, London (1971)
- [38] W. Walter: *Gewöhnliche Differentialgleichungen*. Springer, Berlin, 6th edition (1996)
- [39] M. Nakahara: *Geometry, Topology and Physics*. Adam Hilger, Bristol (1990)

**[Computer stuff]**

- [40] J.A. Nelder, R. Mead: *A simplex method for function minimization*. Computer J. **7** 308-313 (1965)
- [41] P. Musgrave, D. Pollney, K. Lake: *GrTensorII documentation A-F*, Queen's University at Kingston, Ontario (1996), <http://grtensor.phy.queensu.ca/>
- [42] E. Schrüfer, F.W. Hehl, J.D. McCrea: *Exterior calculus on the computer: The Reduce-package Excalc applied to general relativity and to the Poincaré gauge theory*. Gen. Rel. Grav. **19** 197-218 (1987)
- [43] J. Socorro, A. Macías, F.W. Hehl: *Computer algebra in gravity: Programs for (non-) Riemannian spacetimes I*. Comp. Phys. Comm. **115** 264-283 (1998) Los Alamos e-Print Archive [gr-qc/9804068](http://arxiv.org/abs/gr-qc/9804068)

**[Metric-affine gravity]**

- [44] F.W. Hehl, J.D. McCrea, E.W. Mielke, Y. Ne'eman: *Metric-affine gauge theory of gravity: Field equations, Noether identities, world spinors, and breaking of dilation invariance*. Phys. Rep. **258** 1-171 (1995)
- [45] F.W. Hehl, A. Macías: *Metric-affine gauge theory of gravity: II. Exact solutions*. Int. J. Mod. Phys. **D8** 399-416 (1999)

- [46] F. Gronwald: *Metric-affine gauge theory of gravity: I. Fundamental structure and field equations*. Int. J. Mod. Phys. **D6** 263-304 (1997) Los Alamos e-Print Archive [gr-qc/9702034](#)
- [47] F. Gronwald, F.W. Hehl: *On the gauge aspects of gravity*. Proc. of the 14th Course of the School of Cosmology and Gravitation on Quantum Gravity, Erice, Italy, (1995)
- [48] J.D. McCrea: *Irreducible decompositions of the non-metricity, torsion, curvature and Bianchi identities in metric-affine spacetimes*. Class. Quantum Grav. **9** 553-568 (1992)
- [49] M. Toussaint: *Gauge theory of gravity: Foundations, the charge concept and a numeric solution*. Diploma thesis, University of Cologne (1999)
- [50] Y.N. Obukhov, R. Tresguerres: *Hyperfluid - a model of classical matter with hypermomentum*. Phys. Lett. **A184** 17-22 (1993)
- [51] I. Kirsch, D. Sijacki: *From Poincaré to affine invariance: how does the Dirac equation generalize?* Class. Quantum Grav. **19** 3157-3178 (2002) Los Alamos e-print Archive [gr-qc/0111088](#)
- [52] O. Preuss: *Astronomical tests of the Einstein equivalence principle*. PhD. thesis, Universität Bielefeld (2002)
- [**Alternative models**]
- [53] I. Prigogine et al.: *Thermodynamics and cosmology*. Gen. Rel. Grav. **21** 767-776 (1989)
- [54] M. Gasperini: *Repulsive gravity in the very early universe*. Gen. Rel. Grav. **30** 1703-1709 (1998)
- [55] L.C. Garcia de Andrade: *On dilaton solutions of the de Sitter inflation and primordial spin-torsion density fluctuations*. Phys. Lett. **B468** 28-30 (1999)
- [56] D. Palle: *On primordial cosmological density fluctuations in Einstein-Cartan gravity and COBE data*. Nuov. Cim. **114B** 853-860 (1999)
- [57] W.F. Kao: *Inflationary solution in Weyl invariant theory*. Phys. Lett. **A149** 76-78 (1990)
- [58] E.A. Poberii: *Nonmetricity driven inflation*. Helv. Phys. Acta **67** 745-752 (1994)
- [59] A.V. Minkevich: *Generalized cosmological Friedmann equations without gravitational singularity*. Phys. Lett. **A80** 232-234 (1980)
- [60] A.V. Minkevich: *Generalized cosmological Friedmann equations and the de Sitter solution*. Phys. Lett. **A95** 422-424 (1983)

- [61] A.V. Minkevich, I.M. Nemenman: *On the influence of the gravitating vacuum on the dynamics of homogeneous isotropic models in gauge theories of gravity*. Class. Quantum Grav. **12** 1259-1265 (1995)
- [62] A.V. Minkevich, A.S. Garkun: *Isotropic cosmology in metric-affine gauge theory of gravity*. Los Alamos e-print Archive [gr-qc/9805007](#)
- [63] R.W. Tucker, C. Wang: *Dark matter gravitational interactions*. Class. Quantum Grav. **15** 933-954 (1998) Los Alamos e-print Archive [gr-qc/9612019](#)
- [64] T. Dereli, R.W. Tucker: *On the detection of scalar field induced spacetime torsion*. Mod. Phys. Lett. **A12** 421-428 (2002) Los Alamos e-print Archive [gr-qc/0104050](#)
- [65] T. Dereli, R.W. Tucker: *On the motion of matter in spacetime*. Los Alamos e-print Archive [gr-qc/0107017](#)
- [66] P. Peter, N. Pinto-Neto: *Primordial perturbations in a non singular bouncing universe model*. Phys. Rev. **D66** 063509 (2002) Los Alamos e-print Archive [hep-th/0203013](#)
- [67] D. Langlois: *Brane cosmology: an introduction*. Los Alamos e-print Archive [hep-th/0209261](#)

#### [Weyl-Cartan models]

- [68] D. Puetzfeld, R. Tresguerres: *A cosmological model in Weyl-Cartan spacetime*. Class. Quantum Grav. **18** 667-693 (2001) Los Alamos e-Print Archive [gr-qc/0101050](#)
- [69] D. Puetzfeld: *A cosmological model in Weyl-Cartan spacetime: I. Field equations and solutions*. Class. Quantum Grav. **19** 3363-3280 (2002) Los Alamos e-Print Archive [gr-qc/0111014](#)
- [70] D. Puetzfeld: *A cosmological model in Weyl-Cartan spacetime: II. Magnitude-redshift relation*. Class. Quantum Grav. **19** 4463-4482 (2002) Los Alamos e-Print Archive [gr-qc/0205052](#)
- [71] D. Puetzfeld: *A non-standard cosmological model*. Int. J. of Mod. Phys. **A17** 2772 (2002)
- [72] O.V. Babourova, B.N. Frolov: *Matter with dilaton charge in Weyl-Cartan spacetime and evolution of the universe*. Los Alamos e-print Archive [gr-qc/0209077](#)

#### [Triplet models]

- [73] T. Dereli et al.: *Non-Riemannian gravity and the Einstein-Proca system*. Class. Quantum Grav. **13** L103-L109 (1996)

- [74] Y.N. Obukhov, E.J. Vlachynsky, W. Esser, F.W. Hehl: *Effective Einstein theory from metric-affine gravity models via irreducible decompositions*. Phys. Rev. **D56** 7769-7778 (1997)

[Large scale structure]

- [75] C. Alcock, B. Paczyński: *An evolution free test for non-zero cosmological constant*. Nature **281** 358-359 (1979)
- [76] J.A. Peacock et al.: *A measurement of the cosmological mass density from clustering in the 2dF galaxy redshift survey* Nature **410** 169-173 (2001)
- [77] M. Bernardi: *Large scale structure in the Sloan Digital Sky Survey*. Los Alamos e-Print Archive [gr-qc/0111014](http://arxiv.org/abs/gr-qc/0111014)
- [78] <http://www.sdss.org>

[Inflation]

- [79] A.H. Guth: *Inflationary universe: A possible solution to the horizon and flatness problems*. Phys. Rev. **D28** 347-356 (1981)
- [80] *A new inflationary universe scenario: A possible solution of the horizon, flatness, homogeneity, isotropy and primordial monopole problems*. Phys. Lett. **108B** 389-393 (1982)
- [81] A.H. Guth: *Inflationary models and connections to particle physics*. Los Alamos e-print Archive [astro-ph/0002188](http://arxiv.org/abs/astro-ph/0002188)
- [82] A. Linde: *Inflation and string cosmology* Int. J. Mod. Phys. **A17S1** 89-104 (2002)  
Los Alamos e-print Archive [hep-th/0107176](http://arxiv.org/abs/hep-th/0107176)

[Reviews]

- [83] J. Bicák: *Selected solutions of Einstein's field equations: Their role in general relativity and astrophysics*. Lect. Notes Phys. **540** 1-126 (2000) Los Alamos e-Print Archive [gr-qc/0004016](http://arxiv.org/abs/gr-qc/0004016)
- [84] J. Bartels, D. Haidt, A. Zichichi eds.: *Review of particle physics*. Eur. Phys. J. **C15** 1-878 (2000)
- [85] K. Hagiwara et al.: *Review of particle physics*. Phys. Rev. **D66** 010001 (2002)
- [86] M.S. Turner: *Why cosmologists believe the universe is accelerating*. (published in [18]) Los Alamos e-print Archive [astro-ph/9904049](http://arxiv.org/abs/astro-ph/9904049)
- [87] M.S. Turner: *Dark energy and the new cosmology*. SNAP Yellow Book (Snowmass2001) Los Alamos e-print Archive [astro-ph/0108103](http://arxiv.org/abs/astro-ph/0108103)

- [88] M.S. Turner: *A sober assessment of cosmology at the new millennium*. Los Alamos e-print Archive [astro-ph/0102057](#)
- [89] M.S. Turner: *Dark matter and energy in the universe*. Phys. Scripta **T85** 210-220 (2000) Los Alamos e-print Archive [astro-ph/9901109](#)
- [90] M.S. Turner: *Dark matter and energy: The critical questions*. Los Alamos e-print Archive [astro-ph/0207297](#)
- [91] S. Weinberg: *Conference summary: 20th Texas symposium on relativistic astrophysics*. Los Alamos e-print Archive [astro-ph/0104482](#)
- [92] S.M. Carroll: *Dark energy and the preposterous universe*. Los Alamos e-print Archive [astro-ph/0107571](#)
- [93] C.H. Lineweaver: *Cosmological parameters*. Los Alamos e-print Archive [astro-ph/0112381](#)
- [94] P.J.E. Peebles: *The cosmological tests*. Int. J. Mod. Phys. **A16** 4223-4233 (2001)
- [95] M.S. Turner: *The new cosmology*. Int. J. Mod. Phys. **A17** 3446-3458 (2002) Los Alamos e-print Archive [astro-ph/0202007](#)
- [96] M.S. Turner: *Making sense of the new cosmology*. Int. J. Mod. Phys. **A17S1** 180-196 (2002) Los Alamos e-print Archive [astro-ph/0202008](#)
- [97] M.S. Turner: *A cosmic perspective from Lapland in 2001*. Los Alamos e-print Archive [astro-ph/0202005](#)
- [98] S. Sarkar: *New results in cosmology*. Los Alamos e-print Archive [hep-ph/0201140](#)
- [99] T. Padmanabhan: *Cosmic inventory of energy densities: issues and concerns*. Los Alamos e-print Archive [gr-qc/0112068](#)
- [100] M. White: *Complementary measures of the mass density and cosmological constant*. Astrophys. J. **506** 495-501 (1998) Los Alamos e-print Archive [astro-ph/9802295](#)
- [101] O. Lahav: *Observational tests of FRW world models*. Class. Quantum Grav. **19** 3517-3526 (2002) Los Alamos e-print Archive [astro-ph/0112524](#)
- [102] R. Durrer: *Frontiers of the universe: What do we know, what do we understand?* Los Alamos e-print Archive [astro-ph/0205101](#)
- [103] A. Melchiorri: *Cosmology rounding the cape*. Los Alamos e-print Archive [astro-ph/0204262](#)
- [104] A.R. Zentner, T.P. Walker: *Constraints on the cosmological relativistic energy density*. Phys. Rev. **D65** 063506 (2002) Los Alamos e-print Archive [astro-ph/0110533](#)

- [105] A.D. Dolgov: *Neutrinos in cosmology*. Phys. Rep. **370** 333-535 (2002)
- [106] D.J. Schwarz: *The first second of the universe*. Los Alamos e-print Archive astro-ph/0303574
- [Chaplygin gas]
- [107] J.D. Barrow: *Graduated inflationary universes*. Phys. Lett. **B235** 40-43 (1990)
- [108] M. Hassaïne et al.: *Relativistic Chaplygin gas with field-dependent Poincaré symmetry*. Lett. Math. Phys. **57** 33-40 (2001) Los Alamos e-print Archive hep-th/0101044
- [109] J.C. Fabris et al.: *Density perturbations in an universe dominated by the Chaplygin gas*. Gen. Rel. Grav. **34** 53-63 (2002) Los Alamos e-print Archive gr-qc/0103083
- [110] A. Kamenshchik et al.: *An alternative to quintessence*. Phys. Lett. **B511** 265-268 (2001) Los Alamos e-print Archive gr-qc/0103004
- [111] A. Dev, J.S. Alcaniz, D. Jain: *Cosmological consequences of a Chaplygin gas dark energy*. Los Alamos e-print Archive astro-ph/0209379
- [112] J.S. Alcaniz, D. Jain, A. Dev: *High-redshift objects and the generalised Chaplygin gas*. Los Alamos e-print Archive astro-ph/0210476
- [113] N. Bilić, G.B. Tupper, R.D. Jain: *Unification of dark matter and dark energy*. Phys. Lett. **B535** 17-21 (2002) Los Alamos e-print Archive astro-ph/0111325
- [114] V. Gorini, A. Kamenshchik, U. Moschella: *Can the Chaplygin gas be a plausible model for dark energy?* Los Alamos e-print Archive astro-ph/0209395
- [115] P.F. González-Díaz: *Unified model of dark energy*. Los Alamos e-print Archive astro-ph/0212414
- [116] M. Makler et al.: *Constraints on the generalized Chaplygin gas from supernovae observations*. Los Alamos e-print Archive astro-ph/0209486
- [117] M.C. Bento, O. Bertolami, A.A. Sen: *Generalized Chaplygin gas as a scheme for unification of dark energy and dark matter*. Los Alamos e-print Archive astro-ph/0210375
- [118] M.C. Bento, O. Bertolami, A.A. Sen: *Generalized Chaplygin gas and CMBR constraints*. Los Alamos e-print Archive astro-ph/0201468
- [119] H.B. Sandvik et al.: *The end of unified dark matter?* Los Alamos e-print Archive astro-ph/0212114



**[Accelerating universe & SN Ia & Distance-redshift relations]**

- [120] E. Hubble: *A relation between distance and radial velocity among extragalactic nebulae*. Proceedings of the National Academy of Science **15** 168 (1929) (reprinted in [1], [7])
- [121] S. Perlmutter et al.: *Measurements of  $\Omega$  and  $\Lambda$  from 42 high-redshift supernovae*. Astrophys. J. **517** 565-586 (1999)
- [122] S. Perlmutter et al.: *Cosmology from type Ia supernovae*. Bull. Am. Astron. Soc. **29** 1351 (1997) Los Alamos e-print Archive astro-ph/9812473
- [123] S. Perlmutter et al.: *Measurements of the cosmological parameters  $\Omega$  and  $\Lambda$  from the first seven supernovae at  $z \geq 0.35$* . Astrophys. J. **483** 565-581 (1997)
- [124] B.P. Schmidt et al.: *The high- $z$  supernova search: Measuring cosmic deceleration and global curvature of the universe using type Ia supernovae*. Astrophys. J. **507** 46-63 (1998)
- [125] A.G. Riess et al.: *The farthest known supernova: Support for an accelerating universe and a glimpse of the epoch of deceleration*. Astrophys. J. **560** 49-71 (2001) Los Alamos e-print Archive astro-ph/0104455
- [126] A.G. Riess et al.: *Observational evidence from supernovae for an accelerating universe and a cosmological constant*. Astrophys. J. **116** 1009-1038 (1998)
- [127] M. Hamuy et al.: *The absolute luminosities of the Calán/Tololo type Ia supernovae*. Los Alamos e-print Archive astro-ph/9609059
- [128] R.G. Vishwakarma: *Study of the magnitude-redshift relation for type Ia supernovae in a model resulting from a Ricci-symmetry*. Gen. Rel. Grav. **33** 1973-1984 (2001) Los Alamos e-print Archive gr-qc/0106021
- [129] R.G. Vishwakarma: *Consequences on some dark energy-candidates from SN 1997ff*. Mon. Not. Roy. Astron. Soc. **331** 776-784 (2002) Los Alamos e-print Archive astro-ph/0108118
- [130] R.G. Vishwakarma: *Consequences on variable  $\Lambda$ -models from distant type Ia supernovae and compact radio sources*. Class. Quantum Grav. **18** 1159-1172 (2001) Los Alamos e-Print Archive astro-ph/0012492
- [131] M.S. Turner, A.G. Riess: *Do SNe Ia provide direct evidence for the past deceleration of the universe?* Los Alamos e-print Archive astro-ph/0106051
- [132] W. Mattig: *Über den Zusammenhang zwischen Rotverschiebung und scheinbarer Helligkeit*. Astron. Nach. **284** 109-111 (1958)
- [133] P.M. Garnavich et al.: *Supernova limits on the cosmic equation of state*. Astrophys. J. **509** 74-79 (1998)

- [134] P.M. Garnavich et al.: *Constraints on cosmological models from Hubble space telescope observations of high- $z$  supernovae*. *Astrophys. J.* **493** L53-L57 (1998)
- [135] D. Behnke et al.: *Description of supernova data in conformal cosmology without cosmological constant*. *Phys. Lett.* **B530** 20-26 (2002) Los Alamos e-print Archive gr-qc/0102039
- [136] P.P. Avelino et al.: *Modified median statistics and type Ia supernova data*. *Astrophys. J.* **575** 989-995 (2002) Los Alamos e-print Archive astro-ph/0111195
- [137] Y. Wang: *Flux-averaging analysis of type Ia supernova data*. *Astrophys. J.* **536** 531-539 (2000)
- [138] Y. Wang, P.M. Garnavich: *Measuring time-dependence of dark energy density from type Ia supernova data*. *Astrophys. J.* **552** 445-451 (2001) Los Alamos e-print Archive astro-ph/0101040
- [139] K. Tomita: *Analysis of type Ia supernova data in cosmological models with a local void*. Los Alamos e-print Archive astro-ph/0104141
- [140] M. Rowan-Robinson: *Do type Ia supernovae prove  $\Lambda > 0$ ?* Los Alamos e-print Archive astro-ph/0201034
- [141] K. Freese, M. Lewis: *Cardassian expansion: a model in which the universe is flat, matter dominated, and accelerating*. *Phys. Lett.* **B540** (2002) 1-8 Los Alamos e-print Archive astro-ph/0201229
- [142] Y. Wang, G. Lovelace: *Unbiased estimate of the dark energy density from type Ia supernova data*. *Astrophys. J.* **562** (2001) L115-L120 Los Alamos e-print Archive astro-ph/0109233
- [143] J.C. Niemeyer et al.: *Models of type Ia supernova explosions*. Los Alamos e-print Archive astro-ph/0203369
- [**Dimming & magnification of SN Ia**]
- [144] C. Csáki, N. Kaloper, J. Terning: *Dimming supernovae without cosmic acceleration*. *Phys. Rev. Lett.* **88** 161302 (2002) Los Alamos e-print Archive hep-ph/0111311
- [145] C. Csáki, N. Kaloper, J. Terning: *Effects of the intergalactic plasma on supernova dimming via photon-axion oscillations*. *Phys. Lett.* **B535** 33-36 (2002) Los Alamos e-print Archive hep-ph/0112212
- [146] C. Deffayet et al.: *Dimming supernovae by photon-pseudoscalar conversion and the intergalactic plasma*. *Phys. Rev.* **D66** 043517 (2002) Los Alamos e-print Archive hep-ph/0112118

- [147] E. Mörtzell, L. Bergström, A. Goobar: *Photon-axion oscillations and type Ia supernovae*. Phys. Rev. **D66** 047702 (2002) Los Alamos e-print Archive astro-ph/0202153
- [148] E. Mörtzell, C. Gunnarsson, A. Goobar: *Gravitational lensing of the farthest known supernova SN1997ff*. Astrophys. J. **561** 106-110 (2001) Los Alamos e-print Archive astro-ph/0105355
- [149] Y. Wang: *Analytical modeling of the weak lensing of standard candles I. Empirical fitting of numerical simulation results*. Astrophys. J. **525** 651-658 (1999) Los Alamos e-print Archive astro-ph/9901212
- [150] Y. Wang, D.E. Holz, D. Munshi: *A universal probability distribution function for weak-lensing amplification*. Astrophys. J. **572** L15-L18 (2002) Los Alamos e-print Archive astro-ph/0204169
- [151] N. Dalal, D.E. Holz, X. Chen, J.A. Frieman: *Corrective lenses for high redshift supernovae*. Astrophys. J. **585** L11-L14 (2003) Los Alamos e-print Archive astro-ph/0206339

[**Future SN Ia experiments**]

- [152] M. Lampton et al.: *SNAP Telescope*. Los Alamos e-print Archive astro-ph/0209549
- [153] G. Aldering et al.: *Overview of the SuperNova/Acceleration Probe (SNAP)*. Los Alamos e-print Archive astro-ph/0209550

[**Alternative distance notions**]

- [154] C.C. Dyer, R.C. Roeder: *Distance-redshift relations for universes with some intergalactic medium*. Astrophys. J. **180** L31-L34 (1973)
- [155] C.C. Dyer, R.C. Roeder: *Observations in locally inhomogeneous cosmological models*. Astrophys. J. **189** 167-175 (1974)
- [156] E. Mörtzell: *The Dyer-Roeder distance-redshift relation in inhomogeneous universes*. Los Alamos e-print Archive astro-ph/0109197

[**Nucleocosmochronology**]

- [157] B. Chaboyer et al.: *The age of globular clusters in the light of HIPPARCOS: Resolving the age problem?* Astrophys. J. **494** 96-110 (1998)
- [158] J.W. Truran et al.: *Nucleosynthesis clocks and the age of the galaxy*. ASP Conference Series, Vol. TBD, 2001, Eds. T. von Hippel, N. Manset, C. Simpson Los Alamos e-print Archive astro-ph/0109526

**[Pioneer effect]**

- [159] J.D. Anderson et al.: *Study of the anomalous acceleration of Pioneer 10 and 11*. Phys. Rev. **D65** 082004 (2002) Los Alamos e-print Archive [gr-qc/0104064](#)
- [160] C.B. Markwardt: *Independent confirmation of the Pioneer 10 anomalous acceleration*. Los Alamos e-print Archive [gr-qc/0208046](#)

**[Cosmic microwave background]**

- [161] R.K. Sachs, A.M. Wolfe: *Perturbations of a cosmological model and angular variations of the microwave background*. Astrophys. J. **147** 73-90 (1967)
- [162] P.J.E. Peebles, J.T. Yu: *Primeval adiabatic perturbation in an expanding universe*. Astrophys. J. **162** 815-836 (1970)
- [163] W. Hu et al.: *Complete treatment of CMB anisotropies in a FRW universe*. Phys. Rev. **D57** 3290-3301 (1998)
- [164] W. Hu, S. Dodelson: *Cosmic microwave background anisotropies*. Ann. Rev. Astron. and Astrophys. **40** 171-216 (2002) Los Alamos e-print Archive [astro-ph/0110414](#)
- [165] C.P. Ma, E. Bertschinger: *Cosmological perturbation theory in the synchronous and conformal Newtonian gauges*. Astrophys. J. **455** 7-25 (1995)
- [166] V.F. Mukhanov, H.A. Feldman, R.H. Brandenberger: *Theory of cosmological perturbations*. Phys. Rep. **215** 203-333 (1993)
- [167] U. Seljak, M. Zaldarriaga: *A line of sight integration approach to cosmic microwave background anisotropies*. Astrophys. J. **469** 437-444 (1996) Los Alamos e-print Archive [astro-ph/9603033](#)
- [168] M. Zaldarriaga, U. Seljak: *CMBFAST for spatially closed universes*. Astrophys. J. Supp. **129** 431-434 (2000) Los Alamos e-print Archive [astro-ph/9911219](#)
- [169] A. Lewis, A. Challinor, A. Lasenby: *Efficient computation of CMB anisotropies in closed FRW models*. Astrophys. J. **538** 473-476 (2000) Los Alamos e-print Archive [astro-ph/9911177](#)
- [170] M. Doran: *CMBEASY:: an object oriented code for the cosmic microwave background*. Los Alamos e-print Archive [astro-ph/0302138](#)
- [171] <http://physics.nyu.edu/matiasz/CMBFAST/cmbfast.html>
- [172] <http://camb.info/readme.html>
- [173] <http://www.cmbeasy.org>

- [174] G.F. Smoot: *The CMB spectrum*. Los Alamos e-print Archive [astro-ph/9705101](#)
- [175] C.L. Bennett: *4-Year COBE DMR cosmic microwave background observations: Maps and basic results*. *Astrophys. J.* **464** L1-L4 (1996) Los Alamos e-print Archive [astro-ph/9601067](#)
- [176] S. Hanany et al.: *Maxima-1: A measurement of the cosmic microwave background anisotropy on angular scales of  $10'$  to  $5^\circ$* . *Astrophys. J.* **545** L5-L9 (2000) Los Alamos e-print Archive [astro-ph/0005123](#)
- [177] A.H. Jaffe et al.: *Cosmology from MAXIMA-1, BOOMERANG & COBE/DMR CMB observations*. *Phys. Rev. Lett.* **86** 3475-3479 (2001) Los Alamos e-print Archive [astro-ph/0007333](#)
- [178] D.N. Spergel et al.: *First year Wilkinson microwave anisotropy probe (WMAP) observations: Determination of cosmological parameters*. Los Alamos e-print Archive [astro-ph/0302209](#)
- [179] L. Page et al.: *First year Wilkinson microwave anisotropy probe (WMAP) observations: Interpretation of the TT and TE angular power spectrum peaks*. Los Alamos e-print Archive [astro-ph/0302220](#)
- [180] [http://space.gsfc.nasa.gov/astro/cobe/cobe\\_home.html](http://space.gsfc.nasa.gov/astro/cobe/cobe_home.html)
- [181] <http://map.gsfc.nasa.gov>
- [Nucleosynthesis]
- [182] L.H. Kawano: *Let's go: Early universe - Guide to primordial nucleosynthesis programming*. FERMILAB-PUB-88/34-A (1988)
- [183] L.H. Kawano: *Let's go: Early universe II - Primordial nucleosynthesis the computer way*. FERMILAB-PUB-92/04-A (1992)
- [184] M.S. Smith, L.H. Kawano: *Experimental, computational, and observational analysis of primordial nucleosynthesis*. *Astrophys. J. Suppl.* **85** 219-247 (1993)
- [185] K.A. Olive: *Primordial big bang nucleosynthesis*. Los Alamos e-print Archive [astro-ph/9901231](#)
- [186] K.A. Olive: *Big-bang nucleosynthesis*. *Rev. of Particle Phys.* **15** 133-135 (2000)
- [187] K.A. Olive, G. Steigman, T.P. Walker: *Primordial nucleosynthesis: Theory and observations*. *Phys. Rept.* **333** 389-407 (2000) Los Alamos e-print Archive [astro-ph/9905320](#)
- [188] R.V. Wagoner, W.A. Fowler, F. Hoyle: *On the synthesis of elements at very high temperatures*. *Astrophys. J.* **148** 3-48 (1967)

- [189] R.V. Wagoner: *Big-bang nucleosynthesis revisited*. *Astrophys. J. Suppl.* **179** 343-360 (1973)
- [190] R.V. Wagoner: *Synthesis of the elements within objects exploding from very high temperatures*. *Astrophys. J. Suppl.* **162** 247-295 (1969)
- [191] W.A. Fowler, G.R. Caughlan, B.A. Zimmerman: *Thermonuclear reaction rates*. *Annual Rev. Astron. & Astrophys.* **5** 525-570 (1967)
- [192] R. Esmailzadeh, G.D. Starkman, S. Dimopoulos: *Primordial nucleosynthesis without a computer*. *Astrophys. J.* **378** 504-518 (1991)
- [193] J. Bernstein, L.S. Brown, G. Feinberg: *Cosmological helium production simplified*. *Rev. Mod. Phys.* **61** 25-39 (1989)
- [194] S.M. Carroll, M. Kaplinghat: *Testing the Friedmann equation: The expansion of the universe during big-bang nucleosynthesis*. *Phys. Rev.* **D65** 063507 (2002) Los Alamos e-print Archive [astro-ph/0108002](#)
- [195] L. Knox, A. Kosowsky: *Primordial nucleosynthesis in conformal Weyl gravity*. FERMILAB-PUB-93/322-A (1993)
- [196] M. Kaplinghat, G. Steigman, T.P. Walker: *Nucleosynthesis in power-law cosmologies*. *Phys. Rev.* **D61** 103507 (2000) Los Alamos e-print Archive [astro-ph/9911066](#)
- [197] X. Chen: *The helium abundance problem and non-minimally coupled quintessence*. Los Alamos e-print Archive [astro-ph/0011533](#)
- [198] X. Chen: *How to get less helium and more neutrinos from BBN*. *Int. J. Mod. Phys.* **A16S1C** 1025-1027 (2001) Los Alamos e-print Archive [astro-ph/0011532](#)
- [199] T. Damour, B. Pichon: *Big bang nucleosynthesis and tensor-scalar gravity*. *Phys. Rev.* **D59** 123502 (1999) Los Alamos e-print Archive [astro-ph/9807176](#)
- [200] F.G. Alvarenga et al.: *An analysis of helium primordial nucleosynthesis with a variable cosmological coupling*. *Braz. J. Phys.* **31** 546-551 (2001) Los Alamos e-print Archive [gr-qc/0105062](#)
- [201] E. Massó, F. Rota: *Primordial nucleosynthesis as a test of the Friedmann equation in the early universe*. Los Alamos e-print Archive [astro-ph/0302554](#)
- [202] D.I. Santiago, D. Kalligas, R.V. Wagoner: *Nucleosynthesis constraints on scalar-tensor theories of gravity*. *Phys. Rev.* **D56** 7627-7637 (1997) Los Alamos e-print Archive [gr-qc/9706017](#)
- [203] J.H. Applegate, C.H. Hogan, R.J. Scherrer: *Cosmological baryon diffusion and nucleosynthesis*. *Phys. Rev.* **D35** 1151-1160 (1987)

- [204] R.T. Hammond: *Helicity flip cross section from gravity with torsion*. *Class. Quantum Grav.* **13** 1691-1697 (1996)
- [205] M. Brüggen: *Effects of a torsion field on big bang nucleosynthesis*. *Gen. Rel. Grav.* **31** 1935-1939 (1999)

#### [Historical nucleosynthesis & CMB]

- [206] S. Chandrasekhar, L.R. Henrich: *An attempt to interpret the relative abundances of elements and their isotopes*. *Astrophys. J.* **95** 288-298 (1942)
- [207] G. Gamow: *Expanding universe and the origin of elements*. *Phys. Rev.* **70** 572-573 (1946)
- [208] R.A. Alpher, H. Bethe, G. Gamow: *The origin of chemical elements*. *Phys. Rev. Lett.* **73** 803-804 (1948)
- [209] G. Gamow: *On relativistic cosmogony*. *Rev. of Mod. Phys.* **21** 367-373 (1949)
- [210] A.A. Penzias, R.W. Wilson: *A measurement of excess antenna temperature at 4080 Mc/s*. *Astrophys. J.* **142** 419-421 (1965)
- [211] R.H. Dicke et. al: *Cosmic black-body radiation*. *Astrophys. J.* **142** 414-419 (1965)
- [212] P.J.E. Peebles: *Primeval helium abundance and the primeval fireball*. *Phys. Rev. Lett.* **16** 410-413 (1966)
- [213] P.J.E. Peebles: *Primordial helium abundance and the primordial fireball*. *Astrophys. J.* **146** 524-552 (1966)

#### [Nucleosynthesis measurements]

- [214] Y.I. Izotov, T.X. Thuan, V.A. Lipovetsky: *The primordial helium abundance from a new sample of metal-deficient blue compact galaxies*. *Astrophys. J.* **435** 647-667 (1994)
- [215] Y.I. Izotov, T.X. Thuan: *The primordial abundance of  $^4\text{He}$  revisited*. *Astrophys. J.* **500** 188-216 (1998)
- [216] K.A. Olive, G. Steigman: *On the abundance of primordial helium*. *Astrophys. J. Supp.* **97** 49-58 (1995)
- [217] J.K. Webb et al.: *A high deuterium abundance at redshift  $z = 0.7$* . *Nature* **388** 250-252 (1997)
- [218] S. Burles, D. Tytler: *The deuterium abundance toward QSO 1009+2956*. *Astrophys. J.* **507** 732-744 (1998)

- [219] S. Burles, D. Tytler: *The deuterium abundance toward Q 1937-1009*. *Astrophys. J.* **499** 699-712 (1998)
- [220] D.S.P. Dearborn, G. Steigman, M. Tosi: *Galactic evolution of D and  $^3\text{He}$  including stellar production of  $^3\text{He}$* . *Astrophys. J.* **465** 887-897 (1996)
- [221] K.A. Olive et al.: *What is the problem with  $^3\text{He}$ ?* *Astrophys. J.* **444** 680-685 (1995)
- [222] D. Galli et al.: *Galactic evolution of D and  $^3\text{He}$* . *Astrophys. J.* **443** 536-550 (1995)
- [223] D.S. Balser et al.: *The cosmic abundance of He-3. 3. Improved line parameters for selected sources*. *Astrophys. J.* **430** 667-681 (1994)
- [224] D.S. Balser et al.: *The  $^3\text{He}$  abundance in planetary nebulae*. *Astrophys. J.* **483** 320-334 (1997)
- [225] R.T. Root, T.M. Bania, T.L. Wilson: *Detection of helium-3 in a planetary nebula*. *Nature* **355** 618-620 (1992)
- [226] J. Geiss, G. Gloecker: *Abundance of deuterium and helium-3 in the protosolar cloud*. *Space Sci. Rev.* **84** 239-250 (1998)
- [227] P.R. Mahaffy et al.: *Galileo probe measurements of D/H and  $3\text{He}/4\text{He}$  in Jupiter's atmosphere*. *Space Sci. Rev.* **84** 251-263 (1998)
- [228] J.L. Linsky: *Deuterium abundance in the local ISM and possible spatial variations*. *Space Sci. Rev.* **84** 285-296 (1998)
- [229] J. Geiss, H. Reeves: *Cosmic and solar system abundances of deuterium and helium-3*. *Astron. & Astrophys.* **18** 126-132 (1972)
- [230] P. Bonifacio, P. Molaro: *The primordial lithium abundance*. *Mont. Not. R. Astron. Soc.* **285** 847-861 (1997)
- [231] D.T. Tytler, X.M. Fan, S. Burles: *Cosmological baryon density derived from the deuterium abundance at redshift  $z = 3.57$* . *Nature* **381** 207-209 (1996)
- [232] N. Christlieb et al.: *A stellar relic from the early milky way*. *Nature* **419** 904-906 (2002)
- [233] R. Salvaterra, A. Ferrara: *Is primordial  $^4\text{He}$  truly from big bang?* Los Alamos e-print Archive astro-ph/0302285
- [234] L. Searle, W.L. Sargent: *Inferences from the composition of two dwarf blue galaxies*. *Astrophys. J.* **173** 25-33 (1972)
- [235] R.H. Cyburt, B.D. Fields, K.A. Olive: *Primordial nucleosynthesis in the light of WMAP*. Los Alamos e-print Archive astro-ph/0302431



**[Precision nucleosynthesis]**

- [236] S. Dodelson, M.S. Turner: *Nonequilibrium neutrino statistical mechanics in the expanding universe*. Phys. Rev. **D46** 3372-3387 (1992)
- [237] R.E. Lopez, M.S. Turner: *Precision prediction for the big-bang abundance of primordial  ${}^4\text{He}$* . Phys. Rev. **D59** 103502 (1999)



# Index

- baryon, 116
- baryon-to-photon ratio, 41
- binding energy, 30
- Boltzmann equation
  - FLRW model, 33
  - Weyl-Cartan model, 98
- boson, 116
  
- capture time, 40
  - parameter dependence of, 42
- chi square, 80
- CMB
  - spectrum, 28
  - timetable, 26
- computer algebra systems, 121
- critical density, 13
- curvature
  - decomposition of, 119
  - definition of, 51
  - rotational, 117
    - decomposition of, 117
  - strain, 117
    - decomposition of, 118
  
- deceleration parameter
  - alternative Weyl-Cartan model, 90
  - definition of, 21
  - FLRW model, 23
  - sign of, 87
  - triplet model, 93
  - Weyl-Cartan model, 84
- deuterium abundance
  - observational bounds, 46, 47
  - parameter dependence of, 42, 100
- dimensions, 50, 59, 106
- downhill simplex, 122
  
- energy density
  - cosmological-thermodynamical, relation between, 27
  - thermodynamical, definition of, 25
- energy-momentum
  - ideal fluid, 10
  - triplet field, 55
- exterior multiplication, 107
  
- field equations
  - triplet model, 92
  - Weyl-Cartan model
    - alternative approach, 89
    - final form, 70
    - general case, 66
    - special case, 68
- Friedmann equation, 12
  
- hadron, 116
- helium abundance
  - definition of, 43
  - observational bounds, 46, 47
  - parameter dependence of, 44
  - precision estimate, 102
  - triplet model
    - parameter bounds, 101
    - parameter dependence of, 100
- hodge dual, 108
- horizon
  - event, 15
  - particle, 15
- Hubble
  - flow, 11
  - law, 9
    - derivation of, 21
    - deviation from, 22
  - radius, angular scale of, 105

- rate
  - alternative Weyl-Cartan model, 90
  - definition of, 13
  - FLRW model, 17
  - triplet model, 93
  - Weyl-Cartan model, 78
- interior multiplication, 107
- Lagrangian
  - Einstein-Proca, 55
  - MAG, general, 53
  - triplet, 54
  - Weyl-Cartan model, 62
- lepton, 115
- luminosity distance
  - alternative Weyl-Cartan model, 90
  - definition of, 18
  - FLRW model, 20
  - triplet model, 93
  - Weyl-Cartan model, 78
- MAG
  - field equations, general form, 52
  - gauge field excitations, 52
  - gauge fields, 52
  - matter fields, 52
  - summary of definitions, 54
- magnitude-redshift relation
  - alternative Weyl-Cartan model, 90
  - comparison at high redshift, 88
  - definition of, 23
  - FLRW model, 23
    - approximated, 24
    - parameter dependence of, 22
  - Weyl-Cartan model, 78
- meson, 116
- neutron-to-baryon ratio
  - definition of, 31
  - final form, 37
    - with chemical potential, 39
  - parameter dependence of, 38, 40
- Noether identity
  - alternative Weyl-Cartan model, 89
  - FLRW model, 12
  - MAG, general, 52
  - Weyl-Cartan model, 64
  - Weyl-Cartan, general, 58
- nonmetricity
  - decomposition of, 119
  - definition of, 51
- nuclear reactions, 43
- number density
  - non-relativistic limit, 29
  - thermodynamical, definition of, 25
- pp chain, 45
- quark, 115
- reaction rate
  - final form, 35
    - with chemical potential, 39
    - neutron-proton conversion, 32
- redshift, 16
- Robertson-Walker metric, 10
- singularity, 15
- supernova
  - best-fit parameters
    - alternative Weyl-Cartan model, 92
    - FLRW model, 82
    - other groups, 84, 85
    - triplet model, 95
    - Weyl-Cartan model, 83
  - confidence contours
    - alternative Weyl-Cartan model, 95
    - FLRW model, 81
    - triplet model, 95
    - Weyl-Cartan model, 83
  - data set, 145
  - data sets, overview of, 79
- temperature
  - dimensionless, definition of, 35
  - photons-neutrinos, relation between, 40, 97
- temperature-time relation, 40
- torsion

- decomposition of, 119
- definition of, 51
- triplet
  - ansatz, 55
  - ansatz, field equations of, 55
  - excitations, explicit form, 56
- units
  - natural, 111
  - SI, 112
- Weyl-Cartan spacetime
  - definition of, 57
  - field equations, 58

Table E.2: Acronyms

<b>Acronym</b>	
2dFGRS	<b>2</b> degree <b>F</b> ield <b>G</b> alaxy <b>R</b> edshift <b>S</b> urvey
ART	Allgemeine <b>R</b> elativitätstheorie
BBN	<b>B</b> ig <b>B</b> ang <b>N</b> ucleosynthesis
BOOMERANG	<b>B</b> alloon <b>O</b> bservations of <b>M</b> illimetric <b>E</b> xtragalactic <b>R</b> adiation and <b>G</b> eophysics
CMB	<b>C</b> osmic <b>M</b> icrowave <b>B</b> ackground
COBE	<b>C</b> osmic <b>B</b> ackground <b>E</b> xplorer
DMR	<b>D</b> ifferential <b>M</b> icrowave <b>R</b> adiometer
FIRAS	<b>F</b> ar <b>I</b> nfra <b>R</b> ed <b>A</b> bsolute <b>S</b> pectrophotometer
FLRW	<b>F</b> riedmann- <b>L</b> emaître- <b>R</b> obertson- <b>W</b> alker
GR	<b>G</b> eneral <b>R</b> elativity
LSS	<b>L</b> arge- <b>S</b> cale <b>S</b> tructure
MAG	<b>M</b> etric- <b>A</b> ffine <b>G</b> ravity
MAXIMA	<b>M</b> illimeter <b>A</b> nisotropy <b>E</b> Xperiment <b>I</b> Maging <b>A</b> rray
MLCS	<b>M</b> ulticolor <b>L</b> ight <b>C</b> urve <b>S</b> hape
SCP	<b>S</b> upernova <b>C</b> osmology <b>P</b> roject
SDSS	<b>S</b> loan <b>D</b> igital <b>S</b> ky <b>S</b> urvey
SNAP	<b>S</b> upernova <b>A</b> cceleration <b>P</b> robe
WMAP	<b>W</b> ilkinson <b>M</b> icrowave <b>A</b> nisotropy <b>P</b> robe
XMM-LSS	<b>X</b> -ray <b>M</b> ulti <b>M</b> irror telescope - <b>L</b> arge- <b>S</b> cale <b>S</b> tructure survey

## Acknowledgements

The author is grateful to Friedrich W. Hehl (Cologne), Xuelei Chen (Santa Barbara), Carsten Raas (Cologne), Christian Heinicke (Cologne), Guillermo Rubilar (Conception), Yun Wang (Ohio State), Volker Perlick (Cologne), Yuri N. Obukhov (Cologne) and the members of the gravity group at the University of Cologne for their support.

## Erklärung

Ich versichere, daß ich die von mir vorgelegte Dissertation selbständig und ohne unzulässige Hilfe angefertigt, die benutzten Quellen und Hilfsmittel vollständig angegeben und die Stellen der Arbeit – einschließlich Tabellen, Karten und Abbildungen –, die anderen Werken im Wortlaut oder dem Sinn nach entnommen sind, in jedem Einzelfall als Entlehnung kenntlich gemacht habe; daß diese Dissertation noch keiner anderen Fakultät zur Prüfung vorgelegen hat; daß sie abgesehen von den unten angegebenen Teilpublikationen noch nicht veröffentlicht worden ist, sowie daß ich eine solche Veröffentlichung vor dem Abschluß des Promotionsverfahrens nicht vornehmen werde. Die Bestimmungen der geltenden Promotionsordnung sind mir bekannt. Die von mir vorgelegte Dissertation ist von Herrn Prof. Dr. F.W. Hehl betreut worden.

## Teilveröffentlichungen

1. D. Puetzfeld, R. Tresguerres: *A cosmological model in Weyl-Cartan spacetime*. Class. Quantum Grav. **18** (2001) 667-693 Los Alamos e-Print Archive [gr-qc/0101050](#)
2. D. Puetzfeld: *A cosmological model in Weyl-Cartan spacetime: I. Field equations and solutions*. Class. Quantum Grav. **19** (2002) 3363-3280 Los Alamos e-Print Archive [gr-qc/0111014](#)
3. D. Puetzfeld: *A non-standard cosmological model*. Int. J. of Mod. Phys. A **17** (2002) 2772
4. D. Puetzfeld: *A cosmological model in Weyl-Cartan spacetime: II. Magnitude-redshift relation*. Class. Quantum Grav. **19** (2002) 4463-4482 Los Alamos e-Print Archive [gr-qc/0205052](#)
5. D. Puetzfeld, X. Chen: *Analysis of the supernova data within a non-standard cosmological model*. In preparation (2003)





# Lebenslauf

**Name** Dirk Pützfeld

**Geburtsdatum** 15.07.1975

**Geburtsort** Köln

**Familienstand** ledig

**Staatsangehörigkeit** deutsch

## Schulbildung

August 1981 – August 1985 Städt. Gemeinschaftsgrundschule, Köln-Mülheim

August 1985 – Mai 1994 Städt. Rhein-Gymnasium, Köln-Mülheim

Juni 1994 Abitur

## Studium

Oktober 1994 Aufnahme des Physikstudiums (Universität zu Köln)

April 1997 Vordiplom in Physik (Universität zu Köln)

August 2000 Diplom in Physik (Universität zu Köln),  
Aufnahme der Promotionsarbeit

April 2000 – August 2000 Studentische Hilfskraft

Januar 2001 – Juni 2003 Stipendiat im Graduiertenkolleg *Scientific computing*